Optical studies of the pre-breakdown mechanism in dielectronic liquids.

McGrath, P. B.

OPTICAL STUDIES OF THE PRE-BREAKDOWN MECHANISM IN DIELECTRIC LIQUIDS

by

P.B. McGrath, B.Sc. (Eng.)

Department of Electrical and Electronic Engineering
Queen Mary College (University of London)

Thesis presented for the degree of Doctor of Philosophy
in the Faculty of Engineering of the University of London

February 1977

ABSTRACT

The work described in this thesis provides an optical study of pre-breakdown events in liquid dielectrics. A small scale rig employing a 50Ω test cell with viewing windows, as part of a high voltage co-axial line, enabled short rise time pulses to be applied to a non-uniform test gap. For the liquid dielectric, changes of refractive index resulting from applied voltage were rendered visible by means of a Schlieren optical system. A high speed image converter camera enabled rapidly changing pre-breakdown phenomena to be photographically recorded at framing speeds up to 10^7 per second. Scattered light photographs were taken by orthogonal flash illumination under both pulse and direct voltage conditions, allowing large format macrophotography. Using a piezo-electric transducer placed within the test cell, and a photomultiplier to view the gap region, a relationship has also been established between the generation of mechanical waves, light scintillation and conduction current pulses.

From the photographic records and conventional parameter measurements there exists strong evidence for the presence of a gaseous phase in processes leading to the electrical breakdown of liquid dielectrics even under pulse conditions.

CONTENTS

CHAPTER ONE

INTRODUCTION AND SUMMARY

The use of optical probe techniques enables information to be gathered that is not accessible at the terminals of a test cell. Stress induced refractive index perturbations may be rendered visible by the use of Schlieren optics, whilst light scattering can be used to detect interfacial sites. Coupled with high speed photography, these methods provide a powerful diagnostic tool in the study of events leading to liquid dielectric failure.

Previous photographic studies have indicated the existence of pre-breakdown events, although a unified theory has not been established. The survey presented in Chapter 2 provides a coverage of the existing photographic work in addition to various aspects of conduction behaviour.

In order to construct a model for the sequence of events leading to gap failure, the problem was investigated using a variety of experimental methods. Several experiments were performed using either a co-axial or orthogonal viewing port test cell. An outline of the test techniques employed together with a description of the specialised apparatus is included in Chapter 3.

The work presented in this thesis not only augments earlier photographic findings, but the new techniques

adopted have also allowed the advancement of an explanation of events based on a cavitation process. Both time resolved Schlieren records and scattered light photographs are presented in Chapter 4. The findings show the existence of a pre-breakdown event that is composed of a multitude of densely packed microbubbles.

A study of direct stress conduction, light and acoustic emissions in both n-hexane and transformer oil is also reported. The transitional nature of the three parameters is highlighted by presenting integrated plots whilst the pulse activity is illustrated by oscillographic recordings.

The new techniques and findings associated with this study may be summarised as follows.

Step Voltage

1. Time resolved Schlieren photography up to 1×10^7 frames per second.
2. The use of static pre-stress in conjunction with high speed photography.
3. Externally generated impinging and standing acoustic waves.
4. Scattered light photographic sequences.
5. Temperature variation for Schlieren and scattered light photography.

Direct Voltage

1. Using a point cathode, coincident transitions were recorded for integrated conduction current, light and acoustic emissions at room temperature.

2. A differential shift in the transitions was induced by temperature variation.

3. A coincident pulse behaviour was observed for the three quantities measured, with the conduction pulses superimposed on a direct current offset.

4. A shift in the point cathode light emission spectrum for transformer oil was affected by either stress or thermal variation.

Interpretations are placed on the findings with particular emphasis on cavitation and its generation at gaseous, solid and liquid interfaces. A breakdown model is advanced in Chapter 5 in which it is proposed that event precipitation is rooted in electrostatic traction.

CHAPTER TWO

REVIEW OF PREVIOUS WORK

2.1 INTRODUCTION

The insulating properties and events leading to failure of dielectric liquids have attracted considerable interest over many years. The diverse nature of research involved with liquid behaviour has provided a wealth of published information[1-6]. Not only has the work in this field of study been extensive but the conclusions drawn from the findings have often been conflicting, with no apparent convergence to a unified theory.

It is intended to provide a review that is relevant to the topic under investigation and to include information sufficient to add completeness to the interpretation. The differing mechanisms that have been proposed to explain dielectric failure, throughout the published work, have been included in the main body of the review in an attempt to maintain continuity. Investigations of an optical nature, conduction current measurement, the external effects of pressure and temperature, and the influence of a gaseous phase are included in this survey.

2.2 OPTICAL STUDIES

In 1961 Hakim and Higham[7] made a preliminary optical study of pre-breakdown phenomena. Employing a

Schlieren[8] optical system a region of differing refractive index was observed when a voltage pulse was applied to the point cathode of a test gap in n-hexane. The event once generated could disappear without breakdown; but for a higher applied voltage a spark breakdown, accompanied by the formation of a bubble, was seen to ensue. Photographic evidence supporting the observations was obtained using a rotating mirror camera, but due to optical limitations the time resolved event presented appeared only as a blur between the electrodes. Using a Toepler-Schlieren optical system Farazmand[9] obtained photographs with an improved definition. A high voltage negative going step function was applied to the point of a non-uniform test gap in n-hexane. Single-shot photographs were taken, and by selection of the time delay from voltage application, a sequence for the growth of a pre-breakdown disturbance was predicted from the individually recorded events. An explanation of the phenomenon was suggested invoking electron emission; followed by streamers that spanned part of the gap, forming numerous branches until the earthed electrode was reached.

A continuous record of a pre-breakdown disturbance, by the use of a streak camera, was presented in an M.Sc. dissertation by Chadband[10]. The test liquid was hexane, and the pre-breakdown event was seen to originate at the point cathode when an impulse voltage was applied. It was found that a time lag existed between voltage

application and the appearance of a disturbance, and a two stage decay occurred after voltage chopping. A rapid initial decay, lasting approximately 10μs, was followed by a faint disturbance lasting about 100μs. The disturbance then disappeared. Chadband and Wright[11] continued with tests using streak photography in conjunction with a Schlieren optical system to show that shock waves were associated with breakdown. A shock wave was also seen to accompany the first appearance of the disturbance, when an overvoltage was applied to the test gap. Electron emission from the point cathode was considered to form a weak plasma in the liquid, propagating towards the plane anode surface under the influence of the applied field. Later, Chadband et al employed a shadowgraph optical system for a pre-breakdown study[12], providing an improved resolution over that offered by the Schlieren technique[8]. A non-uniform test gap in n-hexane was used to show pre-breakdown phenomena for both a positive and a negative point polarity. The positive point disturbance was filimentary, and that for the negative point, brush like in appearance. When the voltage was insufficient to precipitate breakdown, the disturbance faded to discrete spots 20μs after voltage application. The spots subsequently disappeared 200μs later. It was not known whether this was a characteristic of the pre-breakdown behaviour, or related to the properties of the film emulsion used to photograph the event.

A large scale test chamber was used by Morikawa[13]

to observe highly stressed transformer oil both before and after electrical breakdown. Laser illuminated Schlieren photography was used to investigate the discharges that appeared between a needle and a flat plate when an impulse voltage was applied. Streamer propagation was observed for a positive point and the generation of localised regions of oil vaporisation occurred when the streamers had spanned the electrode gap. The regions were shown to be located at the tip of the needle, at the branching points of the streamers and along the streamers themselves. With increased time after breakdown the discrete vaporous regions expanded and coalesced to form a single bubble. When the point electrode was made negative, the time to breakdown was extended and bubble formation was shown to be less rapid. Corona was said to accompany the appearance of the disturbance and the inception stress increased with pressure over the oil.

Schlieren photography was also used by Thomas[14] who incorporated a Q-switched ruby laser to obtain time resolution in the nanosecond range. With this time resolution, photographs were taken 180ns before and 150ns after breakdown in n-hexane, between uniform field electrodes. Isolated regions, exhibiting a refractive index different from that of the surrounding liquid, occurred over the plane cathode surface and were typically 10μm in diameter. After breakdown, many streamers were shown to span the gap, originating from a common location on the anode surface, branching toward the cathode and

linking with several of the many isolated regions on its surface. The unconnected regions at the cathode remained unchanged in dimension after breakdown. As the discrete cathode regions appeared opaque using the Schlieren technique, it was thought that they could be cavities in which localised breakdown had occurred. The field in the cavity would be low and so be considered as an extension of the cathode surface. In contrast, the field in the liquid at the tip of the cavity may then become very large and so initiate impact ionization in the liquid, and generate anode directed streamers.

Later with the influence of Forster, this breakdown hypothesis was extended[15,16] to invoke electron emission as an initiating step. Thomas proposed that electron emission from cathode located asperities could cause local heating of the test liquid. Only then could a cavity be formed by the expanding low density region. A computer program was developed[17] to mathematically describe the process of charge emission in the presence of space charge distortion of the electric field. An emission related profile was predicted showing that only small temperature increases occurred in the liquid prior to cavitation. The regions of increased temperature were shown to possess complex and irregular shapes resulting from an instability of the space charge cloud.

A different technique was used by Hizal[18,19] to obtain temporal resolution for high speed photography. A step voltage was applied to a test gap of non-uniform

geometry in transformer oil, the voltage was then chopped so arresting the growth of the disturbance. This enabled a 3μs duration flashlight source to be used in conjunction with a conventional Schlieren optical system, to photograph the event. Using the cut-off characteristics of the Schlieren technique,[8] Hizal related the change of refractive index observed to a maximum temperature increase of 48°C; measured in a separate experiment. An explanation involving the generation of a plasma region by an electron collision process in the liquid phase was postulated, and the observed regions of increased temperature were thought to be formed by vibrational collisions. Nelson and Hashad[20] incorporated a Schlieren arrangement in a study of perfluoro n-hexane when variable frequency alternating voltages were applied to a divergent test gap. Discrete cavity formation was found to readily occur throughout the gap, within the frequency range of 150 Hz to 400 Hz, with a peak activity at 270 Hz. Data on gap failure, accompanying the report, also showed a minimum breakdown voltage at 270 Hz. Supporting an earlier electroluminescent study on transformer oil by Malik[21], it was thought that nucleation sites could be precipitated in regions remote from the point electrode, as a result of particle motion induced by the applied alternating field.

Without resorting to specialised optical methods, Krasucki et al[22] found that by using the highly viscous liquid dielectric hexachlorodiphenyl, relatively slow

moving pre-breakdown phenomena could be directly observed. Well defined channels were seen to emanate from the point electrode of a liquid immersed test gap when a direct voltage was applied. The channels were considered to be regions of localised breakdown within the liquid, and the breakdown products of carbon and gas bubbles remained where they were formed. The tree-like conductivity channels extended into the electrode gap and eventually led to total breakdown. At the time of the investigation the authors did not consider that a breakdown sequence could occur in less viscous insulating media. Later the study was extended by Krasucki[23] to include time sequence photography of vapour bubble formation and breakdown channels in hexachlorodiphenyl, in which the formative time lag could be extended to 30 minutes. Using silicone oil, a less viscous liquid, the time to breakdown was considerably reduced, although similar localised breakdown channels were observed. This enabled Krasucki to make the tentative suggestion that the observed breakdown sequence may be extended to include the far less viscous insulating oils. It was considered that above a certain critical voltage, electron emission and ionization became sufficient to cause local vaporisation of the liquid. The increased mean free path presented by the vapour compared with the liquid phase would allow electrons and ions to attain higher energies between collisions under the influence of the applied field, and so increase the probability of ionization on collision. The electrons and ions could

first produce a region in which to acquire more energy and then dissociate the liquid molecules by collision, to further increase the size of this region. Traces of solid matter remaining in the liquid after a bubble had completely faded were considered to be substances formed by dissociation of the liquid. The presence of contamination in the form of a small water globule in silicone fluid was also investigated[23]. The sphere was shown to elongate in the direction of the applied field and breakdown channels extended from the ends of the elongated region toward the electrodes. Breakdown then ensued. In a subsequent publication Krasucki[24] postulated an amended breakdown theory. Under the influence of a high electric field, points of zero pressure may be generated in an insulating liquid. As a result of electron bombardment of the liquid at the cavity boundary so generated, vapourisation would allow the bubble to grow and precipitate breakdown. The formation of a vapour bubble in a uniform field gap was suggested to result at a point of field intensification possibly caused by the presence of particles or surface irregularities on a microscopic scale. Photographic evidence for the growth of a single vapour bubble in hexachlorodiphenyl was presented, showing a formative time in excess of one second. By temperature variation of a hexachlorodiphenyl sample, the dependence of time to breakdown and electric strength, on viscosity, was investigated. Figures 2.1 and 2.2 show both time to breakdown at constant stress and impulse breakdown strength

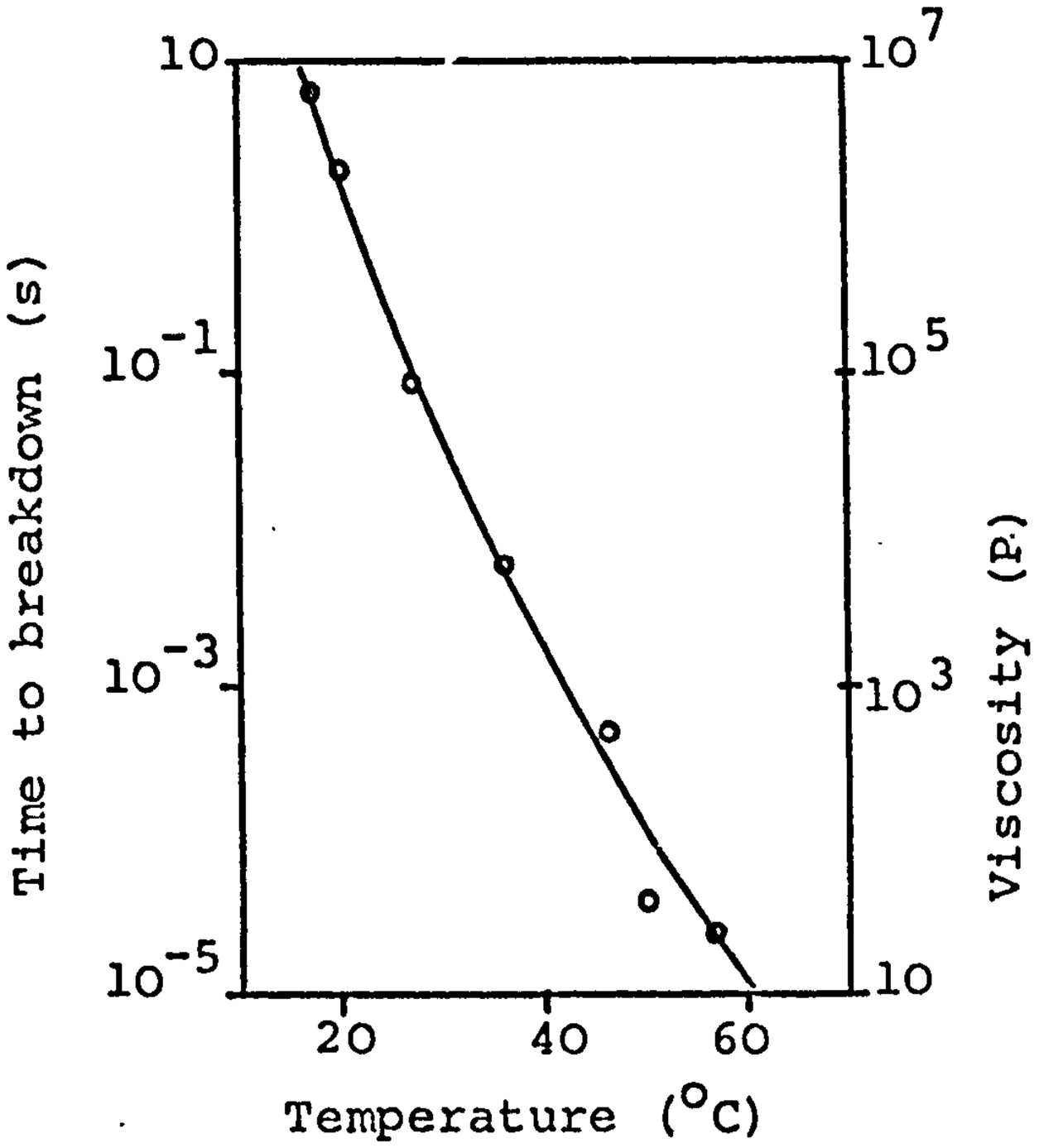

Fig. 2.1 Time to breakdown in hexachlorodiphenyl, stressed at 1.3MVcm^{-1}, as a function of temperature (o); viscosity as a function of temperature (–). (Krasucki 1966)

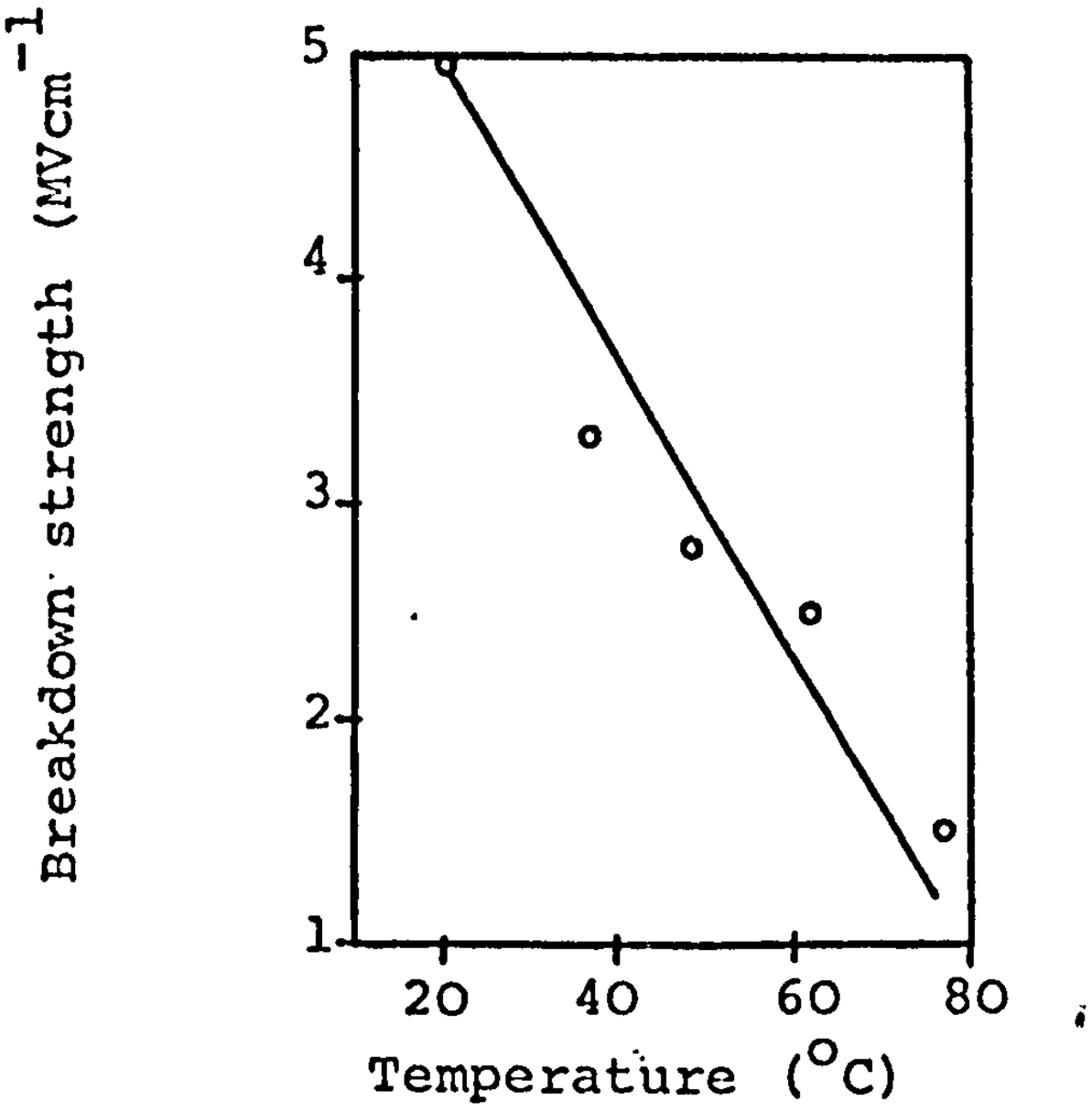

Fig. 2.2 Impulse breakdown strength as a function of temperature. (Krasucki 1966)

to be directly proportional to viscosity. An essentially steady state equation for bubble lift was presented by relating the hydrostatic pressure in the liquid to pressures stemming from the applied field Coulomb force, and surface tension, giving

$$E = 358\sqrt{\frac{1}{\varepsilon}\left[P_\infty + \frac{2\sigma}{R}\right]} \quad Vcm^{-1}$$

where E is the uniform electric field in the absence of a point of intensification; ε is the permittivity; P_∞ the hydrostatic pressure in the liquid (in dyne $cm^{-2}=10^{-1}Nm^{-2}$); σ the surface tension (in dyne $cm^{-1}=10^{-3}Nm^{-1}$) and R the radius of the particle (cm). If the electric stress was removed before breakdown occurred, the disturbance was seen to fade. When a bubble of air was deliberately introduced into the test liquid it was found that the decay time was greater by several orders of magnitude. From this comparative test it was considered that the observed disturbance was a bubble of vapour.

Mirza et al[25] used a point to plane electrode system in which the plane electrode was a layer of mercury. When a direct electric stress was applied, liquid jet motion in the hexane dielectric caused a depression in the centre of the mercury electrode. A photograph was shown in which a light scattering region could be seen in the test gap. The cause, it was suggested, might prove to be a spray of bubbles. Singh et al[26] used a spectroscope and a photomultiplier to measure the angle through which incident light was

scattered by this phenomenon. The results revealed the existence of a spray, which was found to be composed of many isolated regions of unity refractive index. These could only be bubbles, having radii 0.7μm and 1μm for negative and positive point polarity, respectively. Photographs were presented[27] to show light scattering for both positive and negative point polarity, utilising a laser light source to provide a 30 second exposure. Using a shadowgraph optical technique in conjunction with a flashlight source, discrete bubbles were shown to form a spray moving away from the point electrode. A later study[28] provided evidence to support these findings and show the growth of a pre-breakdown disturbance by scattered light photography. The divergent test gap was illuminated by a flashlight source and a number of large format, single shot photographs were taken. A representative sequence of events was constructed and shown to possess similar characteristics to those depicted by time resolved Schlieren records taken under similar conditions.

Murooka et al[29] used a gas bubble chamber to photograph the formation of bubbles in diethyl ether. Supersaturation was achieved by heating the liquid to $140^{o}C$ and then reducing the pressure by $10kgcm^{-2}$. A high voltage pulse was applied to the test gap when the pressure attained its minimum value. Employing a symmetrical divergent geometry for the test gap, bubbles formed preferentially at the cathode and extended into the gap towards the anode. The appearance of the phenomenon

required the presence of both superheating and the application of a high voltage pulse. It was suggested that electron emission from the point cathode was responsible for the initiation of the bubble phase. Later a modified technique was used[30,31], again incorporating a gas bubble chamber and divergent electrode geometry, but using diethyl ether saturated with carbon dioxide. Carbon dioxide gas was dissolved to 100% saturation in the test liquid at a pressure of 9-13 $kgcm^{-2}$, the sample was then compressed to 40-45 $kgcm^{-2}$. Super-saturation was achieved by allowing the pressure to fall to 4 $kgcm^{-2}$. A voltage pulse was then applied to the test gap and bubbles were seen to grow from the point cathode. A sequence of photographs was taken at a time interval of 200μs between frames. The relative slow bubble formation appeared similar to the rapidly developing phenomena photographed by other workers using fixed pressure test techniques in conjunction with liquid hydrocarbons[12,13].

Shadow patterns of pre-breakdown phenomena have also been reported when using water as a test liquid, by Yanshin et al[32]. For a negative point polarity, pre-breakdown channels were shown to be denditric in nature. The disturbance was seen 100ns after voltage application and breakdown followed within a further 100ns. When the point electrode was made positive, the event was seen to be self-luminous 10ns after voltage application and could be photographed directly. Microbubble formation was observed but as a conventional ionic heating mechanism could not be invoked to explain the rapid development of the process,

a hole transport mechanism was considered to occur by H_3O^+ hydronium ions, under the influence of the high electric field the appearance of electron vacancies on the anode surface was thought to attract electrons from the nearby water molecules, so forming hydronium ions, the subsequent charge carrier motion then led to local heating and the formation of gas nuclei.

Lichtenberg figures were used to show pre-breakdown disturbances in an insulating oil by Toriyama et al[33]. A photosensitive plate was placed in light contact with a point plane gap immersed in transformer oil. Photographs were shown indicating thin streamers surrounded by wider regions for both positive and negative point polarity. At reduced pressure, broadening of the wider regions occurred, the thin streamers remaining unchanged. It was suggested that the thin regions were electronic in origin and the broader areas were pre-breakdown gaseous volumes. A breakdown mechanism was proposed that originated from collision ionization by electrons. This was then followed and emphasised by successive discharges in the gaseous phase caused by rupture of liquid molecular bonding, by electron bombardment. Breakdown for a non-uniform geometry could take place from either a point anode or cathode, and appeared similar to the treeing observed in solid dielectrics, this suggesting that breakdown may involve more than just electron emission from the cathode. However, the presence of a photographic plate in the high field region may have modified the observed partial break-

down process, the effects of which were not taken into account. Working in conjunction with Mitsui and Calderwood, Toriyama also produced Lichtenberg and dust figures in liquid nitrogen[34]. A 1 x 40μs impulse voltage was applied to the point electrode of a divergent test gap. The needle was placed in light contact with a photosensitive plate mounted on the plane electrode, to obtain Lichtenberg figures. In the absence of a photographic plate, dust figures were formed by sprinkling a mixture of electrified sulphur and red lead on the ebonite surface of the plane electrode, after an electrical discharge but before removal of the test liquid. The images formed by both techniques, showed finely detailed, tree-like discharge patterns that were continuous for a negative point, but exhibiting broken branches for a positive point polarity. The results were thought to support the earlier breakdown hypothesis involving electron multiplication by ionization on collision and bubble production due to local boiling, with breakdown ensuing in the gaseous phase.

2.3 LIGHT EMISSION STUDIES

In 1940 Race[35] reported the appearance of a diffuse glow emitted from electrically stressed dowtherm (73.5% diphenyl oxide, 26.5% diphenyl) well below its breakdown strength. The appearance of this emission was different from the spark discharges that precipitated breakdown and was believed to originate from an entirely

different mechanism. The blue glow was similar in appearance to that seen in the same liquid under x-ray or mercury arc irradiation. It was found that a few cm partial pressure of air over the sample would completely extinguish the glow. An attempt was made to obtain electroluminescence, as Race named the phenomenon, in mineral oil but this proved to be unsuccessful. However, whilst investigating pre-breakdown pulse activity in transformer oil, Darveniza[36] found that light was emitted from the highly stressed gap region. The colour was seen to be similar to that of the blue fluorescence observed when the oil was irradiated with an ultraviolet source. Microscopic examination showed filimentary luminous streamers which completely spanned the gap without precipitating breakdown, and upon increasing the electric stress the glow became more diffuse, extending throughout the whole test gap. The light intensity increased exponentially with applied electric field but without noticeable change in spectrum to the unaided eye. Using n-hexane no light emission was observed but when the sample was doped with anthracene, a characteristic emission of the dissolved impurity occurred, appearing similar in nature to transformer oil. Pressure and tension were alternately applied to the test samples but there was no apparent change in the respective emission properties. Darveniza and Tropper[37] continued the study of dielectric liquids containing fluorescent solutes. A light emission spectrum was measured for transformer oil and an emission peak was

observed at 530nm for a direct uniform stress of 900kVcm^{-1}. Upon increasing the stress to 1.3MVcm^{-1} the emission peak shifted to 480nm. Both integrated light emission and conduction current were measured and found to be similar increasing exponential functions of applied voltage. For n-hexane doped either with anthracene or p-terphenyl, light was emitted that was characteristic of the fluorescent solute utilised. Using commercially pure benzene very intense blue light was observed which was accompanied by a considerable conduction current even for a low applied field. The liquids exhibited an increasing electric strength, but a reduction of light emission, as the number of conditioning breakdowns increased. Filimentary streamers similar to those in transformer oil but of a higher intensity, were observed in both benzene and doped n-hexane.

Dakin and Berg[38] observed luminous spots on the cathodesurface of a highly stressed gap in an insulating oil. It was presumed that electrons were emitted from sites of high localised stress on the cathode surface, these then causing fluorescence of the adjacent oil molecules. The light emission was unaffected by pressure variation between 10 torr and 2 atmospheres, but oil preparation and filtration details were not presented. Gosling[39] investigated light emission for both uniform and non-uniform field conditions in transformer oil. In contrast with the observations of Darveniza[37,40] where streamers were seen to span the gap, light was confined to

the cathode surface, and for degassed oil, occasionally at the anode. With an increase of nitrogen in solution the observed glow extended from the cathode region into the gap, and the light intensity increased at the anode. Conversely, with oxygen in solution, the light intensity decreased and was confined to the cathode: upon increasing the gas concentration the glow was completely quenched, supporting the findings of Race[35]. For a non-uniform electrode geometry, luminescence could be seen at the surface of the spherical electrode when the point was made positive. With an initial tip radius of 16μm a faint glow was once observed at the point cathode, but luminescence was never seen near the anode for a divergent field geometry. Moving particles were believed to cause streamers and stationary, attached,particles caused the spots of light on the electrode surfaces, especially during stress conditioning of uniform electrodes. The behaviour of the particles was identified by viewing the test gap alternately with and without background illumination.

Applying direct stress to spherical electrodes Kalinowski and Dera[41] studied the luminescence of various dielectric liquids with fluorescent admixtures. Measurements of the characteristic radiation from small solutions of anthracene in either benzene or n-hexane yielded similar findings to those of Darveniza and Tropper[37], where plots of totalluminescence against conduction current was shown to be linear. For POPOP

doped benzene a spectral plot was undertaken and it was found that the wavelength of the light emitted was 438nm and furthermore, this was independent of the applied voltage. A plot of intensity at 438nm against conduction current was essentially linear, but for total light emission some departure from linearity was observed. Direct photography of the pronounced light emission from electrically stressed and doped benzene showed that the luminescence was confined to regions near the spherical electrodes,and that it was far more intense at the cathode. A tentative proposition was made in which the observed luminescence occurred solely in the liquid phase as a result of charge carriers being accelerated by the high field existing between the electrodes. On using a photo-multiplier, the light emission from stressed transformer oil and liquid paraffin was seen to be composed of discrete pulses, by Jones and Angerer[42]. A bi-spherical electrode geometry was used and plots of integrated light emission against conduction current yielded straight lines when plotted on logarithmic axes. Using a similar electrode geometry Gzowski et al[43] studied the light emitted from anthracene doped n-hexane when a step function voltage was applied. Light pulses were detected which were random in occurrence and magnitude and both were found to increase markedly with stress. Measurements were made for the time to appearance of the first light pulse after voltage application. From a statistical interpretation of the results it was believed that particles arriving at the

electrodes were responsible for the generation of light pulses. In an attempt to prevent possible particle effects, Malik[21] applied a sinusoidal voltage to observe electroluminescence in a transformer oil sample. The alternating field caused the particles to oscillate in the gap and so prevent them from discharging at the surface of the electrodes. Electroluminescence was seen to occur near the negative going electrode and light pulses were shown to be directly related to conduction current. Light emission was believed to originate from the downward transition of π electrons associated with the polycyclic aromatic molecules present in the oil, being excited into higher energy states as a result of the applied field.

A bi-spherical electrode geometry, forming part of a 50Ω coaxial system was the basis for tests performed by Palmer and House[45]. A high voltage impulse was applied to the test gap and light pulses were seen to be emitted from the hexane sample, just prior to total gap failure. The short rise time of the coaxial line and measuring equipment enabled light pulses, generated only nano-seconds before breakdown, to be recorded. From oscillo-graphic records of the photomultiplier output, light scintillations were shown to increase in magnitude just prior to breakdown. The discrete pulses observed were believed to correspond to abortive breakdown events, and analysis showed that the light emission occurred in the traditionally defined formative period of the breakdown process. Whilst photographically studying the pre-

breakdown behaviour of electrically stressed transformer oil, Kishida et al[44] made a photomultiplier observation of the non-uniform test gap. For a positive point polarity with a 400/3300μs impulse waveshape, a single light pulse was observed. However, with a point cathode many light pulses were recorded over the same 30μs emission period. Secondary discharges resulting from electron emission were believed to be responsible for the enhanced, negative point, luminescence.

Smith et al[46] demonstrated that for a highly stressed non-uniform gap in n-hexane, light could be seen at the tip of the point electrode; and the self luminous event was photographed with the aid of an image intensifier. Electron emission from the cathode was proposed as the initiating step of a light radiating process. The electrons may gain energy in the high electric field and by attachment to neutral molecules, form ions; with subsequent light emission from the plasma region. It was also shown[47] that the appearance of pre-breakdown light was accompanied by current fluctuations well below breakdown for a negative point but much closer to its occurrence for a positive point polarity. Furthermore, luminescence was more readily observed for a negative point, the opposite polarity yielding a very weak emission, the origin of which was confined to the plane cathode region. In both instances the light intensity decreased with time for constant applied voltage. Spectral analysis of individual light pulses was undertaken and a

broad distribution of wavelength was found, this extending from 250nm to 700nm. Viewing a point-point electrode system with a photomultiplier, light emission was detected 15ns before breakdown when an overvoltage was applied to the gap[48,49]. The emission was seen to commence at the cathode, this was then followed by an intense light at the anode: the two regions then extended and met in the gap at the instant of breakdown. Acoustic radiation was also detected after the light emission had commenced. Extending the field emission model to include the situation at breakdown stress, it was postulated that light emission was associated with the presence of a bubble of gas attached to the cathode surface. A cavity may possibly be generated as a result of an expanding electron cloud, producing local heating and turbulence. The large mean free path presented would allow electrons to gain sufficient energy to ionize molecules in the gas phase. The region may contain a plasma, and light emission at breakdown stress could then be attributed to space charge recombination.

Mirza et al[50] observed that spraying of gas bubbles from the highly stressed region of a point-plane gap in n-hexane coincided with the appearance of light at the tip of the point. The emission seen was considered to emanate from a region of plasma in contact with the point electrode and of sufficient density to be at the same potential. The region would expand until the field at the plasma-liquid interface was insufficient for field

ionization to occur.

Rashwan and Kao[51] investigated electroluminescence in n-hexane, transformer oil and benzene when subjected to direct electric fields. Using a multiple point or sphere to plane system, light was seen only at the cathode irrespective of the electrode geometry. The emission took the form of light bursts which were found to be associated with current bursts, and both exhibited some degree of pressure dependence. When measuring the integrated characteristics of light emission for dielectric liquids[52] it was found that inception voltage for electroluminescence was highly sensitive to temperature, fig. 2.3. In addition, light intensity decreased markedly with increase in both pressure and temperature for hexane, but an opposite characteristic was observed for benzene of commercial purity, fig. 2.4. Under the influence of an electric field it was proposed that electrons from cold cathode emission could gain sufficient energy to excite liquid molecules. After transferring their energy to molecules, the electrons could become attached to neutral molecules to form negative ions. Electroluminescence was thought to be associated with the energy released from excited molecules. The negative ion cloud coupled with light emission could produce local heating to form low density zones, electrons would be able to gain sufficient energy from the high field to cause impact ionization and precipitate breakdown. The observed coincidence of conduction current and light bursts in n-hexane was later

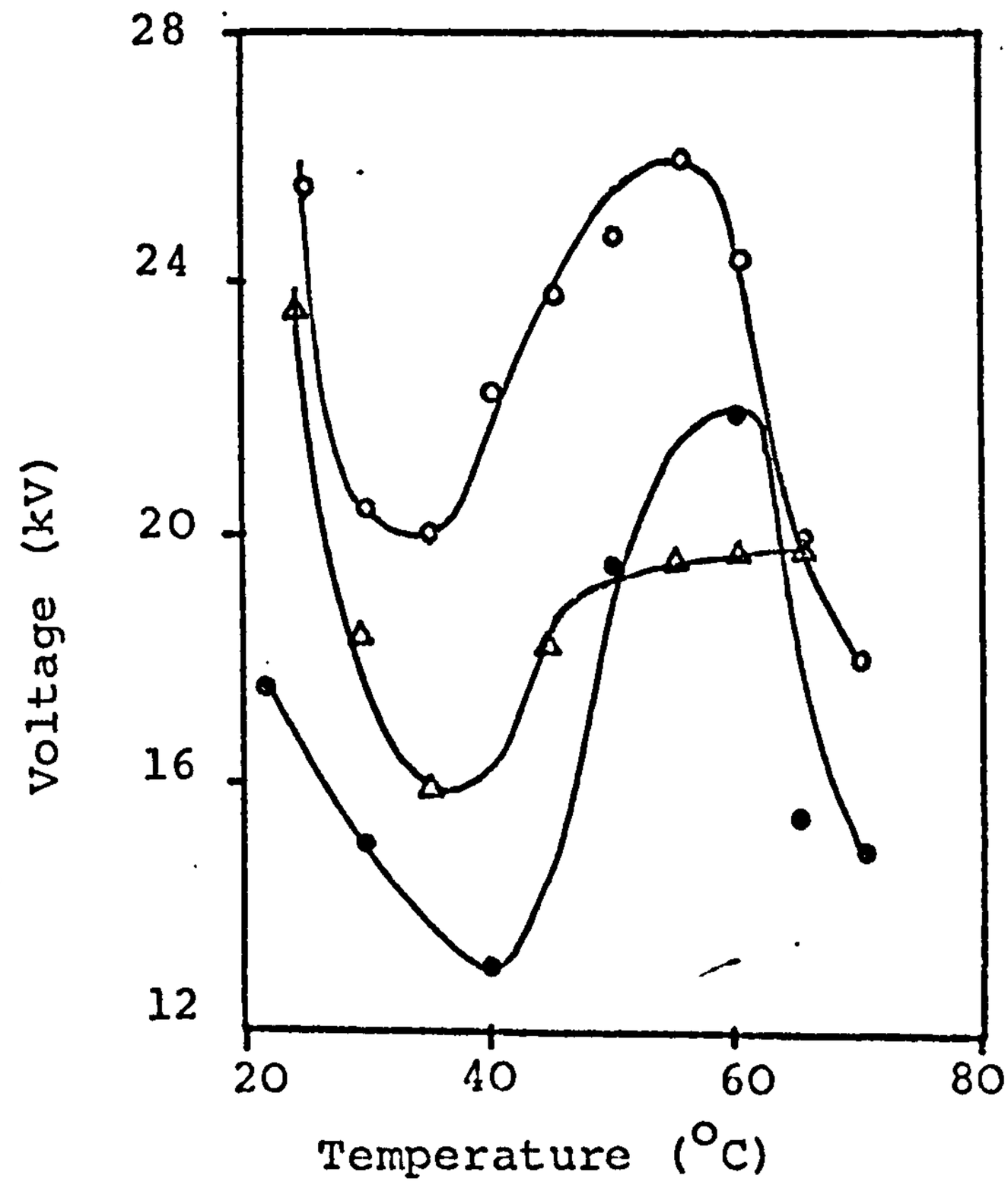

Fig. 2.3 Electroluminescence inception voltage for:
• cyclohexane, 4mm gap; o benzene, 5mm gap;
Δ n-hexane, 2mm gap, (Rashwan and Kao 1972)

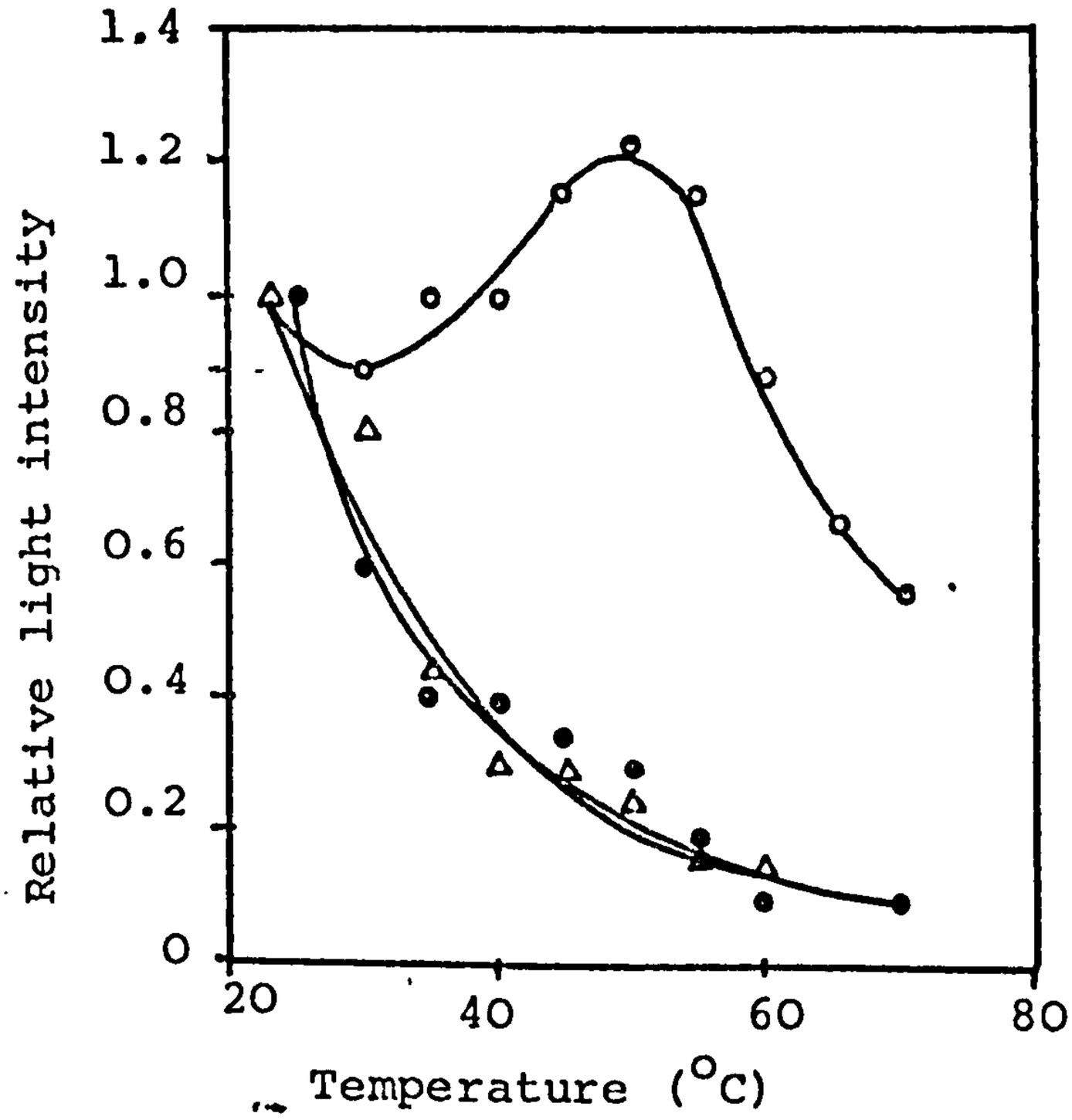

Fig. 2.4 Relative light intensity as a function of temperature for:
• cyclohexane, 4mm gap -25kV;
o benzene, 4mm gap, -40kV;
Δ n-hexane, 3mm gap, -25kV.
(Rashwan and Kao 1972)

shown by Kao and Rashwan[53]. A low speed (1s cm^{-1}), pen recorder trace was presented to show the relationship between the current and light pulses occurring at the point cathode of a highly stressed test gap. The light intensity was shown to be pressure dependent suggesting the presence of pre-breakdown cavities, possibly formed by electro-hydrodynamic motion at the cathode. In conflict with earlier interpretations, the presence of a transient cavity near the cathode could account for the generation of current bursts as electrons were accelerated in this region. The light bursts associated with the conduction behaviour were thought to result from the excitation of molecules by these electrons.

Jayasakera[54] observed that prior to complete gap failure, a partial breakdown occurred in the form of corona, for a negative point to plane geometry in degassed transformer oil. The partial breakdown appeared as luminous streamers, starting at the tip of the point and extending into the gap towards the plate electrode. No visible bubbles were formed as a result of these discharges but the appearance of a streamer was accompanied by a faint click, and an enhanced conduction current pulse activity. For gap spacings of 1.5 to 5cm, the corona inception occurred at approximately 75% of the breakdown voltage and was found to be pressure dependent. When the point was made positive no pre-breakdown discharges appeared and conduction current pulses were not detected. Krasucki[24] observed a faint blue glow at the point of

a highly stressed divergent test gap in an unspecified hydrocarbon oil. The diffuse glow did not produce perceptible decomposition of the liquid. As the applied voltage was increased, well defined sparks were formed that extended from the point into the gap and were accompanied by gas bubble formation. Shammas et al[55] studied a number of dielectric liquids under conditions of high local stress. The light emission studied was described as corona and photographs were taken of the luminous region for varying levels of applied voltage. Over a limited range, it was found that the radius of curvature, r, at the tip of the corona was proportional to the applied voltage V. Measurements of dV/dr were assumed to give values of the local electric field at the boundary of the corona, and at about 1 $MVcm^{-1}$ was considered to be equal to the breakdown strength of the liquid. For hexachlorodiphenyl, corona inception was found to decrease linearly with temperature between 20°C and 50°C, above which a constant value was approached, fig. 2.5. For a fixed applied voltage the corona radius was shown to increase with temperature between 50°C and 90°C, fig. 2.6. It was inferred that the main effect of temperature variation was on its control of viscosity. Coronas were photographed up to breakdown, when sudden propagation of a breakdown channel occurred, rather than a gradual extension of the region across the gap.

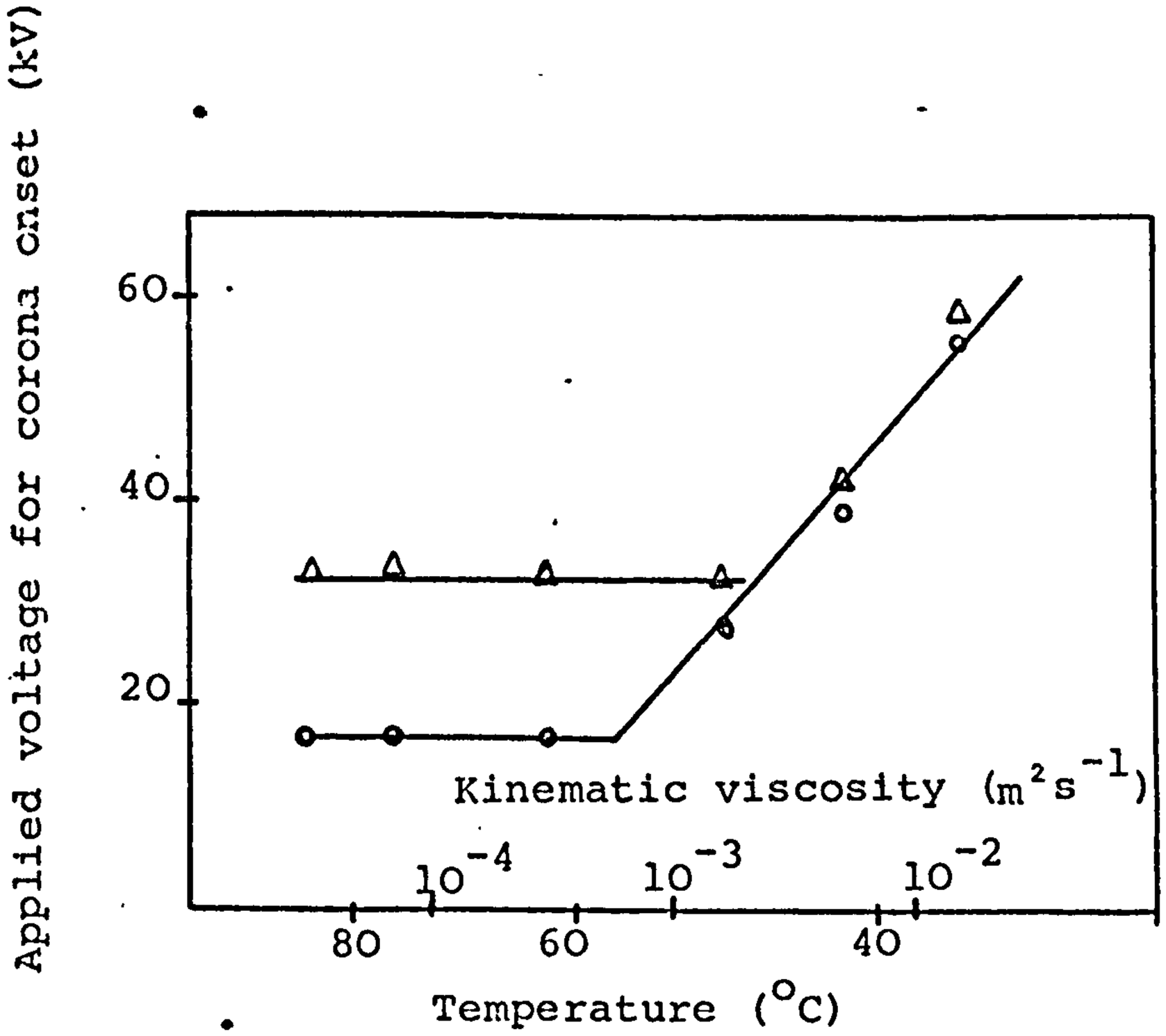

Fig. 2.5 Corona inception in hexachlorodiphenyl as a function of temperature and viscosity (Shammas et al 1974)

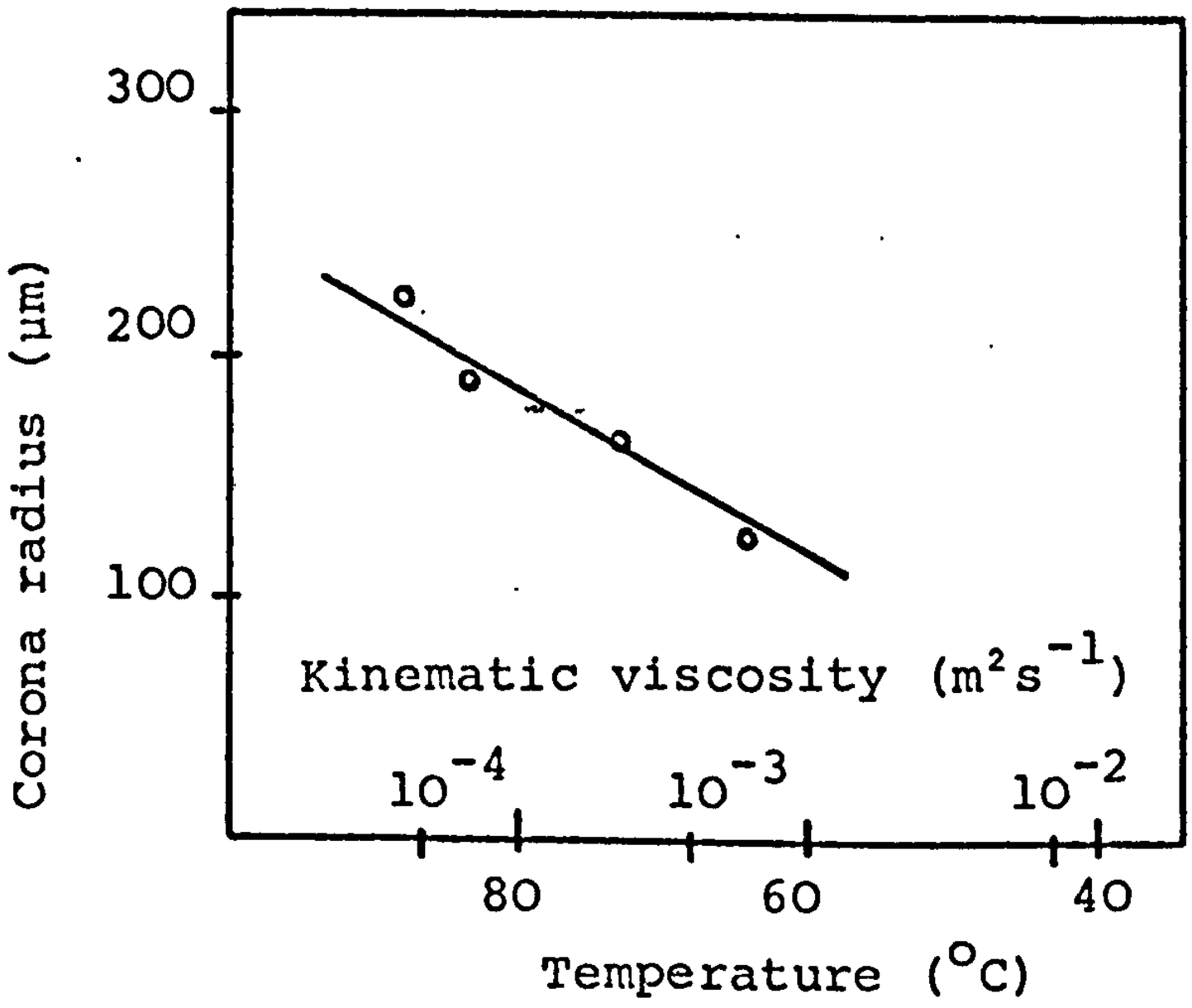

Fig. 2.6 Corona radius for a point cathode at 50kV in hexachlorodiphenyl as a function of temperature and viscosity (Shammas et al 1974)

2.4 CONDUCTION CURRENT MEASUREMENT

2.4.1 Studies of Integrated Conduction

Numerous conduction current studies have been made, often with conflicting interpretations as to the underlying mechanism. In 1937 Baker and Boltz[56] used platinum irridium electrodes in toluene and plotted conduction current characteristics for a number of gap settings. The conduction current was shown to obey a modified Schottky characteristic which led the authors to the conclusion that thermionic emission was responsible for the observed behaviour. The emission from a hot cathode into a vacuum is given by the Richardson equation,

$$j = AT^2 \exp(-e\phi/kT)$$

where j is the current density, A a constant and ϕ the work function. The absolute temperature is given by T, the change on an electron e, and Boltzman constant, k. If sufficient extracting field is applied to the cathode, the current becomes saturated except for the Schottky correction which introduces a dependence on the field E of the form,

$$j = AT^2 \exp(-e\phi/kT) \exp(e(eE)^{\frac{1}{2}}/kT)$$

$$= j_o \exp(e(eE)^{\frac{1}{2}}/kT)$$

The Schottky relationship was modified by Baker and Boltz to include a term to take into account the relative permittivity of the liquid, ε_r, giving,

$$j = j_o \exp(e(eE\varepsilon_r)^{\frac{1}{2}}/kT)$$

Le Page and Du Bridge[57] believed, however, that the agreement of the Baker and Boltz plot with the Schottky conduction regime was accidental. From tests made on nickel electrodes in toluene, log I vs $\sqrt{E}$ plots were made by Le Page and Du Bridge and shown to be linear, with over twice the slope predicted by invoking a simple Schottky relationship. The results were, however, shown to obey Richardson's equation for thermionic emission over a temperature range of -15°C to 70°C. The authors considered that neither relationship was sufficient to confirm or disprove the thermionic origin of conduction current. It was thought that a more fundamental conduction process was possible. Field emission could occur but from the experimental findings it proved difficult to clearly separate the mechanisms involved.

Dornite[58] plotted current vs voltage characteristics for gas free and dried samples of heptane and benzene, using both a uniform and a divergent electrode geometry. The slopes of the conduction characteristics proved to be greater than was predicted by thermionic emission theory alone. For a uniform electrode geometry, the conduction current was found not to be proportional to electrode area and was influenced by the surface finish of the electrodes and adsorbed gases, this supporting the viewpoint that emission originated from sharp points on the cathode surface. Cold cathode emission of electrons was suggested as a possible mechanism for electrical conduction in dielectric liquids.

The conductivity of highly purified heptane was measured by Plumley[59] for field strengths approaching 600kV cm^{-1} and a temperature range from -190°C to 20°C. In an attempt to minimise space charge effects and ionic recombination, tests were performed with a small electrode separation, down to 0.05mm. Electronic or collision processes were thought to be unlikely sources of high field conductivity, and the highly non-conducting dielectrics were categorised as extreme examples of weak electrolytes. The presence of an appreciable conductivity under the influence of a high electric stress was ascribed to the lowering of the C-H bond energy by the applied field and effecting ionic dissociation of the liquid. Repeated purification produced little change in the measured characteristics and so an impurity agency for conduction was discarded. An approximate calculation was presented showing that even if water were contained to 1/10 of the saturation value, then for a conduction current of 1μA, this content would be completely ionized out of solution after several minutes, so quenching the observed current. Experimentally, however, the current was only shown to fall to half its value after a two hour period.

Large plane electrodes with guard rings were immersed in purified and filtered n-hexane and used for an integrated conduction current study by Goodwin and Macfadyen[60]. The treated liquid exhibited a conductivity of approximately $10^{-18}\Omega^{-1}cm^{-1}$. When a voltage was applied, cold field emission of electrons from the cathode occurred,

obeying a Fowler Nordheim[61] relationship. The emission characteristic exhibited the low work function of an oxidised cathode, consistent with the findings of Llewellyn Jones and de la Perrelle[62] giving the Fowler-Nordheim equation

$$I = 38.5 \times 10^{12} \frac{\xi^{\frac{1}{2}}}{(\phi+\xi)\phi^{\frac{1}{2}}} E^2 S \exp(-6.8 \times 10^7 \phi^{3/2}/E)$$

where I is the number of electrons emitted per second from a surface of area S and an electric field E. ϕ is the work function and ξ the Fermi energy. Collision ionization of the emitted electrons was then believed to take place under the influence of the strong field. A plot of log current density vs gap spacing, for moderate stresses, up to 220kV cm^{-1} exhibited curves not too remote from the straight line form that Macfadyen attributed to the simple Townsend theory.

A sphere anode to plane cathode electrode system with a spacing of a few hundred microns in n-hexane was used by Green[63]. The observed conduction current proved not to obey field enhanced thermionic emission or customary cold field emission relationships. Surface layers on the cathode were believed to play a dominant role in the conduction behaviour. Heat treatment of the cathode was found to radically modify its emissivity, but the nature of the anode material and its treatment had little effect on the measured conduction current. A model was proposed in which emission was controlled by the collection of positive ions on the semi-insulating cathode

surface layer, so producing an intense local field across this layer that would aid electron emission. The magnitude of the local field generated by the ions would be related to a balance between the supply of ions from the liquid and their neutralisation by the electrons emitted from the cathode. The liquid purification treatment was varied but this had little controlling influence on the integrated conduction current. For certain electrode materials the measured conduction current at constant average stress exhibited an increase with gap spacing, indicating a possible impact ionization process. However, this characteristic was electrode dependent and occurred only for stresses approaching a breakdown value. This was followed by another conduction current study[64] using a coaxial test cell constructed from a brass cylindrical anode and rod cathode. A modification of the earlier view of electrical conduction was advanced, extending the dominant role of ion behaviour. For low applied voltages the movement of ions in the liquid was believed to be responsible for the observed conduction current. Accompanying an increase in applied voltage, the enhanced ionic current was thought to precipitate field emission, the emission current being dependent on the cathode material, adsorbed gas and surface layer thickness. The high field current density was believed to be governed by a modified form of Fowler-Nordheim relationship, consistent with electron emission into gases from oxidised electrodes possessing surface charge layers.

Electrical conductivity was measured by House[65]. A bi-spherical electrode geometry was used and the test liquid was filtered and purified n-hexane of spectroscopic grade. For a gap spacing of 25μm, conduction current was measured up to a breakdown stress of 1.5MVcm^{-1}. By observation of the conduction current pulse activity, and selecting a stress just above the inception threshold it was possible to condition out the current pulses and attain high values of electric strength. It was found that once a conditioning procedure had been followed, a test could be repeated using a reversed electrode polarity without the need to extend conditioning. Furthermore, with identical electrode materials, a reverse polarity test yielded curves similar to the initial conditioned characteristics up to 1.15MVcm^{-1}. For differing electrode materials, the conduction current was found to be cathode dependent. The results furnished the impression that conductivity was determined largely by the presence of adsorbed surface layers on the electrodes and, in turn, on the liquid purity; it was further suggested that the two factors may be intimately related. Later this study was extended[66] to include a consideration of both field aided thermionic emission, as described by Schottky equations, and cold field emission described by a modified Fowler-Nordheim relationship. For a low work function of 1.2eV and stresses below 2MVcm^{-1}, it was shown that the Schottky relationship was predominant. The experimental findings generally supported this dependence. However, an

increase in conduction current with gap spacing was observed for constant stress plots above $1MVcm^{-1}$, this suggesting the presence of an ionization process similar to the classical Townsend multiplication theory for gases. The use of a bi-spherical electrode geometry, however, prohibited an estimation of the multiplication coefficient. The conditioning process was believed to procure the removal of minute gas bubbles from the high stress region of the liquid and the central portion of the electrode surface, or perhaps the stripping of lightly adsorbed surface layers from the electrodes.

Cullingford et al[67] used an electrode coating technique in order to separate anode and cathode effects on electrical conduction in filtered transformer oil. Integrated conduction characteristics were presented, showing the effects of both anode and cathode coatings of a thermoplastic layer less than 1mm thick. The presence of a cathode coating severely restricted the conduction current and an anode coating also presented a current limitation, although to a lesser extent. A conduction mechanism was presented stressing the important part played by the anode. When a voltage was applied to uncoated electrodes, space charges of both polarities formed in the oil; the positive ions drifting towards the cathode and the negative ions to the anode. In addition to the negative ions already present in the bulk of the liquid, the electrons emitted from the cathode could readily form negative molecular ions by attachment.

The stability of the negative space charge, and hence its intensity at the anode, would be dependent on the oxygen content of the liquid and the nature of the anode surface. For air saturated transformer oil, and in the presence of an insulating film on the anode surface, a large anode space charge field may be formed, giving rise to an ionization process within the vicinity of this electrode. This process could provide feedback of positive ions to the cathode so enhancing the localised field. At the cathode, two opposing processes may occur. The presence of an insulating film could produce a decrease in electron emission, whilst the establishment of a positive space charge may lead to a considerable enhancement of the local field, yielding an increased emission. The two processes may be inter-related, as the degree of field enhancement would depend on the number of positive ions available and on the blocking nature of the cathode surface.

Evidence of space charge formation was furnished by Zaky and House[68]. A direct electric stress was applied to bi-spherical electrodes in n-hexane until a steady state condition was attained. When the stress was removed, a current flowed in the external circuit as a result of space charge diffusion from localised regions, back into the bulk of the liquid. A charge diffusion equation was presented and the curves plotted were shown to be in agreement with the experimental findings. A polarity reversal technique was also employed and large

currents were shown to flow immediately after stress reversal. A steady state was reached within five minutes whereupon the conduction current attained a magnitude similar to the pre-reversal value. Both an electrode material and a surface layer dependence was demonstrated: aluminium electrodes producing a higher discharge current than copper, and a stainless steel cathode allowing a greater current to flow when the surface was oxidized. A double peak existed in the discharge characteristic particularly for higher fields, which was explained by the presence of not only a positive charge near the cathode, but also a positive charge in the vicinity of the anode. It was then possible for the anode charge to be released to re-establish a potential gradient when the bulk of the charges moved into the gap towards the cathode.

Invoking mechanisms consistent with earlier findings[67,68], Zaky, Tropper and House[69] measured conduction current in extensively purified n-hexane, using a number of electrode materials and gap settings for a bi-spherical electrode geometry. Irrespective of the absolute values encountered, which were thought to be related to liquid purity, three regions for the conduction characteristic were observed. At low stresses, impurity based ionic conduction was apparent and the current increased linearly with voltage. Resulting from electrode surface layers, a saturation effect was seen to occur as the stress was increased and space charge formation limited the conduction current. At higher stresses, the potential drop

across the cathode surface layer was thought to be sufficient to enable field emission, from favourable sites, to become the dominant conduction mechanism.

2.4.2 Conduction Measurements for Step Voltage Application

Whereas many breakdown measurements have been made under pulse conditions, conduction current measurements have generally been taken for direct voltage application. However, Macfadyen and Helliwell[70] used a test cell incorporated in a Schering bridge circuit and a balanced pulse transformer, to eliminate the predominant capacitor charging current and the interference of spurious pulses. Conduction current in n-hexane was measured for a voltage pulse of 5μs; gold plated parallel electrodes were used and the measured conduction current increased with stress, ranging from 5μA at 100kVcm^{-1} to 80μA at 400kVcm^{-1}. The test cell had been connected to a direct voltage: this was then removed and the subsequent pulse conduction current was found to be reduced to half the previous value. Changing the test liquid had little effect but conduction was found to be strongly dependent on electrode surface finish. This provided the authors with an indication that electron emission from the cathode was responsible for the observed current rather than conduction by ionic impurities. A conditioning process that formed wax on the electrode surfaces was also evident.

Watson and Sharbaugh[71,72,73] measured the accumulated charge on a capacitor in series with a parallel plate test cell in order to deduce the conduction current

passed by a hexane sample for pulse voltage application. The conduction current was found to be independent of voltage duration between 1μs and 10ms, but for a pulse duratien extending to minutes and so approaching a direct voltage situation, the current decreased by two orders of magnitude. A series of constant stress tests was performed for selected gap spacings between 62.5μm and 250μm, with a 10ms voltage pulse duration. For stresses in the range 800kVcm^{-1} to 1.2MVcm^{-1} it was evident that the current was independent of electrode spacing.

In excess of 1.2MVcm^{-1} there was some evidence for an electron multiplication process. Placing interpretations on these results, the authors suggested that the multiplication process was relatively unimportant and that electron emission occurred, perhaps as described by Fowler-Nordheim or Schottky characteristics. It was believed that aspherities presented favourable emission sites on the cathode surface and local current densities of 1Acm^{-2} were possible. The average energy input to the liquid at breakdown stress was calculated to be 10^{4}Wcm^{-3},[74], and at the tips of aspherities it was estimated to be as high as 10^{7}Wcm^{-3}. An energy input of this magnitude could lead to local vapourisation of the liquid within a few microseconds. In support of the thermal bubble formation model, comparative breakdown tests were performed on n-hexane for both the liquid and vapour phase[75]. For the same density the high pressure vapour exhibited a superior breakdown strength compared with the liquid phase. As the critical

density was approached, however, the breakdown values were seen to converge. It was believed that low density gas bubbles could form in the liquid and initiate breakdown. In the high pressure vapour phase, low density regions could not readily be formed, so a high breakdown strength would be expected.

A charge storage technique was used by Chadband and Calderwood[76] to measure conduction current resulting from step voltage application. The current flowing through the test cell caused a charge to be accumulated on a series capacitor and the voltage on this capacitor was then measured using a vibron electrometer. From the slope of the charge vs time characteristic, instantaneous values of conduction current could be deduced. A negative going step voltage was applied to the point of a divergent electrode system immersed in n-hexane. A 1μA conduction current pulse occurred 2μs after the application of a 9kV step function. The current pulse decayed to half its maximum value after 30μs, but the tail continued for several milliseconds. The measured conduction was believed to be composed of two components, a field emission current arising from negative charge injection from the cathode, superimposed on a smaller ohmic conduction. A conditioning effect was observed and tests were extended[77] to show the decay of the charge passed in relation to the number of pulses to which the cell had been subjected. As changing the test liquid had no effect, electrode conditioning, particularly of the point cathode, was believed to be

responsible for the observed behaviour. Conditioning was found to be both voltage and time dependent for a negative point polarity, but there was little evidence for this effect when the point was made positive.

2.4.3 Observations of Conduction Current Pulse Activity

Conduction current for direct stress has been treated as a form of noise superimposed on a steady direct current[78]. The analysis of conduction current pulse behaviour provides additional information to that gathered from integrated measurements. As a pressure dependence was observed by Nosseir and Megahed[79,80] they considered that conduction current pulses were related to bubble formation. A model was advanced in which electrons could be emitted from the cathode with sufficient energy to cause chemical dissociation within the liquid. The hydrogen liberated could then form a bubble, which if not absorbed, would allow electrons to accelerate and gain sufficient energy to cause further dissociation at the bubble interface. Breakdown could then ensue if the bubble expanded to sufficient dimensions. Similar viewpoints were advanced by these and other workers[81-83], when temperature and gas content effects on conduction current pulse behaviour were examined. Furthermore, the exponential pulse height distribution of the current fluctuations and the gap dependence[82-84], was indicative of a multiplication process occurring in the liquid. Megahed and Nosseir[85] found that autocorrelation plots for conduction current pulses took the form of either

exponential functions at low stresses, or cosine-exponential functions for high stress and gas content. These results were later confirmed[86] and related to liquid motion by effecting the transition of the auto-correlation function whenliquid was forced through the test gap. The relationship between pulse autocorrelation function and liquid motion was thought to be related to earlier, integrated conduction characteristics as plotted by Ostroumov[87]. When conduction current was plotted against applied voltage on logarithmic axes, abrupt changes of slope were apparent. The slope of a particular portion of the characteristic was thought to be related to the hydrodynamical state of the liquid within the stressed test gap.

2.4.4 Studies Using a Divergent Electrode Geometry

A variation of the electrode geometry is a technique that has been used to separate polarity effects associated with electrical conduction measurements, with particular reference to the emission process. A marked rectification effect was observed by Secker and Aplin[88]. A simple test cell, with a razor blade mounted perpendicularly to a brass plate, was filled with n-hexane and conduction measurements taken. When the blade was made negative,a transition in the conduction characteristic was apparent. The onset of charge injection, at 4kV, provided a current over 100 times larger than that for the reverse, positive point,case. A barrier tunnelling mechanism at the metal to liquid interface was believed to be responsible

for the forward mode current enhancement of this field emission process. For a blade with a tip radius in excess of 100nm, the rectification effect was suppressed. The conduction current increased exponentially with voltage, for either polarity, and corona was thought to be responsible for the generation of charge carriers by local liquid ionization. The experiments were extended to include a point plane system[89] in addition to further blade to plate tests. The emission limited behaviour exhibited by the blade emitter was less apparent when this was replaced by an etched point electrode, but the rectification characteristics were similar. The differences were attributed to the effects of liquid motion on space charge formation around the emission zone. For forward mode conduction no emitter degradation was apparent, but when the voltage was reversed both electrode erosion and wax deposition occurred.

Coelho[90] used a wire to cylinder coaxial test cell to investigate the conduction behaviour of several n-alkanes. The highly purified liquids exhibited resistivities in excess of $10^{18}\,\Omega m$. The measured current was seen to increase markedly with contamination and some doubt was cast on earlier work regarding liquid cleanliness and the possibility of field dissociation of impurities being predominant in the conduction process. It was believed that dissociation of charge carriers occurred near the wire and a conduction model was advanced in which molecular ionization by an internal Schottky effect

occurred, followed by electron trapping by other molecules. A rectifying effect was apparent but this decreased with increase in temperature, perhaps due to a thermal influence on the homocharge formation around the wire.

Using a bladeto plate electrode system in transformer oil, Pugh[91] measured integrated conduction current. In contrast with other findings[88,89], a rectification effect was observed only at intermediate stresses. Electron injection and corona formation were discounted in favour of ionization of a common impurity, perhaps the moisture content of the oil sample.

A considerable body of work exists for conduction in liquified gases and, in some instances, marked similarities in the characteristics of these and liquid hydrocarbons and insulating oils are apparent. A rectifying effect was observed by Coelho[92] using both liquid nitrogen and helium. Field injection and corona provided similar current magnitudes, but the mechanism difference when corona was seen was highlighted by the appearance of light emission. Conduction current pulses appeared as a superposition on a d.c. level and the magnitude of the pulses remained roughly invariant but increased in frequency with applied voltage. When injection occurred without corona, or pulses, it was thought that this was due to the presence of particles near the point electrode.

A space charge limited behaviour was observed by Halpern and Gomer[93] for liquified gases at high stresses. A marked rectifying effect was apparent and the onset of

high level forward mode injection was accompanied by bubble formation, which led to considerable electrode damage, possibily by positive ion sputtering. Coelho and Sibillot[94] used both point to plane electrodes and a coaxial wire to cylinder geometry to measure conduction currents in liquid nitrogen. An abrupt conduction onset occurred, above which the current varied with the square of the applied voltage, indicating a space charge limited behaviour. Localised bubble formation and light emission accompanied the advent of conduction and sustained emission caused considerable electrode damage as was observed by Aplin and Secker[89] when using n-hexane.

2.5 THE EFFECTS OF TEMPERATURE

Many attempts have been made to relate electrical properties of insulating liquids to temperature, particularly by measurement of breakdown strength and conduction current. Early work both by Clark[95,96] and Hoover and Hixson[97] involved measurement of breakdown strength with variation of temperature. On increasing the temperature of a mineral oil sample, Clark showed that this was accompanied by an increase in breakdown strength, attaining a maximum at approximately 100°C. Beyond this temperature the electric strength decreased andit was suggested that this was due to oil vapourisation lowering the quantity of dissolved air by reducing its partial pressure. Breakdown measurements made by Hoover and Hixson showed a similar characteristic for transformer oil, peaking at approximately 80°C. On increasing the pressure

over the oil the peak shifted to 100°C. The results of these tests were explained by consideration of both gas and impurities in the oil. Breakdown was thought to be initiated by ionization of gas present in the oil in suspended form. Such a stable gas suspension could exist at a solid/liquid interface presented by particulate contamination. Later, results were presented both by Salvage[98] and Lewis[99] using n-hexane, showing characteristics that were in direct conflict with the earlier findings.

Crowe, Bragg and Sharburgh[100] measured the electric strength of a range of normal alkanes displaying an increase with liquid density. Choosing n-heptane and measuring breakdown strength with temperature variation, this too was interpreted as a density dependence. These results were supported by the findings of Goodwin and Macfadyen[60] and further discussed by Macfadyen[3]. A breakdown theory was advanced suggesting a mechanism that was initiated by conduction dependent on collision ionization, giving rise to field intensification at the cathode, and instability leading to breakdown. Eldine and Tropper[101] performed breakdown tests on de-gassed and dried transformer oil. Again the results were in conflict with the findings of Clark, and Hoover and Hixson, the difference being attributed to liquid preparation. A breakdown mechanism involving bubble formation at the cathode was advanced. Lewis[102,103] measured the breakdown strength of several n-alkanes over a temperature

range of -50°C to 70°C. By plotting the electric strength divided by the molecular volume against temperature, transitions were evident and were coincident with changes in liquid, rather than molecular structure. Bubble formation and elongation was believed to be responsible for breakdown when Kao and Higham[104] found that the electric strength of n-alkanes decreased with increase in temperature and impulse duration.

Hexachlorodiphenyl was used by Krasucki[24] and more recently by Shammas, et al[55]. Krasucki showed that the electric strength fell from 5MVcm^{-1} at room temperature, when the liquid viscosity was 2MP, to 1.5MVcm^{-1} at 77°C when the viscosity was 2P. The time to breakdown vs temperature at constant stress was also measured and appeared to be highly viscosity sensitive. Vapourisation was suggested as the initiating event leading to bubble formation, elongation and breakdown.

Kao and Calderwood[105] monitored conduction current in both n-hexane and carbon-tetrachloride and found that the current increased with temperature, as did the relative fluidity. Using a wire to cylinder coaxial electrode geometry, Kao[106] measured both breakdown strength and conduction current as a function of temperature. For both wire polarities, the breakdown strength was found to decrease with temperature, whereas the conduction current exhibited a marginal increase with temperature when the wire was negative, a distinct minimum was apparent for the opposite polarity at 45°C. It was thought that the

formation of space charge could modify the effective wire radius. When the wire was made negative, negative space charge could readily be formed by attachment of field emitted electrons to neutral liquid molecules. On top of this layer, positive space charge formation could be produced by separation of dissociated impurity ions. With an increase in temperature, the space charge complex could diffuse away from the wire. For a positive wire situation, negative space charge would be formed as a result of dissociated impurity ions. On increasing the temperature this could lead to a decrease in the number of charge carriers through thermal diffusion and recombination, and increase the mobility of charge carriers. Whilst performing measurements of light emission and the effects of pressure variation, Rashwan and Kao[51] found that transformer oil, hexane and benzene all exhibited a minimum in breakdown strength between 30°C and 40°C, when temperature dependence was investigated. It was maintained that breakdown occurred as a result of local heating and the formation of low density zones rather than bubble formation.

2.6 PRESSURE EFFECTS

Pressure is a variable that has been used to verify the influence of a gaseous phase on the behaviour of both pre-breakdown and breakdown events in liquids. Using alternating and impulse voltages, Hoover and Hixson[97] performed breakdown tests on insulating oils. A pronounced dependence over a gauge pressure range of

0 to 1.4MNm^{-2} was apparent when the electric strength increased threefold with pressure. When the oil was partially de-gassed the pressure effect was far less pronounced, indicating that gas in suspended form was responsible for breakdown initiation.

Watson and Higham[107] made a study of hydrostatic pressure and its effect on the electrical breakdown of transformer oil. Alternating voltage was applied to bi-spherical electrodes in filtered transformer oil, and the electric strength was found to double over a gauge pressure range of 0 to 3.4MNm^{-2}. Impulse voltage tests were performed on both untreated and de-gassed oil samples. The superior insulating property of the de-gassed oil was evident when a gauge pressure dependence existed only between 0 and 0.7MNm^{-2}, above which it remained at a high constant value, but for untreated oil the dependent range extended to 2MNm^{-2}. For a voltage duration in excess of microseconds, cavitation was thought to be the underlying mechanism leading to electrical breakdown. Eldine and Tropper[101] observed a similar electric strength variation with pressure for both uniform and non-uniform electrode configurations. The authors observed bubble formation at the surface of the electrodes when suitable conditions of voltage and pressure were provided, but breakdown was also thought to be related to electrode condition, impurity and gas content.

Darveniza[36,40] applied tension and pressure of approximately 1 atmosphere to an electrically stressed

sample of transformer oil and observed no light emission variation. This led to the conclusion that the light detected was a result of excitation of fluorescent impurities in the liquid phase and not due to microcavity discharges in the oil. Priaroggia and Palandri[157] measured the breakdown strength of an insulating oil over a similar pressure range. The investigation indicated that the electric strength was independent of pressure provided an equilibrium was reached between the gas dissolved in the oil and the free gas remaining above its surface. Also taking measurements over a limited pressure range, Gosling[39] recorded a small increase in breakdown strength with pressure for transformer oil, using both a uniform and a divergent electrode geometry.

A comprehensive study involving the measurement of breakdown voltage for a range of dielectric liquids was made by Kao and Higham[104]. Supporting earlier findings electric strength was found to increase monotonically through the gauge pressure range 0 to $2MNm^{-2}$ for all nine liquids investigated. Later, Kao and Calderwood[105], measured integrated conduction current in both carbon tetrachloride and transformer oil for field strengths up to 90% of the expected breakdown value, but found no pressure dependence, although current bursts were suppressed at higher levels. The pressure range extended from atmospheric to $1MNm^{-2}$ and despite independence of conduction current, the breakdown strength increased with pressure, in support of previous results and the dominance of a

cavitation initiated breakdown mechanism.

Mirza et al[50] applied hydrostatic pressure to a stressed point to plane gap immersed in n-hexane. For a negative point polarity, the conduction current, the onset of light emission and spraying were found to be independent of pressure up to 6.9MNm^{-2}. A pressure dependence was, however, observed when the point was made positive; but it was found impossible to predict a relationship for light emission, spray onset, or breakdown strength, on the basis of a simple Paschen breakdown within a bubble. Rashwan and Kao[51-53] used a multiple point electrode system and incorporated an image intensifier and photomultiplier to investigate the influence of pressure on electroluminescence. Hexane, benzene and transformer oil were subjected to hydrostatic pressure up to 1.4MNm^{-2} and light intensity measurements were taken. For hexane and transformer oil the application of pressure tended to slightly reduce the integrated light emission and almost completely suppressed the random light bursts, but for benzene the light intensity increased with pressure. Light emission was found to be far more pronounced from the less pure technical grade, than that used for spectroscopic analysis indicating the enhancement produced by contamination. For a given sample of benzene, despite an increase in light emission, the electric strength increased with pressure, as was found for hexane and transformer oil.

2.7 THE INFLUENCE OF GAS CONTENT

Electrical properties of insulating liquids have been shown to be influenced by the presence of gas contained in solution. Both cavitation and electronic viewpoints have been advanced to explain the observed behaviour. Clark[95] measured the breakdown strength of mineral oil and found a gas pressure dependence, exhibiting a minimum electric strength at approximately 25 torr. This, he explained, was due to dissolved gases in the oil. Later Clark[96] attempted to explain pressure and temperature effects on breakdown strength by relating these parameters to air solubility in the oil. Assuming a linear relationship between pressure and air solubility, he produced an empirical logarithmic relationship between pressure and oil breakdown strength. The later findings of Khambanonda[108] provided further support for Clark's viewpoint.

Race[35], whilst performing breakdown measurements on cable oil and dowtherm, varied the partial pressure of air in solution from less than 0.01 micron to one atmosphere and found that this had no effect on the electric strength. This result, in conflict with the findings of Clark was thought to be related to electrode and sample preparation. Particulate contamination was removed by fractional distillation and the oil samples were contained in a totally enclosed test cell.

Eldine and Tropper[101] used a divergent electrode geometry in filtered and dried transformer oil,

and measured the direct voltage breakdown strength in relation to its gas content. For a negative point polarity, a pressure dependence was observed irrespective of the gas content, although the de-gassed oil exhibited a generally superior electric strength. When the point was made positive no pressure dependence was observed until air was admitted into solution, when the behaviour became similar to that of the negative point situation.

Sletten[109] used a bi-spherical electrode geometry in dried and filtered n-hexane and performed breakdown and conduction measurements with variation of gas content. The breakdown strength of the de-gassed hexane sample remained unchanged when nitrogen was admitted into solution. However, with a high air or oxygen content, the breakdown strength, for otherwise similar conditions, was found to increase by over 50%. Both a reduction and a stabilisation of conduction current was observed when oxygen was dissolved in the test sample, the electro-negative property of oxygen, allowing low energy electron trapping and negative ion formation, was thought to be responsible for the observed effects[110].

Lewis[103] took the influence of oxygen into account when considering the dependence of electric strength on the molecular structure of liquid hydro-carbons. An attachment process could operate in the presence of oxygen, in which dissociation occurred, with the formation of an atomic ion having a peak energy lying between vibrational and ionizational values for

hydrocarbons. This would remove free electrons with energies above the vibrational peak normally capable of contributing to an α, electron multiplication,process in the liquid. The conversion of electrons into low mobility negative ions would also reduce conduction current fluctuations, as was found by Sletten[109].

Tropper[111] reported on research with specific reference to the effects of gas content on both electrical conduction and breakdown in liquids. Pre-breakdown bubble formation was observed for de-gassed oil at a reduced hydrostatic pressure, especially for oil with particulate contamination. The addition of a small amount of air to a de-gassed oil sample produced an increase in the breakdown strength. The trapping of electrons by oxygen molecules was favoured for this improvement. Further increase in air content, however, produced a degradation of electrical strength, as less energy would be required for the detachment of gas molecules and subsequent aggregation into microbubbles.

Huq and Tropper[78] investigated conduction current pulse activity in both transformer oil and liquid paraffin. When a small amount of oxygen was added to de-gassed transformer oil, a considerable reduction in pulse activity was evident, although similar tests using nitrogen had no effect. The addition of oxygen to liquid paraffin produced an increase in breakdown strength without changing the conduction characteristics. For increasing gas content both oils exhibited a considerable increase in current

fluctuations, suggesting gas evolution as a result of the high electric field. On changing from a uniform to a divergent electrode geometry, little variation was seen for a positive point polarity. For the reverse polarity, however, the electron trapping and quenching effect of oxygen was masked by the presence of gas evolution.

2.8 OBSERVATIONS OF GAS EVOLUTION

Gas evolution from insulating oils under steady state conditions has been evident for many years. Oil filled cables of the late 1920's showed signs of premature failure in which ionization appeared to play a major role. In an attempt to illucidate the problem, Schopfle and Connell[112] irradiated oil samples with electrons in a gassing cell. Hydrogen was evolved which was accompanied by the formation of a wax deposit. Schopfle and Fellows[113] irradiated a number of liquid hydrocarbons and analysed the composition and volume of the gaseous products. Saturated hydrocarbons were found to form much larger volumes of gas, principally hydrogen, than unsaturated hydrocarbons, whereas aromatic compounds formed practically no gaseous products. Straight chained paraffins and in particular n-hexane, produced large volumes of gas, over 90% of which was hydrogen, with a few percent of methane. A comprehensive review of the extensive range of early work performed using gassing cells was presented by Thomas Egloff and Morrell[114] describing both discharge chemistry and experimental techniques.

Basseches and Barnes[115] investigated gassing in relation to pressure and applied electric stress, using a simple aluminium and glass test cell with mineral oil. It was found that gassing was dependent on both pressure and electric stress rather than time. Assuming that an electron could enter a gas nucleus or bubble at the electrode surface, an electron could gain sufficient energy from the electric field to produce C-H bond sission at the boundary, so providing a continual gas evolution process. From the experimental results, the application of hydrostatic pressure caused a reduction in bubble size, and as would be expected from a reduction of the cavity mean free path, gas evolution was suppressed.

Blodgett and Bartlett[116] tested a number of insulating oils in a gassing apparatus. Samples of naphthalene and paraffin oils were bombarded with ions and electrons under hydrogen and the rate of gas evolution or absorbtion was measured. Oils without aromatic compounds were found to be gas evolving, whereas those with a high aromatic content, approaching 20%, absorbed similar amounts of hydrogen. For an aromatic content of 7% a zero gassing coefficient was obtained, but the authors stressed that the optimum value was dependent upon specific conditions of pressure, temperature, the type of test cell and its operation.

Reynolds and Black[117] reviewed a range of more recent work using gassing cells and examined the problem of gas evolution. It was claimed that gassing cell tests

and service conditions were closely related and that the gassing mechanism was explicable in terms of the chemistry of excited species and classical kinetics.

CHAPTER THREE

EXPERIMENTAL APPARATUS AND TECHNIQUE

3.1 INTRODUCTION

The investigation was primarily concerned with optical probe techniques applied to dielectric liquids in the pre-breakdown regime. Methods of both time resolved Schlieren photography, for refractive index gradient detection, and scattered light photography, showing interfacial regions of differing phase, were employed. Conduction current and acoustic vibrations, which were associated with pre-breakdown light emission, were monitored. For integrated parameter measurement, the spectral nature of the light emitted prior to gap failure was also investigated.

Details concerning the relevant experimental apparatus are presented in four sections. However, most of the electrical apparatus is described in section 3.3, with details concerning modifications for subsequent experiments following in the relevant sections.

3.2 GENERAL APPARATUS

3.2.1 Liquid Preparation

Samples of n-hexane, liquid paraffin and Gulf B30 transformer oil were each subjected to tests involving electrical and optical investigations. A simple glass-

ware system was constructed to provide a link with either one of the two test cells used, and to facilitate filtration and storage of the chosen test liquid (plate 3.1). Referring to figure 3.1, the degassing flask was connected to an Edwards ES35 single stage rotary vacuum pump, via a liquid nitrogen cold trap. The ultimate vacuum attained by the liquid free system was approximately 10^{-2}Torr, when measured using an Edwards model B5 Pirani gauge in conjunction with a G6A head.

The test sample was admitted under gravity to the degassing flask via stopcock 1. Whilst under vacuum the liquid passed through a no. 4 and no. 5 filter to the reservoir and then to the test cell. The liquid could be returned to the degassing flask and the filtration process repeated as many times as was necessary to remove particulate contamination. Suspended particles present in the system originated not only from the liquid as supplied, but also from the apparatus itself, particularly after electrode refurbishment and the ensuing test cell reassembly.

On opening stopcock 2, air or nitrogen could be admitted when required, after undergoing filtration and passing over silica gel to suppress the ingress of moisture to the system. With the liquid confined to the degassing flask, stopcock 3 was partially opened and the gas allowed to bubble slowly through the liquid to aid absorption into solution. Gas was then left over the liquid for several hours before filling the test cell

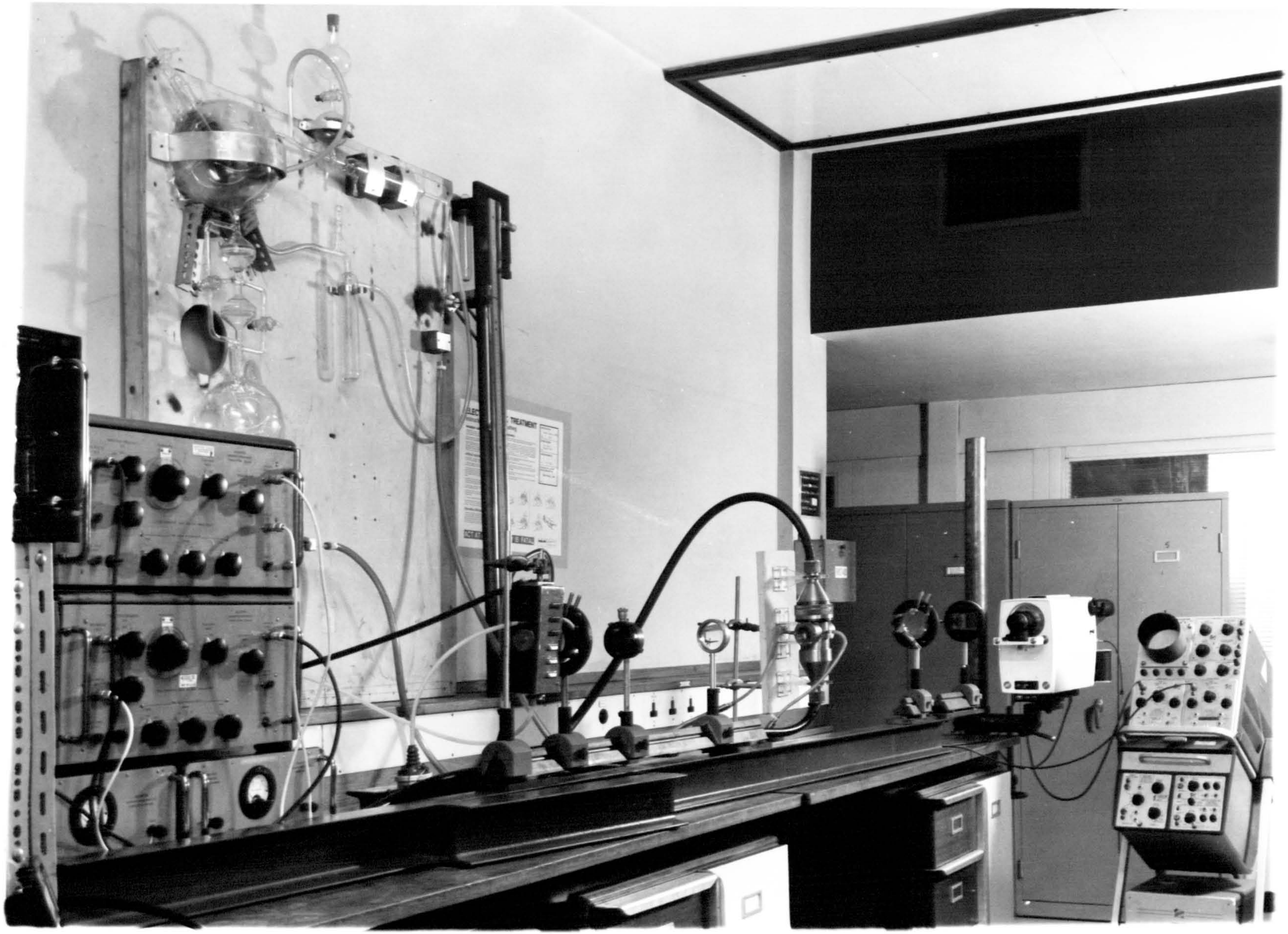

Plate 3.1 Schlieren arrangement of apparatus

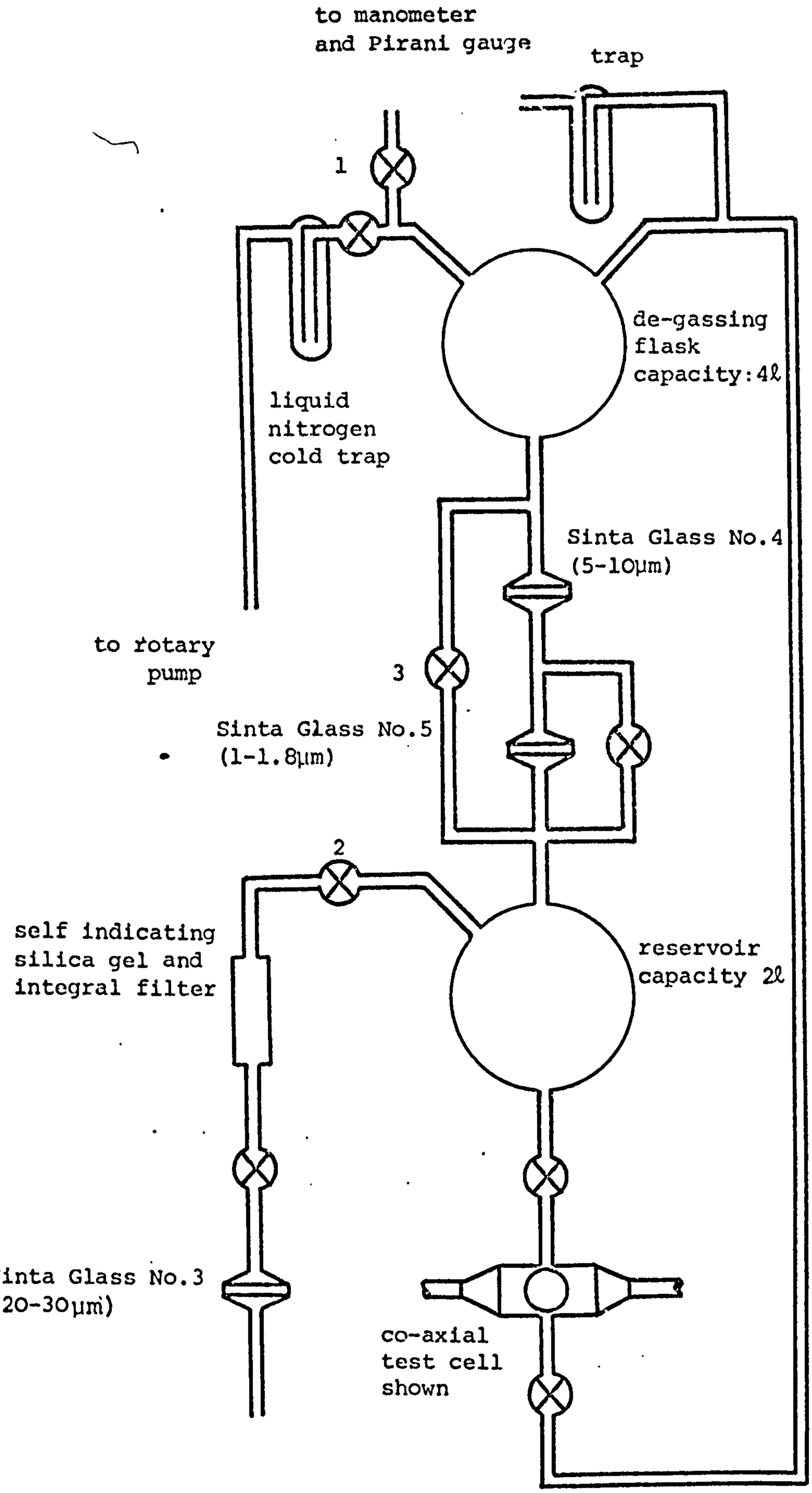

Fig. 3.1 Liquid preparation

under gravity, and the commencement of electrical tests.

3.2.2 Test Cells

In order to fulfil the requirements of the experiments undertaken, two test cells were employed. For the time resolved Schlieren study, the use of a coaxial test cell allowed sub-microsecond rise time step function voltages to be applied to the test gap. For scattered light photography, single shot flashlight illumination provided a less stringent demand on the voltage rise time duration. A four windowed test cell was chosen to allow the use of orthogonal viewing and illuminating planes. The coaxial cell appears in plate 3.1 and the component parts are shown by the reduced scale engineering drawing, fig. 3.2. The main body was constructed from brass, as were the centre electrode support shanks. A point to hemisphere electrode configuration was chosen for most of the tests incorporating this cell. Machined from stainless steel, the hemispherical electrode was formed with a 2BA thread for mounting onto the brass shank. The tungsten point electrode was braised onto a stainless steel disc, with a threaded portion similar to that of the hemisphere. The taper section of the test cell body offered a 50Ω constant impedance transformation from an RG218U coaxial cable to the test gap. Insulation leading from the cable, through the taper section and up to full body diameter, was provided by a solid PTFE dielectric spacer which was machined to suit the dual conical section,

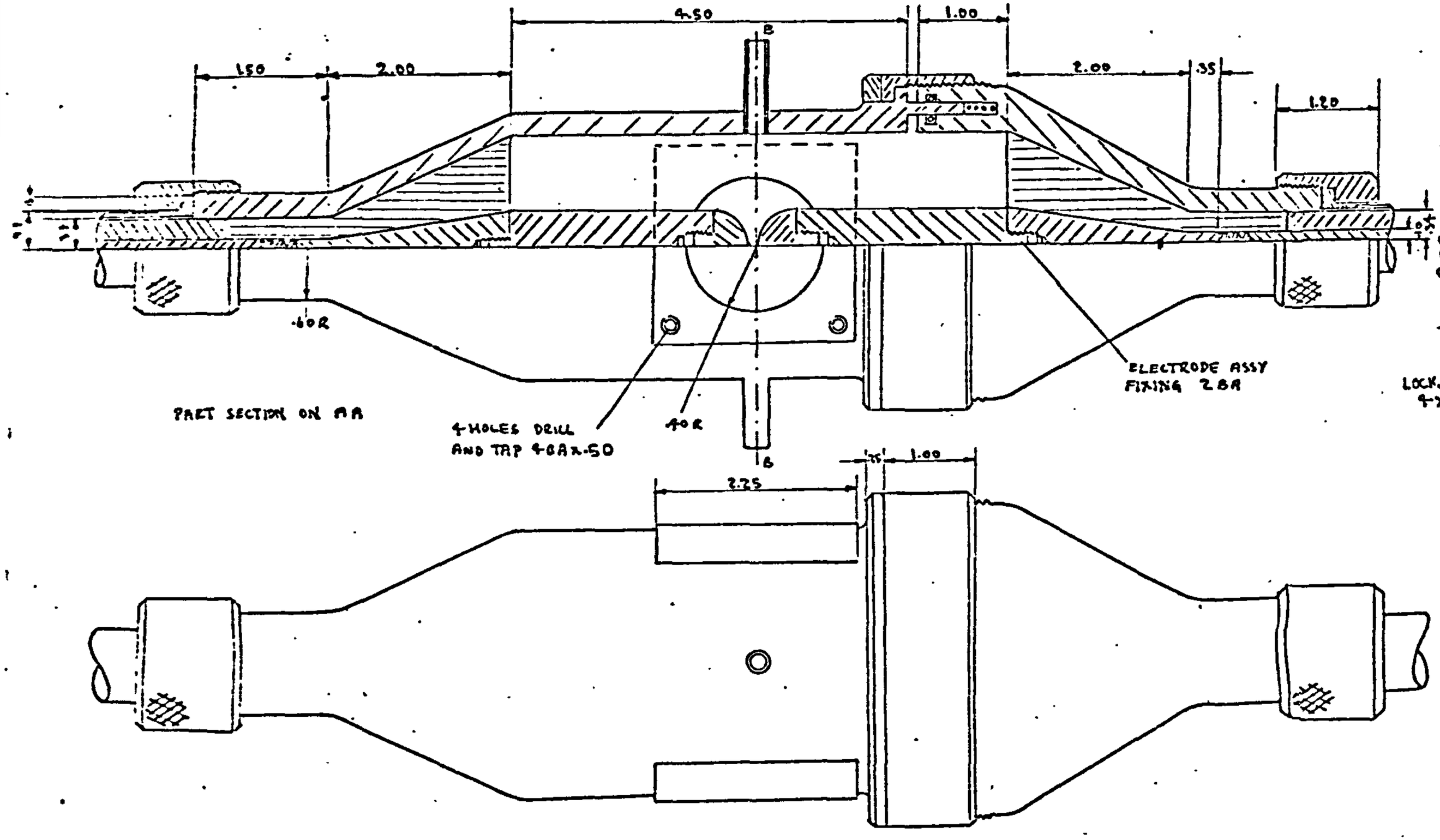

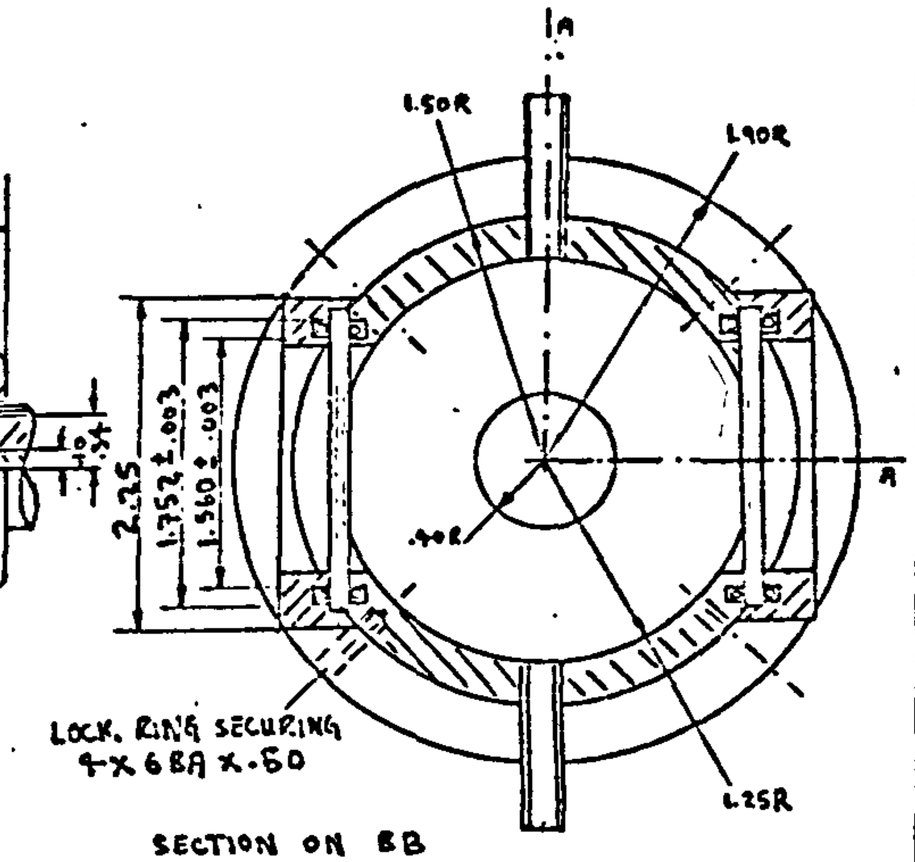

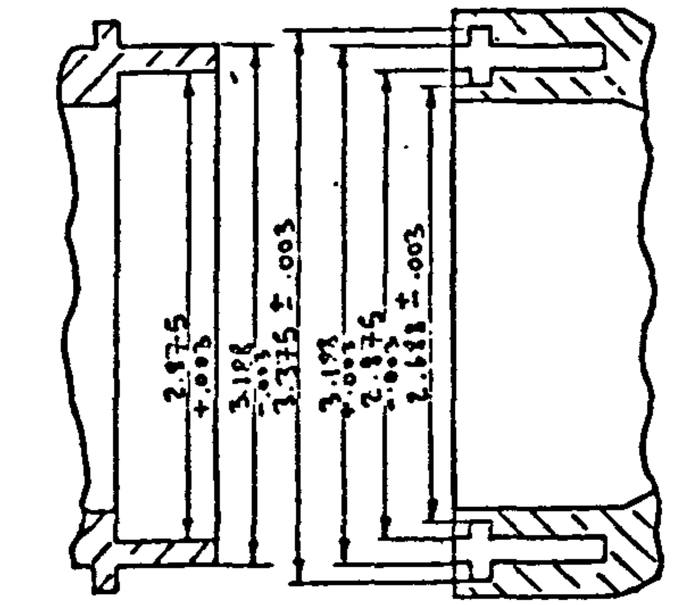

SCRAP VIEW SHOWING MAIN BODY SEALING

QMC ELECTRICAL ENGINEERING DEPT.		
COAXIAL TEST CELL		
SCALE: 0.4 : 1	ALL DIM. IN INCHES	
TOLERANCE UNLESS OTHERWISE STATED FOR RADIAL DIM AND UNDER 1.00 ± 0.005 REMAINDER ± 0.010		
PART DESCRIPTION	MAT'L	No OFF
OPTICAL FLAT 1.96 ϕ x 0.16	PYREX	2
OPTICAL FLAT SEALING 'O' RING DOWTY 200 139 5375	RUBBER	4
INNER BODY 'O' RING DOWTY 200 167 5375	RUBBER	1
OUTER BODY 'O' RING DOWTY 200 692 5375	RUBBER	1
ELECTRODE INSULATOR	PTFE	2
ELECTRODE TIPS	STAINLESS STEEL	2
ALL REMAINING BODY PARTS	BRASS	—
DRAWN BY: PENGOTH	DATE: 18.3.72	

Fig. 3.2 Co-axial test cell

and secured to the main body with spring steel circlips. The centre core of the cable was linked to the end of the electrode support shank by a spring connector, and the braiding secured by an outer threaded collar to complete the coaxial connection. Test gap adjustment could be made by effectively changing the length of the cell body. The two parts of the outer body were linked by an integral annular tongue and groove and sealed by two concentric neoprene 'O' rings. Fine control over the gap adjustment was made possible by a threaded collar on the outside of the main body which was clamped by a steel retaining ring. Two pyrex optical flats formed the viewing ports and were sealed into the test cell body using 'O' rings on both the inner and outer faces.

A four windowed test cell [118], although not offering a constant impedance transformation, was found suitable for long term step function measurements, with time durations extending to milliseconds, and direct voltage application. With reference to fig. 3.3, the test cell body material was again brass, but the electrode shanks were fabricated from stainless steel, and the two sections of the main body were separated by a cast epoxy resin insulator. Test gap adjustment was made possible by a metric micrometer head incorporated into the upper body portion. The four viewing ports allowed orthogonal illumination and viewing planes to be chosen for scattered light photography of the immediate test gap region.

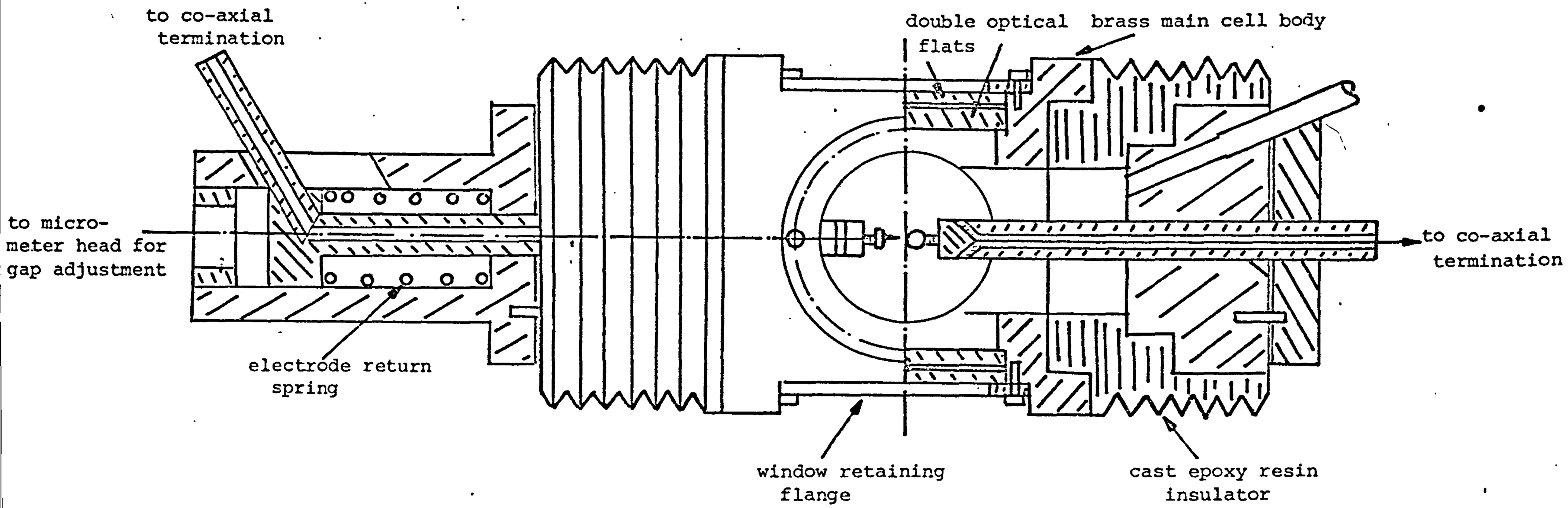

Fig. 3.3 Four window test cell (after Spitzer, 1967)

Window blanking plates were available for both test cells and these could be attached to enable photomultiplier studies to be undertaken under normal room lighting conditions. Barium titanate transducers were suspended in both cells to facilitate either ultrasonic generation, or the detection of stress induced acoustical disturbances in the test liquid.

Although both test cells were provided with calibrated scales for gap adjustment, it was found expedient to use a travelling microscope (Precision Tool and Instrument Co. Ltd., Vernier microscope type 13), with a 10μm vernier scale, for the setting operation. This method was adopted to avoid the electrode damage likely to result at zero gap adjustment when using only the graduated test cell scales.

3.2.3 Electrode Preparation

Stainless steel spherical and hemispherical electrodes were used and the surfaces prepared by firstly hand polishing with fine carborundum, grade 600, then using a rotating buffing wheel and finishing with metal polish. The electrodes were immediately placed in n-hexane until test cell assembly.

In order to produce a highly non-uniform electrode geometry, the point electrode was fabricated from a tungsten wire which was electrolytically etched to present a tip radius of typically 1μm. A saturated aqueous solution of sodium hydroxide provided the electrolyte. A 22 gauge

nickel sheet was used to generate the outer cylindrical field and the tungsten wire acted as the second, inner electrode. The electrodes were connected to a 15V, 50Hz supply, having a 'Variac' voltage control facility. After immersion into the electrolyte, the etched tungsten wire was slowly withdrawn from the solution as the supply voltage was reduced. Removal of caustic contamination from the etched tungsten wire was accomplished by firstly rinsing in de-ionized water and then in n-hexane.

Because the experiments were centred essentially on the pre-breakdown regime,the stainless steel electrodes suffered little damage and so did not require frequent refurbishing treatment. In contrast, however, the small tip radius presented by the tungsten point necessitated frequent etching and replacement of this electrode. It was found that the tip radius increased with stressing time even without breakdown ensuing.

3.3 SCHLIEREN PHOTOGRAPHY

3.3.1 General

The general arrangement of the time resolved Schlieren system is shown by fig. 3.4. This arrangement provided a means of applying a direct pre-stress, and a step function of a pre-determined magnitude and polarity, to a non-uniform test gap. An optical technique was incorporated that was sensitive to changes of refractive index within the highly stressed region. A high speed image converter camera was used to record the rapidly

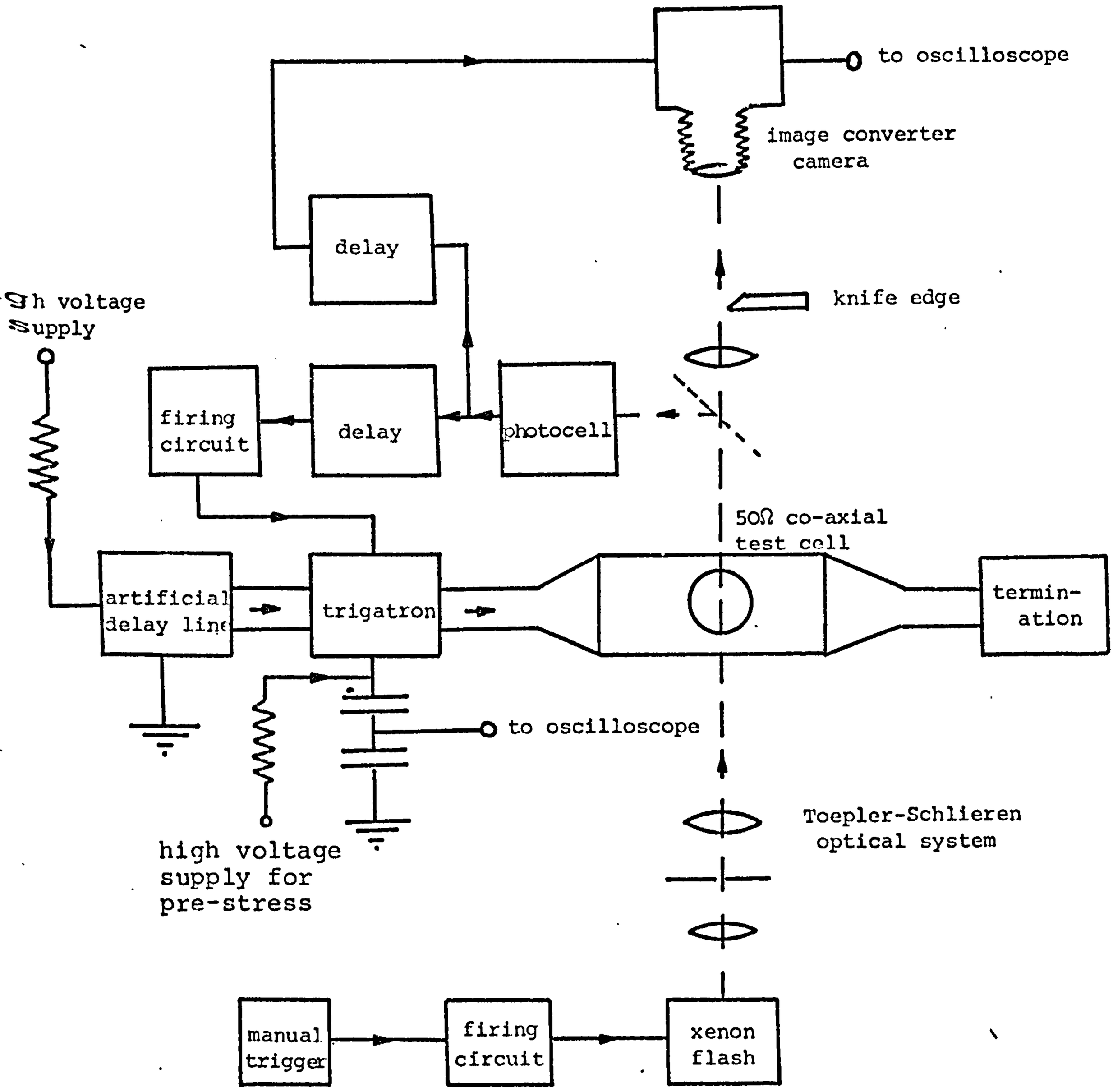

Fig. 3.4 Block diagram of the time resolved Schlieren system

changing disturbance.

3.3.2 The Optical System

The optical technique employed was based on a Toepler-Schlieren system of lenses, as shown by fig. 3.5. The light source used for photography was a Mazda FA5 xenon flash tube, which could be replaced by a Philips 100W strip element projector lamp for focussing and optical alignment. A compound plano-convex condenser lens was used to gather and focus the light onto the rectangular source slit (Hilger F1386). This provided a new source of controllable dimensions, offering a height range of 1mm to 2cm, and a slit width of 1μm to 1mm. Light emerging from the slit was brought to a parallel beam by the collimator lens, and this light passed through the working section in which was sited the test cell. The outgoing parallel beam was re-focussed by the Schlieren head, to form a rectangular image of thelight source in the plane of the knife edge. An adjustment was made to the knife edge position so as to obstruct approximately one half of the source image from the camera. The illumination emerging from the knife edge, $I = K'ha$ where h is the height of the source image, a is the portion of the width w not cut off by the knife edge and K' is a constant. With reference to fig. 3.6, if an optical disturbance produces an angular deflection $\delta\theta$ then the image is displaced by $\delta w = f_2\delta\theta$ and the change in illumination $\delta I = K'hf_2\delta\theta$. The contrast $C = \frac{\delta I}{I} = \frac{f_2\delta\theta}{a}$ and the contrast sensitivity $C_s = \frac{dC}{d\theta} = \frac{f_2}{a}$

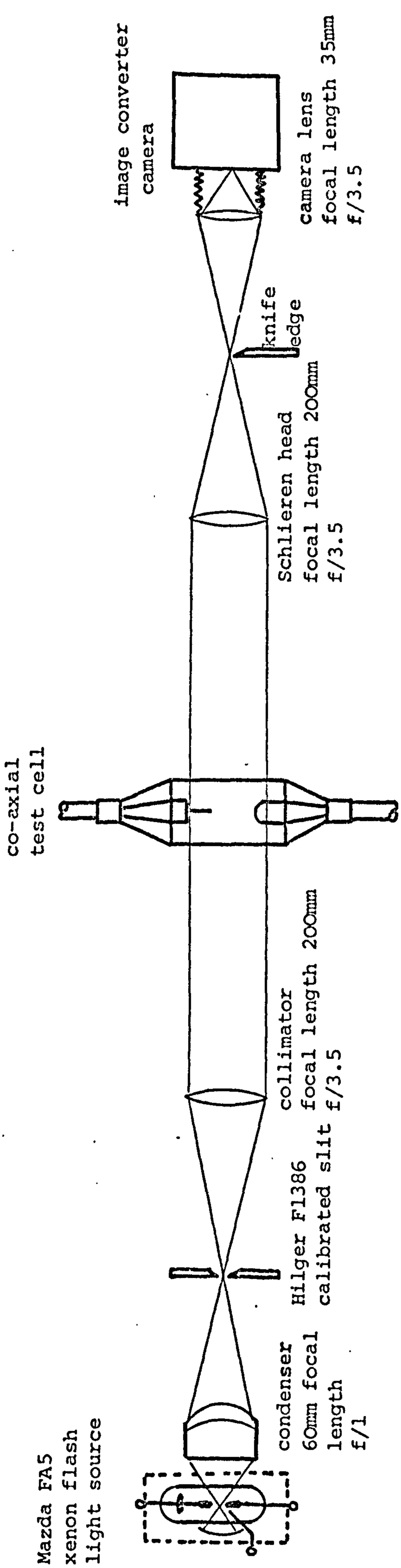

Schlieren optical arrangement

Fig. 3.5

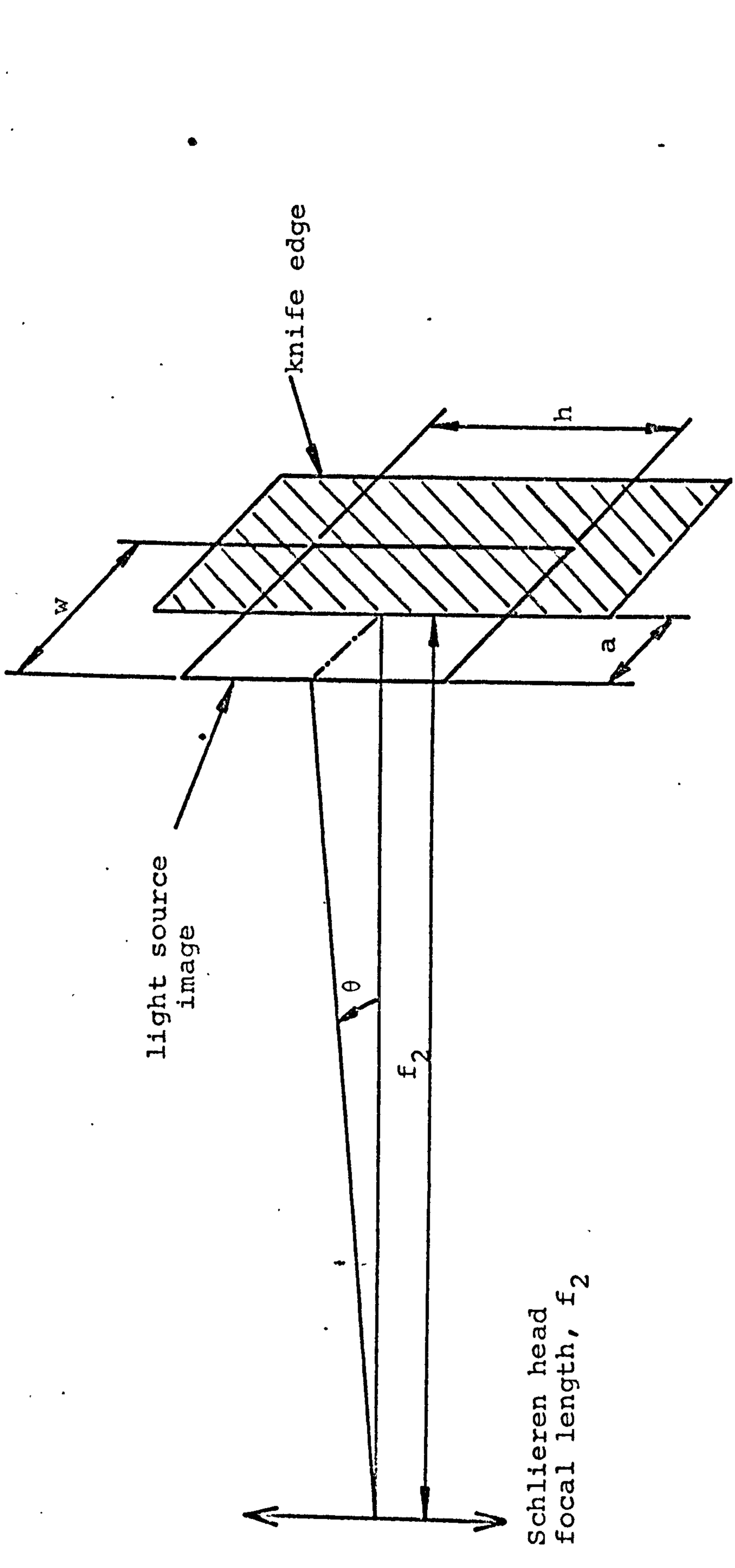

Fig. 3.6 Light source image formation at the knife edge in the Schlieren system

If half the image is cut off, a = ½w.

The range from fully off to fully on the knife edge is $w = f_2\delta\bar{\theta}$ or the range of angular deflection, $\delta\bar{\theta} = \frac{w}{f_2}$.

The lenses for the collimator and Schlieren head were both of twin element plano-convex construction and had standard surface coatings of magnesium fluoride to aid transmission and reduce flare by reduction of surface reflection. In the absence of a disturbance in the working section, the lenses and optical flats were seen to be free from internal Schlieren effects up to the normally used system sensitivity. The lenses and associated optical attachments were mounted with the aid of saddles onto a triangular section optical bench. For additional dimensional stability and to minimise the effects of mechanical vibration, the optical bench was firmly mounted onto an 8 x 10cm 'I' section rolled steel joist.

The Schlieren technique used provided a means of qualitatively identifying a refractive index gradient within the working section. An inhomogeneity generated in the test gap produced a deflection of the parallel beam and so changed the position of the re-focussed source images in the knife edge plane. Either a partial cancellation or reinforcement of the final image occurred, depending upon whether the source image was deflected onto or away from the opaque area presented by the knife edge.

3.3.3 Electrical Equipment

Commercially available power supplies and pulse delay generators were employed in the electrical arrangement but the trigatron, test cell and ancillary triggering circuits were constructed to meet the requirements of the small scale coaxial system. Design details of the component parts forming the electrical circuitry are shown by figs. 3.7 to 3.10. Referring to fig. 3.7, a Brandenburg MR50 was used to charge a pair of Wego HV50BB low inductance capacitors in a simple π reactive circuit. This network was then discharged into a 22mm diameter Suhner RG218U 50Ω radio frequency cable, connected to the coaxial test cell. A trigatron [119] was used as the high voltage switch linking the coaxial cable and the reactive circuit. The trigatron was constructed from two nickel plated hemispheres in a screened tube. The device was triggered by the application of a 20kV pulse to a tungsten wire spark gap, centrally positioned in the cathode hemisphere. A capacitor was discharged into a Lucas SA12 ignition coil to provide the high voltage trigger pulse. The switching operation was accomplished by using a thyristor, the gate of which was driven by a low impedance pulse transformer in an attempt to protect the circuit from triggering by spurious pulse activity. Interconnection between the ignition coil and the trigatron was made via a pair of isolating capacitors and the trigger spark gap was shunted by a resistor to inhibit self triggering of the main gap. The capacitors allowed the operating pulse

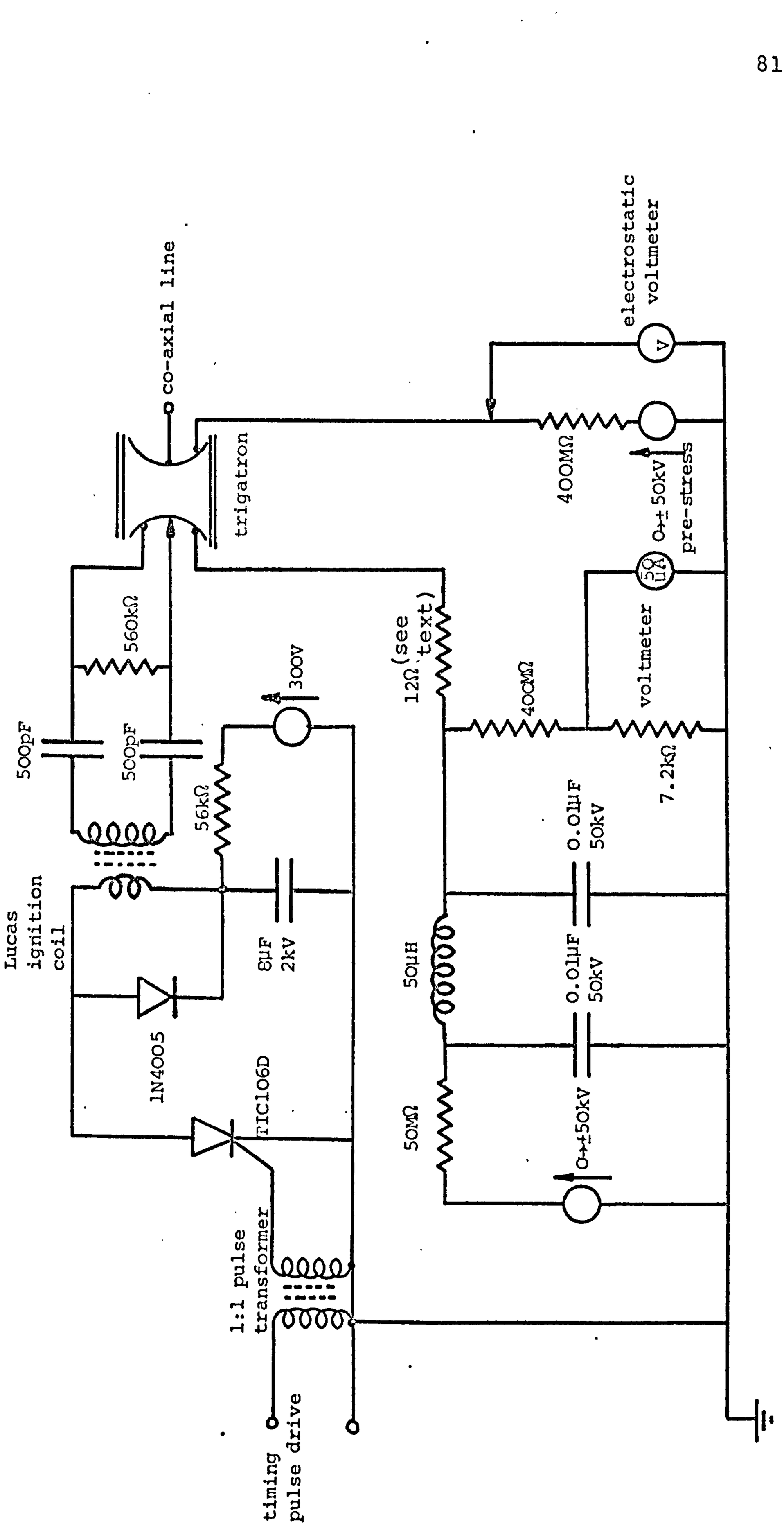

Fig. 3.7 High voltage pulse forming and triggering circuit

to be applied to the trigger spark gap but were of sufficient withstand voltage to protect the transformer and solid state devices from damage due to the presence of the main charging voltage, and its discharge transient. The presence of a charging voltage on the capacitors was monitored using a microammeter (Taylor 500 No. 704787) and a resistance divider. The voltmeter was initially calibrated at a reduced voltage. On comparison with a Pye Scalamp electrostatic voltmeter (No.11310) an indication difference of less than 3% was apparent up to 20kV.

The step function on the coaxial line was measured using a calibrated capacitor divider, fig. 3.8(a), connected to a Tektronix Model 551 oscilloscope. A capacitor divider was chosen, not only for its impulse performance, but also to allow a direct pre-stress to be applied during step voltage trials. By using a coaxial cable to form the high voltage input capacitor, it was possible to reduce the step voltage by the desired ratio with a minimal amount of ringing. Calibration of both the divider ratio and the step function response was accomplished by using a Venner TSA628 pulse generator connected to the trigatron end of the line and simultaneously monitoring the input and output signals. Resistor R_1 and capacitors C_1 and C_2 were adjusted in value to provide a divide ratio of 500:1 and enable the rise time to be reduced to 20ns without overshoot. Using the calibrated divider for measurement under working conditions

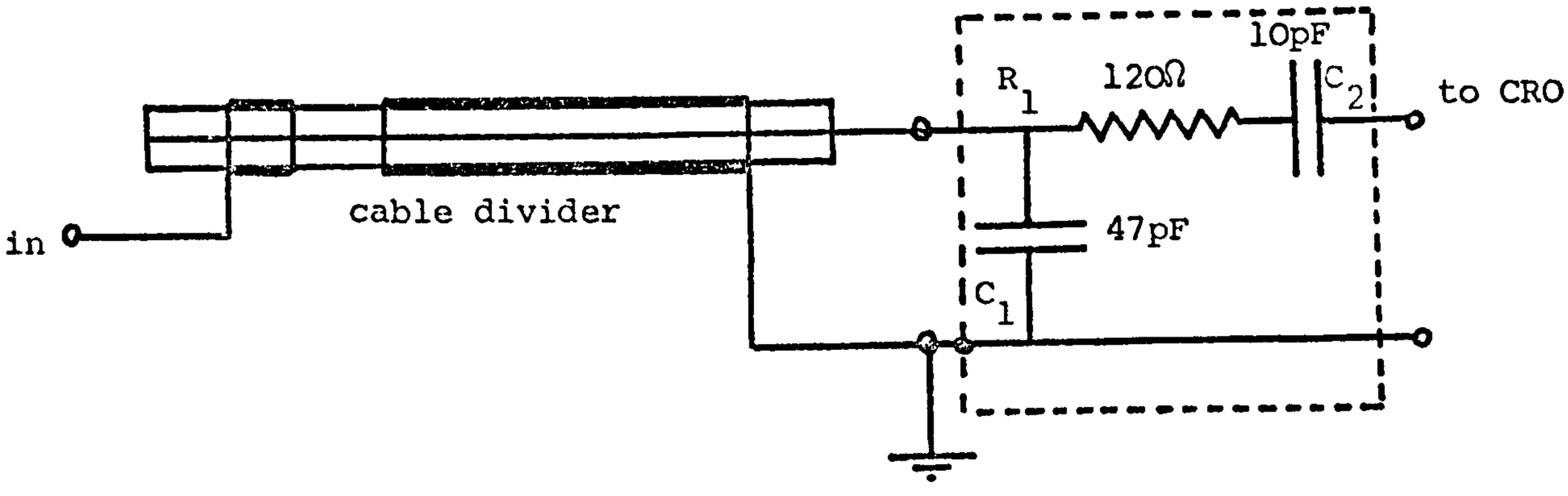

(a) 10ns/50μs time constant for short duration measurements

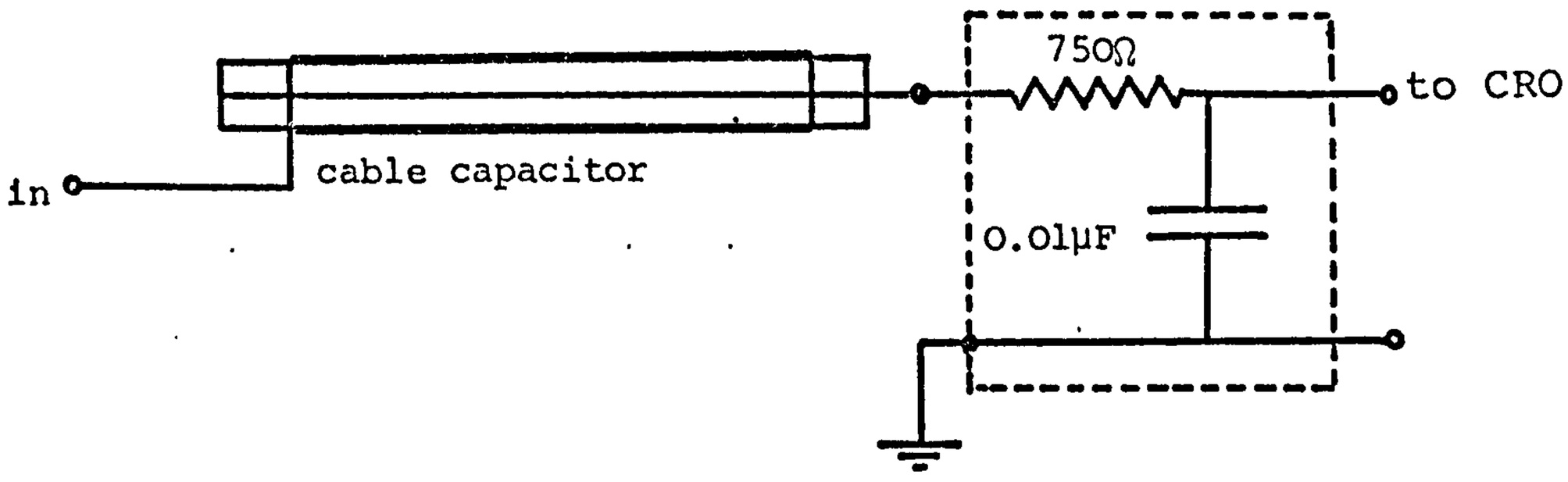

(b) 200ns/10ms time constant for long duration measurements

Fig. 3.8 500:1 dividers for step voltage monitoring

the value of the damping resistor, in series with the trigatron and the end of the coaxial cable, was adjusted to provide the best overall step function response. Upon selecting a resistance of 12Ω optimum suppression of ringing and overshoot occurred and the risetime was approximately 200ns. The high voltage discharge circuit and the trigatron were housed in a screened cage. Coaxial connections were made through the case, and were limited to the direct voltage supplies, the triggering lead and the main high voltage output. This arrangement was adopted in an attempt to suppressimpulse radiation likely to interfere with the overall timing operation.

Direct voltage could be applied to the test gap from a Brandenburg MR50RV via a 500MΩ series resistance, to provide the instrument with impulse isolation. The large series resistance also allowed the step voltage from the 50Ω line to be applied to the test gap without the necessity for the removal of the pre-stress and the large impedance ratio prohibited voltage superimposition at the test cell terminals. A pre-determined level of direct pre-stress was applied prior to selected test sequences and the voltage was measured using a Pye scalamp electrostatic voltmeter prior to step voltage application.

3.3.4 The Flashlight Source

Flashlight illumination for the Schlieren optical system was provided by a Mazda FA5 xenon discharge tube.

Details of the power supply, triggering and waveshaping circuits are shown in Fig.3.9. The firing operation was initiated by closing the microswitch, which produced a positive going impulse at the unijunction emitter. The low output impedance offered by the unijunction lower base to the gate of the thyristor provided a short rise-time pulse and a rapid turn on, within 1μs, for the thyristor. Current then circulated in the loop containing the primary circuit of the transformer, the charged capacitor and the conducting thyristor. A 20kV pulse generated in the secondary of the transformer was then applied to the flash tube anode loop and, via a spark gap, to the trigger electrode. A Wego type 1245, 125μF capacitor was then discharged via a mechanically robust coil, of small inductance, into the flash tube. Using this arrangement it was possible to attain the maximum specified discharge energy of 150J for the light source, with an illumination period extending to 50μs.

3.3.5 Ultrasonic Generation

Whilst Schlieren photography was available, the effects of ultrasonic irradiation on the observed pre-breakdown disturbance was also investigated. Both continuous and synchronous impulse tests were performed. In an attempt to minimise acoustic coupling losses, the barium titanate transducer was suspended in the test liquid inside the cell close to the outer body wall. When the transducer was excited at its resonant frequency

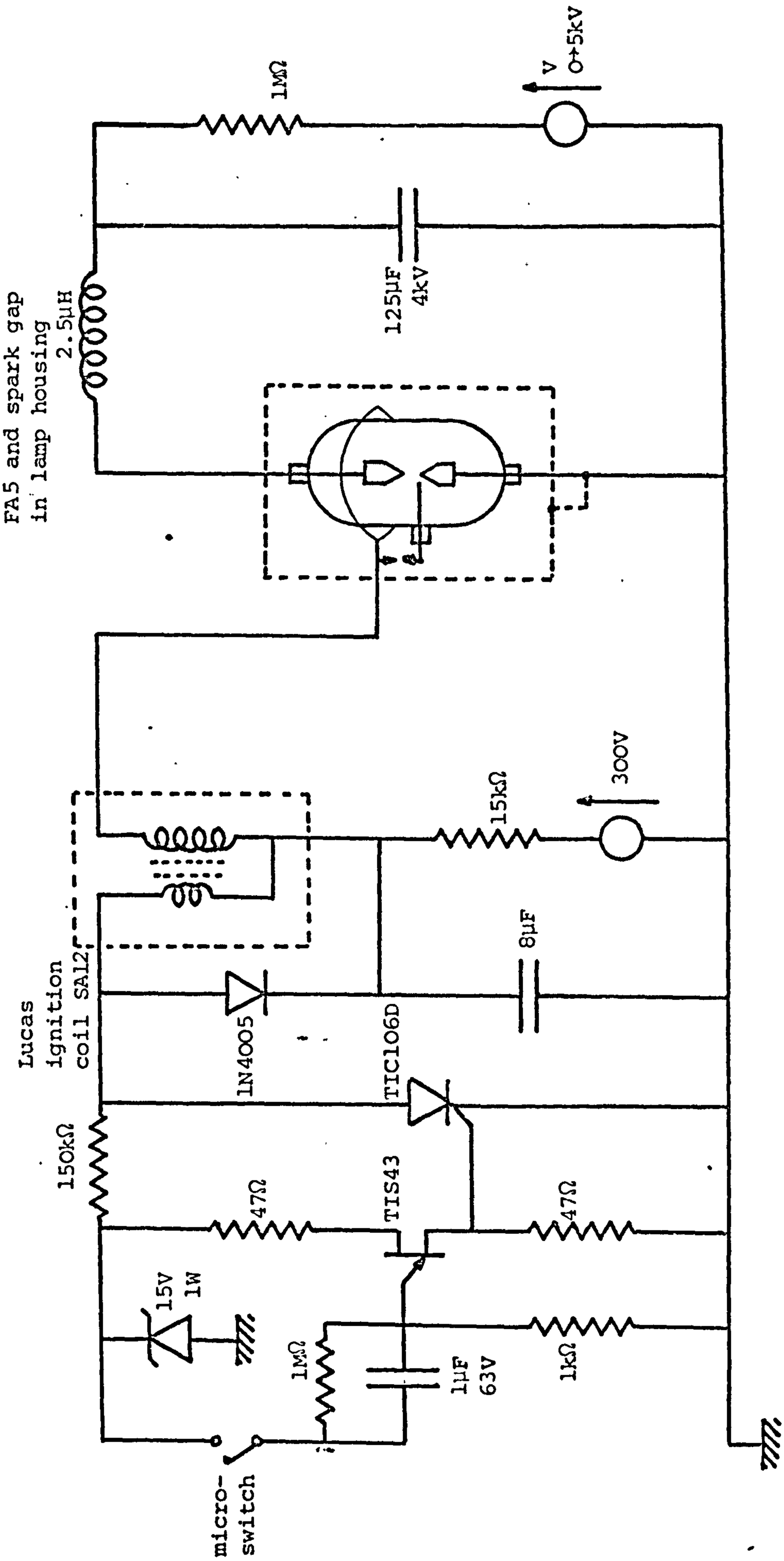

Fig. 3.9 Flashlight timing circuit

of 834kHz it was possible to provide sufficient power to produce cavitation in the test liquid within a range of approximately one centimetre from the transducer. A Marconi TF144H signal generator was used to drive a three valve ultrasonic power amplifier [156] capable of delivering up to 50 watts to the load. As an alternative to the standing wave pattern produced by continuous excitation, a travelling wave could be generated by applying an electrical impulse to the transducer. Fig. 3.10a shows the unijunction and thyristor switching circuit used to drive the transducer. With this arrangement it was possible to provide an impulse of up to 600V without damage to the transducer. The storage capacitor was first charged from the high voltage supply. On receiving an emitter impulse, the unijunction produced a signal sufficient to switch the gate of the thyristor. When thyristor conduction occurred, this produced a crow-bar effect at point A, so providing a negative going impulse to the transducer.

3.3.6 The High Speed Camera

In order to provide temporal resolution for the Schlieren photographic study, an image converter camera was employed. The camera used was a Hadland Imacon type HE700-S11, No. 081. This was supplied with an English Electric P856 tube, which was the larger dimension option, having a photocathode with an S11 response. Using this tube, a maximum individual image format of 18 x 16mm was available in the film plane of the camera.

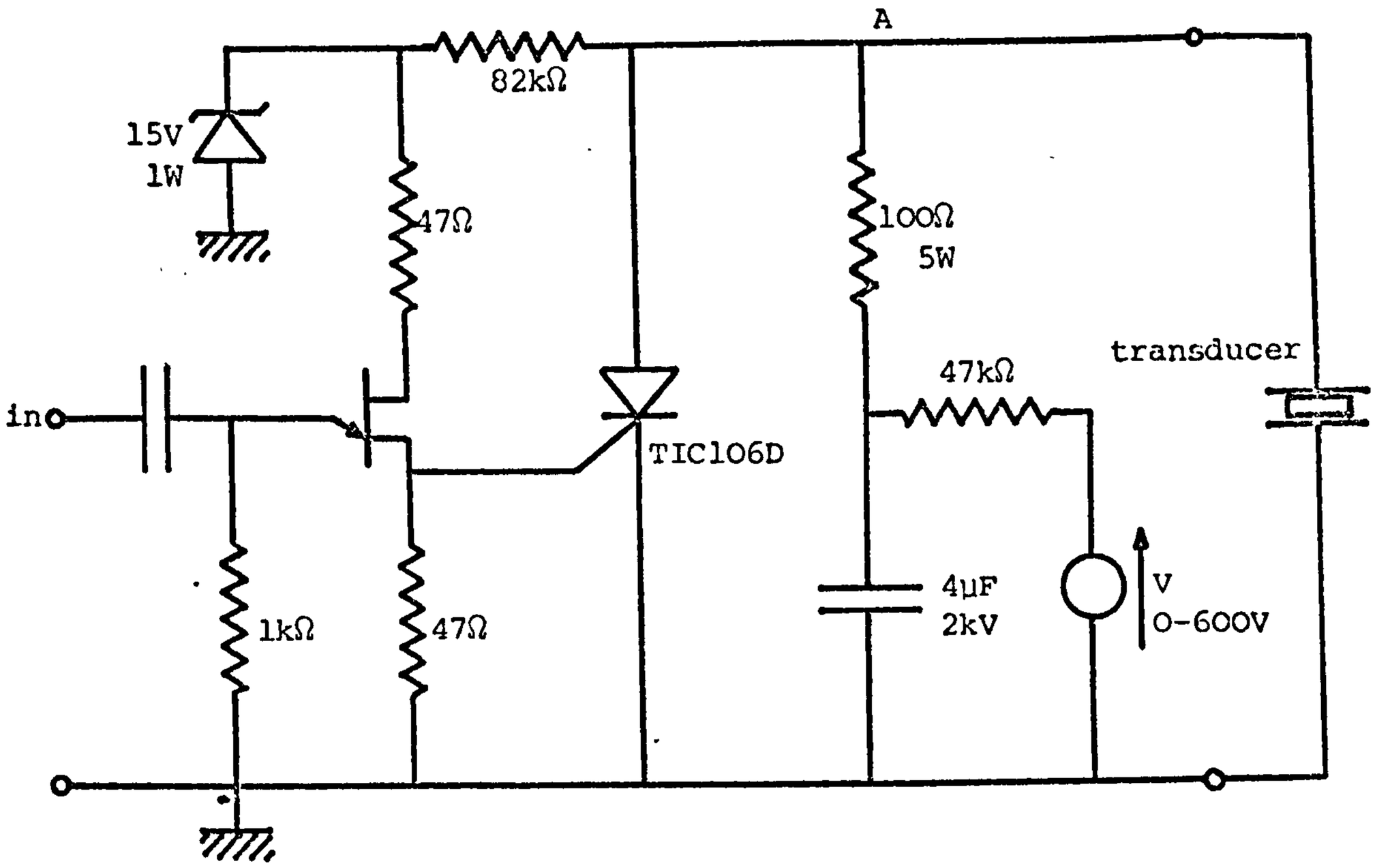

Fig. 3.10(a) Transducer pulse drive circuit

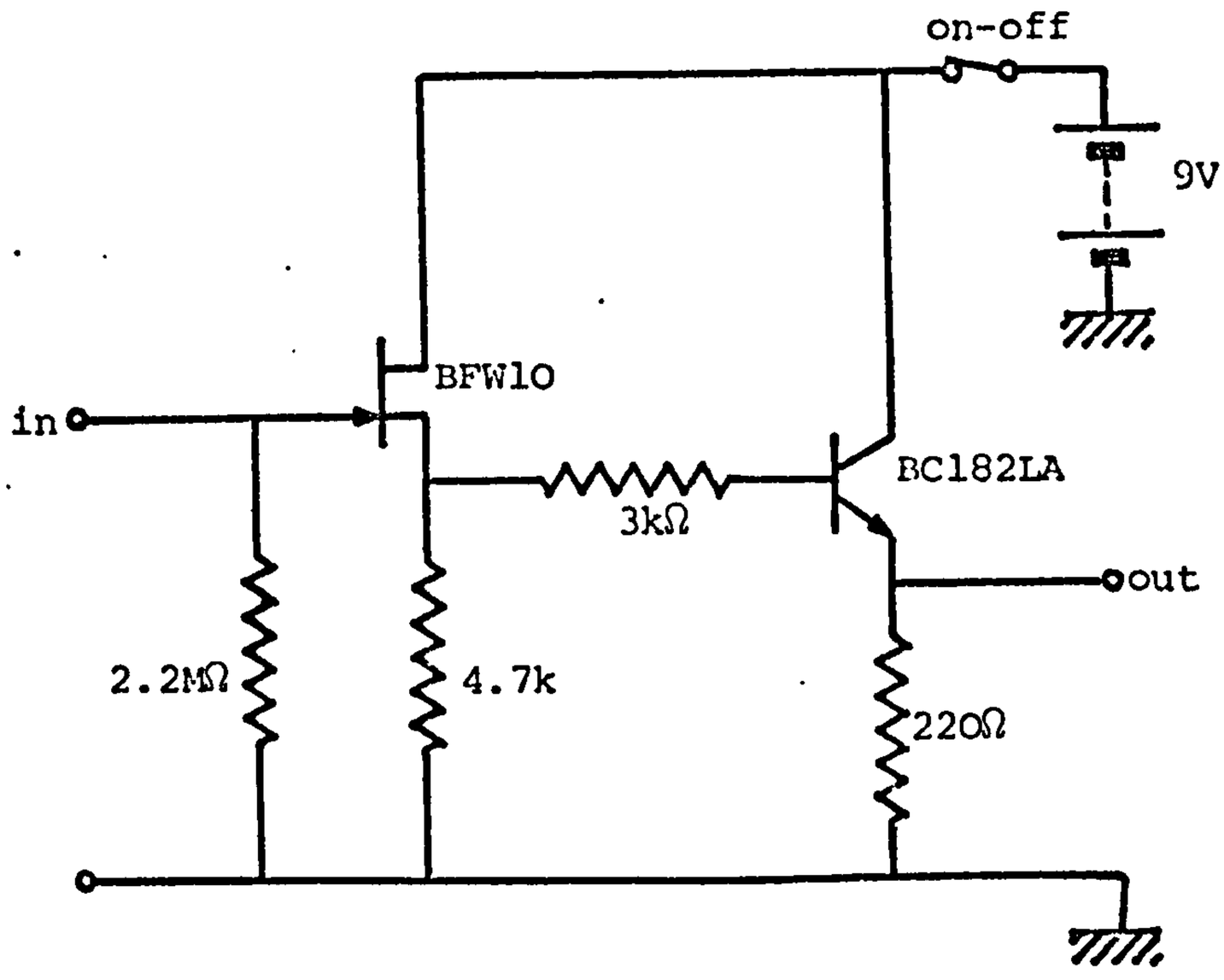

Fig. 3.10(b) Photomultiplier pre-amplifier

A standard framing mode of operation was chosen and two plug-in units were used to span the necessary temporal range. A medium speed plug-in type FT171 was used during most negative point to sphere step voltage tests. This offered a framing rate of 5×10^5 per second and an exposure time of 400ns. A fast plug-in, type FT174, operating at a higher framing speed of 1×10^7 per second and an exposure time of 20ns, was also used. This was found particularly useful during the examination of positive point disturbances, where much higher propagation velocities were encountered compared with the negative point situation. A conventional Hanimex 35mm f/3.5 primary lens was incorporated into the camera focussing system with the aid of a bellows unit. The chosen focal length and extension enabled the aerial image generated by the Schlieren optical arrangement to be brought into focus at the photocathode of the image tube. A polaroid film back was chosen for use with the camera. It was found that type 410, with a film speed rating of 10000ASA, was necessary to obtain optimum exposure, particularly when using the fast plug-in. When the camera was used in conjunction with the Schlieren system it was possible to perform a directly viewed ranging test prior to photo-raphy. With the hinged mirror of the camera in the upper, focussing position, the dynamic images formed on the phosphor screen could be viewed by the dark accustomed eye. On lowering the mirror to the recording position, the phosphor screen image was projected onto the recording film via a Wollensak f/1.2 relay lens, when the remotely

operated Pi Alphax shutter was opened.

3.3.7 Sequence of Operation

Fig. 3.11 shows the electrical interconnection of the component parts comprising the time resolved Schlieren system. Manual closure of the microswitch initiated the operating sequence. This switch produced a trigger pulse to drive the thyristor discharge circuit for the flash-light source. A Mullard 92AV vacuum photocell was used to detect the leading edge of the light pulse and trigger a Solatron OPS100 delay pulse generator. A synchronous signal from the pulse generator was fed to the trigatron firing circuit, whilst a delayed pulse was derived to trigger the image converter camera. An acoustic pulse could also be generated after a pre-determined time lage by using another Solatron delay generator to trigger the transducer drive circuit. Continuous ultrasonic irradiation was introduced into some test sequences. Irradiation was limited to a one minute period prior to each microswitch closure, with a ten minutes waiting period between each test. This precaution was taken in an attempt to suppress the liquid heating effect resulting from transducer power dissipation.

For the temporal relationship between each step voltage application and the corresponding high speed photographic sequence, a dual trace oscillographic recording was taken. With reference to fig. 3.11, the camera monitor pulses from the connection designated CRO_1, and the signal from the high voltage capacitor

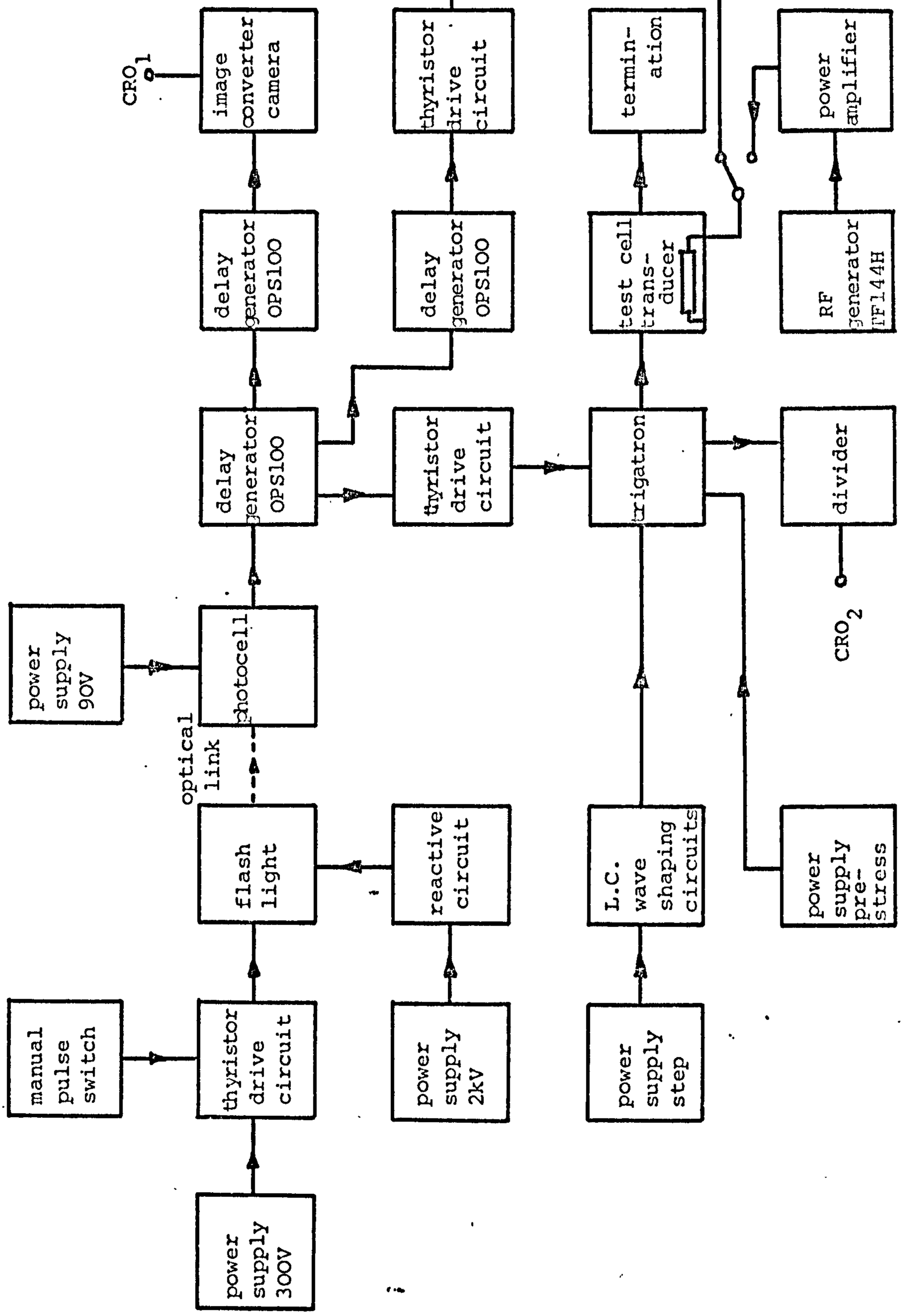

Fig. 3.11 Electrical circuit block diagram for Schlieren photography

divider, connection CRO_2, were displayed on a Tektronix Model 551 oscilloscope. A 35mm format Shakman recording camera, type AC 2/25, was loaded with Ilford HP4 film and used to view the oscilloscope screen and record the timing trace for each test.

3.4 SCATTERED LIGHT PHOTOGRAPHY

3.4.1 General

Fig. 3.12 and plate 3.2 show the essential features of the scattered light technique. The coaxial test cell that was incorporated into the Schlieren system was replaced by one possessing four viewing ports, and the optical arrangement was modified to provide an intense level of illumination in the test gap. Instead of sighting the camera along the illuminating axis, an orthogonal viewing plane was chosen. Scattered light, from the stress induced generation of inhomogenous interfaces within the test gap, was made the subject of large format macrophotography. To fulfil the optical viewing requirement; a Dallmeyr Septac 50mm f/1.5 lens and a 10cm extension tube was attached to a 9 x 12cm format Linhof Color plate camera. Initially a laser was used to align the optical system but temporal resolution was achieved by using the camera with an open shutter and providing flash illumination.

3.4.2 Electrical Equipment

The flashlight source and firing circuit of fig. 3.9, was utilised with a modification to the main capacitor

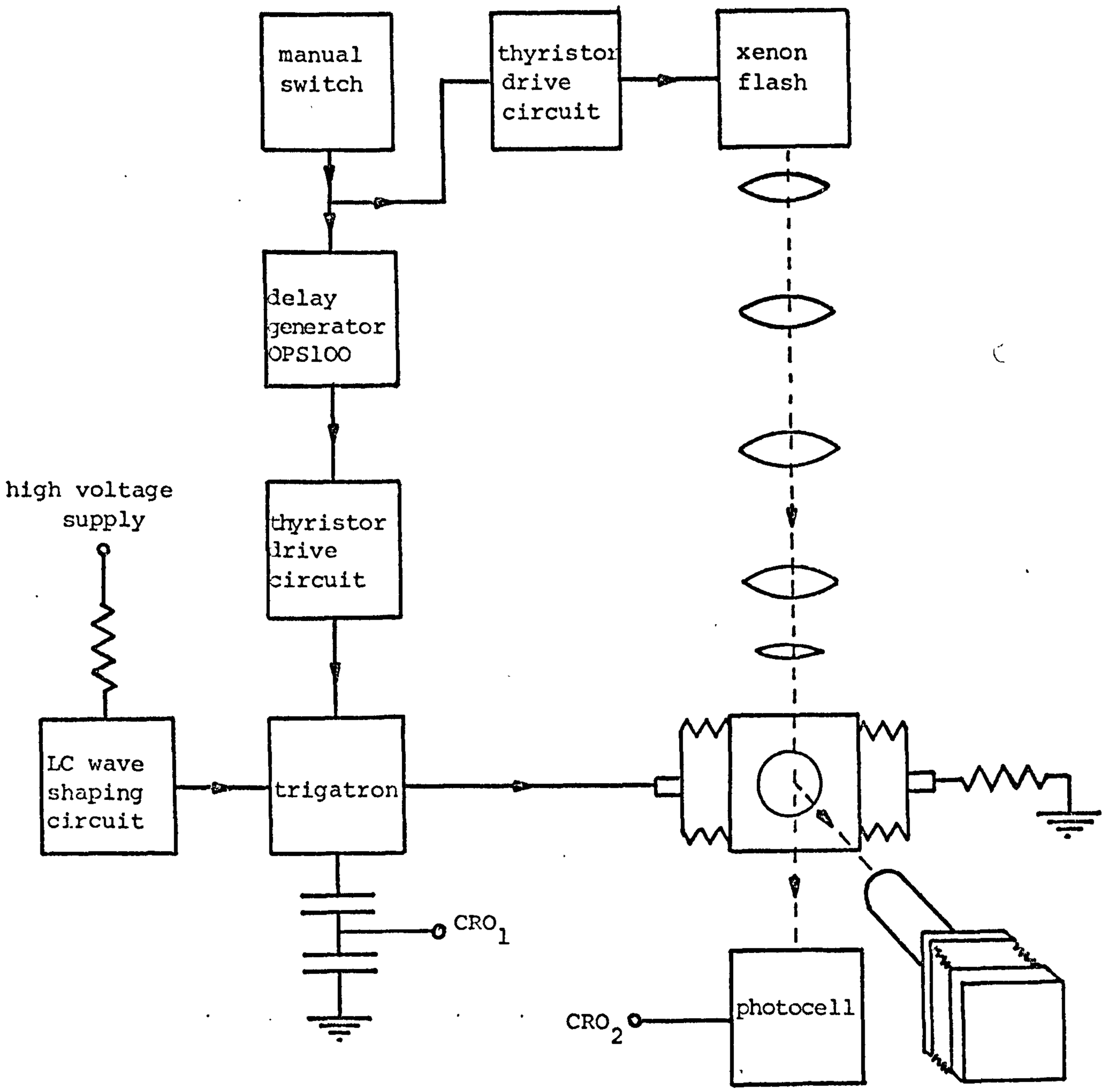

Fig. 3.12 General arrangement of the scattered light system

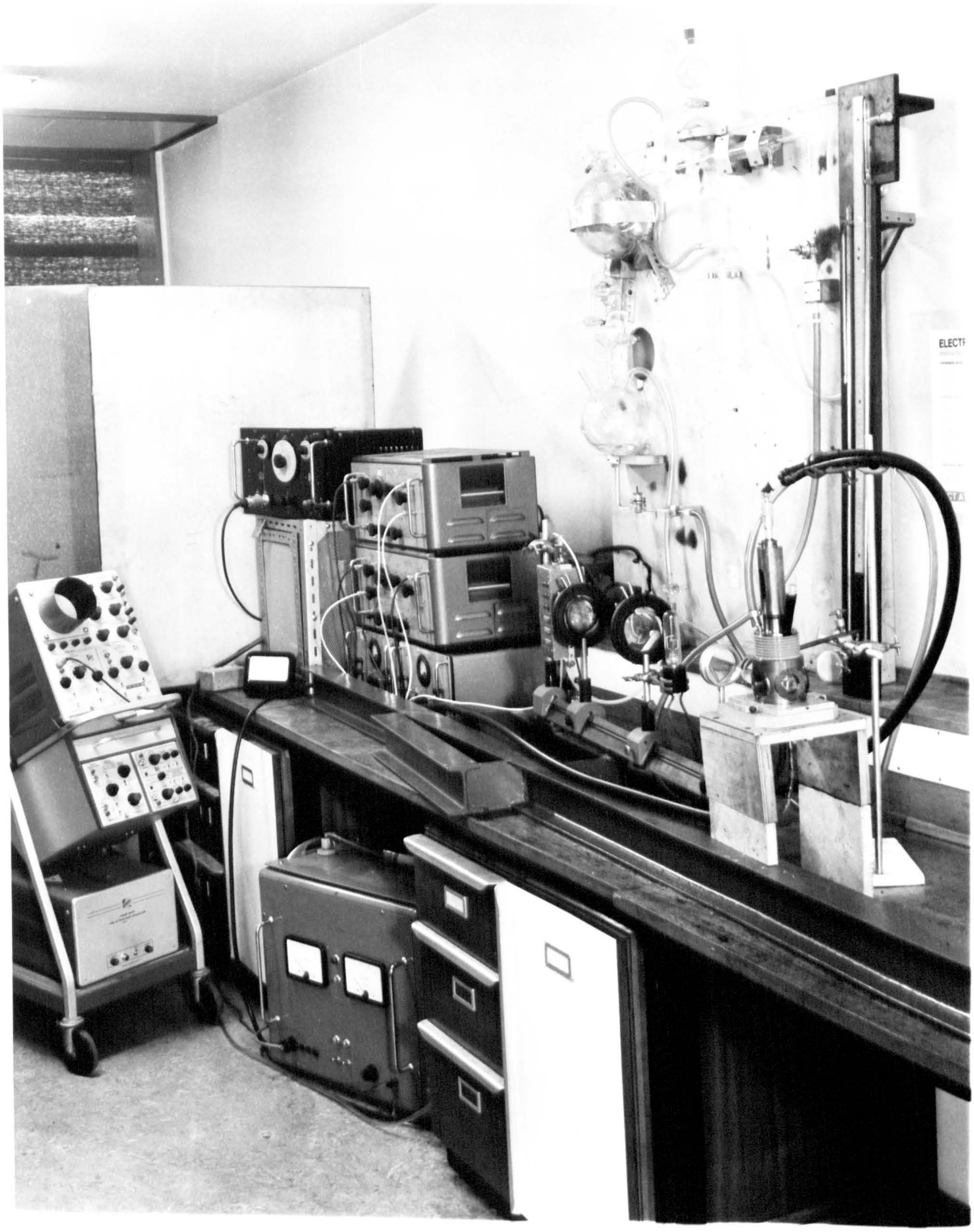

Plate 3.2 The scattered light system

discharge circuit to reduce the illumination time. The 125μF capacitor and inductor were replaced by a Wego 0.5μF low inductance capacitor with direct connections to the flash tube. An estimate of the illumination time was made using the image converter camera operating at 100ns/frame, and observing the number of frames illuminated on the viewing screen. Using a capacitor charging voltage of 5kV gave an illumination time of approximately 2μs.

High voltage was applied to the test cell using the circuit shown by fig. 3.7 for the time resolved Schlieren system. As the delay time between voltage application and flashlight illumination could be extended to several milliseconds, a capacitor divider with a long decay time constant was used as shown by fig. 3.8(b), for the high voltage timing measurements.

3.4.3 Sequence of Operation

Fig. 3.13 shows a block diagram of the complete electrical interconnection arrangement for the scattered light technique. The operating sequence was commenced by manual closure of the microswitch. A synchronous signal was used to apply a high voltage step function to the test gap with the aid of a thyristor switching circuit and the associated trigatron. A delayed signal was then derived to trigger the flashlight source and provide illumination for the scattered light optical arrangement. With reference to fig. 3.13, the voltage signals from the capacitor divider, CRO_1, and the photocell, CRO_2, were used to measure the time delay between each voltage

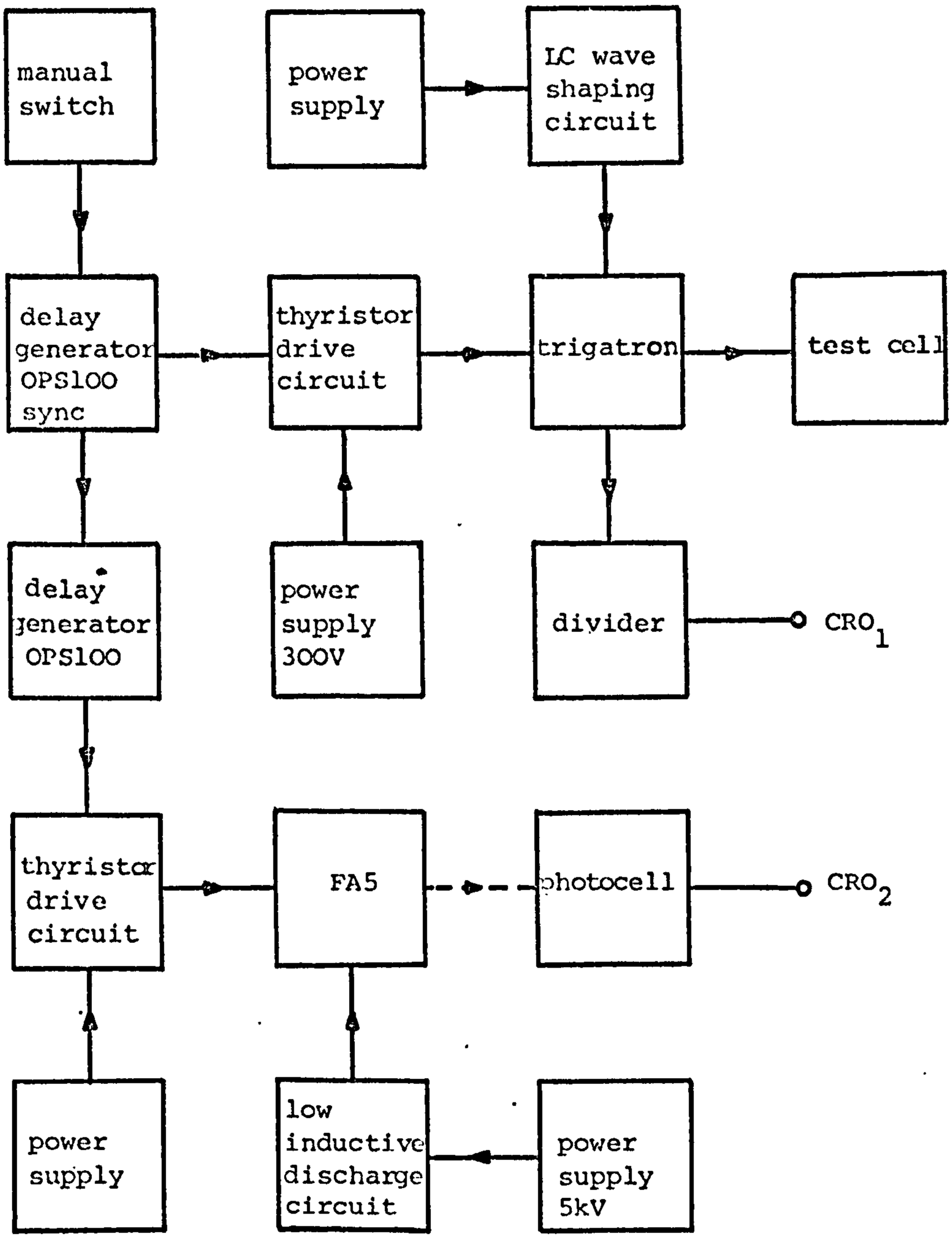

Fig. 3.13 Electrical circuit block diagram for scattered light photography

application and the flashlight illumination of the pre-breakdown event. The timing signals were displayed and recorded in the manner described for the Schlieren techniques, section 3.3.7.

Scattered light images were recorded on Ilford HP4 plate film and developed in Microphen, the combination offering a fine grain resolution coupled with an enhanced film speed extending to 650 ASA. Kodak Royal X Pan plate film, developed in DK50 was also used, with a film speed that could be extended to 3000 ASA. The contrast available was sufficient to allow the pre-breakdown scattered light images to be enlarged and printed onto normal grade photographic paper.

3.5 LIGHT EMISSION STUDIES

3.5.1 General

Measurements of the pre-breakdown light emission from n-hexane and transformer oil were taken for both step function and direct voltages. For step voltage application, individual light scintillations were recorded. When direct stress was applied to the test liquid, conduction current and acoustical disturbances were monitored in addition to the light emission. Both individual pulse and integrated measurements were taken for each parameter.

3.5.2 Step Voltage Investigations

For step voltage application, the high voltage circuit of fig.3.7 was utilised but the overall system arrangement was simplified as shown by fig.3.14. An EMI 6256S photomultiplier was used to view the test gap and monitor the light pulses emanating from the highly stressed liquid as shown by plate 3.3. Prior to commencement of tests, the photomultiplier was connected to the high voltage supply for at least 2 hours to ensure dark current stabilisation, and at no time was the tube subjected to ambient lighting or test cell breakdown whilst voltage was applied. For the examination of individual light pulse behaviour, the photomultiplier was connected for scintillation measurement. With reference to fig.3.15, the cathode connection K was grounded, a positive high voltage from a General Radiological type NE013A stabilised power supply was connected to point A; and the switch S was set to position 2. Connection to the high voltage supply, of typically 1kV, was made via a screened resistor of 500KΩ forming part of a coaxial connecting lead. A mu-metal screen surrounded the body of the photomultiplier tube, and this together with the passive components was placed in a cylindrical brass housing. Access to the electrical components was provided by BNC coaxial connectors, mounted on a rear blanking plate. These screening precautions were taken to ensure pulse immunity from external interference and transients generated by the high voltage system.

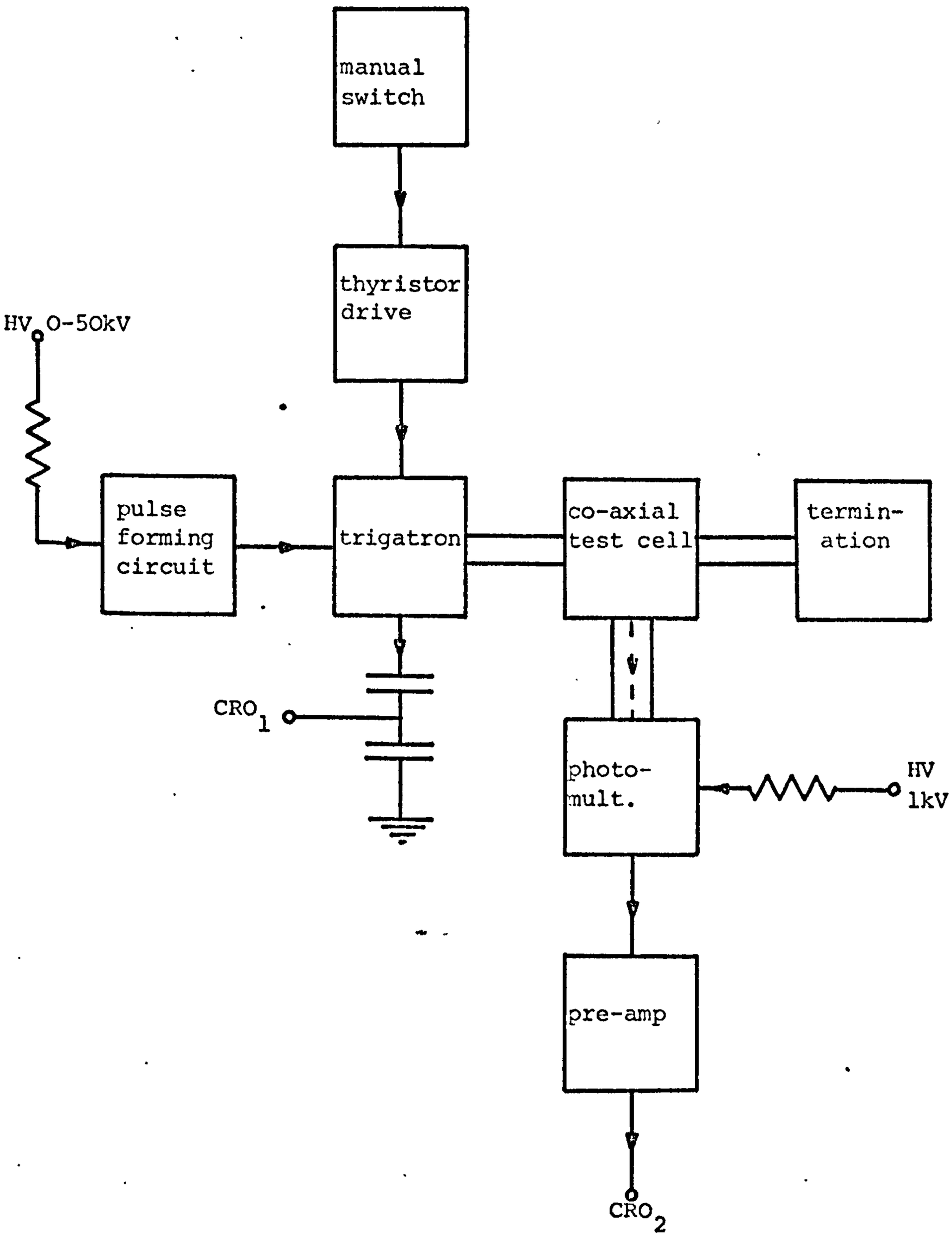

Fig. 3.14 Block diagram of light emission measuring circuit for step voltage application

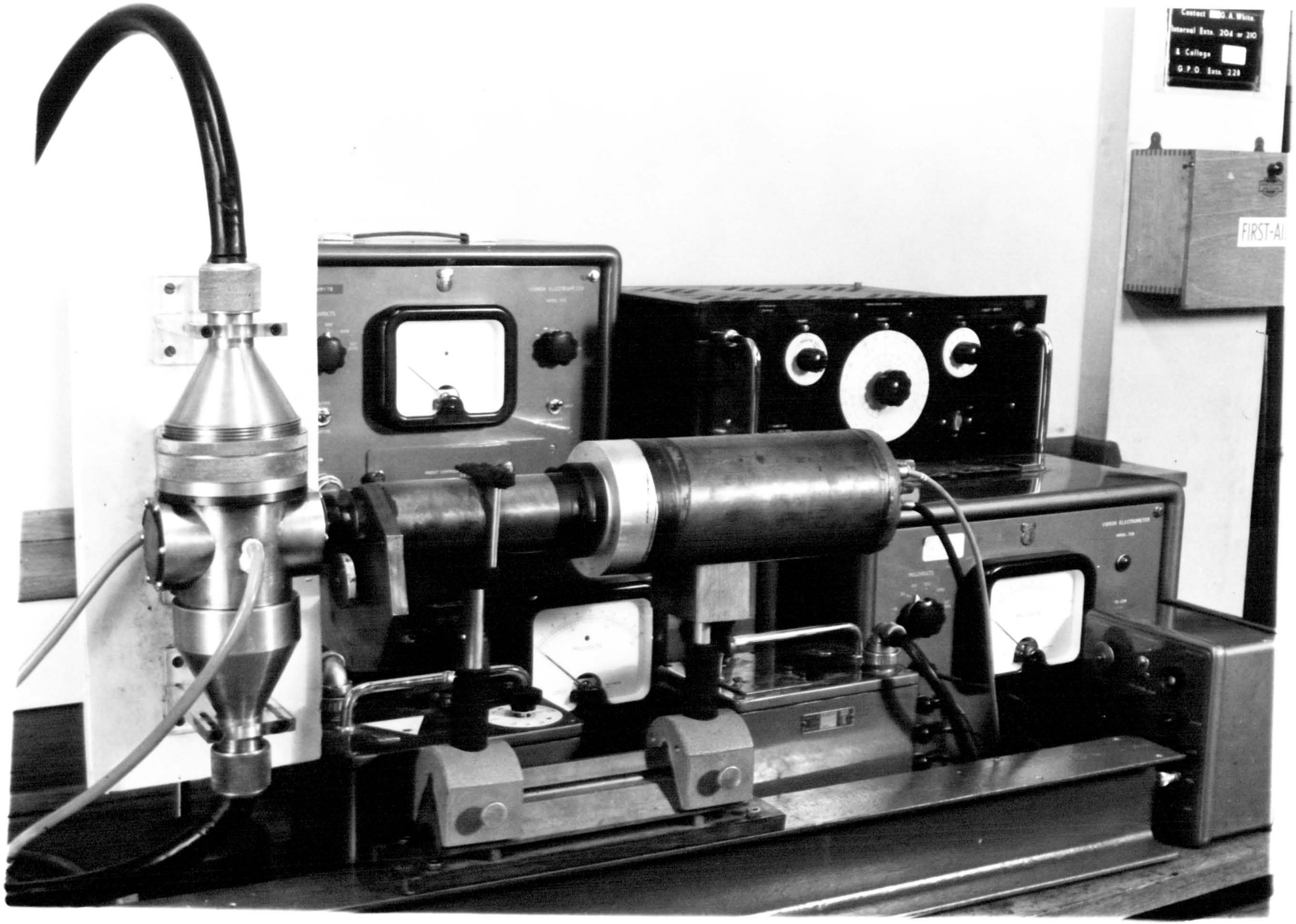

Plate 3.3 Arrangement for light emission studies

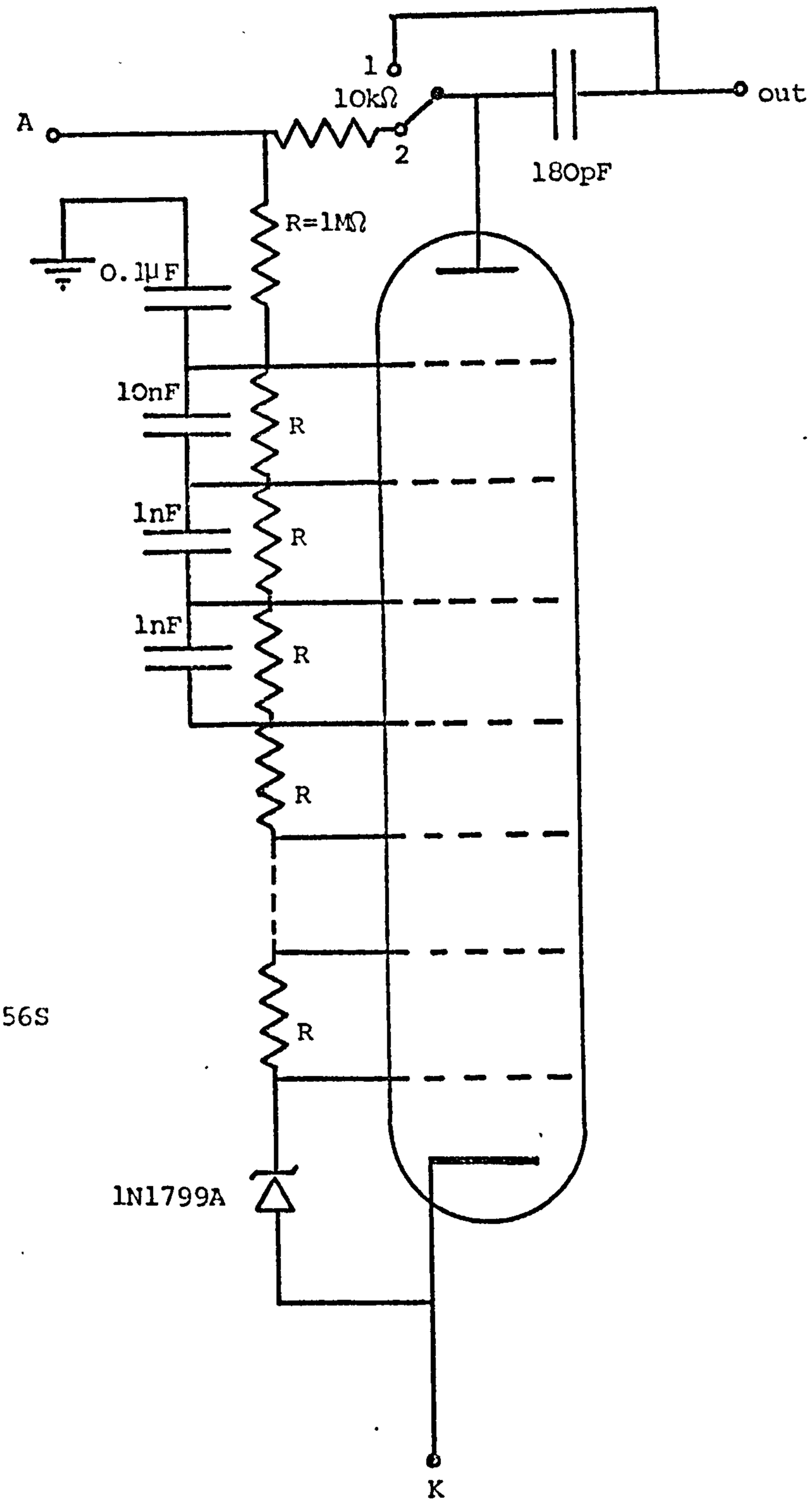

EMI 6256S

Fig. 3.15 Photomultiplier wiring diagram

A pre-amplifier was used in conjunction with the photomultiplier as shown by fig. 3.10(b). An FET source follower was used, which presented an input impedance of approximately 2MΩ. A second stage of current amplification was provided by an emitter follower which produced a low output impedance for the recording instruments. The amplifier was powered by an internal battery and enclosed in a dicast box. Coaxial connections were used throughout for spurious pulse protection. A 10cm length of 50Ω cable was used to connect the photomultiplier output to the pre-amplifier, in an attempt to limit the anode shunt capacitance to approximately 10pF. The pre-amplifier rise and fall time characteristics were measured with the aid of a Venner TSA628 pulse generator and Tektronix model 551 oscilloscope, and found to be less than 20ns. The time between voltage application to the test gap and the subsequent light emission, was oscillographically displayed and recorded, taking pulse measurements from the capacitor divider, CRO_1, and the pre-amplifier output CRO_2, as shown by fig. 3.14. Not only was the test gap viewed directly by the photomultiplier but a screen was also incorporated into the viewing plane. The opaque plastic screen was suspended inside the test cell close to the viewing port. The relative screen to electrode location was then adjusted such that a selected portion of the gap could be obscured from the photomultiplier.

3.5.3 Direct Voltage Investigation

Light scintillation records were also taken in conjunction with conduction current and acoustic vibrations, when direct voltage was applied to the test gap, as shown by fig. 3.16. To facilitate acoustic measurements a lcm diameter barium titanate transducer was lightly suspended inside the test cell, but mechanically isolated from the main body. Using a Tektronix type CA plug-in to provide a third beam, by chopping one of the dual beams provided by the type 551 oscilloscope, all three parameters were simultaneously displayed on the screen and recorded with the aid of the Shakman camera.

In addition to oscillographic observations, integrated values of light emission, conduction current and acoustic vibrations were also recorded when direct voltage was applied to the test gap. Direct scale, integrated values, were displayed by the E.I.L. type 33 vibrating capacitor electrometers shown in the block diagram 3.16. For these tests, the photomultiplier was connected for integrated light measurement. Referring to fig. 3.15: the anode connection A was grounded; the negative high voltage supply was connected to point K, and the switch S was set to position 1.

Spectral analysis was made possible by using a selected range of narrow band interference filters interposed between the test gap and the photomultiplier. The filter characteristics are shown by table 3.1 and the

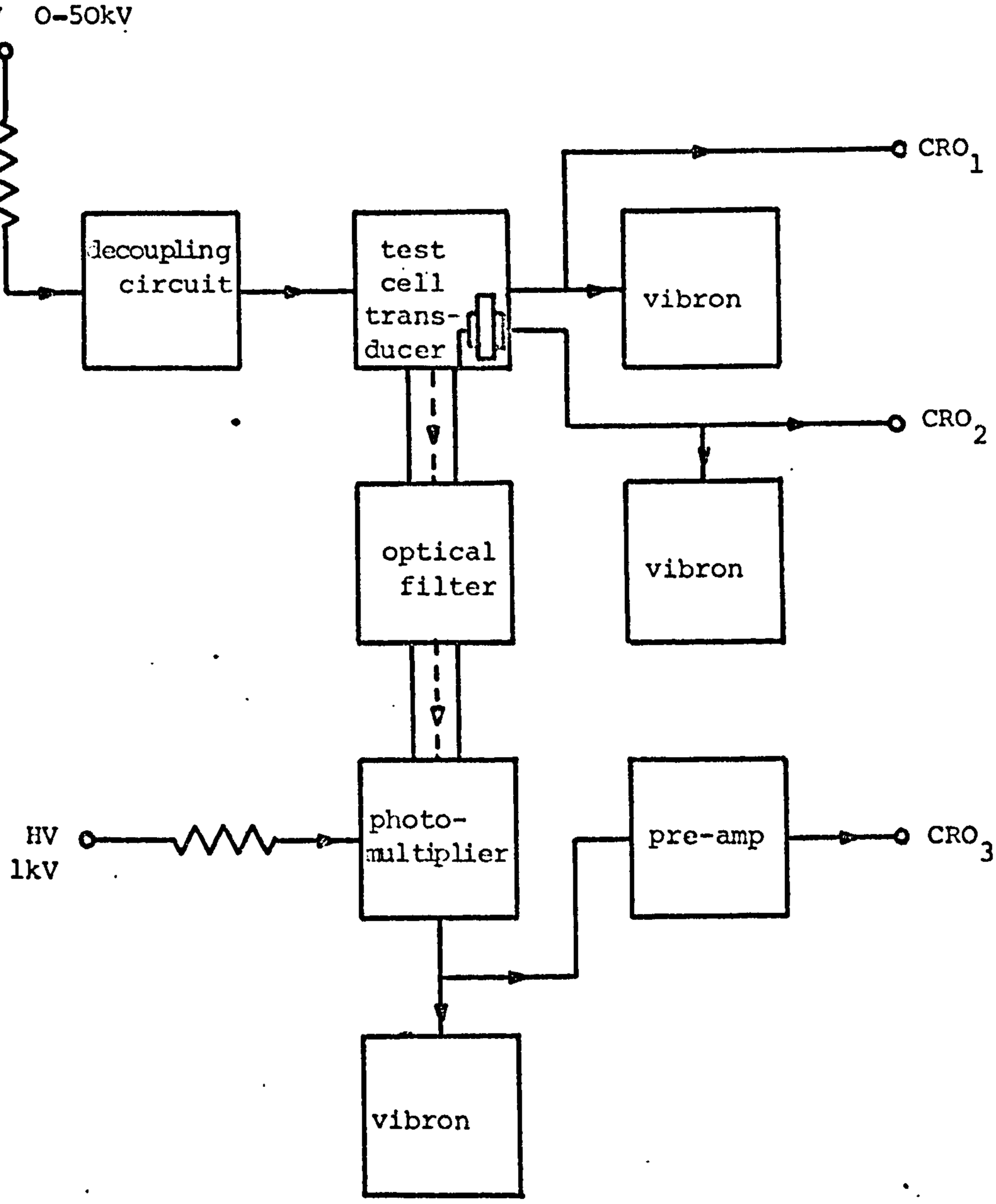

Fig. 3.16 Block diagram of direct voltage conduction and emission measuring circuit

photocathode spectral response by fig. 3.17. Several tests were performed over a controlled temperature range. The temperature of the liquid sample was increased by employing a warm air enclosure for the test cell. For trials below ambient temperature, liquid nitrogen vapour was allowed into the enclosure. This method provided a convenient and contamination free control on the sample temperature, which was monitored using a chromal alumel thermocouple connected to a Jenway 2001 transistorised thermometer.

Filter No.	Peak Wave-length (nm)	Bandwidth (nm)	Bandwidth limits (nm)	Peak Trans-mission (per unit)
1	401	11	395.5-406.5	0.30
2	424	11	418.5-429.5	0.30
3	452	11	446.5-457.5	0.42
4	496	10	491.0-501.0	0.52
5	534	9	529.5-538.5	0.48
6	559	40	539 -579	0.65

Table 3.1 Optical filter transmission characteristics

TEXT BOUND INTO

THE SPINE

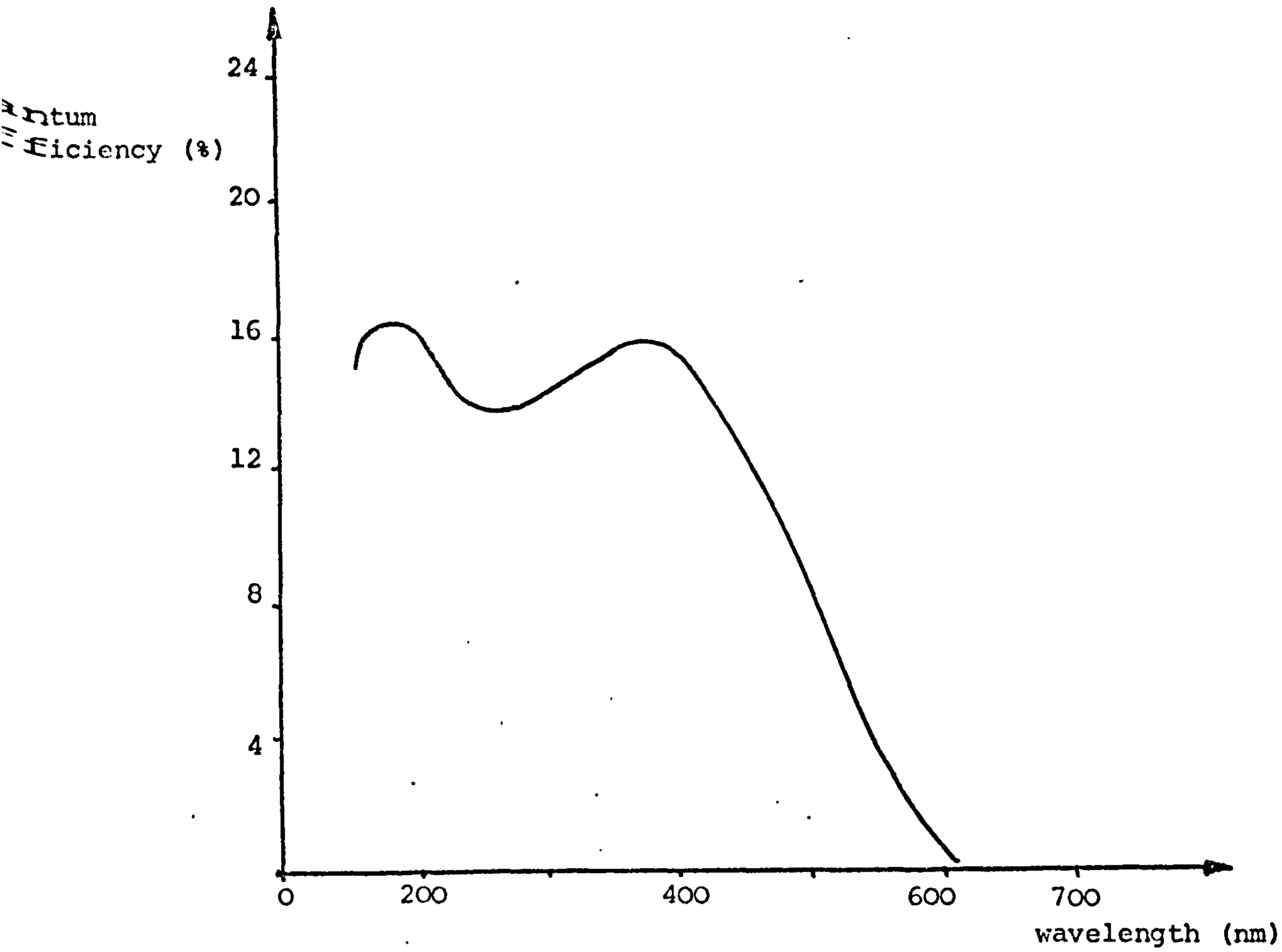

Fig. 3.17 Photomultiplier spectral response

CHAPTER FOUR

RESULTS

4.1 Schlieren Records

4.1.1 Findings for a negative point polarity

A Schlieren study was undertaken in order to provide a sensitive optical probe with which to view the test gap. The dielectric liquid under investigation was freshly filtered n-hexane. The sample was allowed to attain a state of equilibrium at a chosen temperature either in the presence of a selected gas over the liquid, or after an extended period of reduced pressure. On applying a negative going step voltage to the point electrode an inhomogenity appeared in the test gap after approximately 2μs. The disturbance appeared at the tip of the point and extended into the gap toward the hemispherical electrode. The profile of the event appeared to be irregular and possessed several branches. On spanning the gap, a self luminous breakdown spark ensued. Plate 4.1(b) shows a breakdown situation resulting from voltage application during the first frame of the record. The phenomenon may also be precipitated by a voltage insufficient to cause breakdown. Plate 4.1(a) shows a pre-breakdown event that fails to span the gap when an 18kV step is applied during the third frame interval. At the final frame of the record the event appears to be of reduced size despite the continued presence of the applied

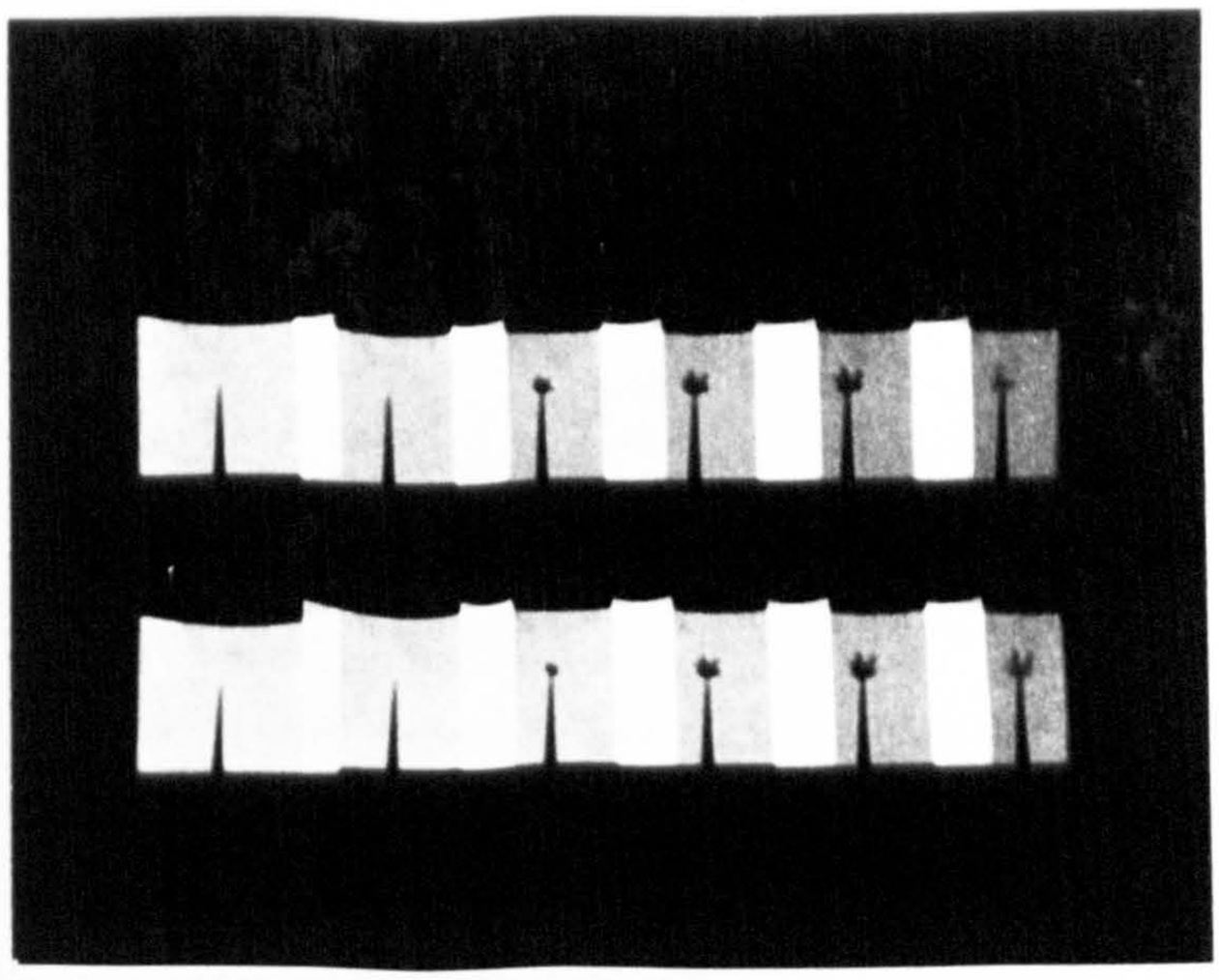

(a)

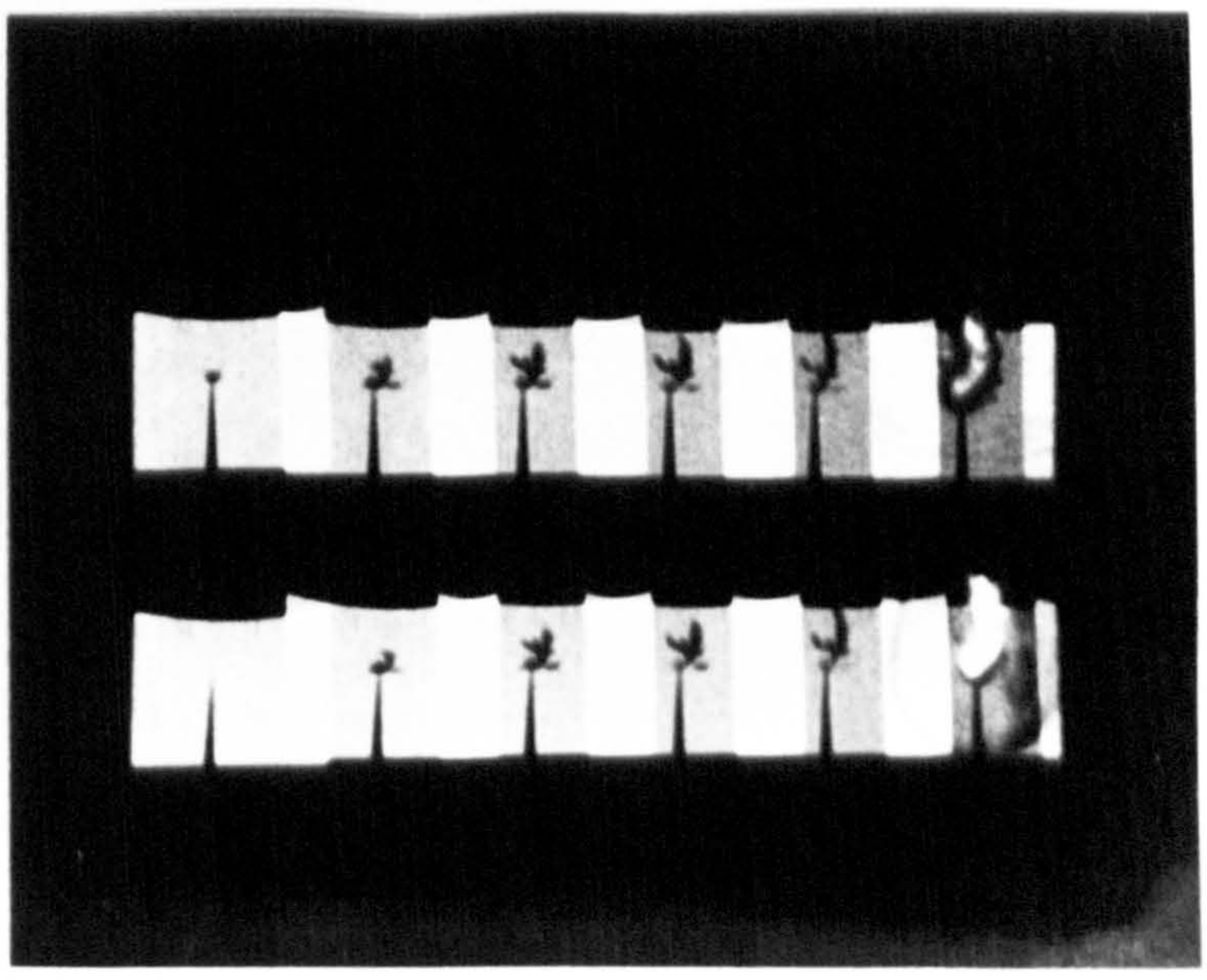

(b)

Plate 4.1 Point polarity: negative going step function.

Voltage amplitude: (a) 18 kV; (b) 20 kV.

Liquid condition: high air content at 25°C and atmospheric pressure.

Temporal resolution: 2μs/frame.

voltage. Increasing the sensitivity of the Schlieren optical system and making adjustments to the camera diaphragm to maintain optimum film illumination, provided additional pre-breakdown information. Referring to plate 4.2(a), after voltage application at the fourth frame, shock waves can be seen that are rooted at the point. These waves accompany the first appearance of the disturbance. At the eighth frame the generation of a new shock wave is evident at a branching point of the growing disturbance and is centred in a mid gap position. Plates 4.2(b) and (c) show a similar acoustic behaviour, but in the final frames the pre-breakdown event appears to fragment and shock wave generation is suppressed, despite a maintained gap potential.

4.1.1.1 An elevated temperature test

In an attempt to identify a possible thermal mechanism associated with the pre-breakdown event an elevated temperature test was performed. The test cell and contained liquid sample were slowly heated to $50^{o}C$. Plate 4.3 shows the pre-breakdown record resulting from a negative going step voltage applied during the period between the first and second frames. Although a static thermal gradient is evident in the top corner of each frame, the event is of the same form as that of the room temperature test depicted by plate 4.1.

4.1.1.2 Tests on samples with reduced oxygen content

The nature of the pre-breakdown event with a change

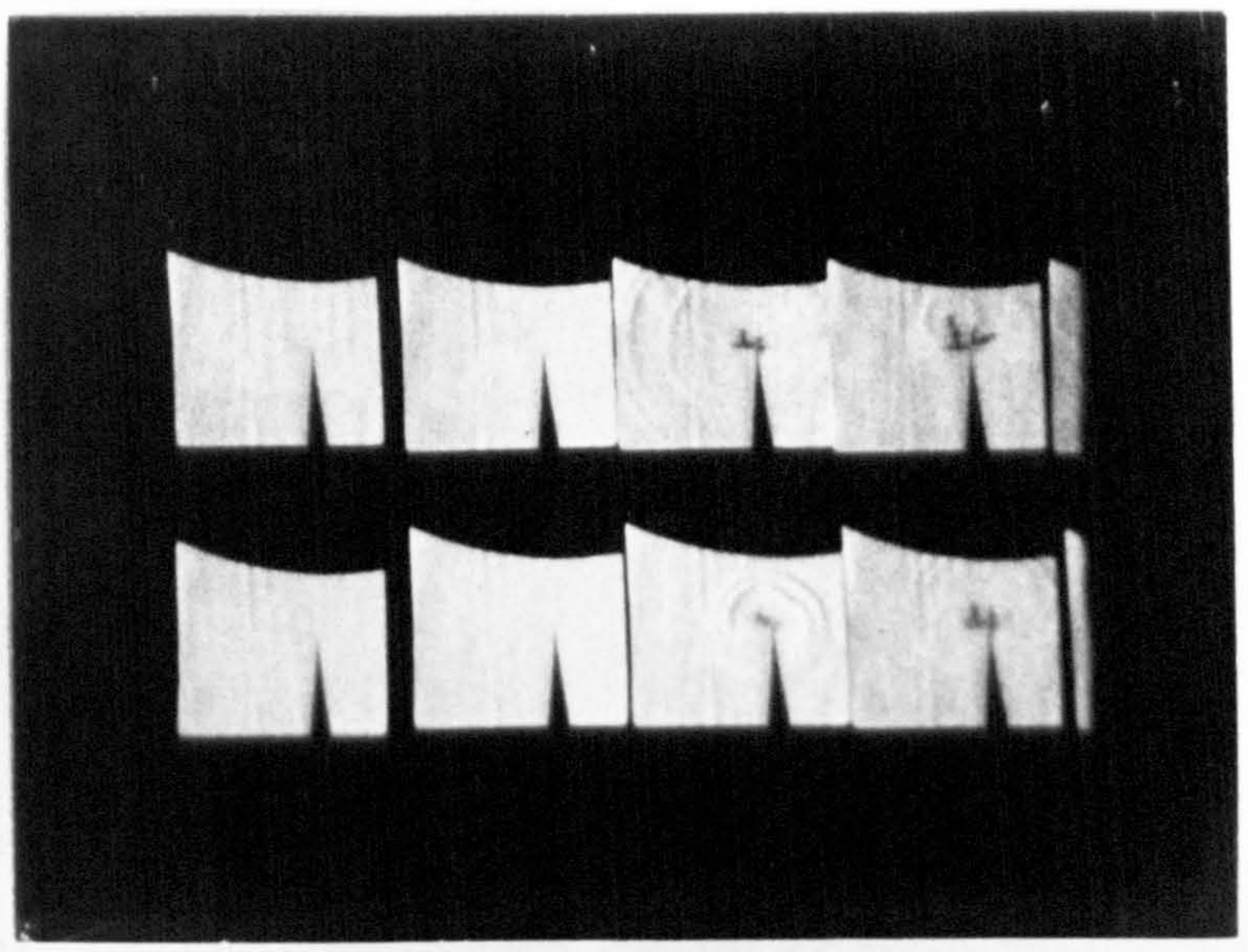

(a)

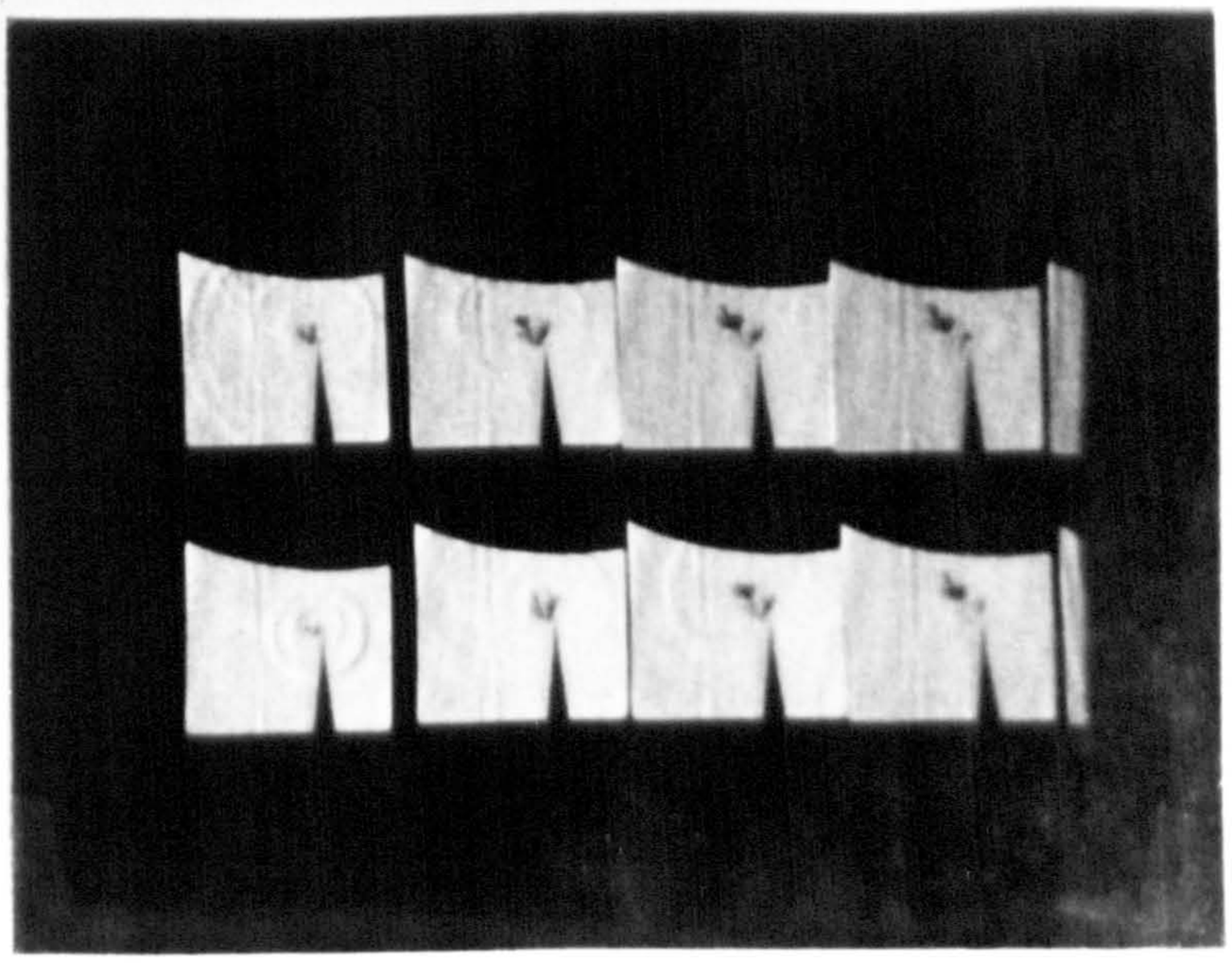

(b)

Plate 4.2 Point polarity: negative going step function.

Voltage amplitude: (a) 23 kV; (b) 23 kV applied 2μs prior to the first frame.

Liquid condition: high air content at 20°C and atmospheric pressure.

Temporal resolution: 2μs/frame.

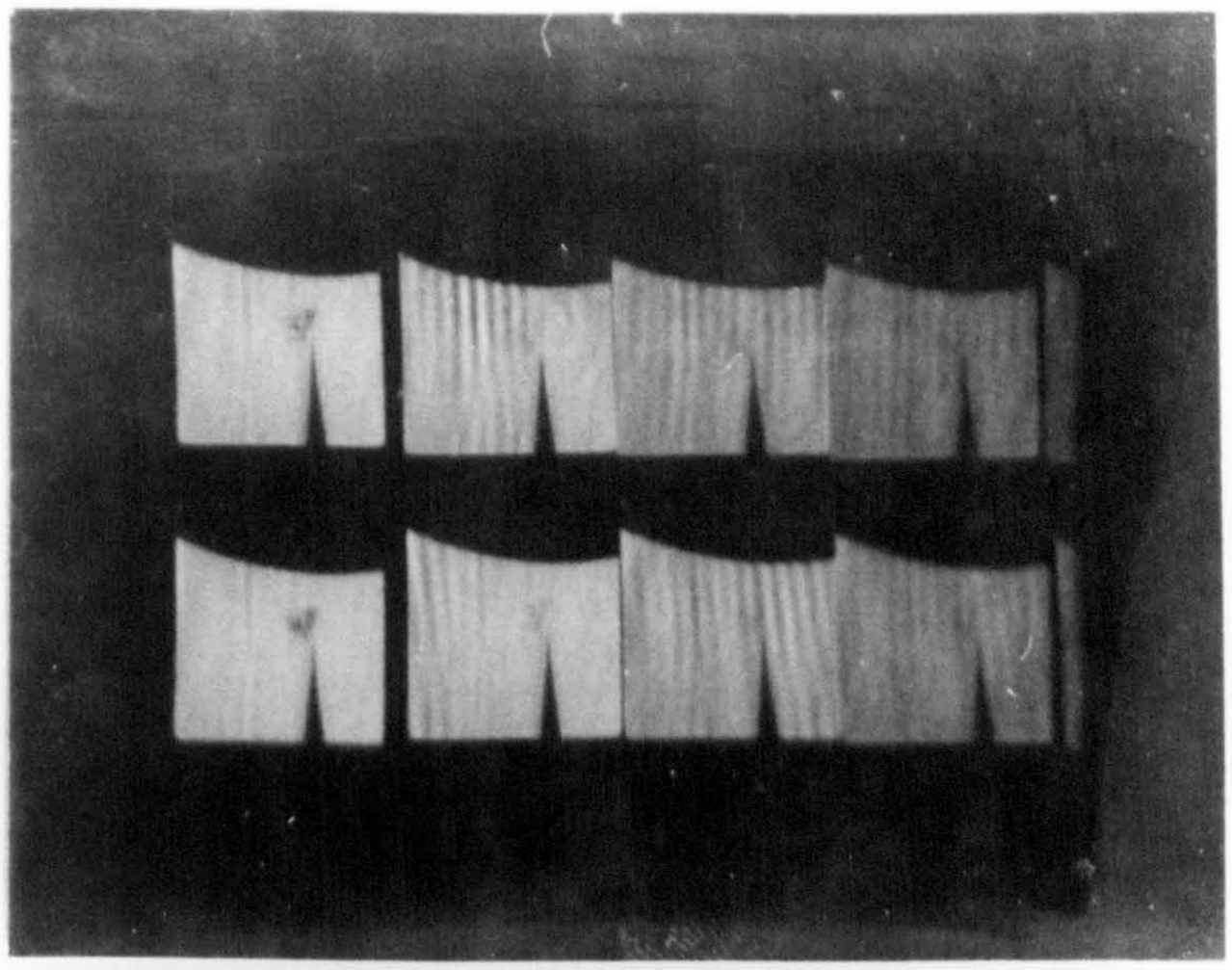

(c)

Plate 4.2 Point polarity: negative going step function.

Voltage amplitude: 23 kV applied 14μs prior to the first frame.

Liquid condition: high air content at 20°C and atmospheric pressure.

Temporal resolution: 2μs/frame.

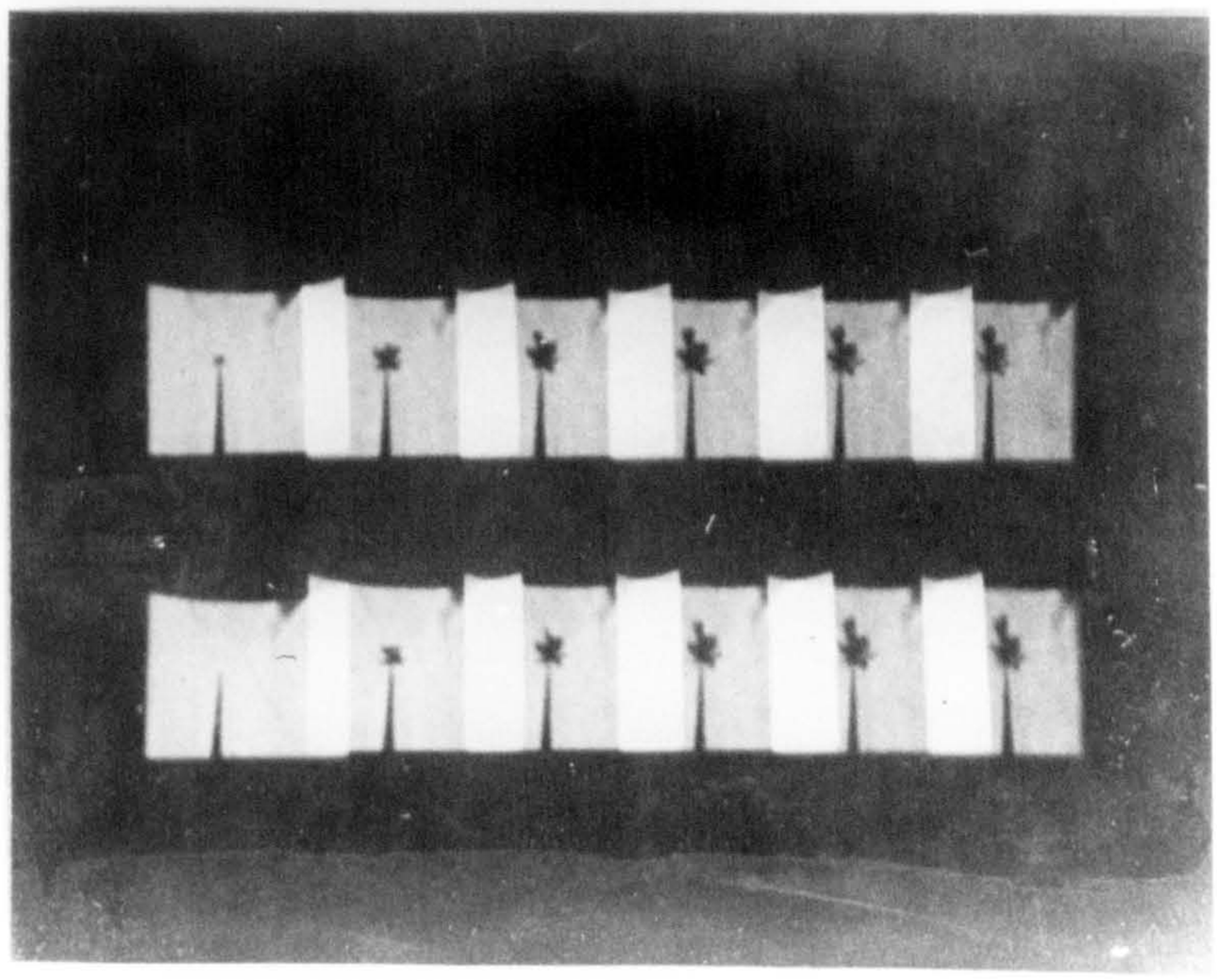

Plate 4.3 Point polarity: negative going step function.

Voltage amplitude: 23 kV.

Liquid condition: high air content at 50°C and atmospheric pressure.

Temporal resolution: 2μs/frame.

in gas content is illustrated by plates 4.4 and 4.5. For a sample possessing a low air content and held at a reduced pressure, the precipitation of the event and breakdown are shown by plate 4.4. At (a) the disturbance appears and spans over 50% of the gap with several branches, after a 16kV step was applied at the fourth frame. Increasing the step voltage to 18kV leads to breakdown as shown by plate 4.4(b), where the voltage was applied at the second frame. Distinct branching is evident from this record and at the last frame it can be seen that the breakdown path occupies the central limb.

Nitrogen was admitted to a de-gassed hexane sample and records were taken of the voltage induced events occurring at atmospheric pressure. Plate 4.5(a) shows the growth and decay of an inhomogenity after a negative voltage step of 20kV was applied at the second frame. Fragmentation of the disturbance is apparent approximately 15μs after voltage application, leaving only the tips of the branches visible by the final frame, despite the continued presence of the impressed voltage. Increasing the voltage by 4kV and applying this at the first frame, plate 4.5(b) provides a breakdown record. Distinctive branching is evident in excess of 6μs from voltage application, with breakdown following after 18μs.

Plates 4.4 and 4.5 show events that are essentially similar in appearance. Both tests were performed on samples possessing a low oxygen content with a consequent reduction of the high electron trapping cross section

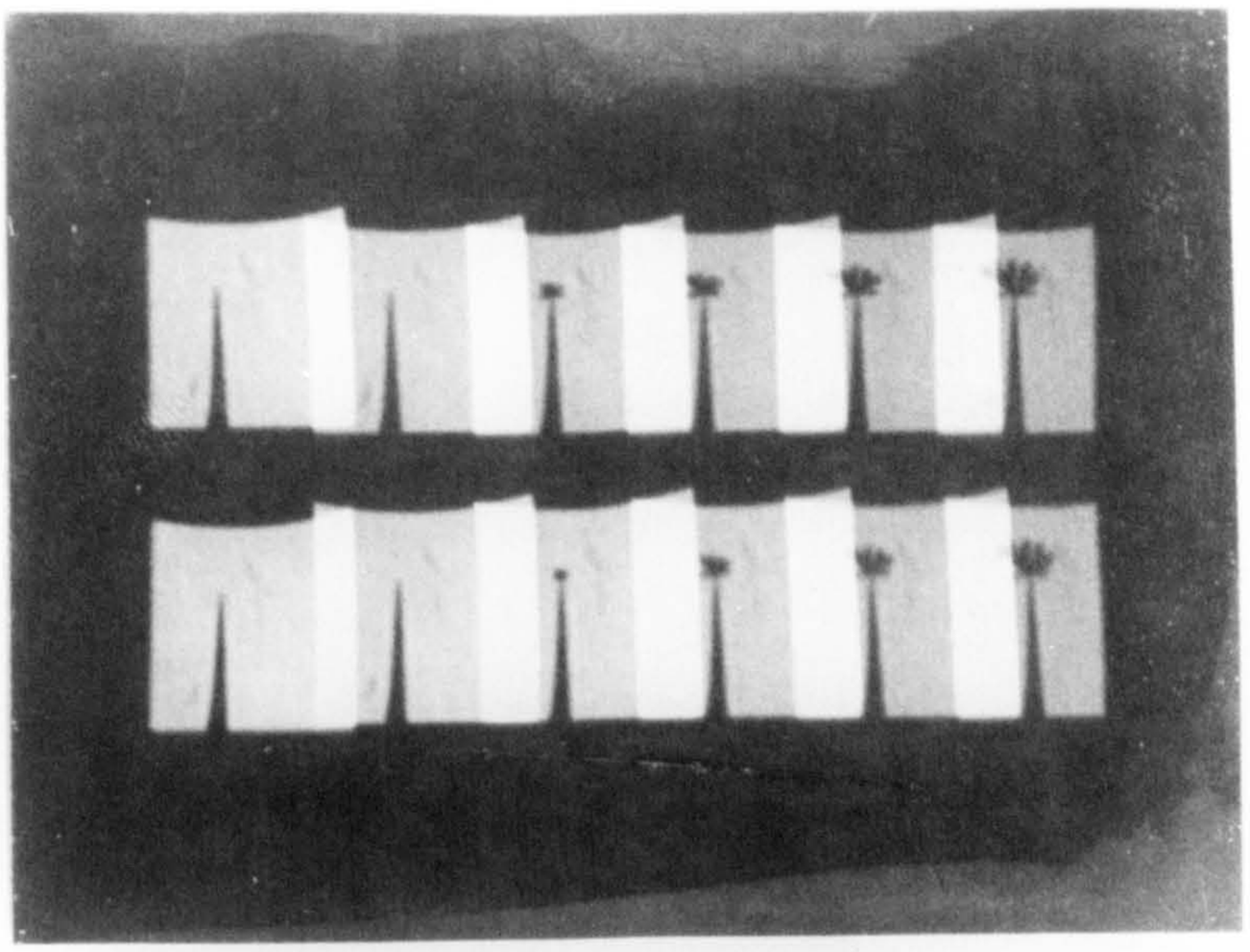

(a)

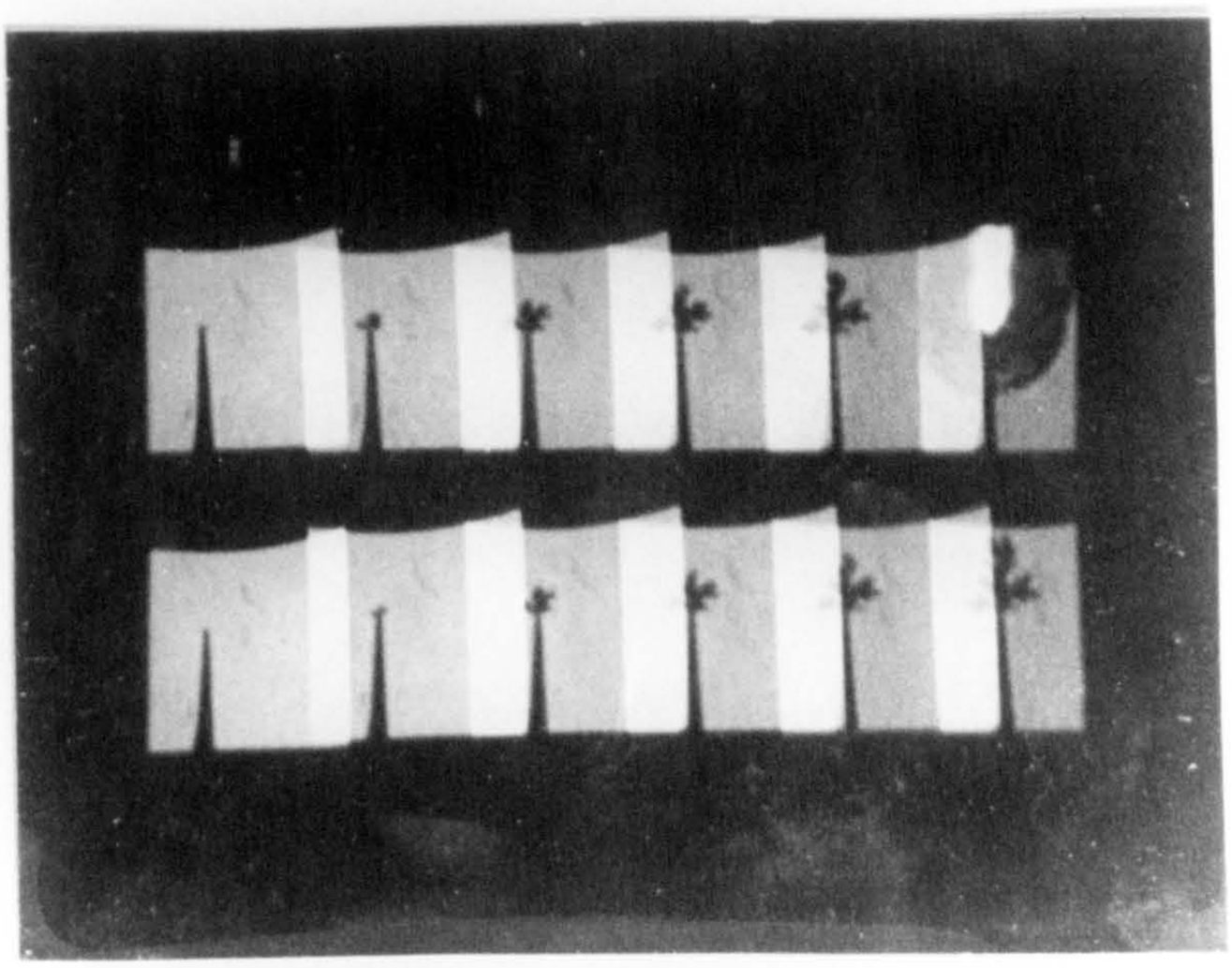

(b)

Plate 4.4 Point polarity: negative going step function.

Voltage amplitude: (a) 16 kV; (b) 18 kV.

Liquid condition: de-gassed at 25°C and vapour pressure.

Temporal resolution: 2μs/frame.

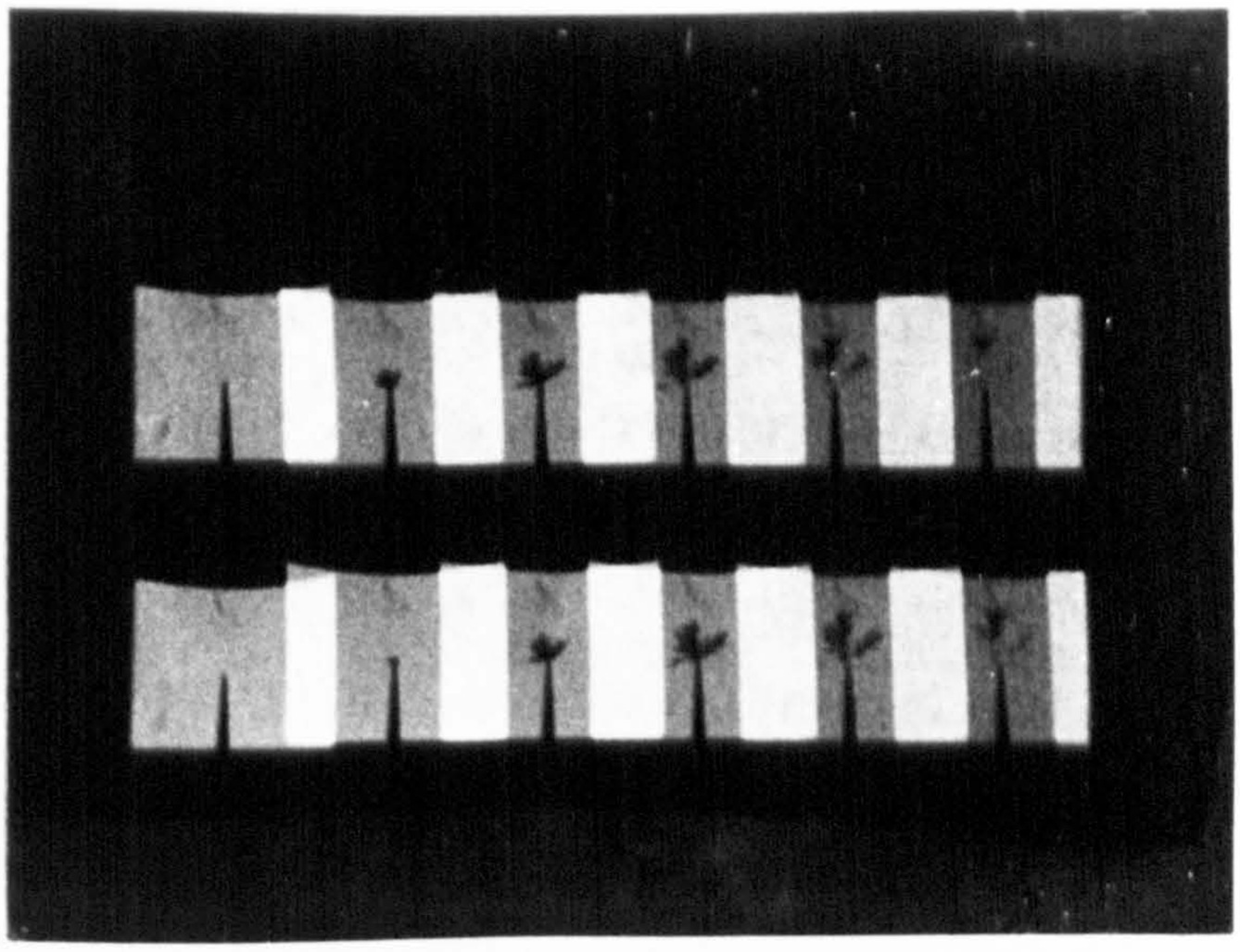

(a)

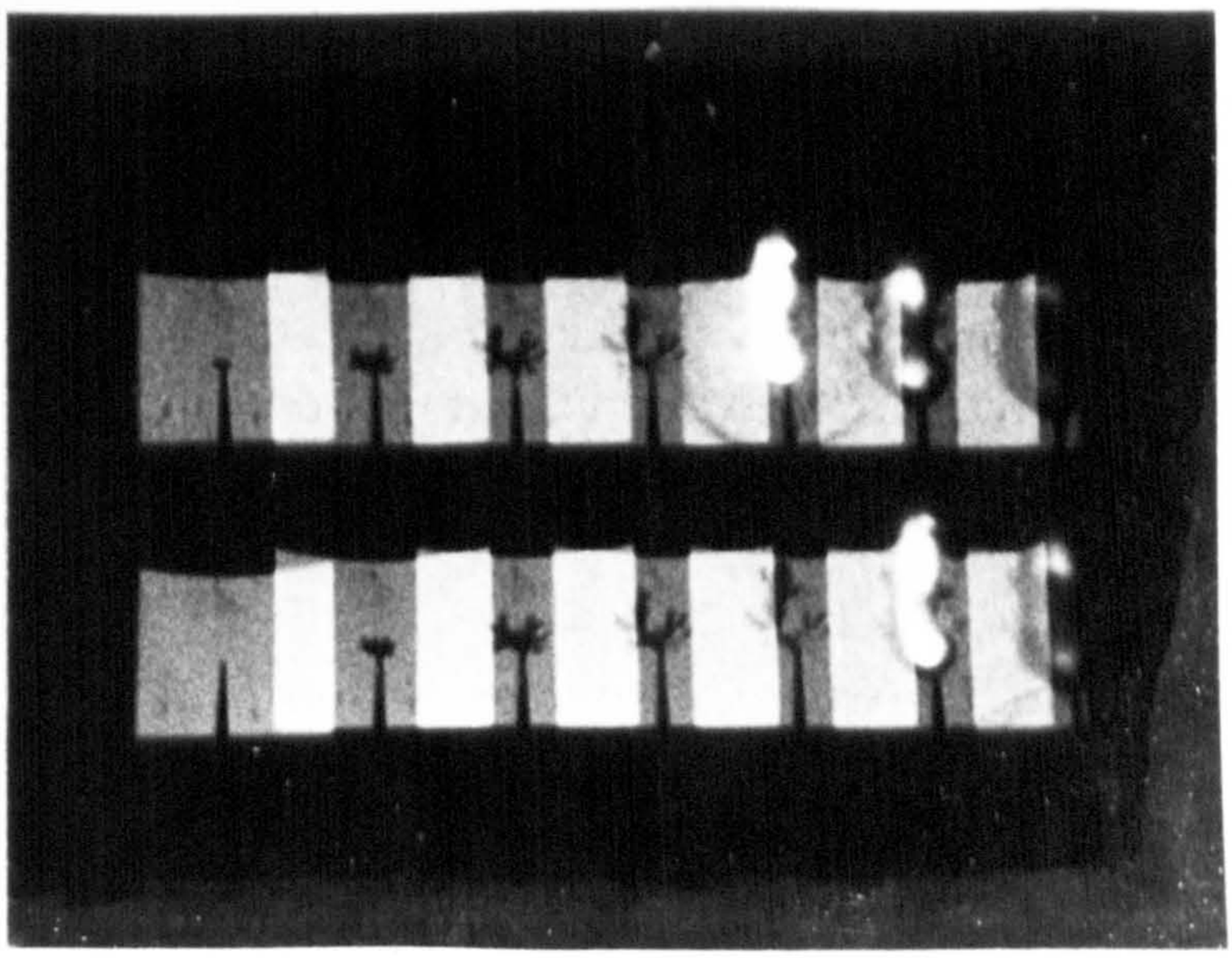

(b)

Plate 4.5 Point polarity: negative going step function.
Voltage amplitude: (a) 20 kV; (b) 24 kV.
Liquid condition: high nitrogen content at 25°C and atmospheric pressure.
Temporal resolution: 2μs/frame.

associated with this gas.[109]

4.1.1.3 Events in the presence of external acoustic waves

Following the observation of pre-breakdown shock wave generation typified by plate 4.2, the possibility of interaction with externally produced acoustic waves was investigaged. A standing wave was produced by continuously exciting an ultrasonic transducer contained within the cell body. Perturbations to the refractive index are clearly shown by the superimposed pattern on each frame of plate 4.6. The appearance of the initiating phase and breakdown showed little change when subjected to this externally generated disturbance. At (a) a 23kV negative going step was applied during the period of the second frame. At (b) breakdown can be seen at the eighth frame 8μs after the application of a 25kV step. An alternative approach utilised a travelling acoustic wave which was made to impinge on the test gap. This was achieved by providing an electrical impulse at the terminals of the transducer. Plate 4.7(a) shows the wavefront traversing the test gap from left to right and reaching the point electrode at the second frame. A 20kV negative step was applied to the point during the first frame interval. Electric stress of the same magnitude was applied to the electrodes during the first frame of the record shown by plate 4.7(b). The acoustic wave can be seen to impinge on the test gap at the sixth frame,coincident with the period of maximum event size. Both the externally produced acoustic wave

(a)

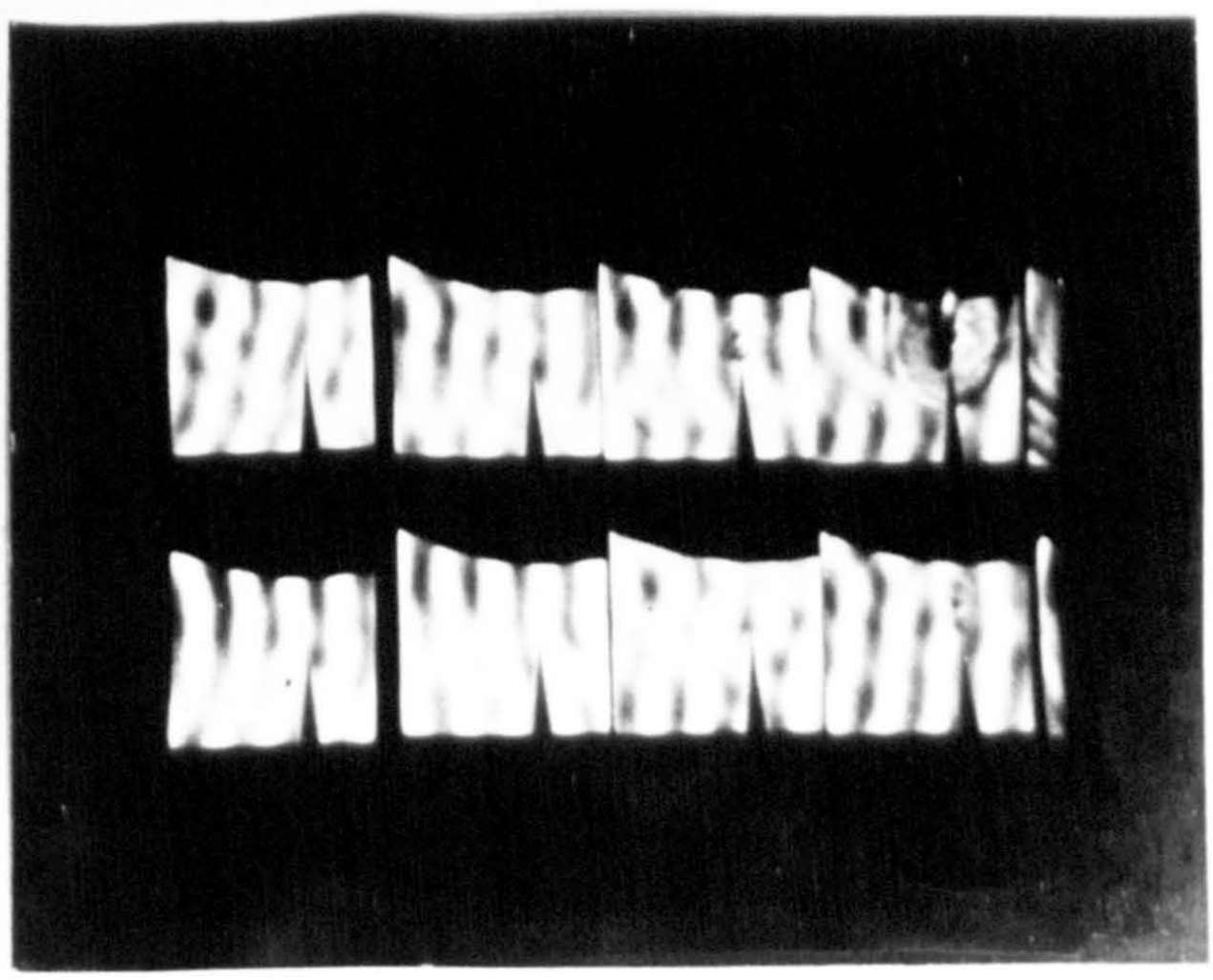

(b)

Plate 4.6 Point polarity: negative going step function.

Voltage amplitude: (a) 23 kV; (b) 25 kV.

Liquid condition: high air content at 20°C and atmospheric pressure.

Temporal resolution: 2μs/frame.

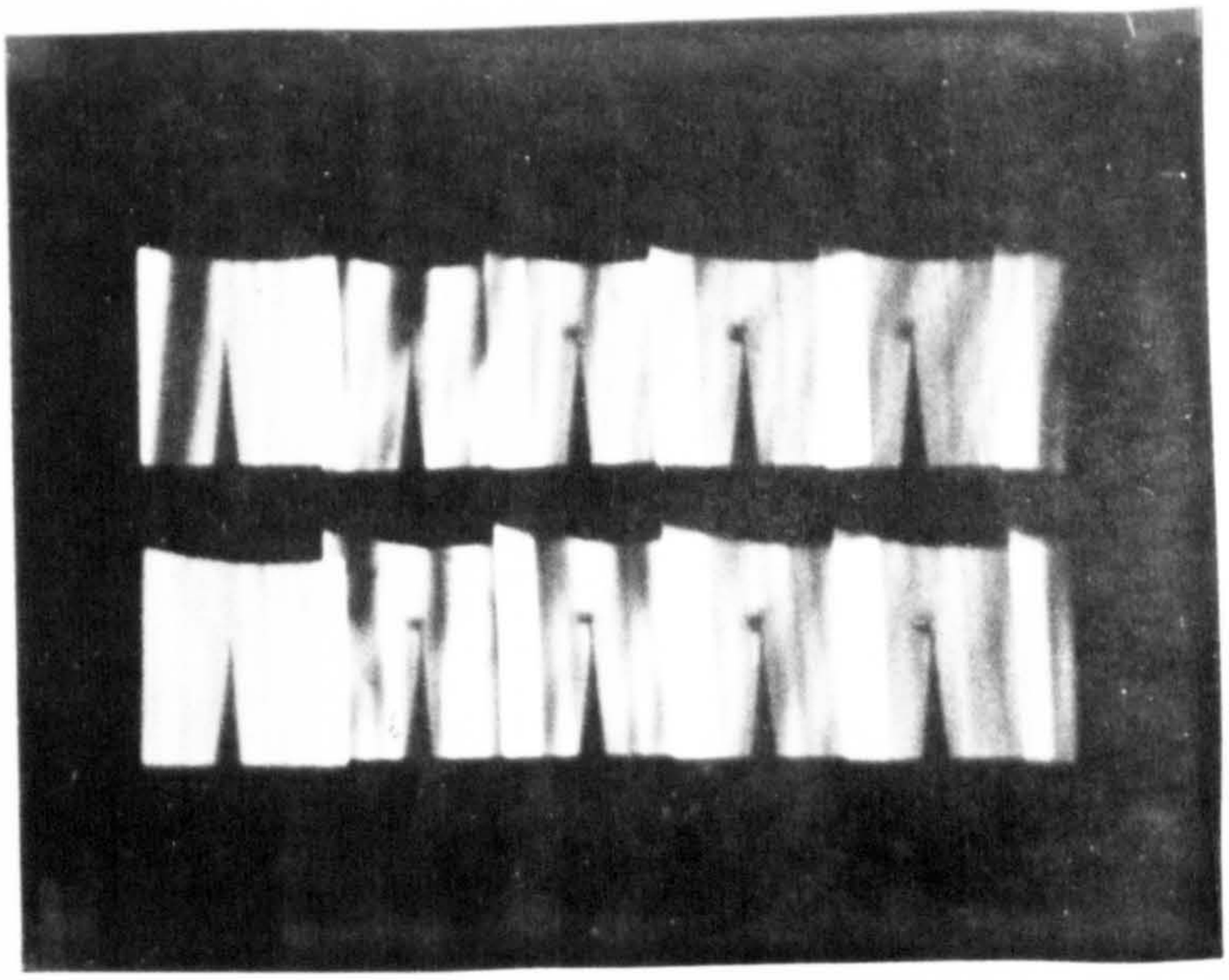

(a)

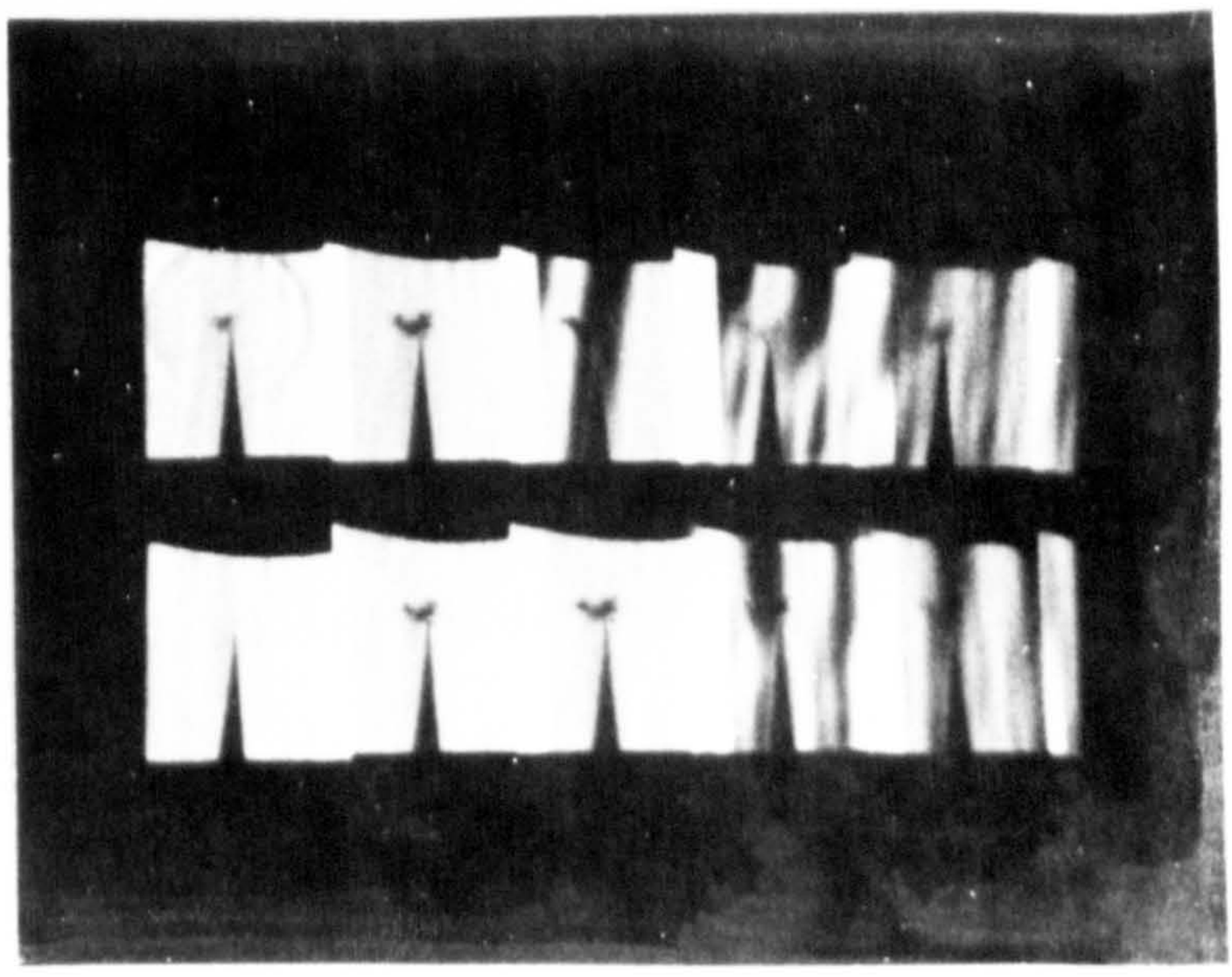

(b)

Plate 4.7 Point polarity: negative going step function.

Voltage amplitude: (a) 20 kV; (b) 20 kV, with 10μs acoustic delay.

Liquid condition: high air content at 20°C and atmospheric pressure, acoustic pulse applied during framing sequence.

Temporal resolution: 2μs/frame.

and the stress induced event appear to be superimposed with little interaction between them. This would tend to support the findings of plate 4.6.

4.1.1.4 The influence of pre-stress

In an attempt to reveal space charge effects a direct pre-stress was applied prior to a step voltage trial. Plate 4.8(a) shows a pre-breakdown record with a negative point pre-stress. The direct voltage was applied an hour before commencement of the sequence to establish a steady state condition. However, some liquid motion is evident throughout the sequence and appears as static striations superimposed on each frame of the record. Although the pre-stress was not removed when the 19kV step was applied, the difference in source impedances was sufficient to ensure superposition of the voltages did not occur. The step voltage was impressed upon the gap at the third frame of the sequence and the ensuing event clearly appears to be flattened in the plane of the earthed electrode. For a change of pre-stress polarity the record of 4.8(b) shows a marked constriction of the disturbance in the vicinity of the tip of the point electrode following step voltage application at the first frame.

4.1.2 Positive point to hemisphere records

For the chosen electrode geometry it was found that a point anode produced a characteristically different breakdown sequence. If the step voltage amplitude was sufficient to initiate a pre-breakdown event then this would

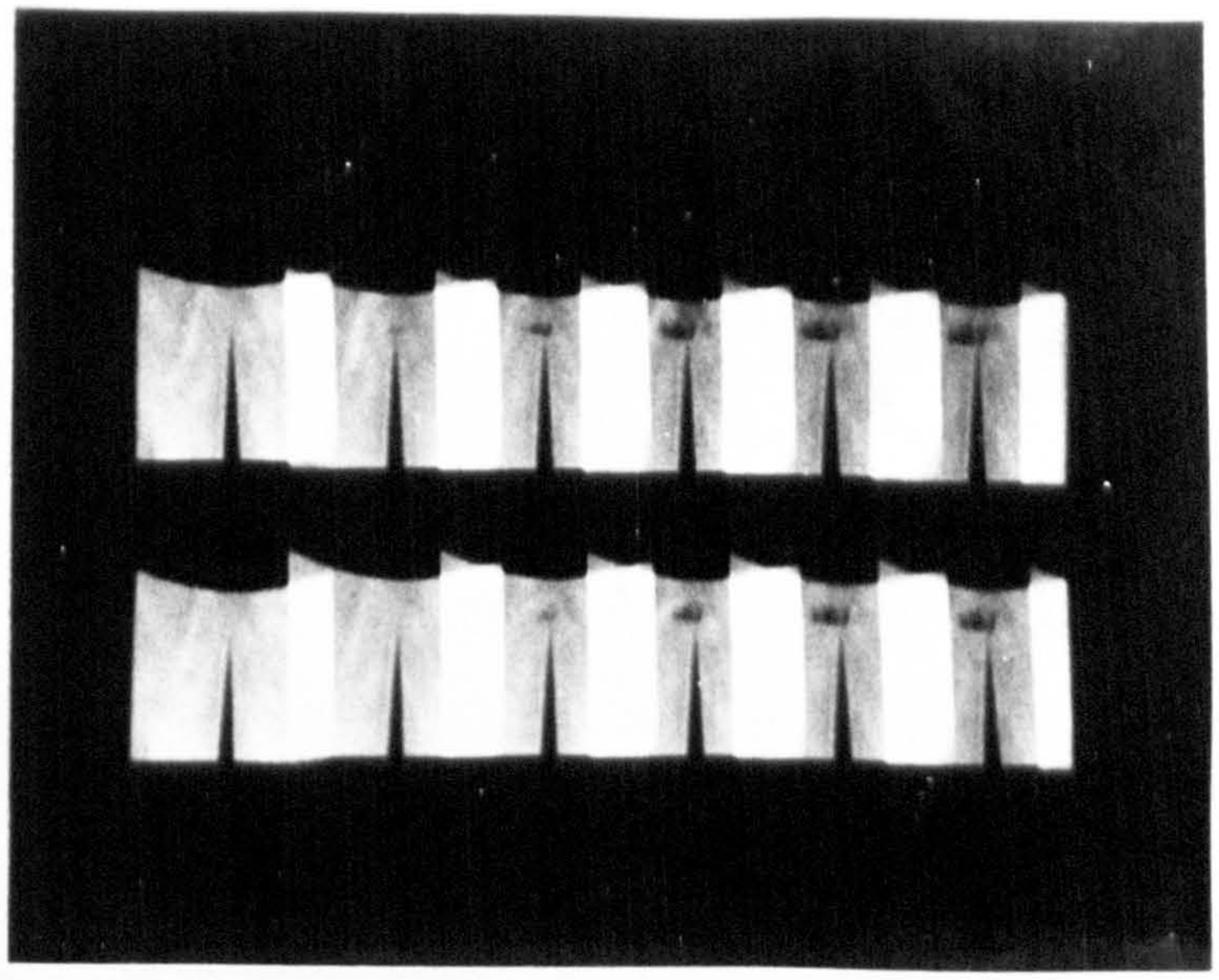

(a)

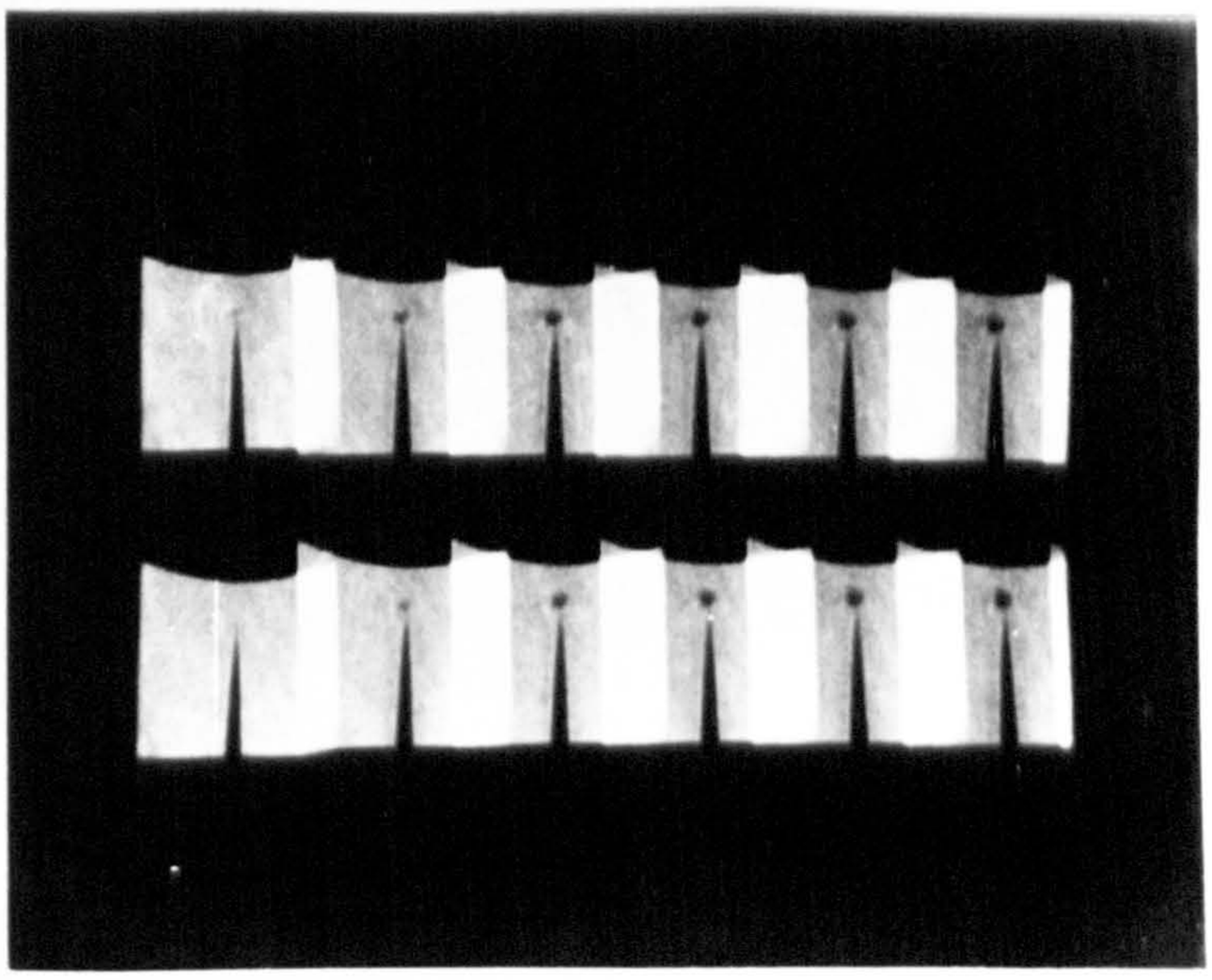

(b)

Plate 4.8 Point polarity: negative going step function.

Voltage amplitude:
(a) 19 kV step, 10 kV negative point pre-stress.
(b) 19 kV step, 10 kV positive point pre-stress.

Liquid condition: high air content at 22°C and atmospheric pressure.

Temporal resolution: 2μs/frame.

invariably lead to total gap failure. The experimental difficulties associated with synchronisation were heightened both by an erratic time to appearance of the event after voltage application and a time to breakdown of less than 1μs. A framing rate of 10^7 per second was chosen to photographically capture the phenomenon. Plate 4.9 depicts a typical breakdown sequence; the results of two tests are presented to provide an extended temporal record. At (a) a 22kV step was applied at the first frame with the event clearly visible by the third frame. The disturbance appears to possess several lobes with the central area rapidly expanding to cross the 1,5mm gap in less than 400ns. A luminous discharge forms at the sixth frame and persists to the end of the sequence. The inhomogeneous pre-breakdown region ceases to expand but is seen to be forced radially outwards from the mid gap location by the breakdown bubble, as is confirmed by the delayed record of plate 4.9(b).

4.1.2.1 The influence of space charge

In the manner described for one of the negative point step function tests, a static electric field was applied to the gap prior to the positive going transient. A negative point pre-stress radically modified both the profile and the propagation velocity of the pre-breakdown event. The behaviour became markedly similar to that resulting from a negative going step voltage at the point electrode. Plate 4.10 shows pre-breakdown phenomena at

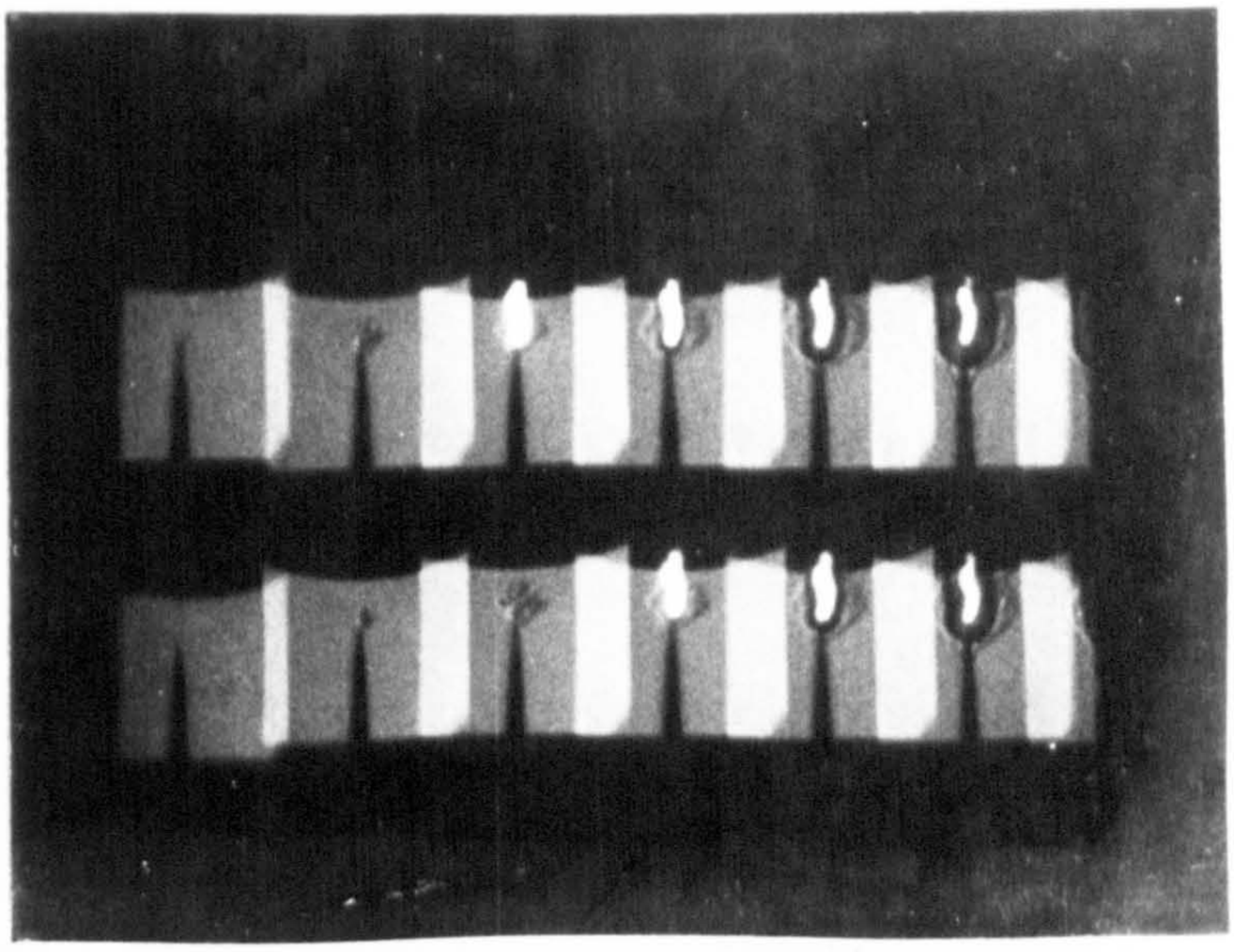

(a)

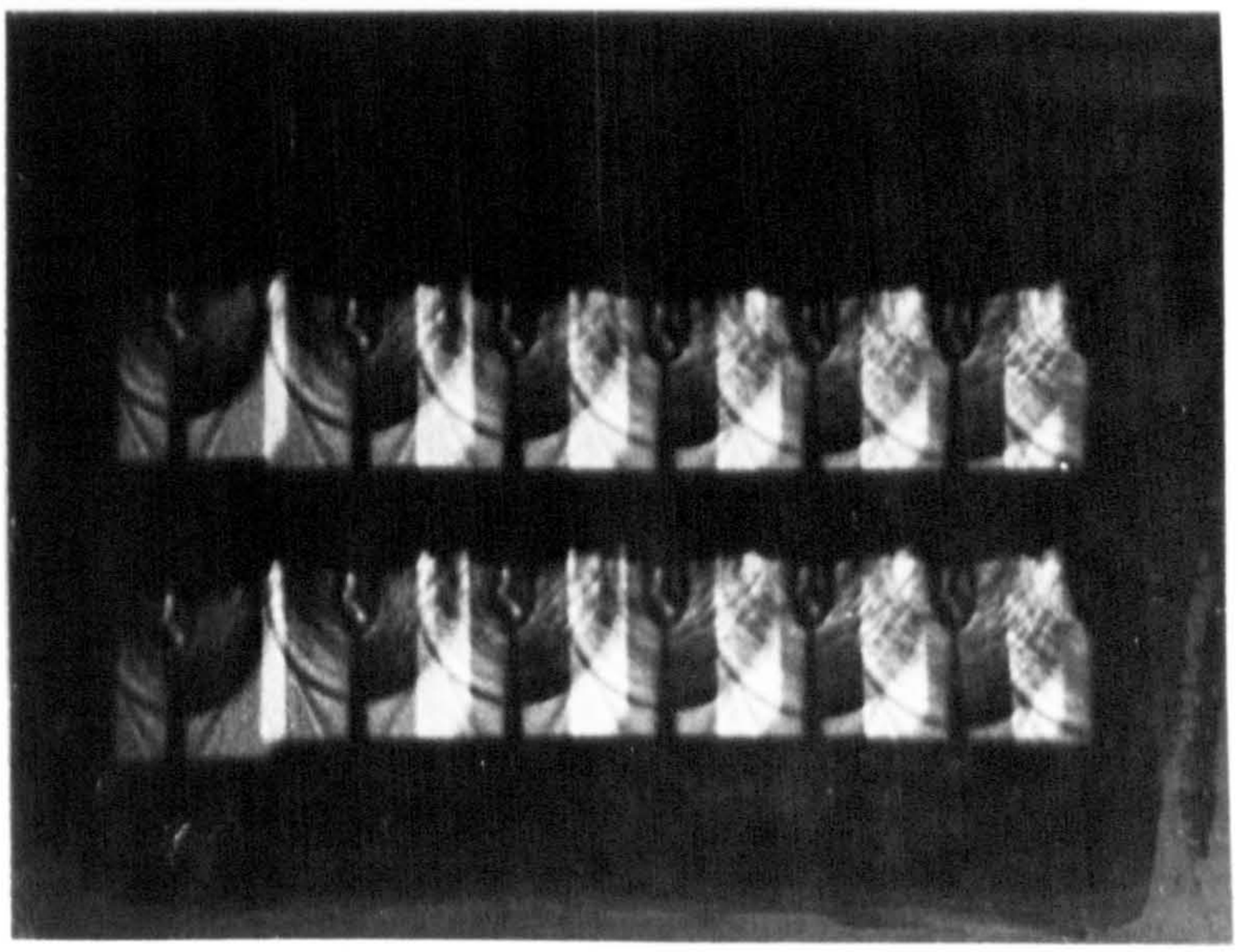

(b)

Plate 4.9 Point polarity: positive going step function.

Voltage amplitude: (a) 22 kV; (b) 22 kV applied 1μs prior to the first frame.

Liquid condition: high air content at 22°C and atmospheric pressure.

Temporal resolution: 100ns/frame.

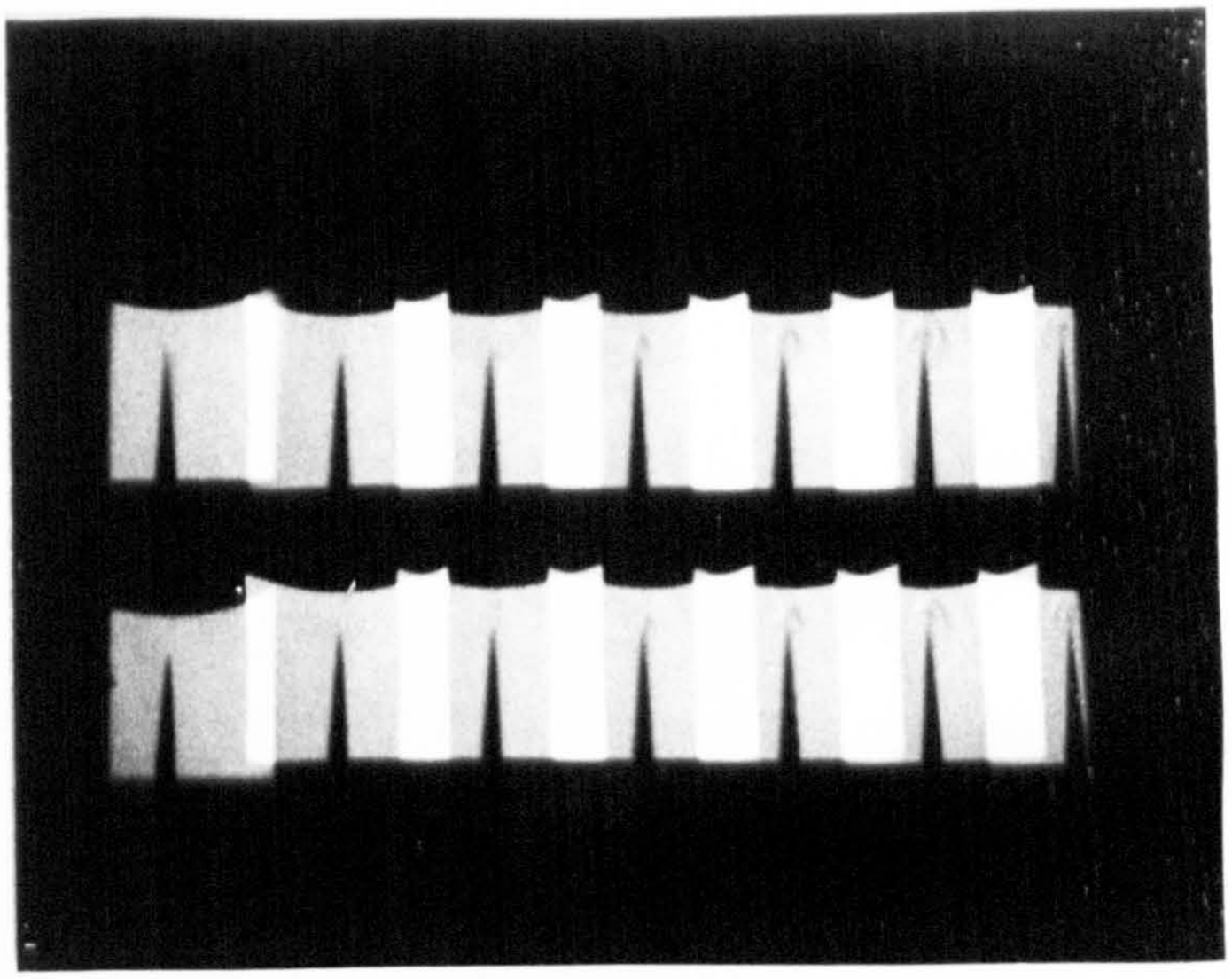

(a)

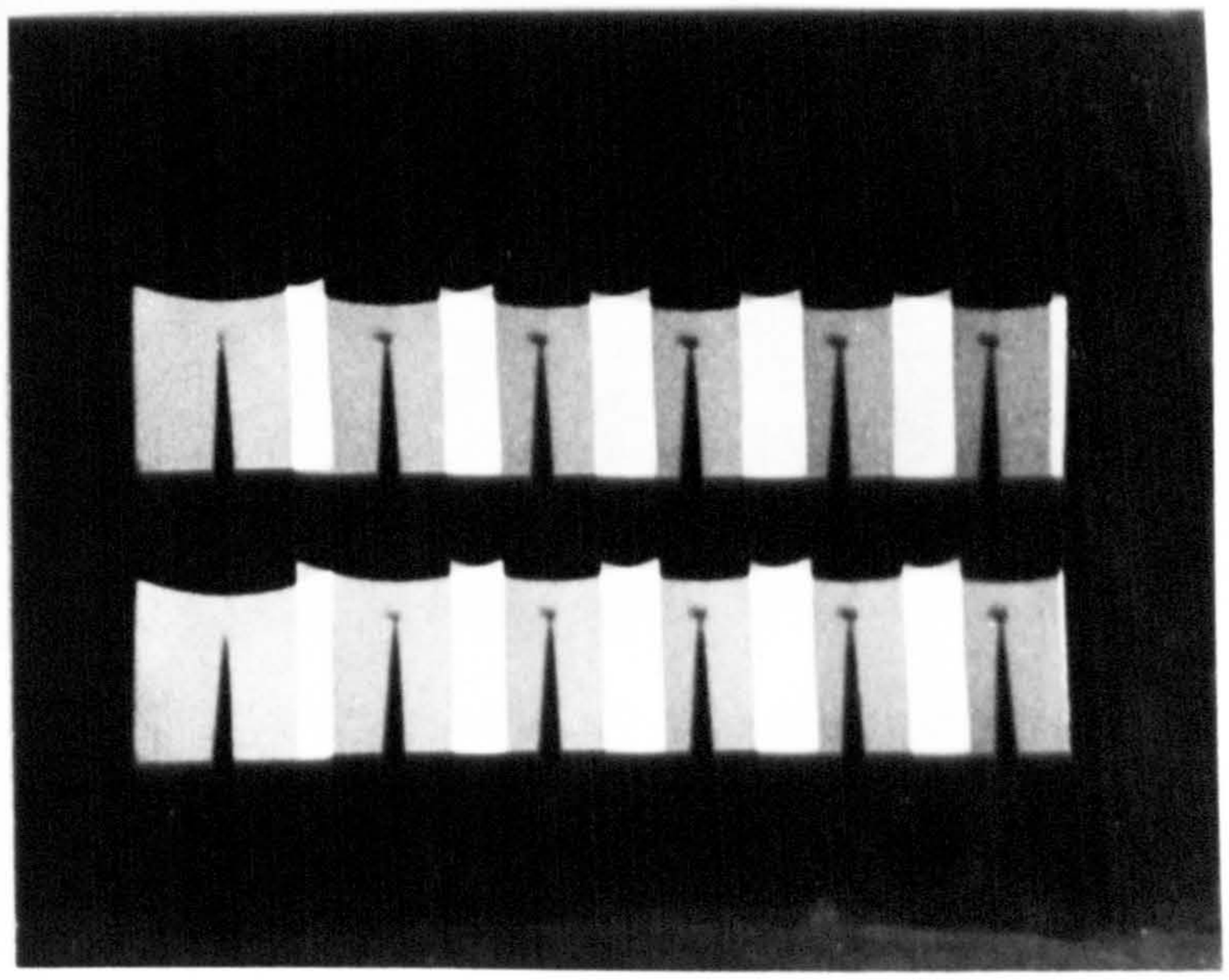

(b)

Plate 4.10 Point polarity: positive going step function, with negative pre-stress.

Voltage amplitude: 13 kV step, 10 kV pre-stress.

Liquid condition: high air content at 20°C and atmospheric pressure.

Temporal resolution: (a) 100ns/frame; (b) 2μs/frame.

similar voltages but at differing framing rates. At (a) the framing rate was 10^7 per second and the voltage was applied during the second frame. A disturbance appears at the seventh frame resembling the point centred shock wave of plate 4.2. The pre-breakdown phenomenon appears later and can be seen to form behind the advancing acoustic disturbance. At (b) the negative pre-stress was maintained at 10kV and the 13kV positive going step was applied at the first frame. The exposure was 5×10^5 per second and the event can be seen to exhibit little expansion over the entire record.

Choosing a positive point pre-stress also modifies the behaviour of the event. The record of plate 4.11(a) is little different from that of 4.9(a) except that breakdown occurs at a reduced voltage of 19kV. A further reduction in the step voltage to 13kV provides an extended time to breakdown in the presence of a positive pre-stress. Plate 4.11(b) shows the expanding event after step voltage application at the second frame. From this record it can be seen that the breakdown spark appears 8μs after the leading edge of the voltage step.

4.1.3 A dual point record

The hemispherical electrode was replaced by an etched tungsten wire to form a dual point geometry. Pre-breakdown disturbances were seen to propagate from the electrode to which the voltage step was applied. Plate 4.12(a) shows the event resulting from a 22kV negative

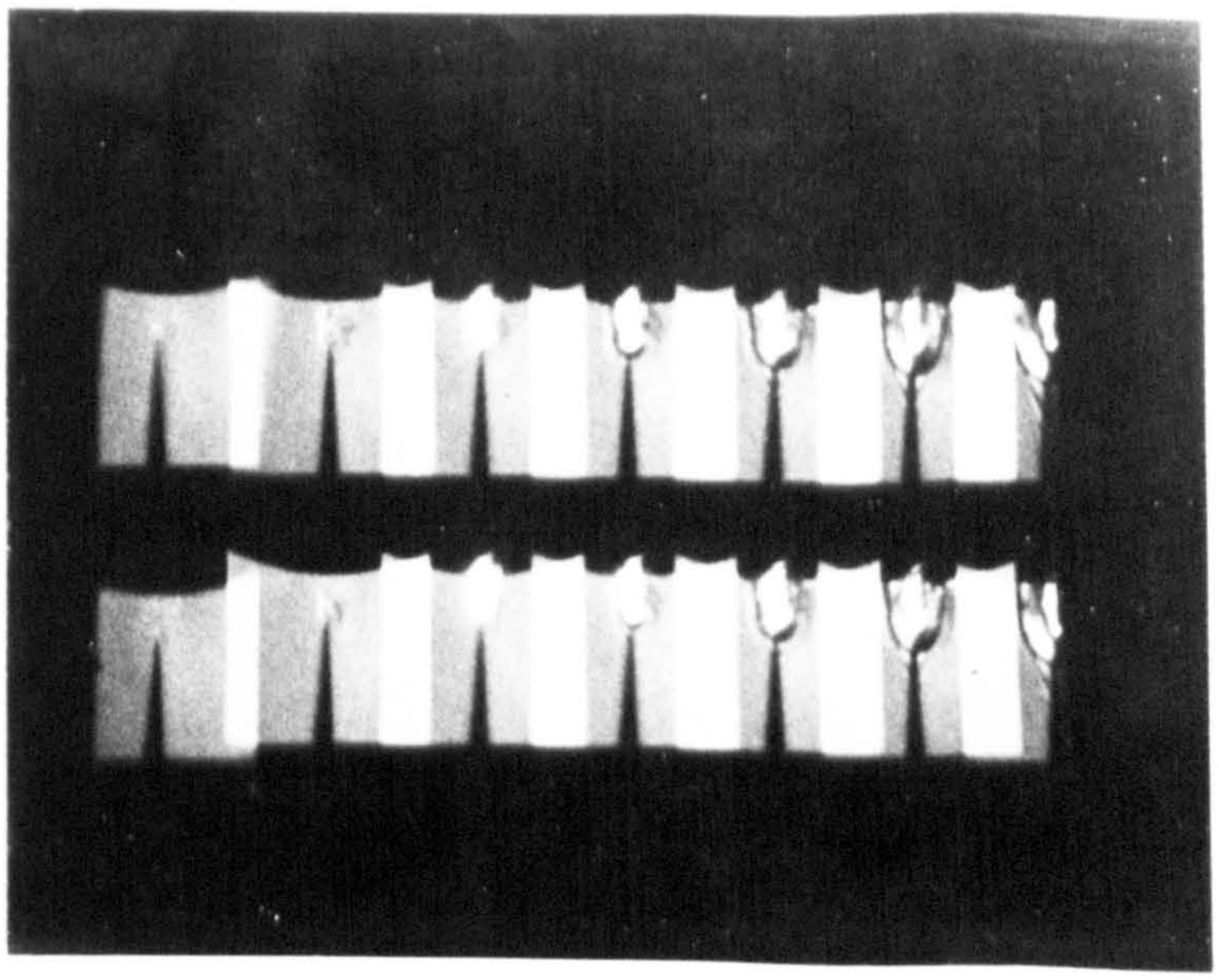

(a)

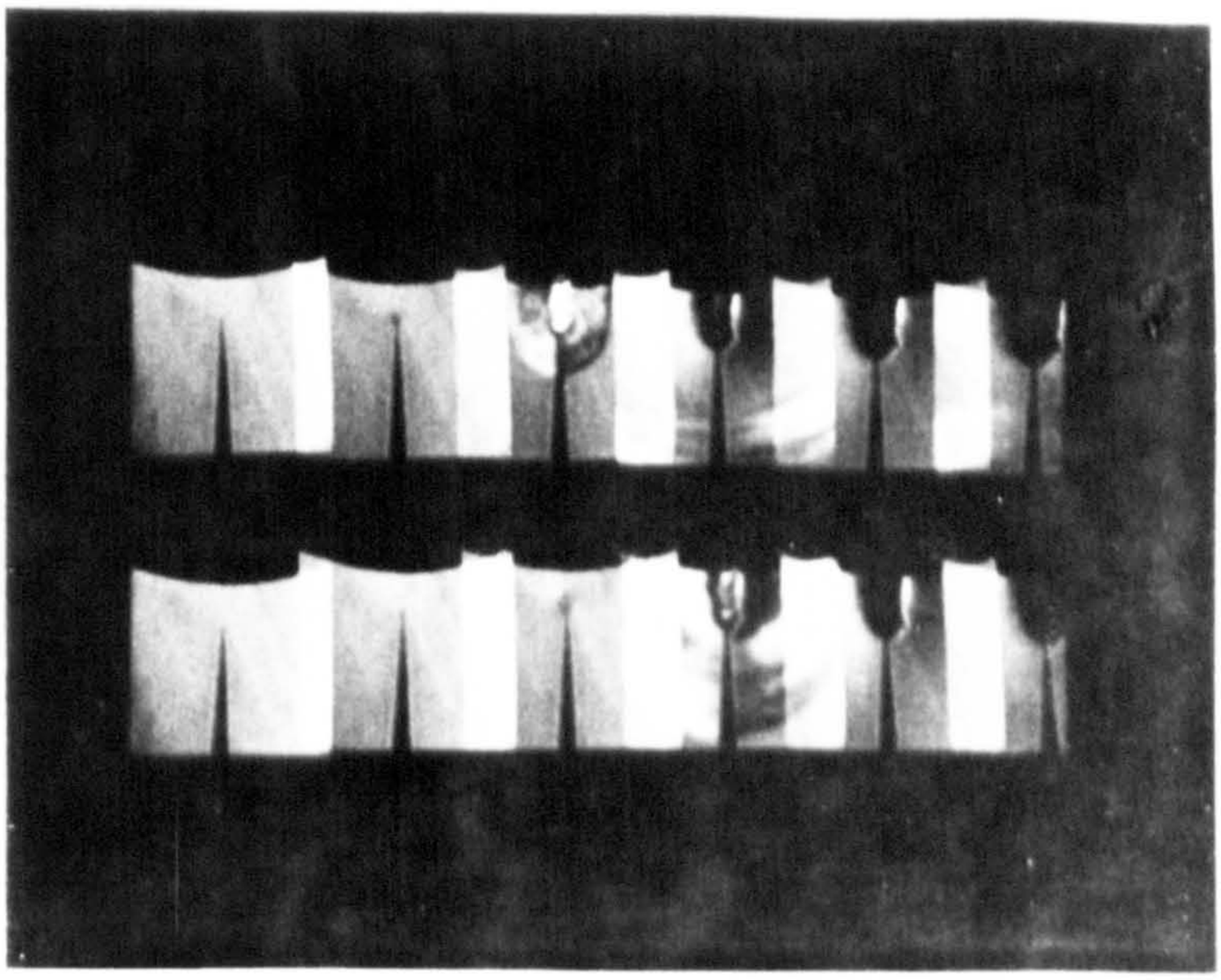

(b)

Plate 4.11 Point polarity: positive going step function, with positive pre-stress.

Voltage amplitude: (a) 19 kV step, 8 kV pre-stress; (b) 13 kV step, 8 kV pre-stress.

Liquid condition: high air content at 20^{o}C and atmospheric pressure.

Temporal resolution: (a) 100μs/frame; (b) 2μs/frame.

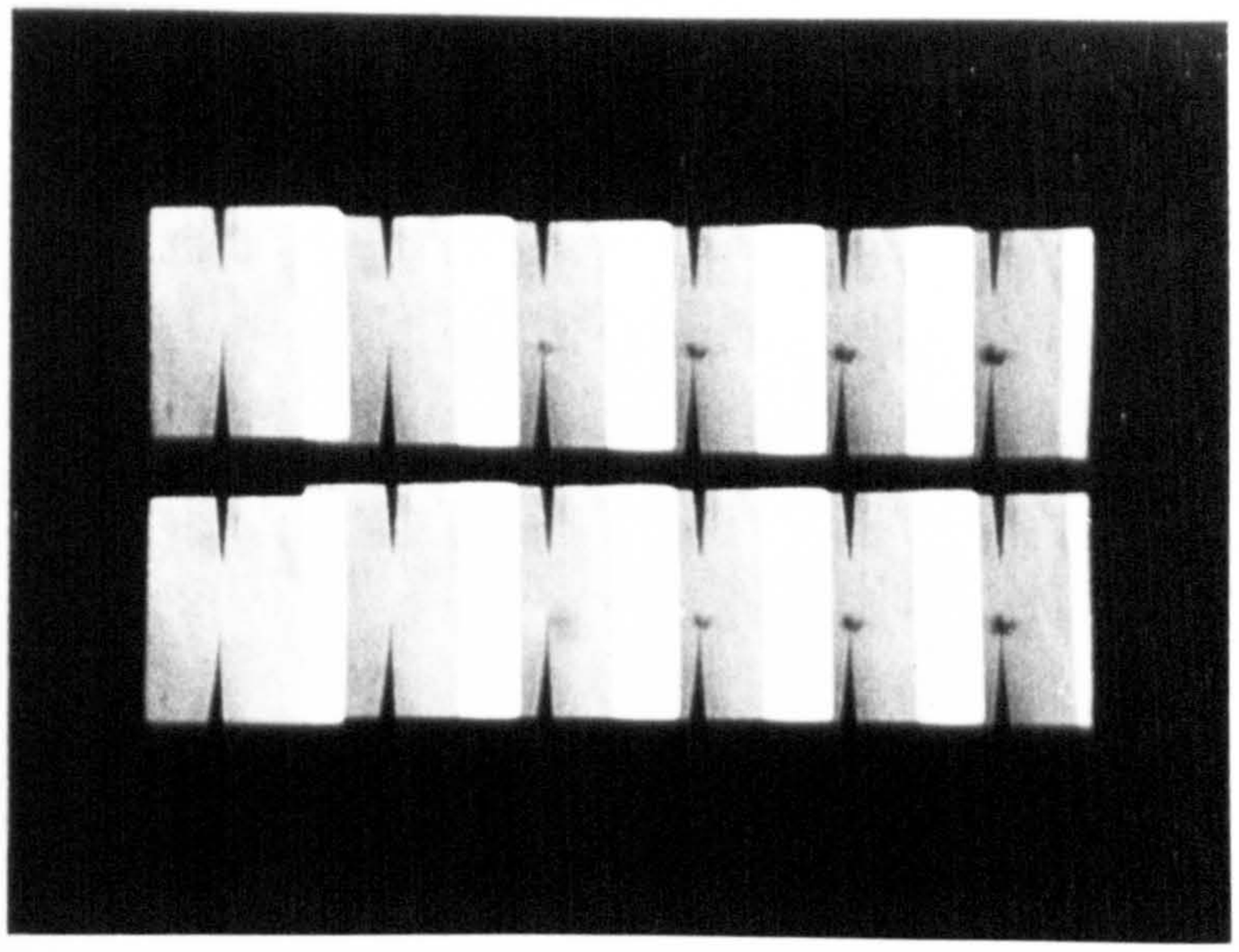

(a)

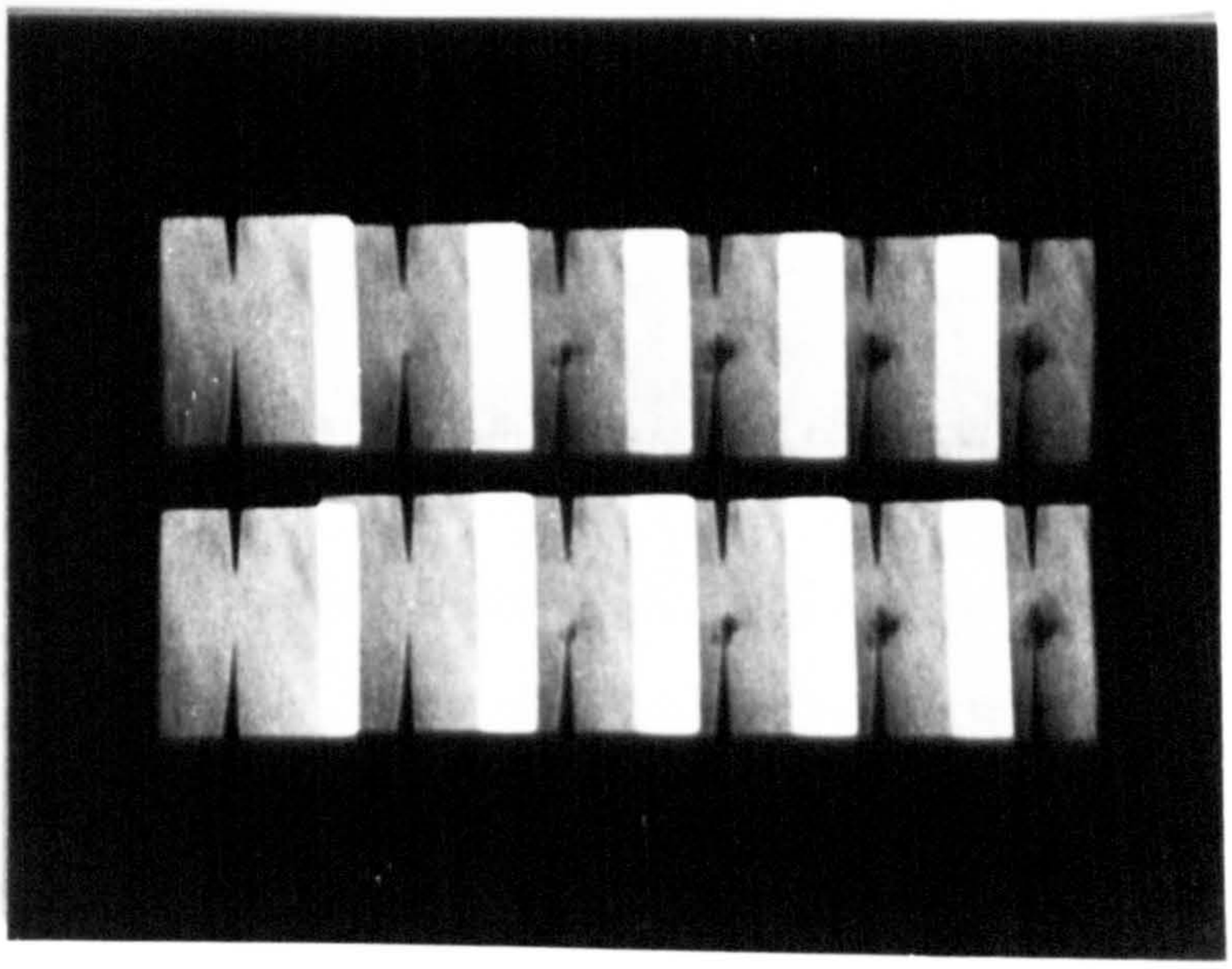

(b)

Plate 4.12 Voltage polarity: (a) negative going; (b) positive going step function.

Voltage amplitude: (a) 22 kV; (b) 19 kV.

Liquid condition: high air content 20°C at atmospheric pressure.

Temporal resolution: 2μs/frame.

step applied to the lower electrode at the fourth frame. For a voltage reversal, plate 4.12(b) shows a disturbance similar in both appearance and propagation velocity which results from the application of a 19kV step at the third frame. The rate of expansion of the region is much reduced compared with the positive point to hemisphere situation depicted by plate 4.9. The test gap was subjected to a direct voltage pre-stress an hour prior to a step voltage trial. It can be seen from plate 4.13 that the shape of the event is modified by the direct stress and is polarity dependent. At (a) a 25kV negative going step was applied in the presence of a negative pre-stress to the same electrode. It can be seen that the pre-stress inhibits progress towards the earthed electrode by inducing a concave profile. Applying a pre-stress of the opposite polarity appears to radially constrict the volume of the disturbance along the electrode axis. Plate 4.13(b) typifies this situation, where a negative going step was applied at the fourth frame of the record.

4.2 Direct Photography of Stress Induced Events

4.2.1 Scattered light photography

Direct macrophotography of the light scattered orthogonally by the pre-breakdown disturbance was undertaken. This produced an enhanced image definition compared with that available from the Schlieren technique. Illumination was provided by a xenon flash of 2μs duration which allowed sufficient film exposure to be coupled with

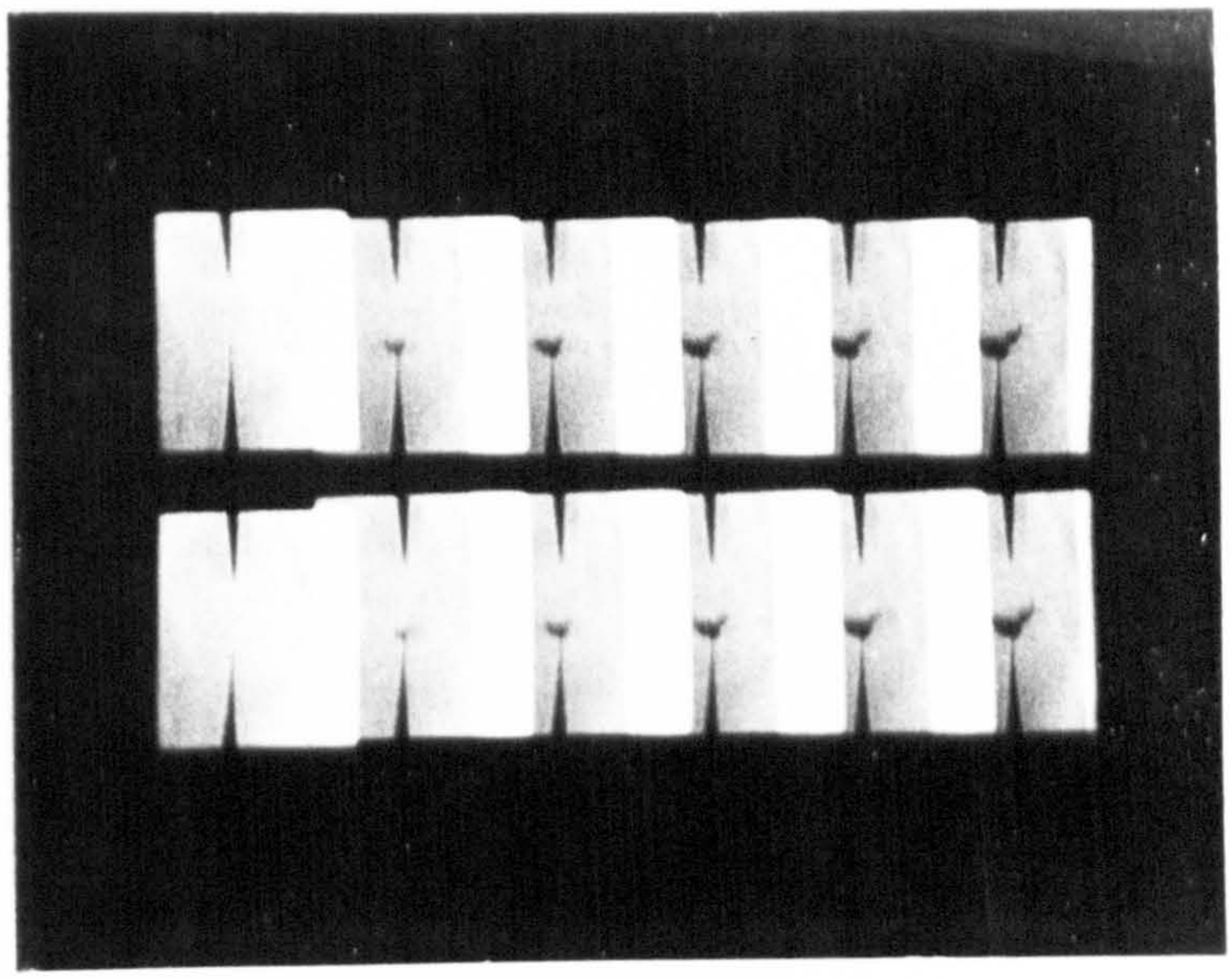

(a)

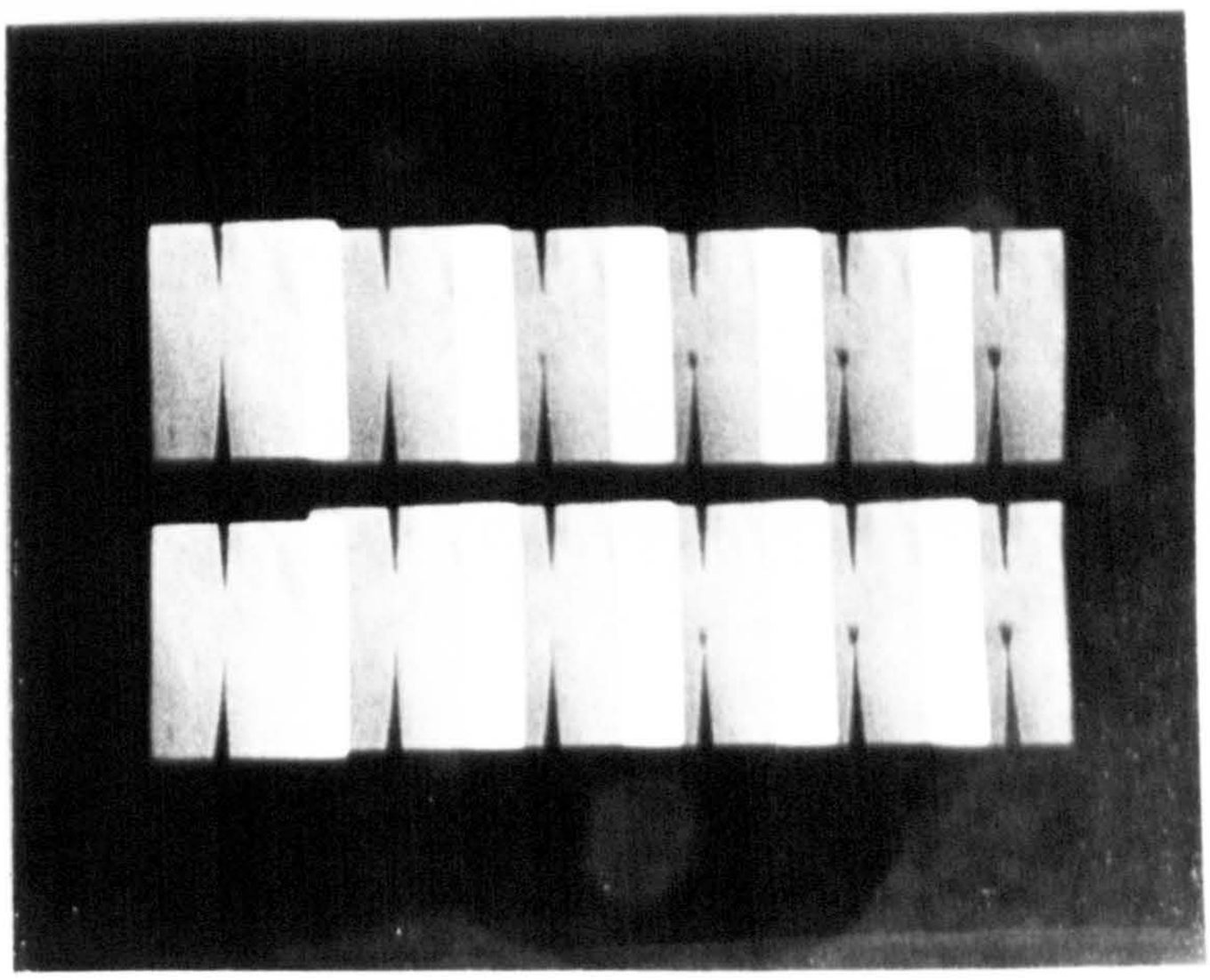

(b)

Plate 4.13 Voltage polarity: negative going step function with pre-stress.

Voltage amplitude:
(a) 25 kV step, 10 kV negative pre-stress.
(b) 20 kV step, 10 kV positive pre-stress.

Liquid condition: high air content at 20°C and atmospheric pressure.

Temporal resolution: 2μs/frame.

capture of the dynamic event, after the initial rapid growth phase. Plates 4.14 to 4.29 are enlargements taken from the original 127 x 102mm negatives. For plates 4.14 to 4.22 a 25kV negative going step was applied to a 2mm point-to-sphere test gap immersed in n-hexane. The filtered liquid was in equilibrium with air at atmospheric pressure and room temperature. A representative sequence depicting propagation of the pre-breakdown event was constructed by taking single photographs at pre-determined delays from voltage application.

A light scattering disturbance can be seen to form within the first 5μs of voltage application, as shown by plates 4.14 and 4.15(a); the appearance of the event may be identified with that seen utilising the Schlieren technique for plates 4.1 to 4.5. After 20μs this region begins to fragment at the extremities of the disturbance as can be seen from plate 4.15(b) when viewing the event 80μs after voltage application. Plate 4.16(a) indicates the presence of discrete light scattering regions. The regions appear as isolated bubbles that separate and disperse away from the point electrode. A new distribution is evident after 300μs when it can be seen that there is no longer a continuous light scattering zone in the centre of the disturbance, as shown by plate 4.16(b). Viewing the test gap 700μs from voltage application, plate 4.17(a) reveals the presence of a conical light scattering region at the tip of the point electrode and a general spherical distribution of bubbles extending into the centre of the gap.

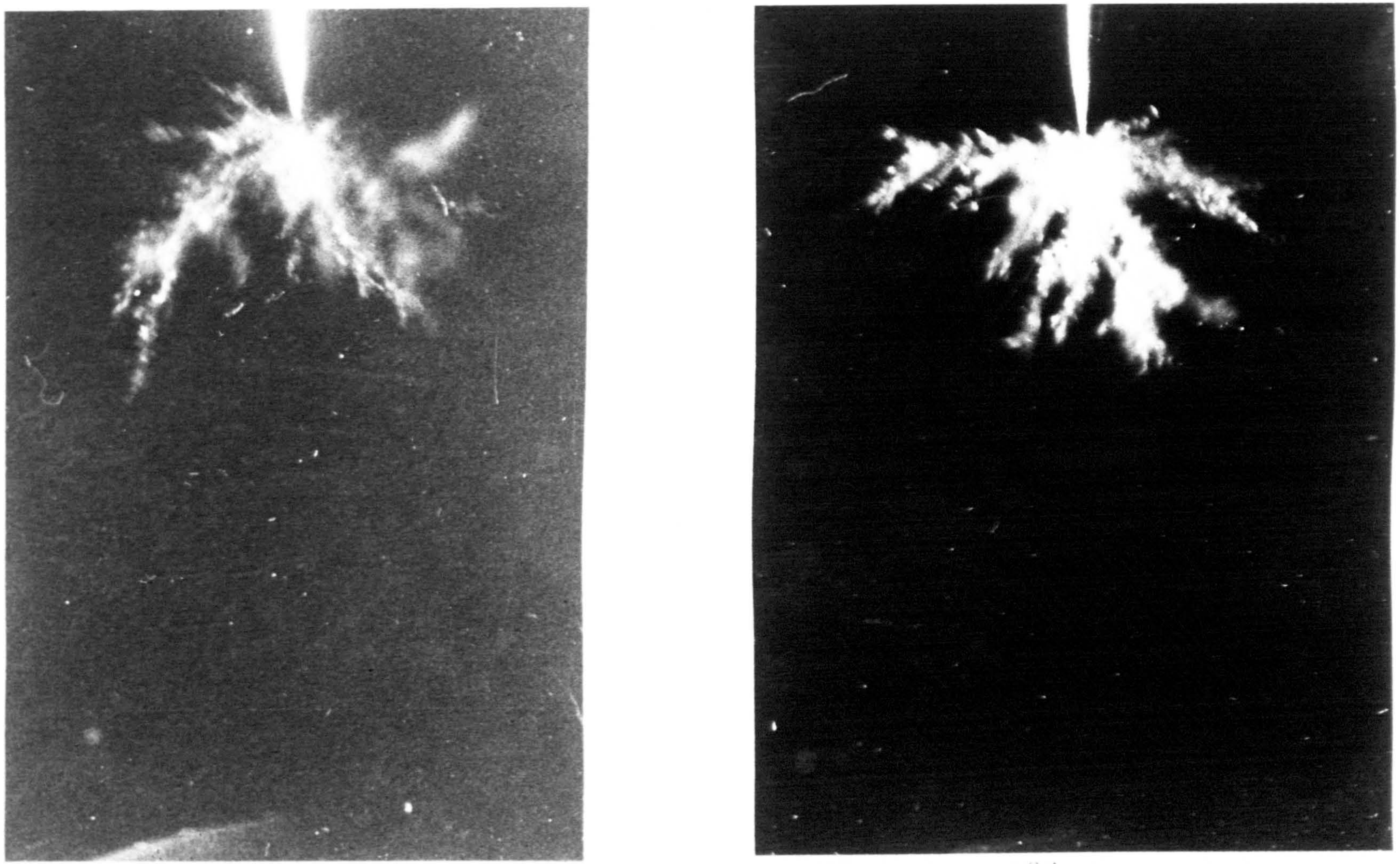

(a) (b)

Plate 4.14 Scattered light records, taken (a) coincident and (b) 2μs after step voltage application. Voltage: 25kV, negative point polarity. Liquid: n-hexane. Gap: 2mm.

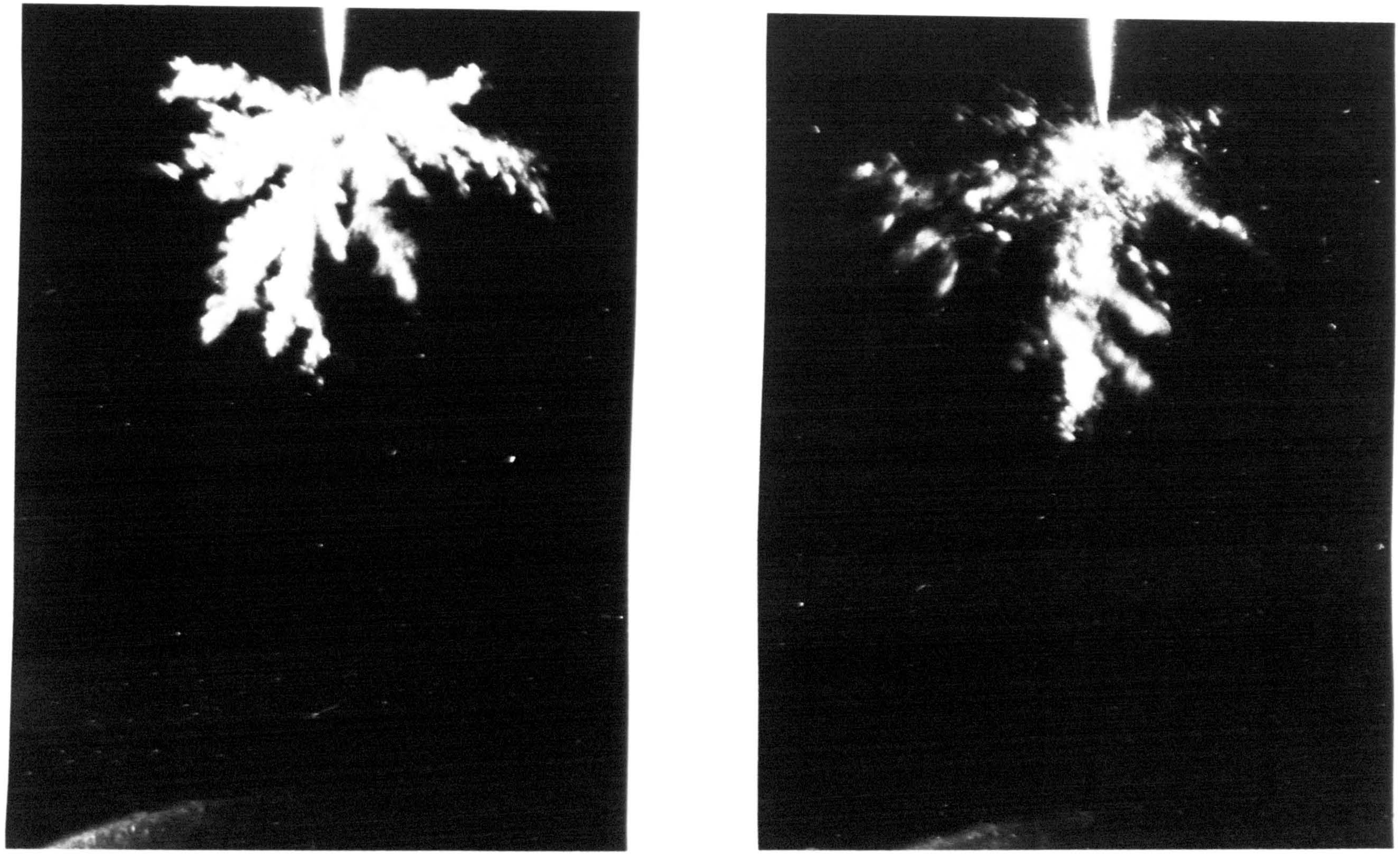

(a) (b)

Plate 4.15 Scattered light records, taken (a) 5μs and (b) 20μs after step voltage application. Voltage: 25kV, negative point polarity. Liquid: n-hexane. Gap: 2mm.

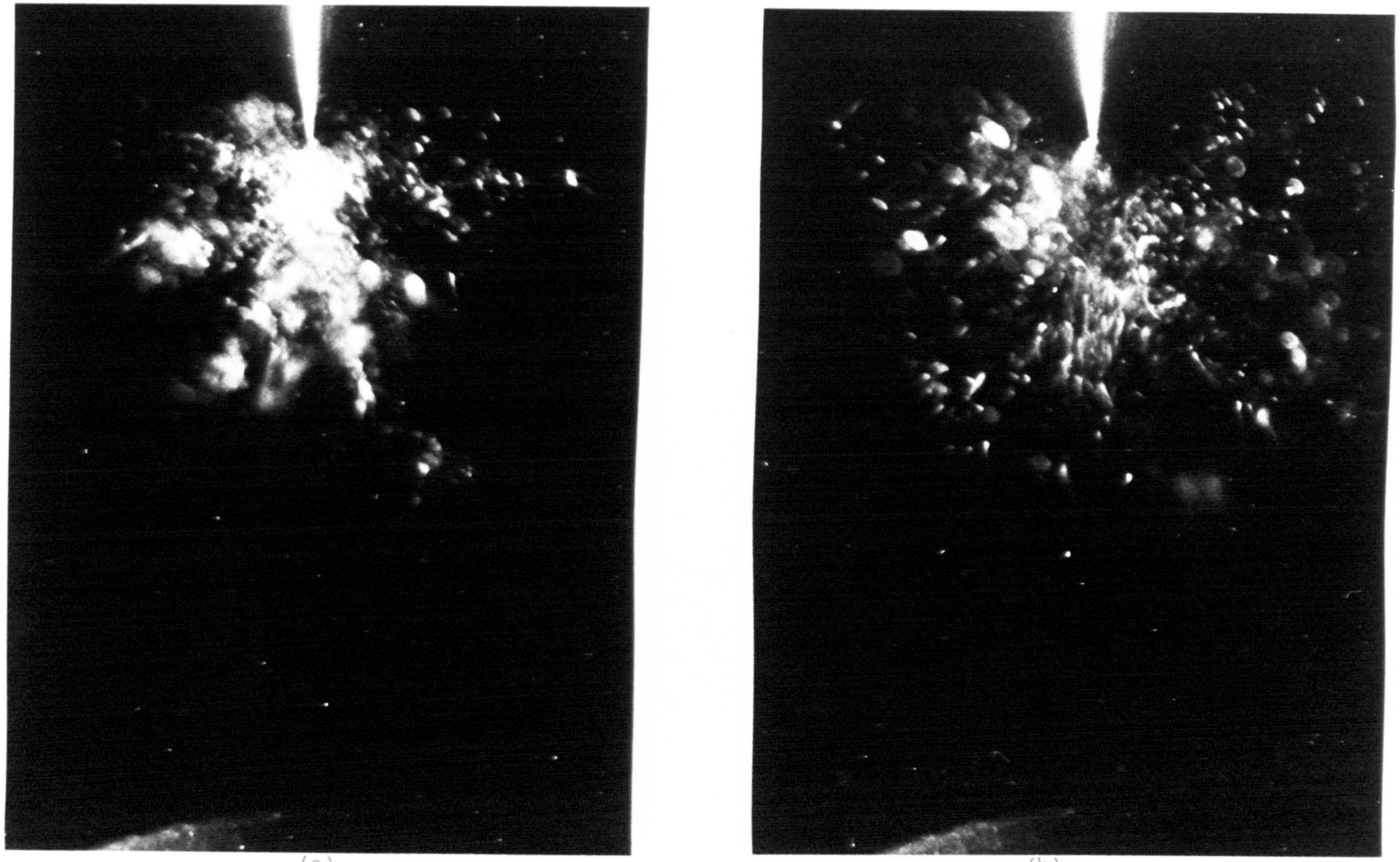

(a) (b)

Plate 4.16 Scattered light records, taken (a) 80μs and (b) 300μs after step voltage application. Voltage: 25kV, negative point polarity. Liquid: n-hexane. Gap: 2mm.

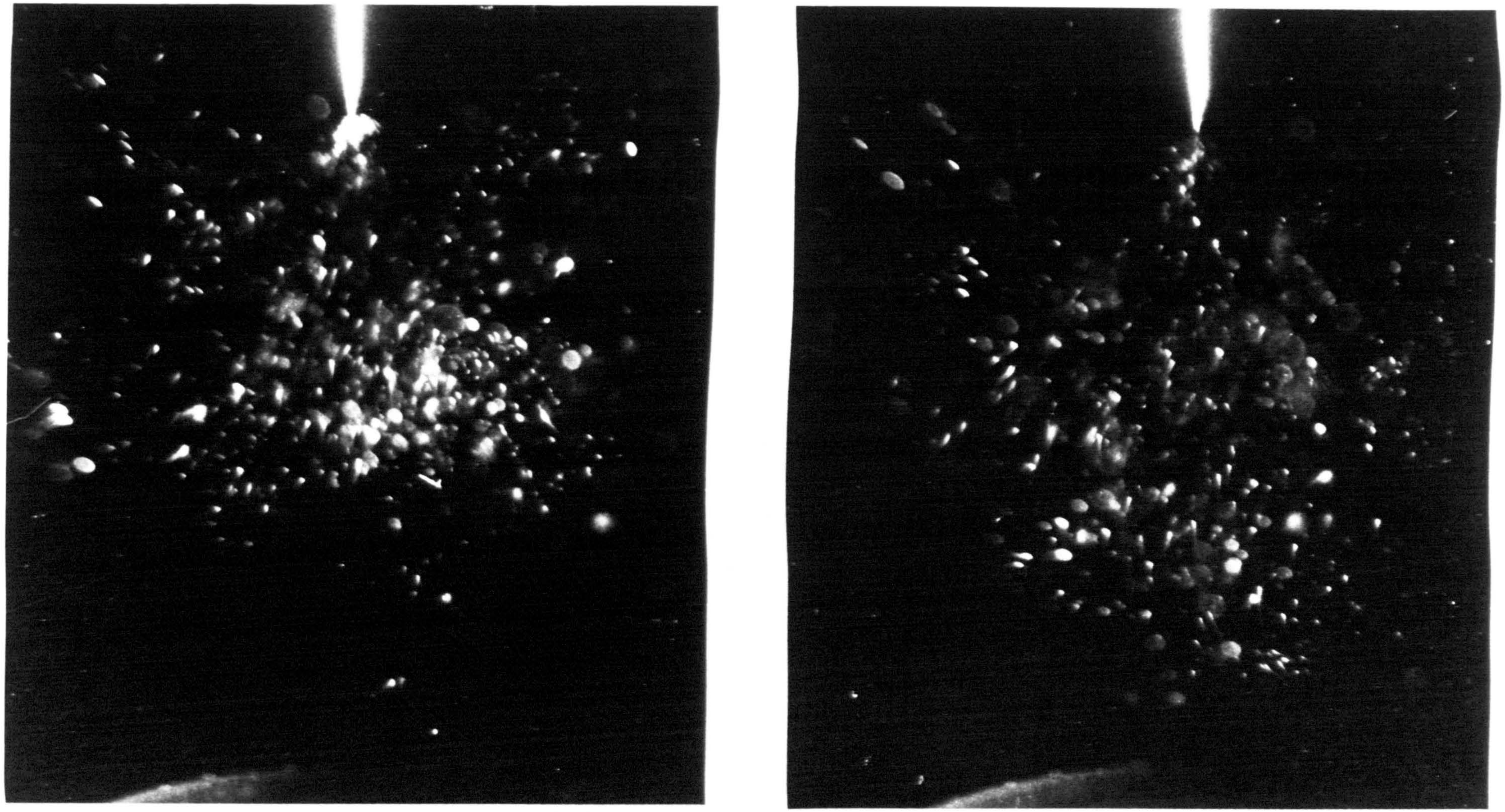

(a) (b)

Plate 4.17 Scattered light records, taken (a) 700μs and (b) 800μs after step voltage application. Voltage: 25kV, negative point polarity. Liquid: n-hexane. Gap: 2mm.

The formation of the disturbance changes as the earthed electrode is approached. Plate 4.17(b) shows a distortion of the spherical distribution as the bubbles stream toward the earthed sphere, along the electrode axis. The bubbles begin to deflect around the surface of the sphere after a delay of 820μs from voltage application, as shown by plate 4.18. After 1.4ms the bubbles begin to disperse throughtout the liquid and leave the mid gap position, as depicted by plate 4.19. Beyond 2ms a direct voltage situation is approached and the disturbance takes on a conical distribution throughout the gap, with the apex at the point electrode. Bubbles appear to stream from the point cathode across the gap and around the anode, as shown by plates 4.20, 4.21 and 4.22; supporting observations made by Mirza et al[25].

Retaining the same electrodes and test liquid a positive going step voltage was applied to the tungsten point. Plate 4.23(a) shows the formation of pre-breakdown bubbles 60μs after voltage application. At (b) a similar situation exists after 90μs. It is evident from plate 4.23(b) that the gap may be spanned by a string of bubbles without the advent of a breakdown spark. After an extended delay of 1ms the bubbles assume a spherical distribution throughout the test gap as shown by plate 4.24.

Step voltage tests were performed using liquid paraffin in place of the n-hexane sample. Choosing the point electrode as the cathode, 30kV was applied to the

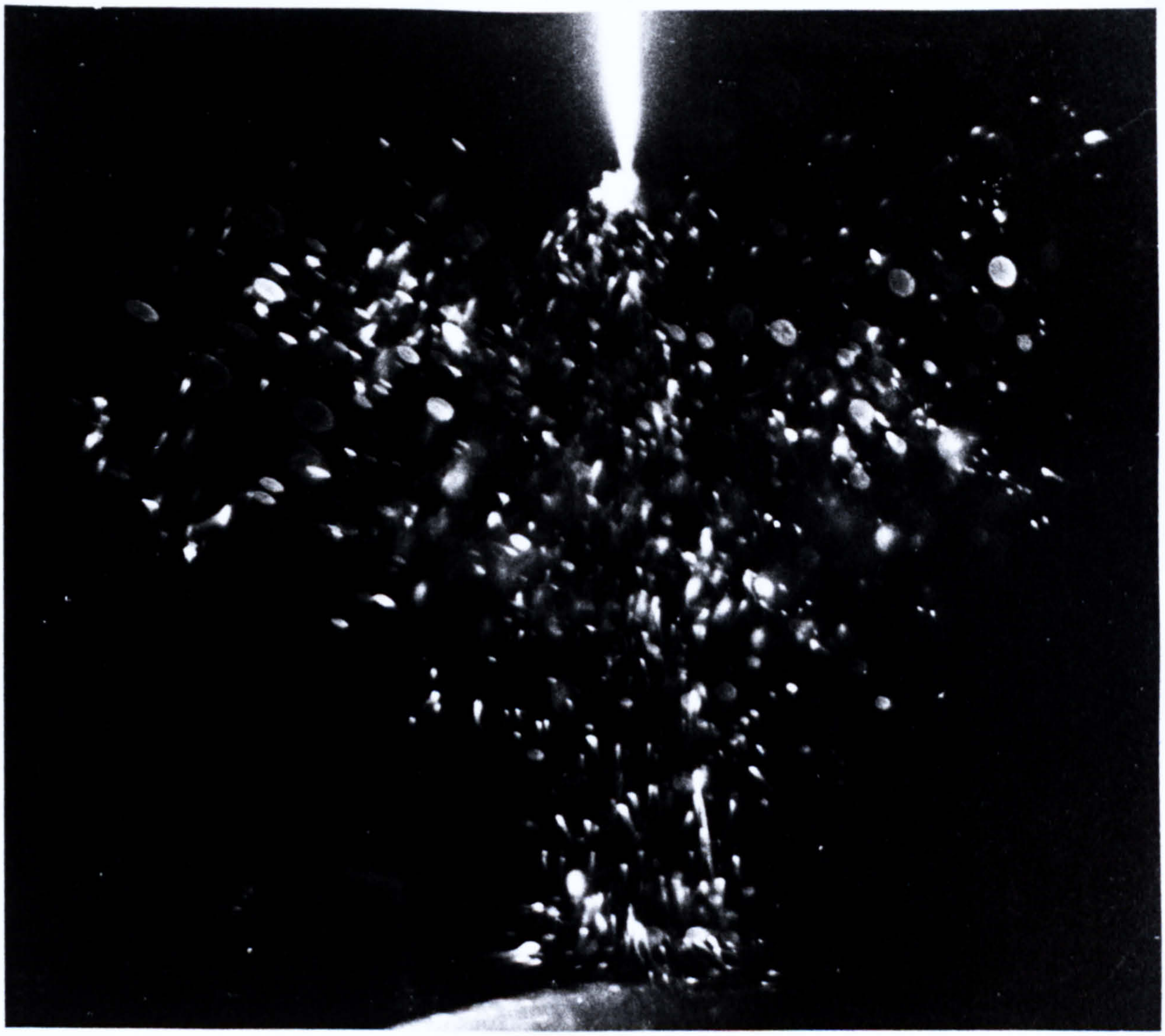

Plate 4.18 Scattered light record taken 820μs after step voltage application. Voltage: 25kV, negative point polarity. Liquid: n-hexane. Gap: 2mm.

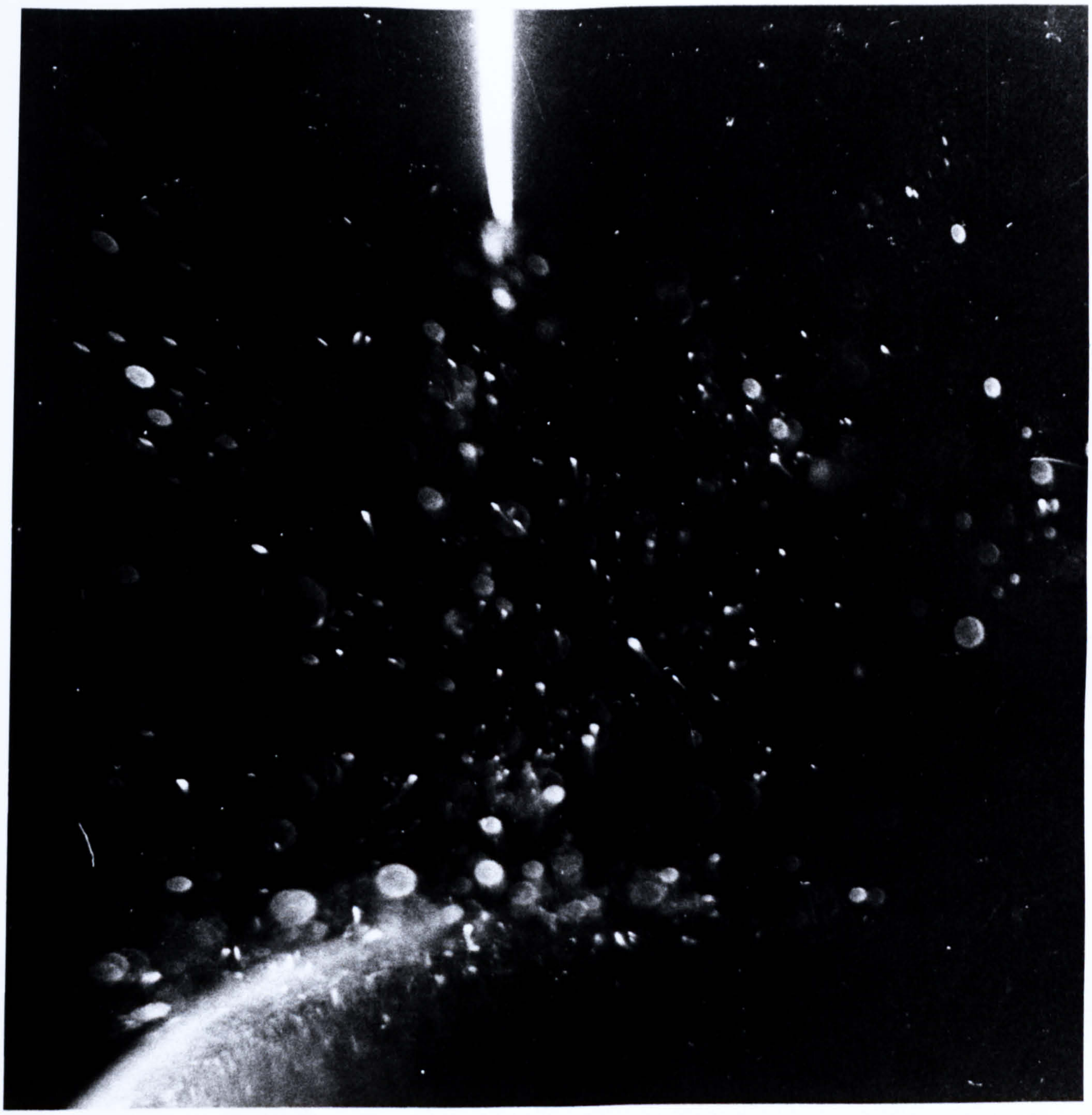

Plate 4.19 Scattered light record taken 1.4ms after step voltage application. Voltage: 25kV, negative point polarity. Liquid: n-hexane. Gap: 2mm.

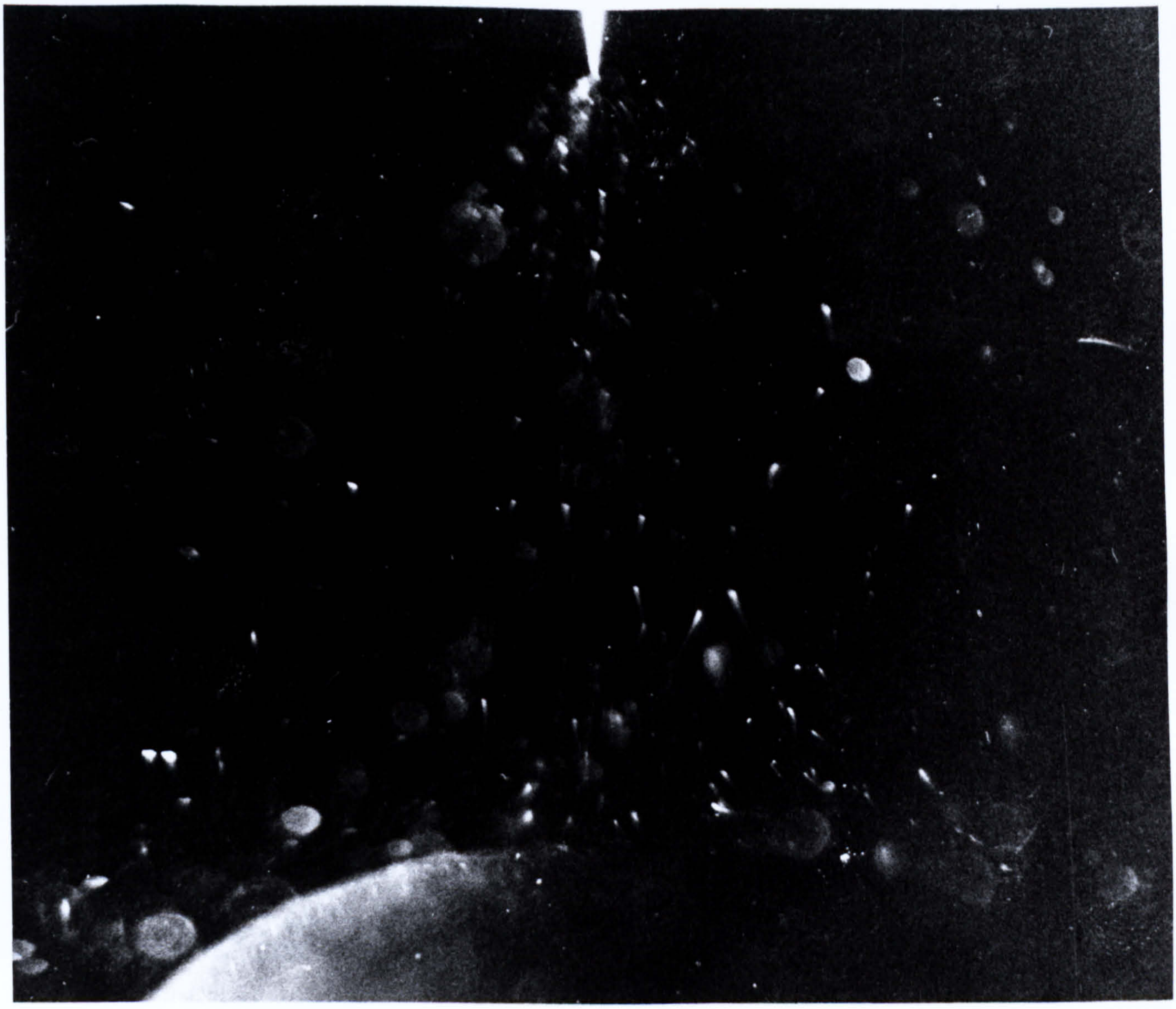

Plate 4.20 Scattered light record taken 2.2ms after step voltage application. Voltage: 25kV, negative point polarity. Liquid: n-hexane. Gap: 2mm.

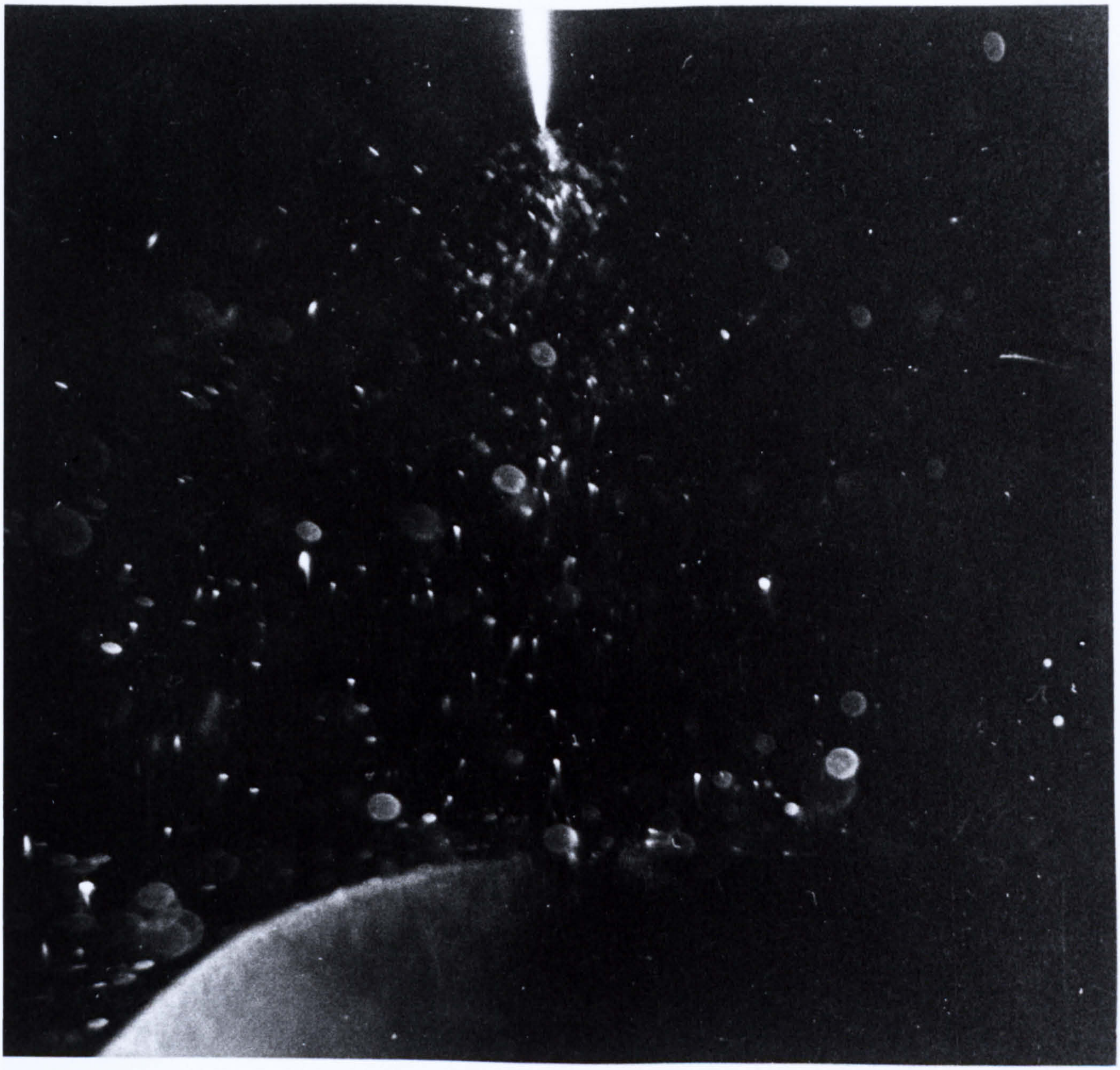

Plate 4.21 Scattered light record taken 2.5ms after step voltage application. Voltage: 25kV, negative point polarity. Liquid: n-hexane. Gap: 2mm.

Plate 4.22 Scattered light record taken 4ms after step voltage application. Voltage: 25kV, negative point polarity. Liquid: n-hexane. Gap: 2mm.

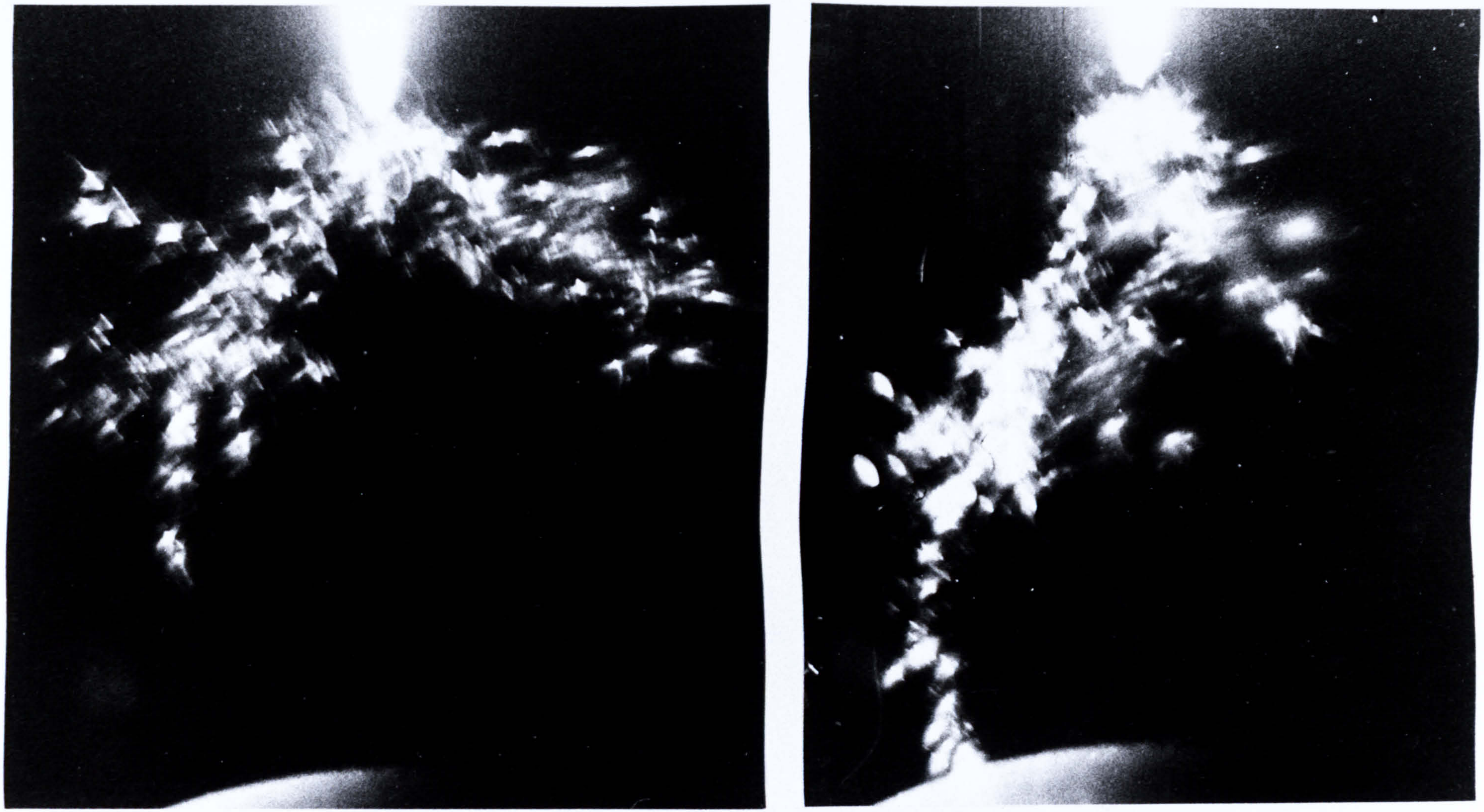

(a) (b)

Plate 4.23 Scattered light records taken (a) 60μs and (b) 90μs after step voltage application. Voltage: 20kV, positive point polarity. Liquid: n-hexane. Gap: 2mm.

Plate 4.24 Scattered light record taken 1ms after step voltage application. Voltage: 20kV, positive point polarity. Liquid: n-hexane. Gap: 2mm.

1.3mm gap. Tests were performed at 22°C and the oil sample was in equilibrium with air at atmospheric pressure. Sequence representation was again achieved by the selection of events from single shot records possessing differing time delays from voltage application.

The formation and propagation of the pre-breakdown event appeared to be essentially similar to that seen for n-hexane with the exception of the generation of larger bubbles during the initiating stage. Plate 4.25(a) shows branching and bubble formation 15μs after a 30kV negative going step was applied to the point electrode. A record taken after 38μs reveals the onset of fragmentation as presented by plate 4.25(b). It can be seen from plate 4.26(a) that after 200μs the bubbles in the gap stream towards the spherical anode. Finally, after 2.4ms, plate 4.26(b) depicts the situation where the bubbles have dispersed throughout the gap. Comparing this result with the records for n-hexane it is evident that for liquid paraffin there are fewer bubbles present in the gap, particularly in the final stages of the event.

4.2.1.1 The influence of temperature elevation

Elevated temperature experiments were performed on both n-hexane and liquid paraffin. Plate 4.27(a) shows a pre-breakdown disturbance in n-hexane at 60°C, 3μs after the application of a negative step voltage to the point electrode. The photograph shows a formation that extends a considerable distance into the gap and is less well

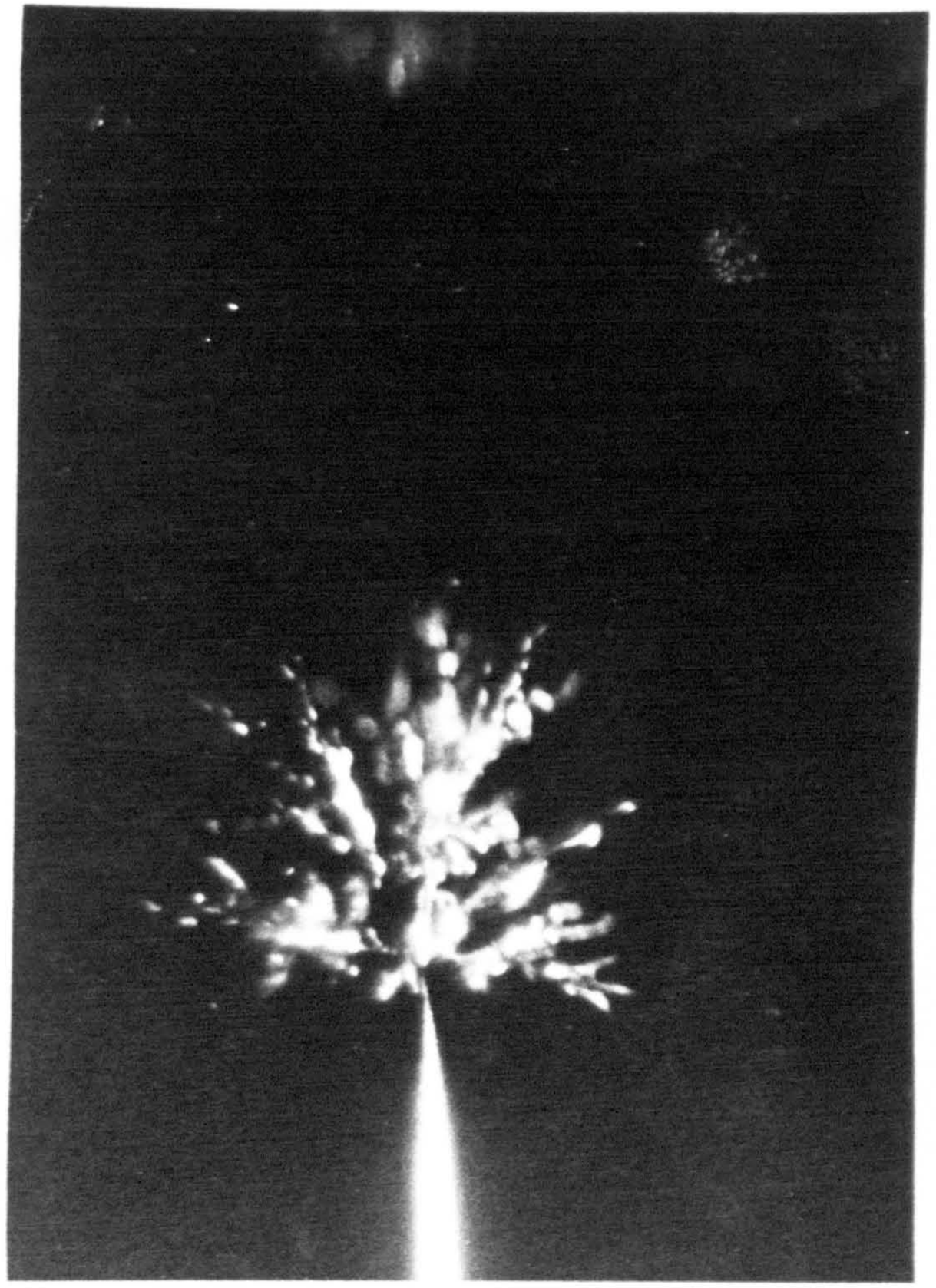

(a)

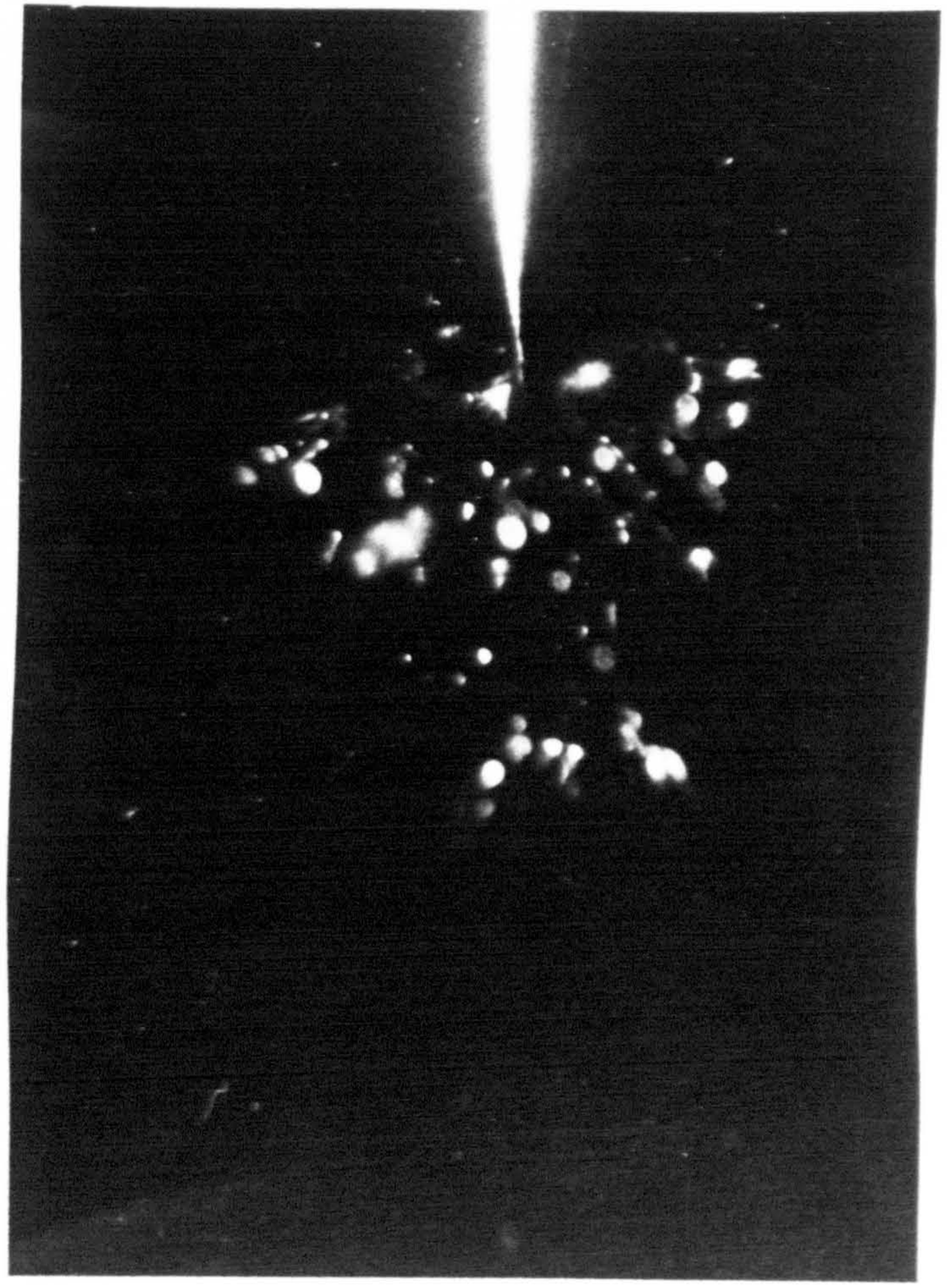

(b)

Plate 4.25 Scattered light records taken (a) 15μs and (b) 38μs after step voltage application. Voltage: 30kV, negative point polarity. Liquid: liquid paraffin. Gap: 1.5mm.

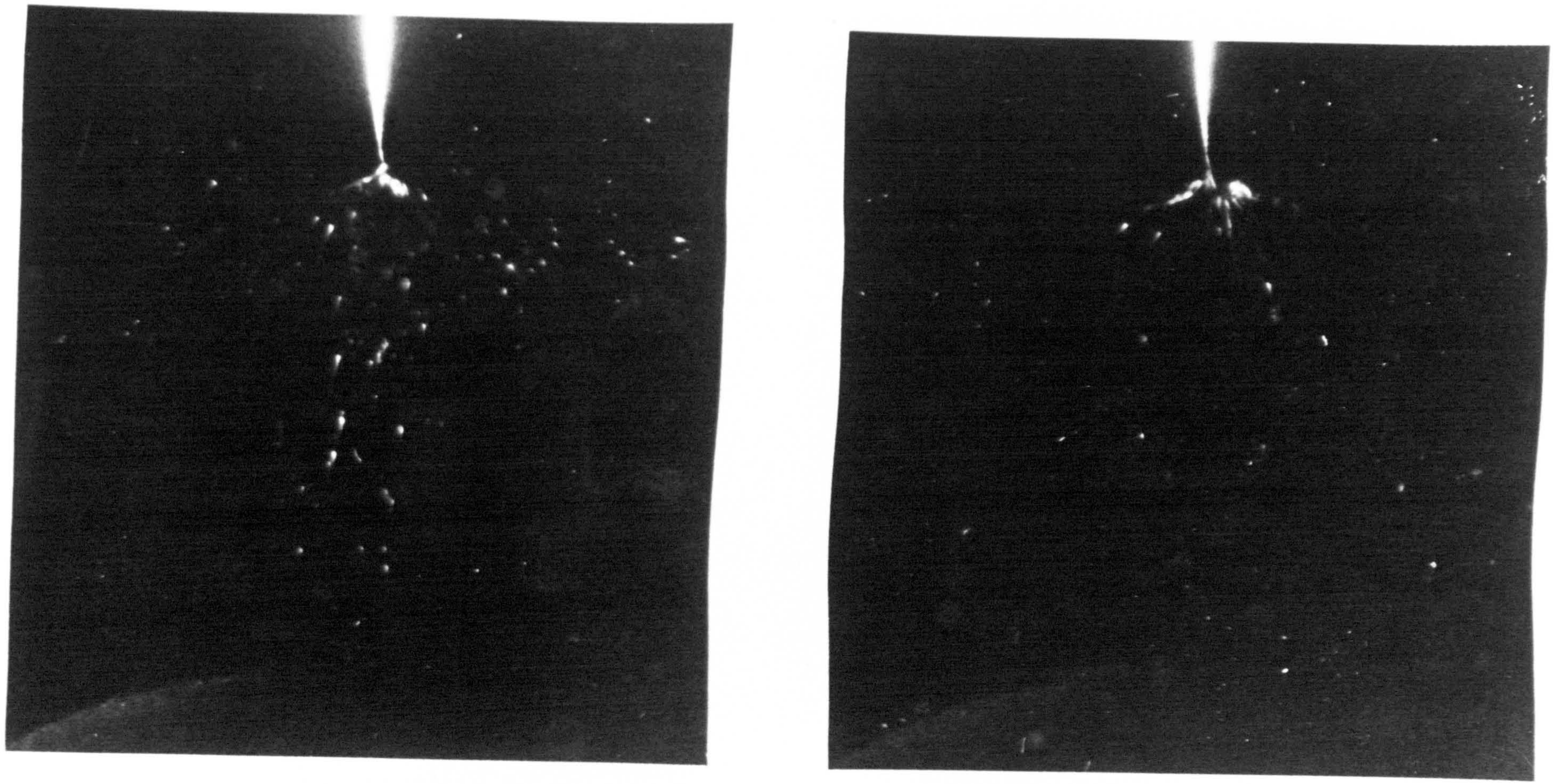

(a) (b)

Plate 4.26 Scattered light records taken (a) 200μs and (b) 2.4ms after step voltage application. Voltage: 30kV, negative point polarity. Liquid: liquid paraffin. Gap: 1.5mm.

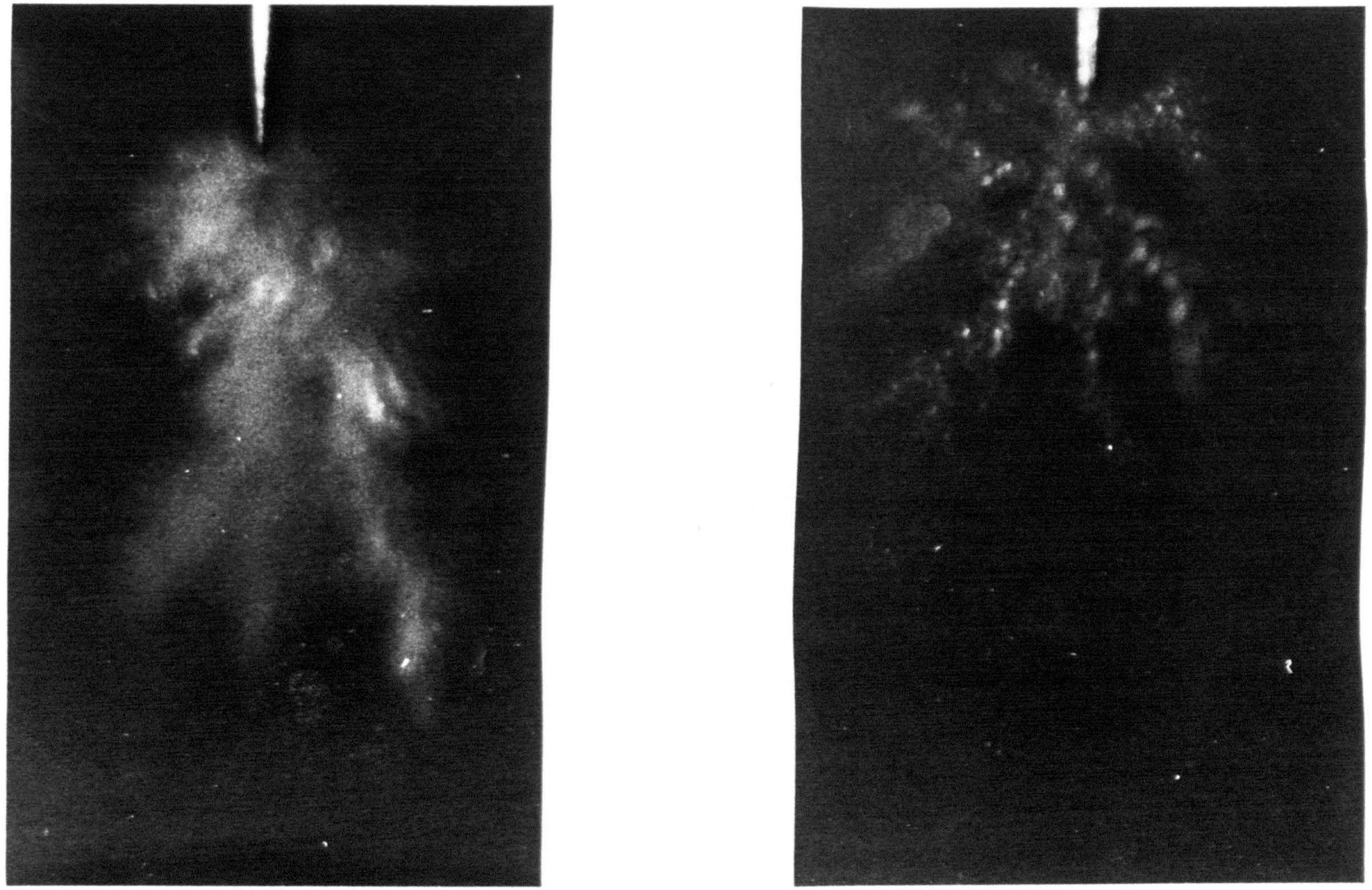

(a) (b)

Plate 4.27 Scattered light records taken (a) 3μs and (b) 10μs after step voltage application. Voltage 25kV, negative point polarity. Liquid: (a) n-hexane at 60°C; (b) liquid paraffin at 66°C. Gap: 2mm.

defined than that seen at room temperature. Liquid paraffin exhibits a similar tendency at 66°C, although some discrete bubbles are evident in plate 4.27(b).

4.2.1.2 Breakdown

Plates 4.28 and 4.29 show negative point breakdown situations in liquid paraffin and n-hexane respectively, flashlight photographs were taken at the instant of breakdown for each case. A continuous breakdown channel for liquid paraffin at 16°C is shown by plate 4.28(a). At 66°C the self luminous spark possesses a discontinuity in the centre of the gap, and small discrete bubbles are evident around the breakdown channel from plate 4.28(b). For n-hexane at 26°C, plate 4.29(a) shows a break in the spark discharge, but several discontinuities are visible at 60°C as shown by plate 4.29(b).

4.2.2 A non-illuminated observation

Applying a negative direct voltage to the point electrode a 30 second exposure was made without background lighting. A self luminous region near the tip of the point electrode can be seen from plate 4.30. The shape of the light emitting cone appears to be similar to the region located nearest the point electrode in the scattered light photographs 4.16 to 4.22.

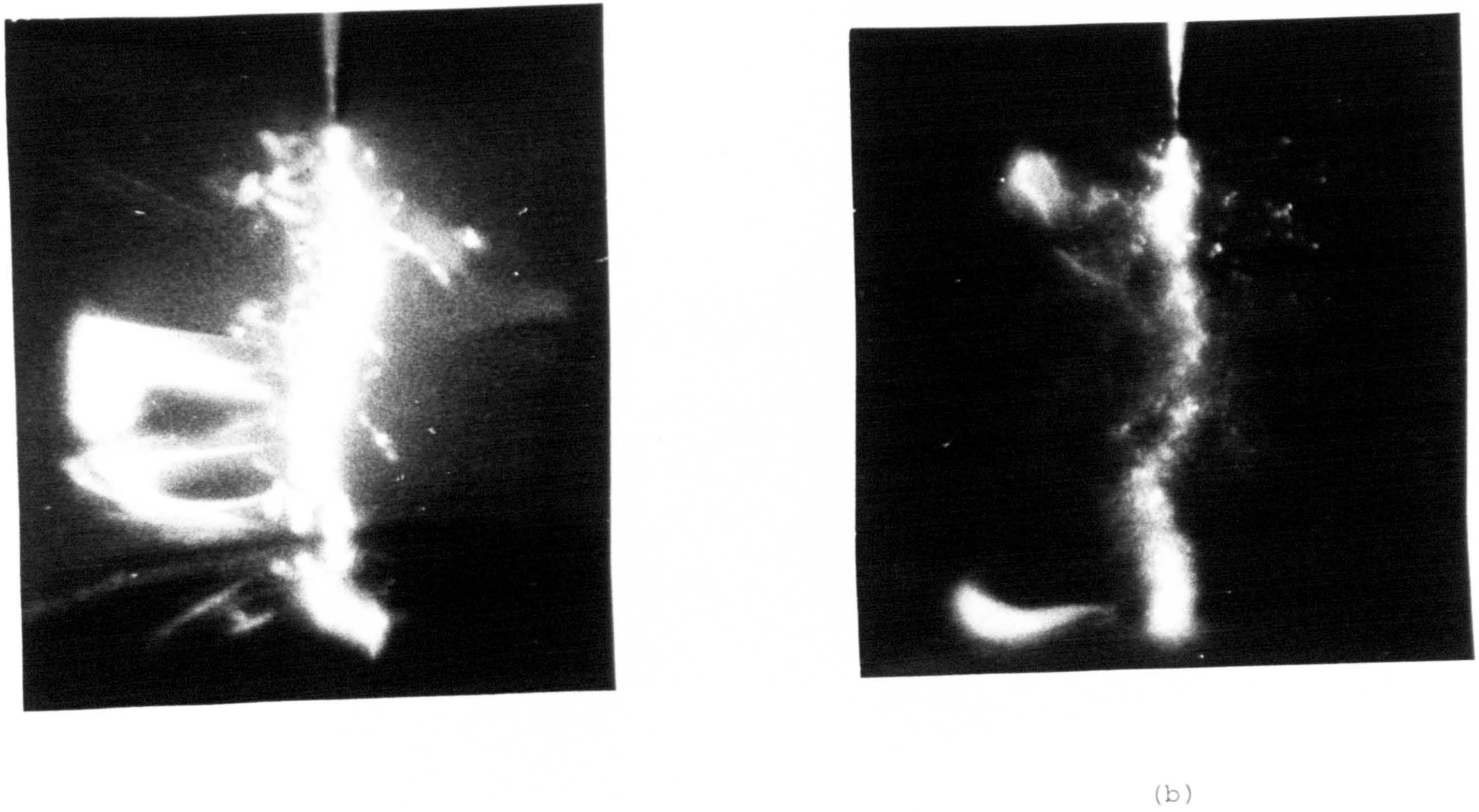

(a) (b)

Plate 4.28 Scattered light breakdown records. Voltage: (a) 25kV and (b) 23kV, negative point polarity. Liquid: liquid paraffin at (a) 16°C and (b) 66°C. Gap: 1.5mm.

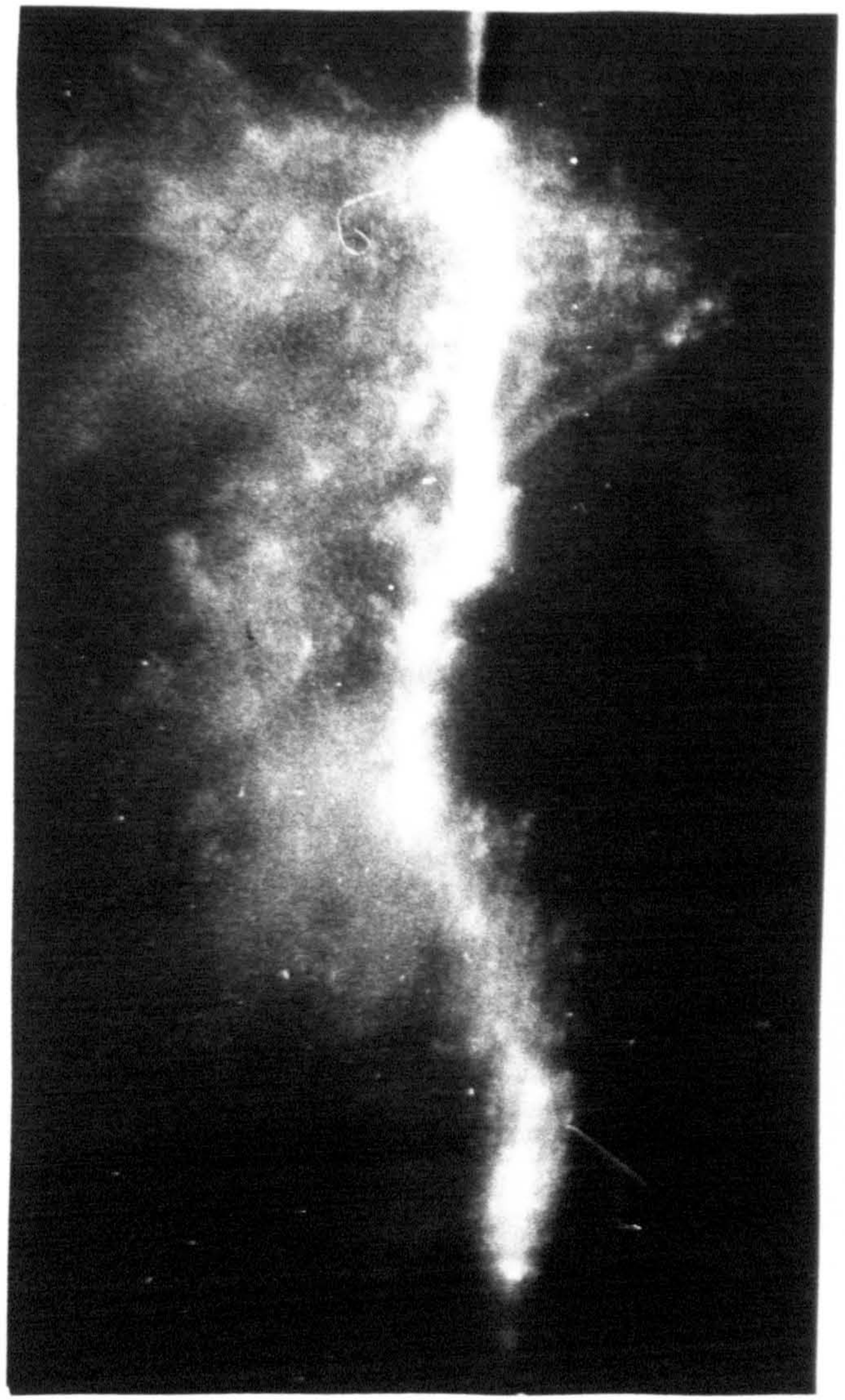

(a)

(b)

Plate 4.29 Scattered light breakdown records. Voltage: 25kV, negative point polarity. Liquid: n-hexane at (a) 26°C and (b) 60°C. Gap: 2mm.

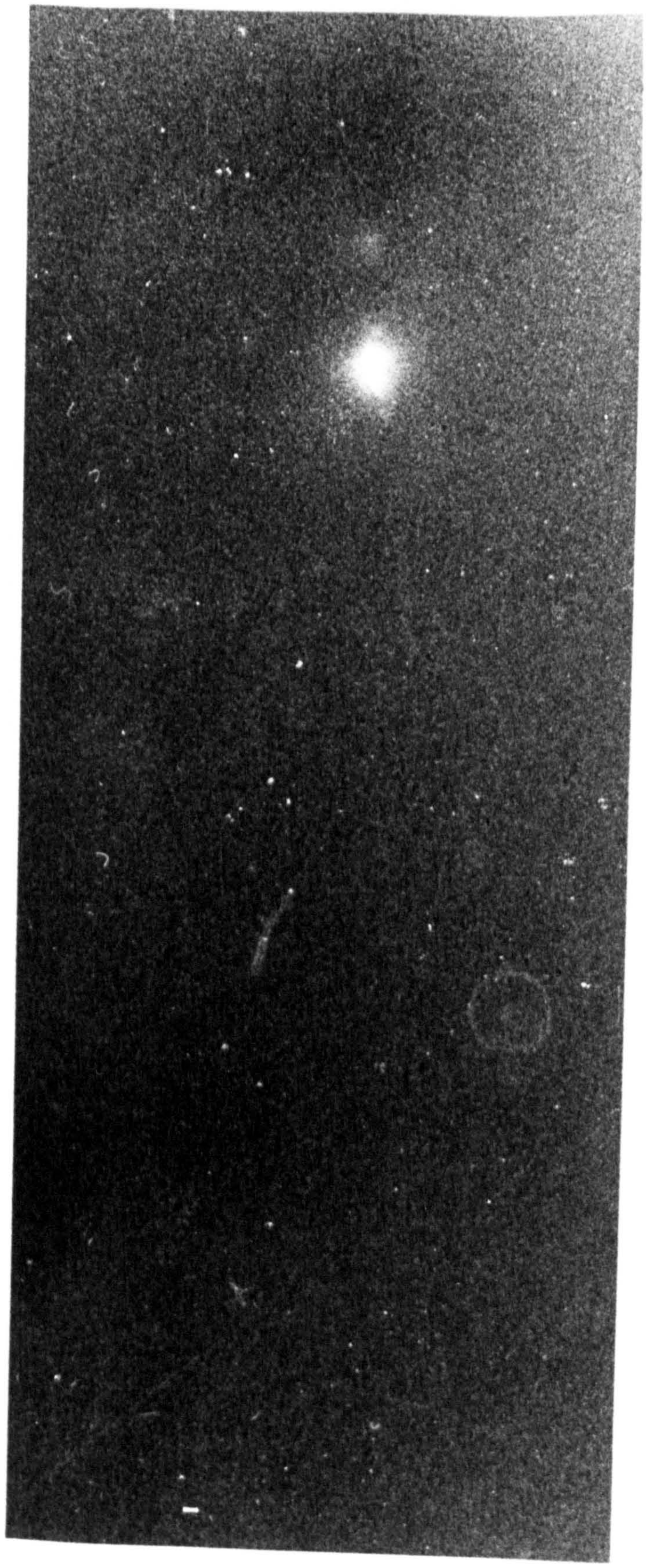

Plate 4.30 A 30 second exposure of direct voltage light emission. Voltage, 30kV, negative point polarity. Liquid: n-hexane. Gap: 3mm.

4.3 Transitional Behaviour of Pre-breakdown Conduction and Emissions

4.3.1 Introduction

Integrated measurements of conduction current, acoustic vibrations and light emission were made under varying, controlled conditions for dielectric liquids subjected to direct electric stress. In addition to integrated plots of the three measured parameters, the pulse behaviour was also monitored and oscillographically recorded. Transformer oil and n-hexane were chosen for the study and both bi-spherical and divergent electrode configurations were adopted. The simultaneous integrated values that were displayed by the electrometers are presented graphically. These are shown plotted on logarithmic axes to highlight the abrupt transitions that occurred in the measured parameters.

4.3.2 Transitions at ambient temperature

4.3.2.1 n-hexane characteristics

Figure 4.1 shows a plot of conduction current and the associated emissions of light and sound from n-hexane for a negative point polarity. On increasing the applied voltage the conduction current passes through a transition from a value below 10nA to that in excess of 100nA. With a voltage in excess of the transitional value, in this instance approximately 14kV, light emission also accompanies the higher level of conduction current, which also marks the onset of acoustic generation. When oscillographically

Fig. 4.1

Conduction current in n-hexane together with associated light and sound emissions.
Negative point/sphere electrodes, 3.0mm gap, 20°C

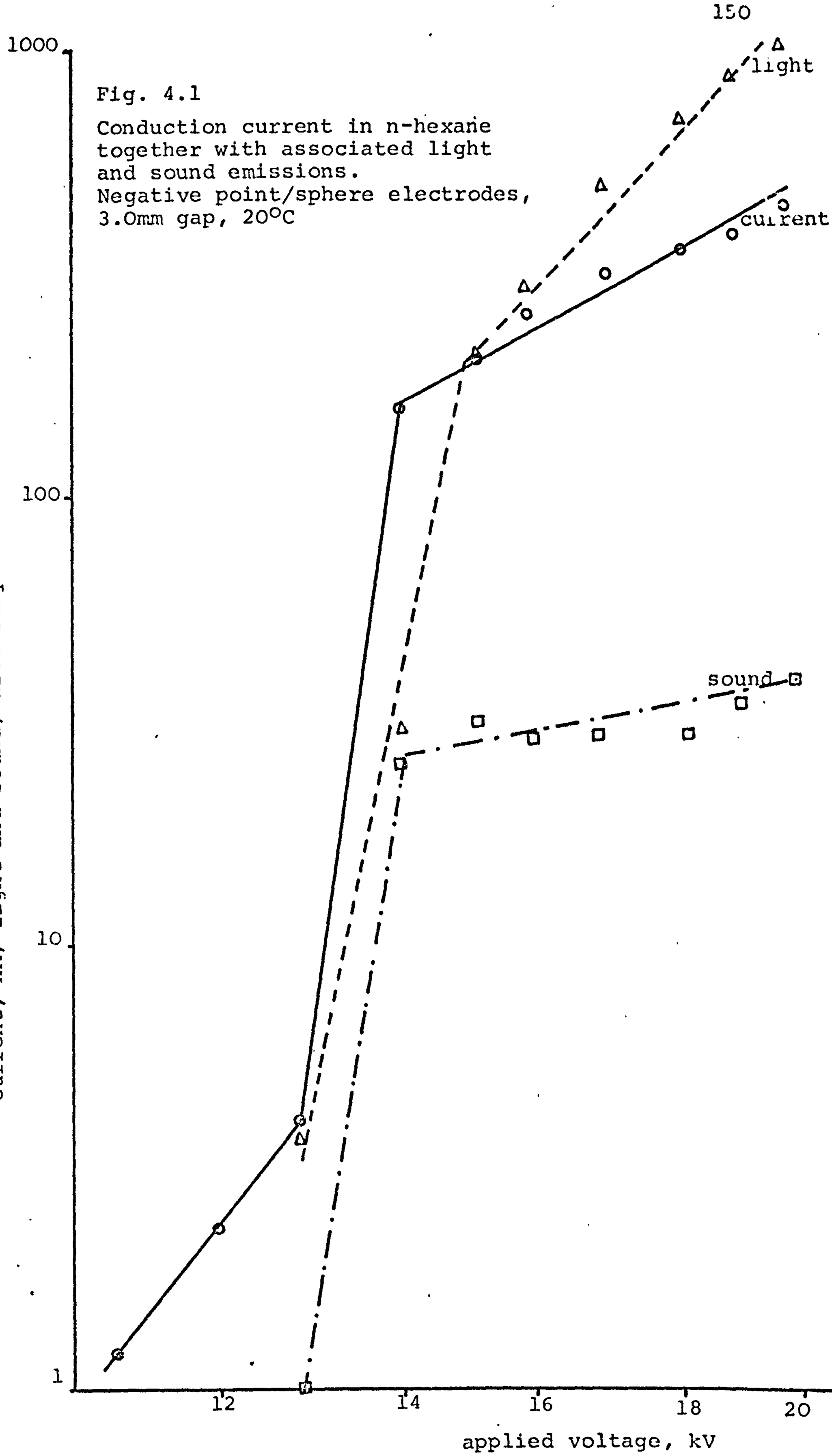

displayed the current bursts and light pulses appeared simultaneously, as depicted by plate 4.31. The appearance of the associated acoustic pulse is delayed by 20μs, which is consistent with the transit time anticipated between the point electrode and the transducer. This is illustrated by the oscillograph plate 4.32, where the time scale is expanded to 10μs cm^{-1}, and conduction current and acoustic pulses are displayed. The coincidence of conduction current and light scintillations is readily shown on a time scale of 50μs cm^{-1} by plate 4.33, in the absence of trace chopping present in plate 4.31.

4.3.2.2 Transformer oil characteristics

Changing the test sample to transformer oil and retaining the divergent electrode geometry a transitional behaviour similar to that for n-hexane was observed, as shown by figure 4.2. However, for transformer oil low level light emission is evident prior to the transition, as may be expected from the presence of polycyclic aromatic compounds in the oil. The post transition pulse activity is shown by plate 4.34. Large light scintillations that are coincident with conduction current pulses can be seen to be superimposed on the lower, uncorrelated light emission.

A comparative test was performed using bispherical stainless steel electrodes in transformer oil. Acoustic generation was absent up to gap failure, but a transition was evident at 10kV which marked the onset of uncorrelated light emission, as shown by figure 4.3.

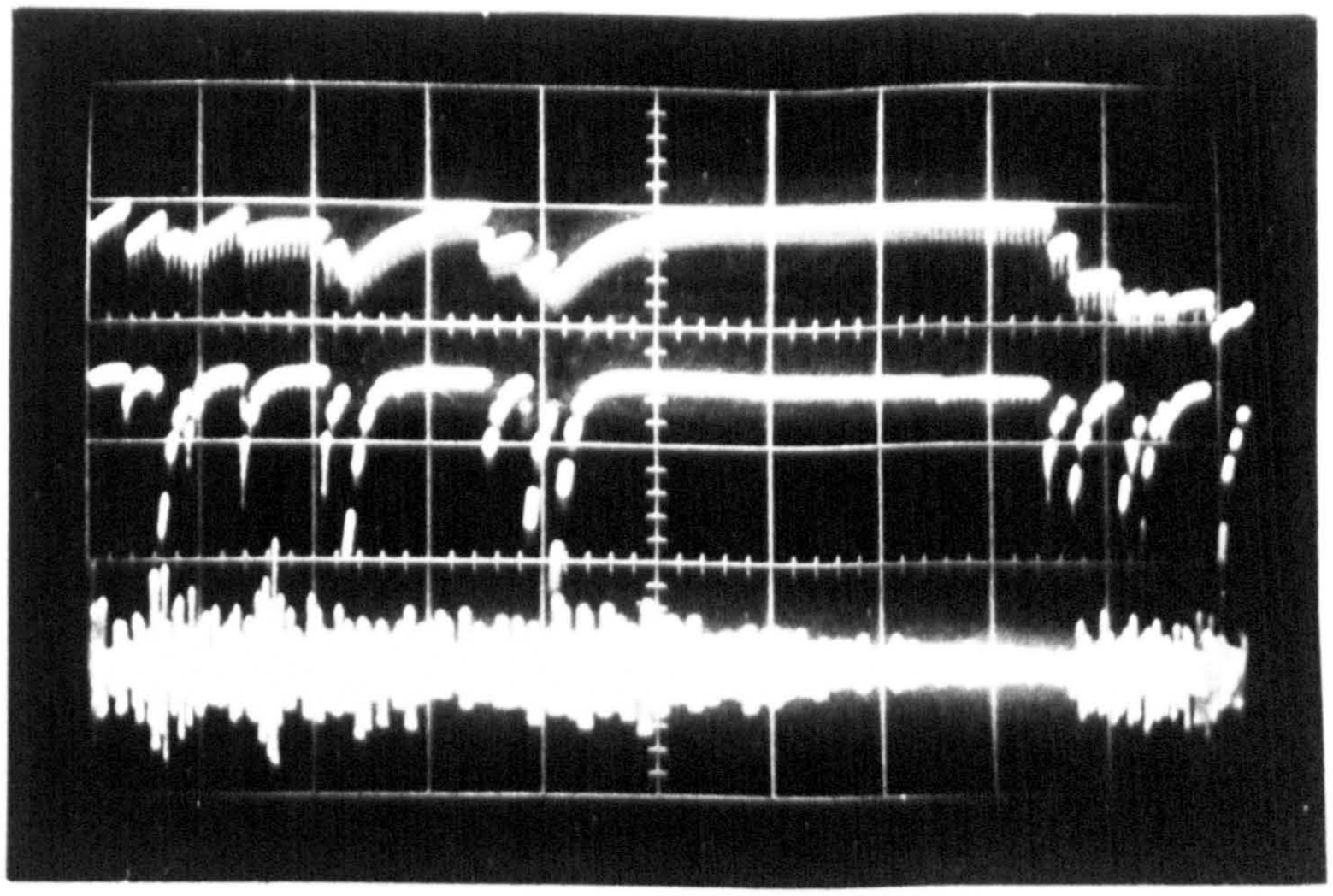

Plate 4.31 Oscillograph showing: upper, conduction current; centre, light emission; lower, acoustic emission. Time scale: 100μs cm^{-1}. Voltage: 22kV direct, negative point polarity. Liquid: n-hexane. Gap: 1.5mm.

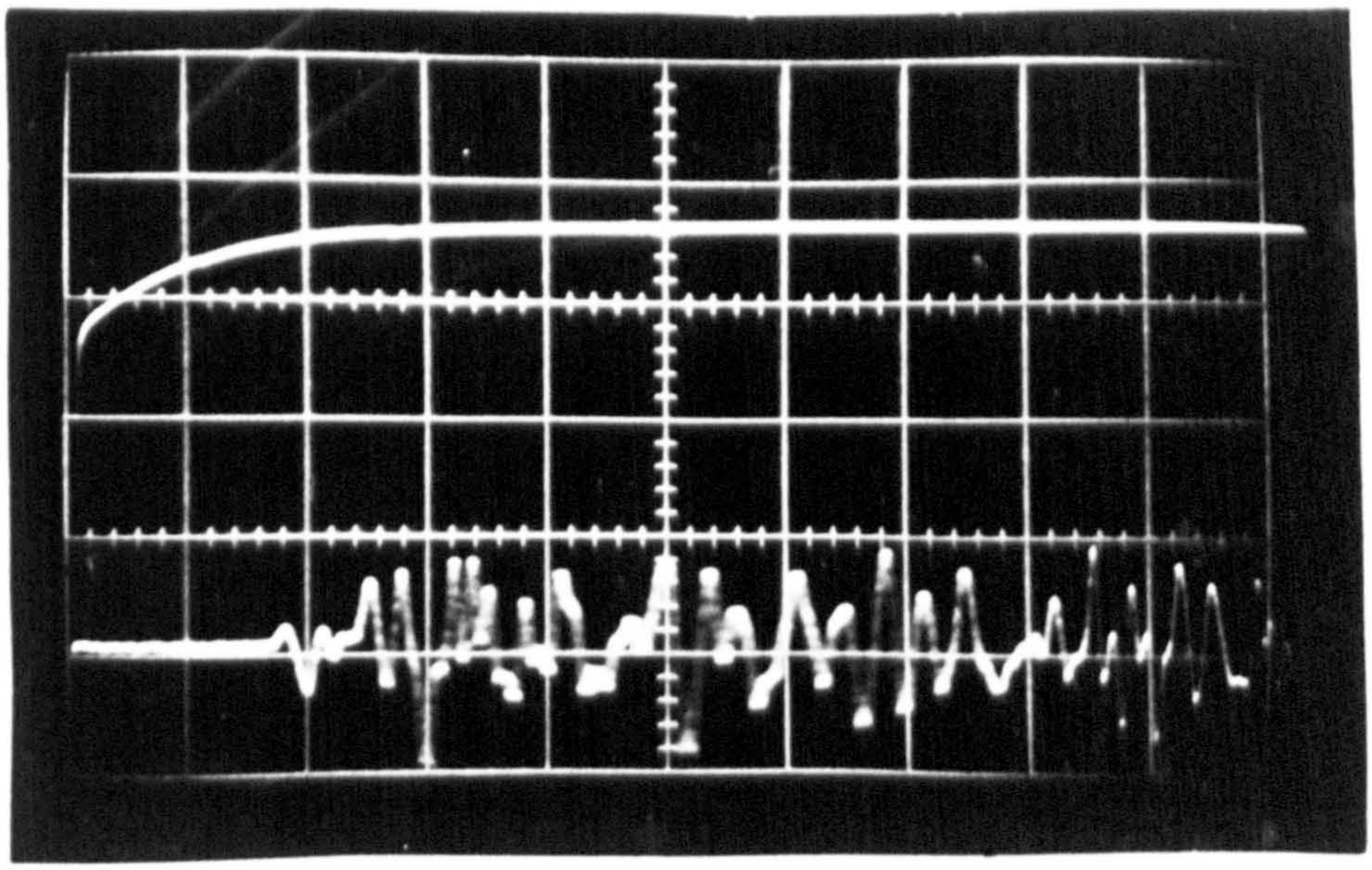

Plate 4.32 Oscillograph showing: upper, conduction current; lower, acoustic emission. Time scale: 10μs cm^{-1}. Voltage: 25kV direct, negative point polarity. Liquid: n-hexane. Gap: 2mm.

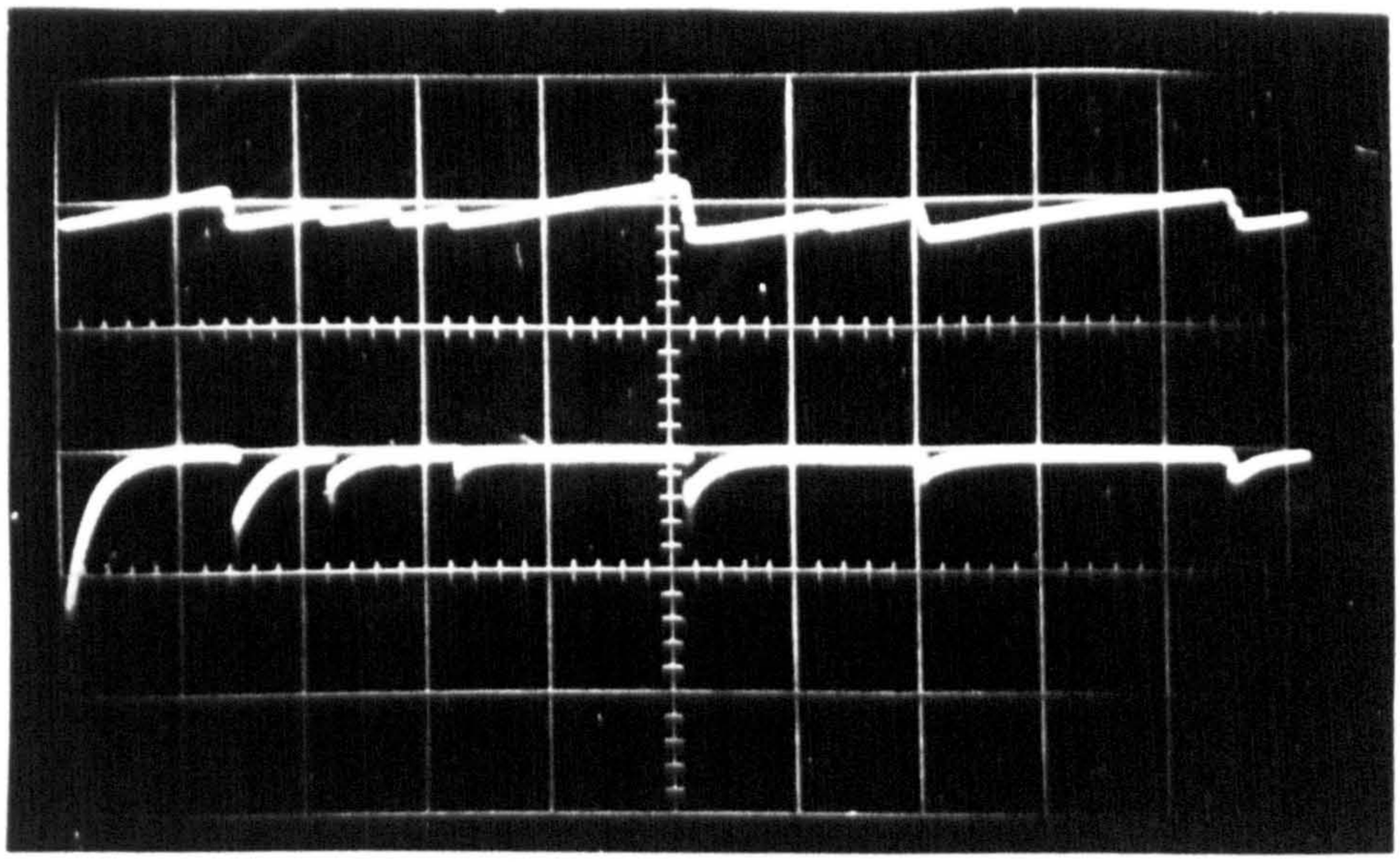

Plate 4.33 Oscillograph showing: upper, conduction current; lower, light emission. Time scale: 50μs cm^{-1}. Voltage: 20kV direct, negative point polarity. Liquid: n-hexane. Gap: 1.5mm.

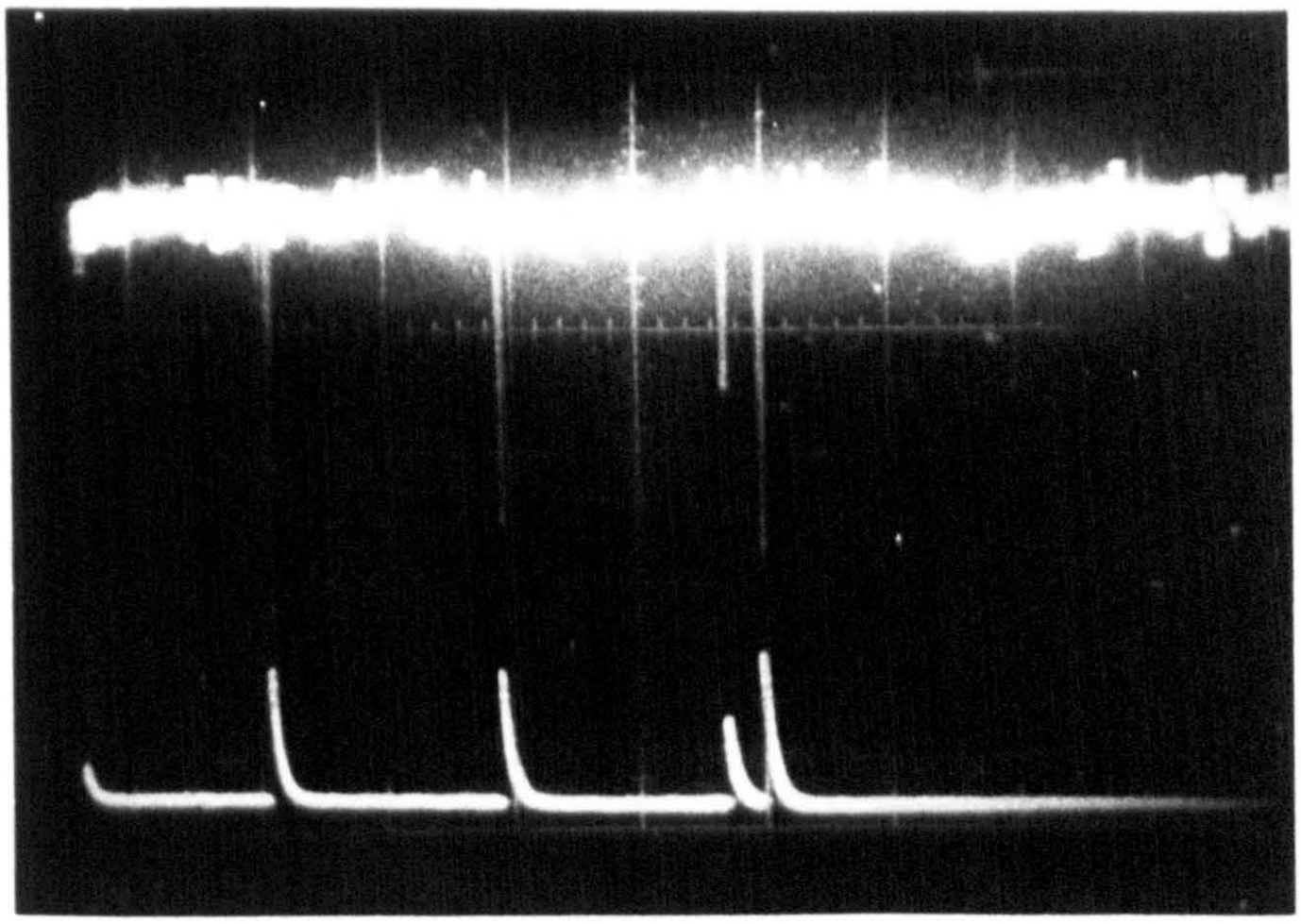

Plate 4.34 Oscillograph showing: upper, light emission; lower, conduction current. Time scale: 20ms cm^{-1}. Voltage: 25kV direct, negative point polarity. Liquid: transformer oil. Gap: 1.5mm.

Fig. 4.2

Conduction current in transformer oil together with associated light and sound emissions.
Negative point/sphere electrodes, 3.0mm gap, 20°C.

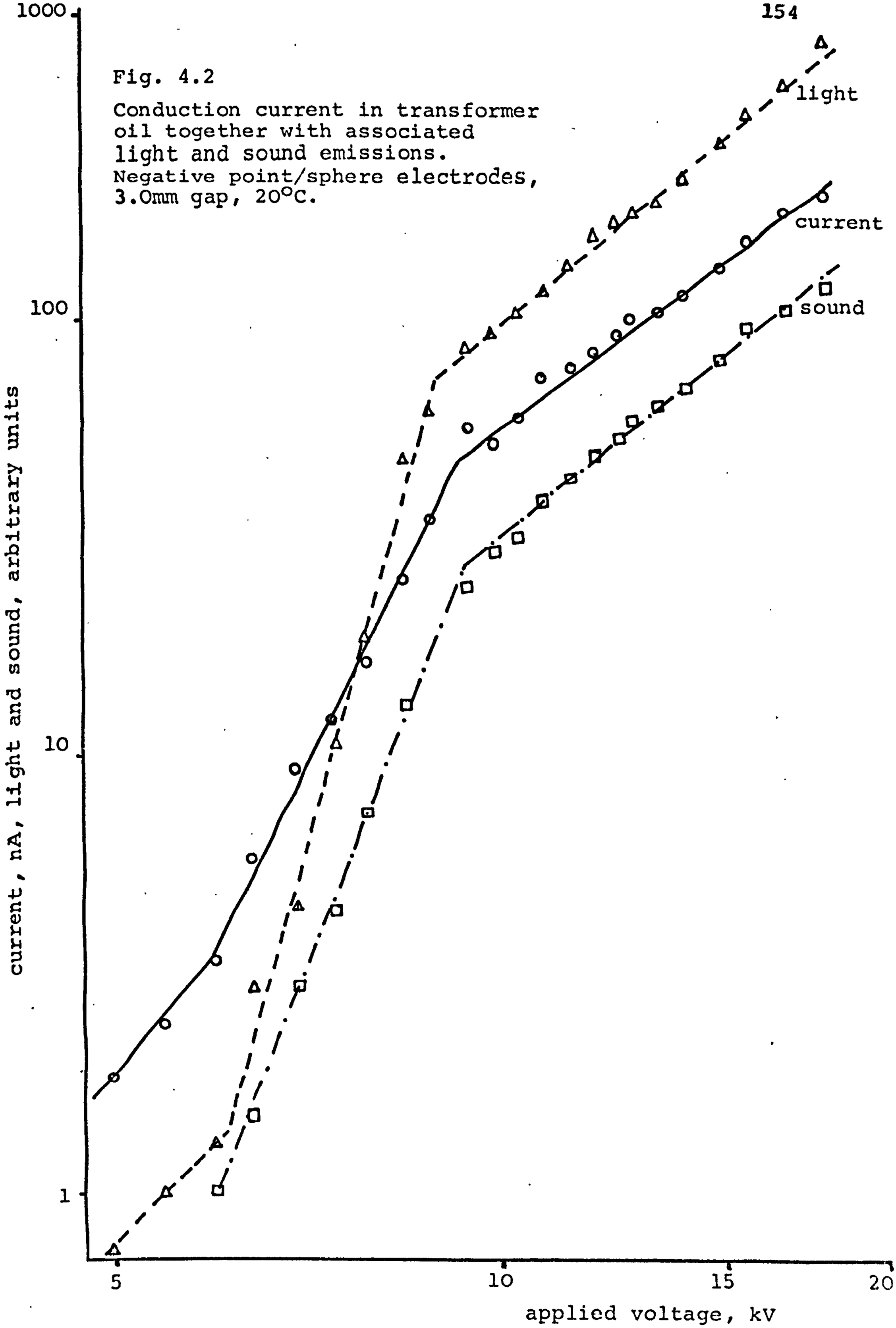

Fig. 4.3

Conduction current in transformer oil together with the associated light emission.
Sphere/sphere electrodes,
0.75mm gap, 20°C.

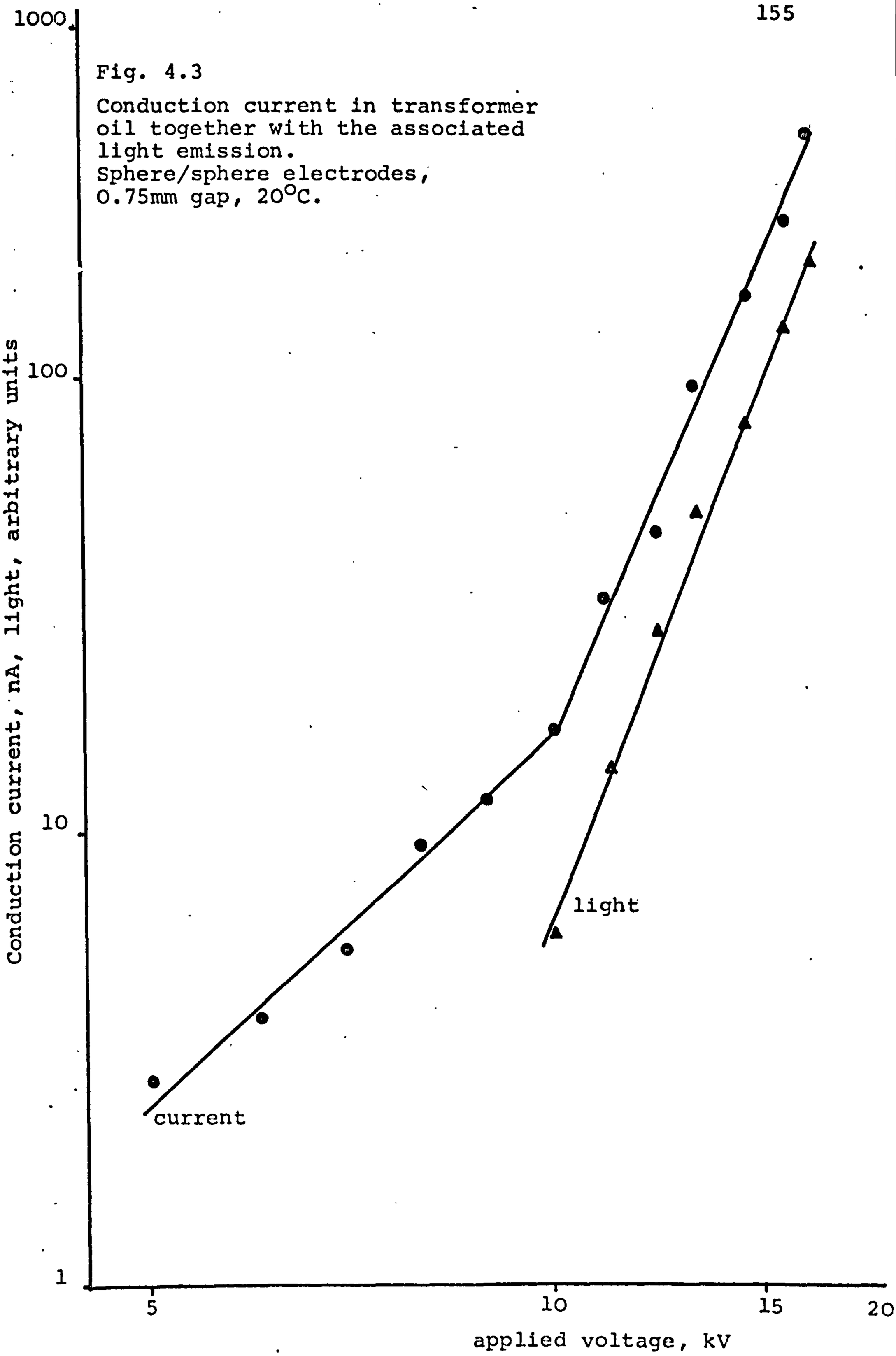

4.3.3 Positive point results

For a divergent geometry with a point anode, a transitional behaviour of the pre-breakdown characteristics is apparent but less well defined for both n-hexane, figure 4.4,and transformer oil, figure 4.5. Although the current and sound magnitudes were similar the light emission was found to be weak and erratic up to the point of gap failure.

4.3.4 Elevated temperature transitions

4.3.4.1 General conditions

Taking measurements for a negative point polarity in transformer oil, the influence of temperature on the discontinuous behaviour of conduction current and light emission is shown by figure 4.6. Acoustic measurements were not recorded at elevated temperatures as the thermal sensitivity of the transducer was unknown.

4.3.4.2 An ambient temperature test

At $25^{o}C$ the transitions shown for conduction current and light emission are essentially similar to those of figure 4.1. The coincident room temperature transitions can be seen to occur at 9kV.

4.3.4.3 Transitions at $50^{o}C$

Retaining the same liquid and electrode combination, but raising the temperature produces a change in the characteristics. At $50^{o}C$ the conduction current can be

Fig. 4.4

Conduction current in n-hexane together with light and sound emission.
Positive point/sphere electrodes, 1.0mm gap, 20°C.

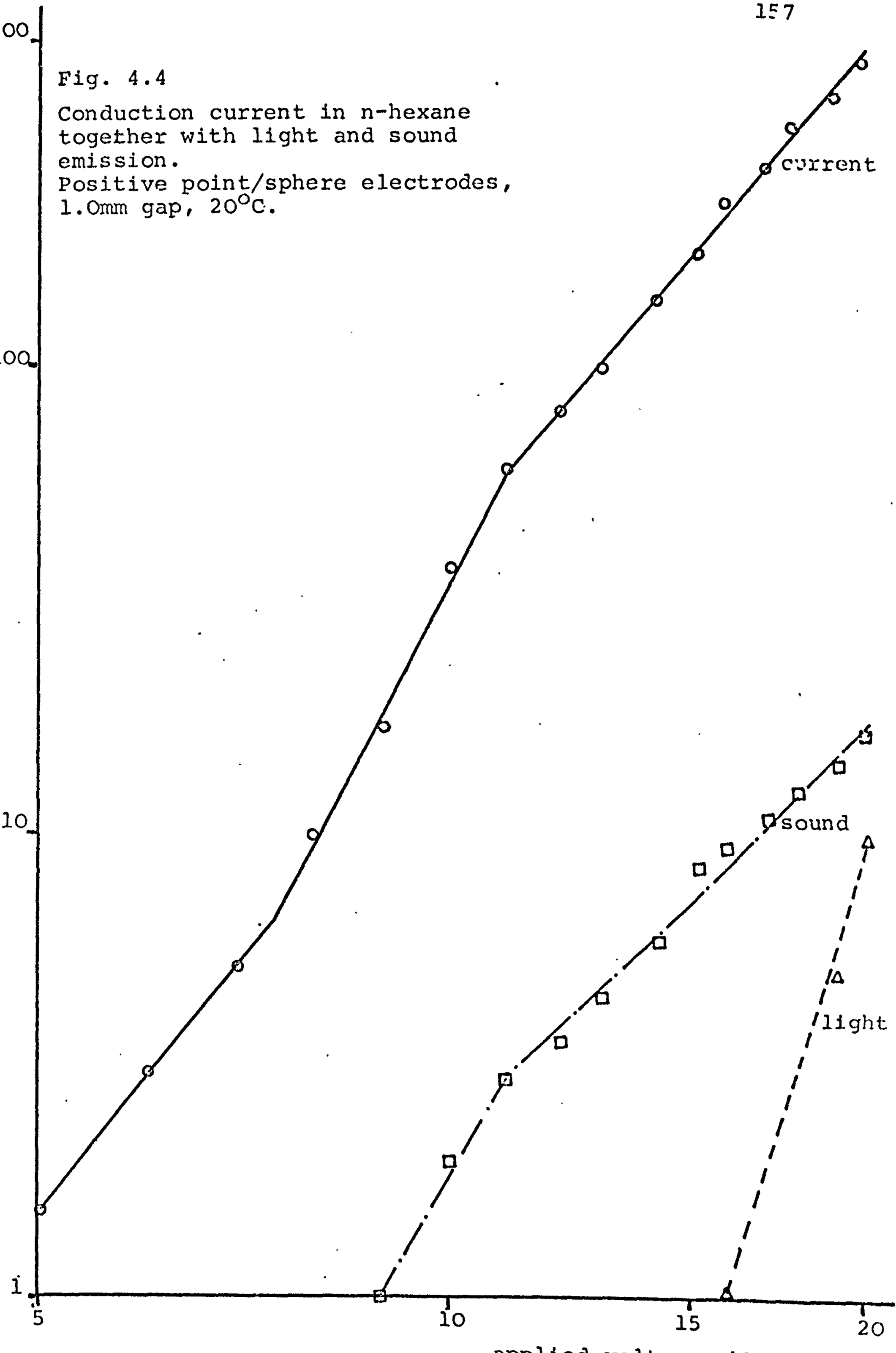

Fig. 4.5

Conduction current in transformer oil together with the associated light and sound emissions.
Positive point/sphere electrodes, 3.0mm gap, 20°C.

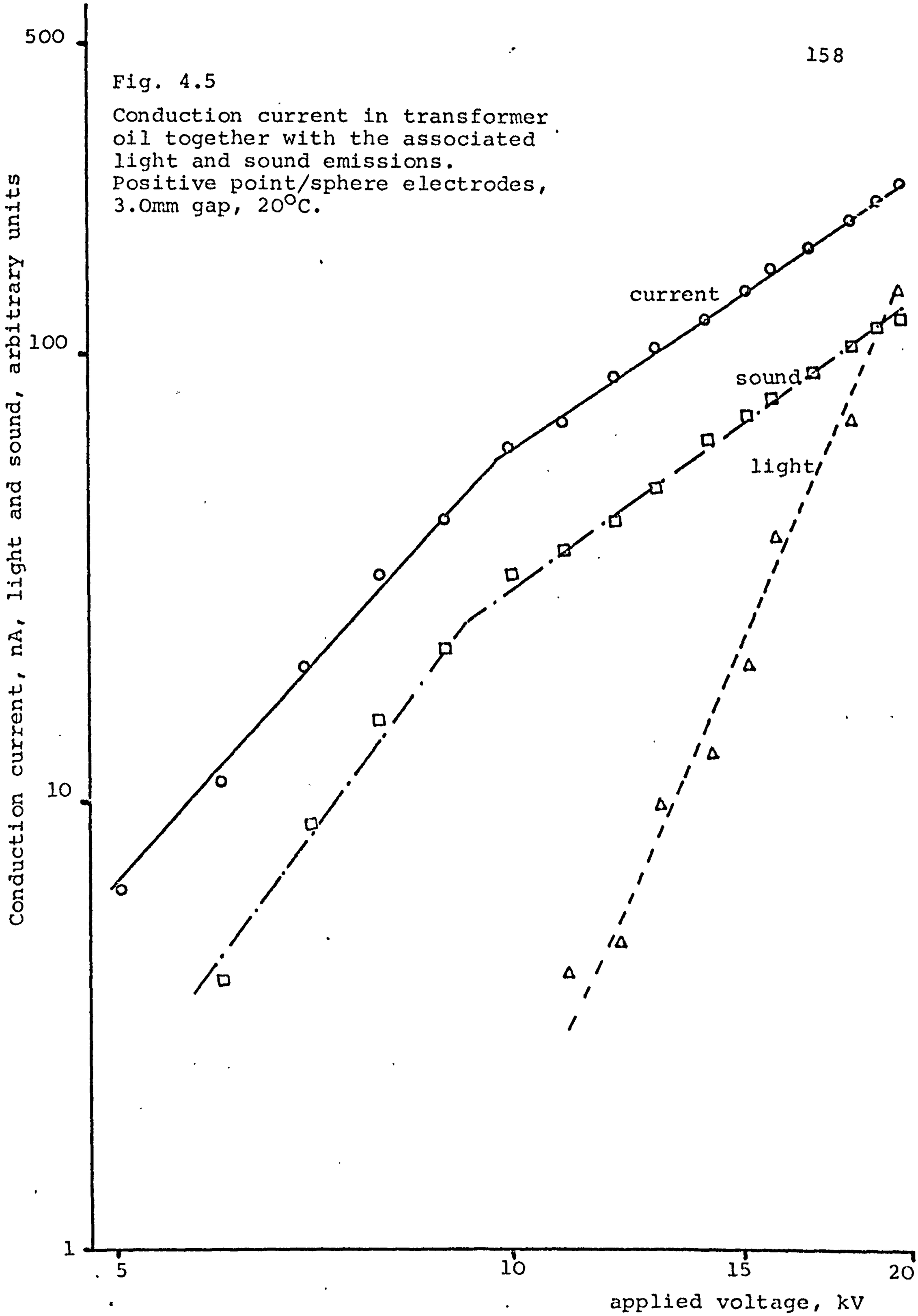

Fig. 4.6

Temperature dependence of conduction current in transformer oil with associated light emission. Negative point/sphere electrodes, 3.0mm gap.

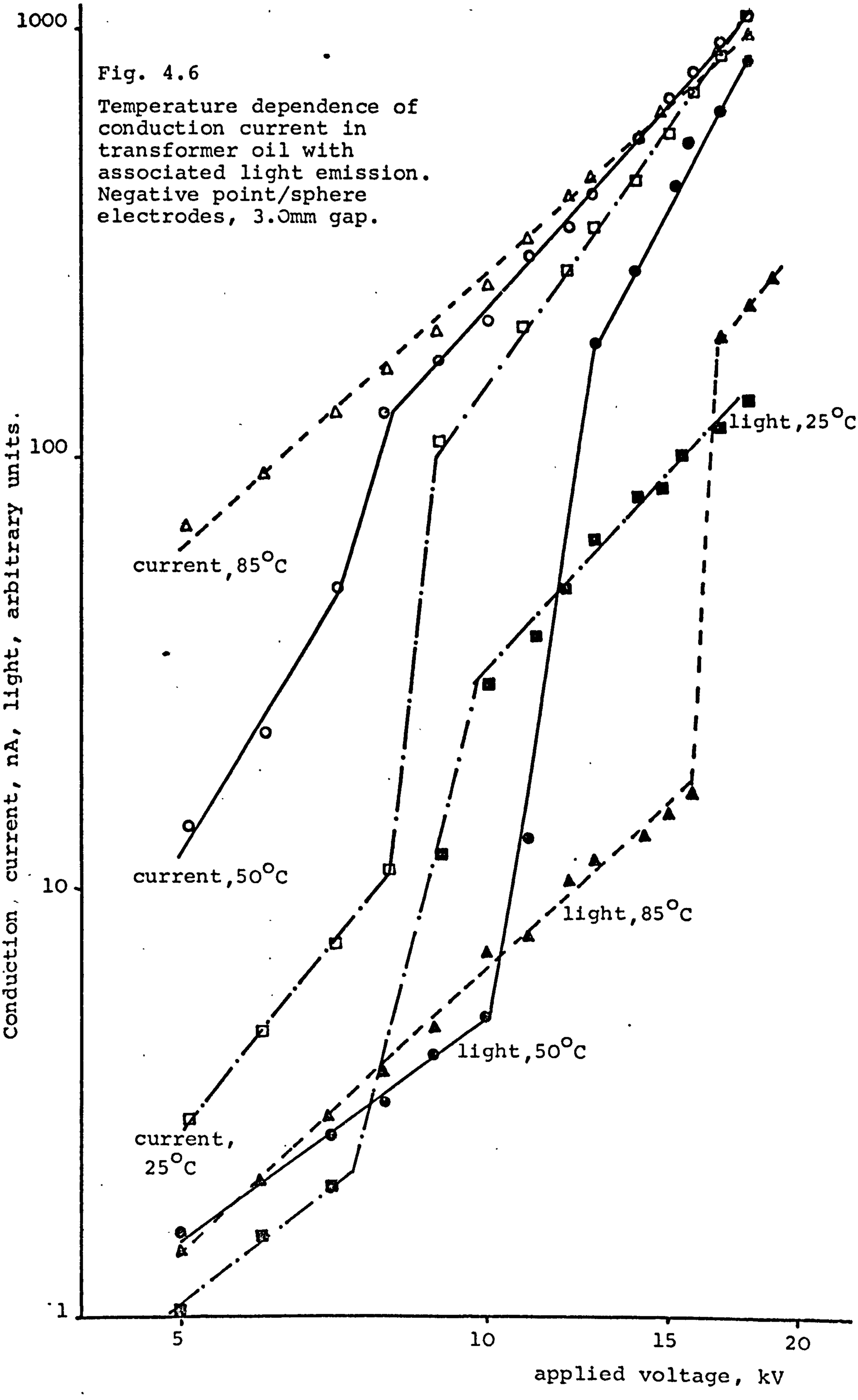

seen to be much larger at 40nA prior to the consequentially reduced transition at 9kV. Associated with this conduction current the light emission possesses a discontinuity at 11kV, being no longer coincident with the conduction current trend.

4.3.4.4 Transitions at 85°C

For an additional temperature increase of 35°C, the conduction current assumes a straight line form. A transition in the accompanying light emission remains evident but this is shifted to 20kV.

4.3.4.5 Trends of thermal dependence

From figure 4.6 it can be seen that the pre-transitional conduction current increases with temperature but beyond the transition the effect is suppressed, particularly as the breakdown voltage is approached. On examining the light emission characteristics it is evident that the transition is forced to a higher voltage as the temperature is raised.

4.3.5 A confirmatory oscillographic study

In order to identify the dominant contribution to the integrated conduction current, a display of the current fluctuations was made on an oscilloscope. The points on the plot of figure 4.7 were derived from the d.c. pedestal measured as the offset on the oscilloscope trace when the input was directly coupled to the current measuring circuit. Discrete pulses were seen to be

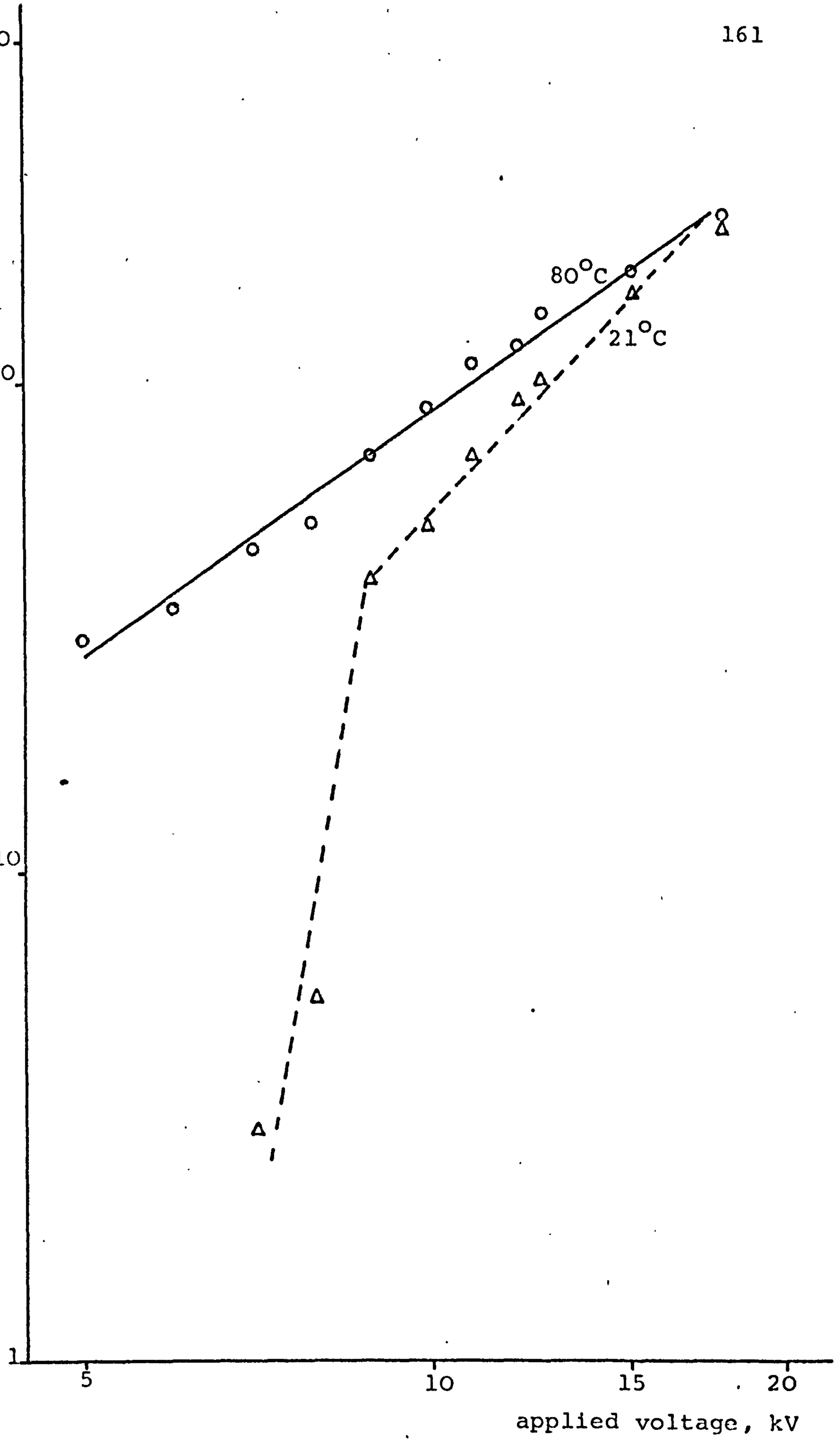

Fig. 4.7 Temperature dependence of the pedestal conduction current in transformer oil, using an oscilloscope Negative point/sphere electrodes, 3.0mm gap.

superimposed on the direct voltage level, but these were at least an order of magnitude below the direct current offset value.

4.3.6 The inception of light emission and its temperature dependence

4.3.6.1 A general description

Plots of the voltage required to produce light emission, and that necessary to initiate the transition to an elevated level are shown by figure 4.8. As would be expected from figure 4.6, the low level light inception is relatively insensitive to temperature but the transitional state is strongly temperature dependent.

Choosing three fixed values of applied voltage, the conduction current and the associated light emission were plotted as a function of temperature, as shown by figure 4.9.

4.3.6.2 Low voltage characteristics

At 5kV the conduction current increases markedly with temperature whereas the light emitted remains relatively unaffected.

4.3.6.3 Plots at 10kV

For an increased voltage, of a magnitude sufficient to exceed the transitional value at room temperature, the conduction current remains constant. The accompanying light emission suffers a reduction commencing at 50^{o}C and on reaching 70^{o}C falls to the pre-transitional, room

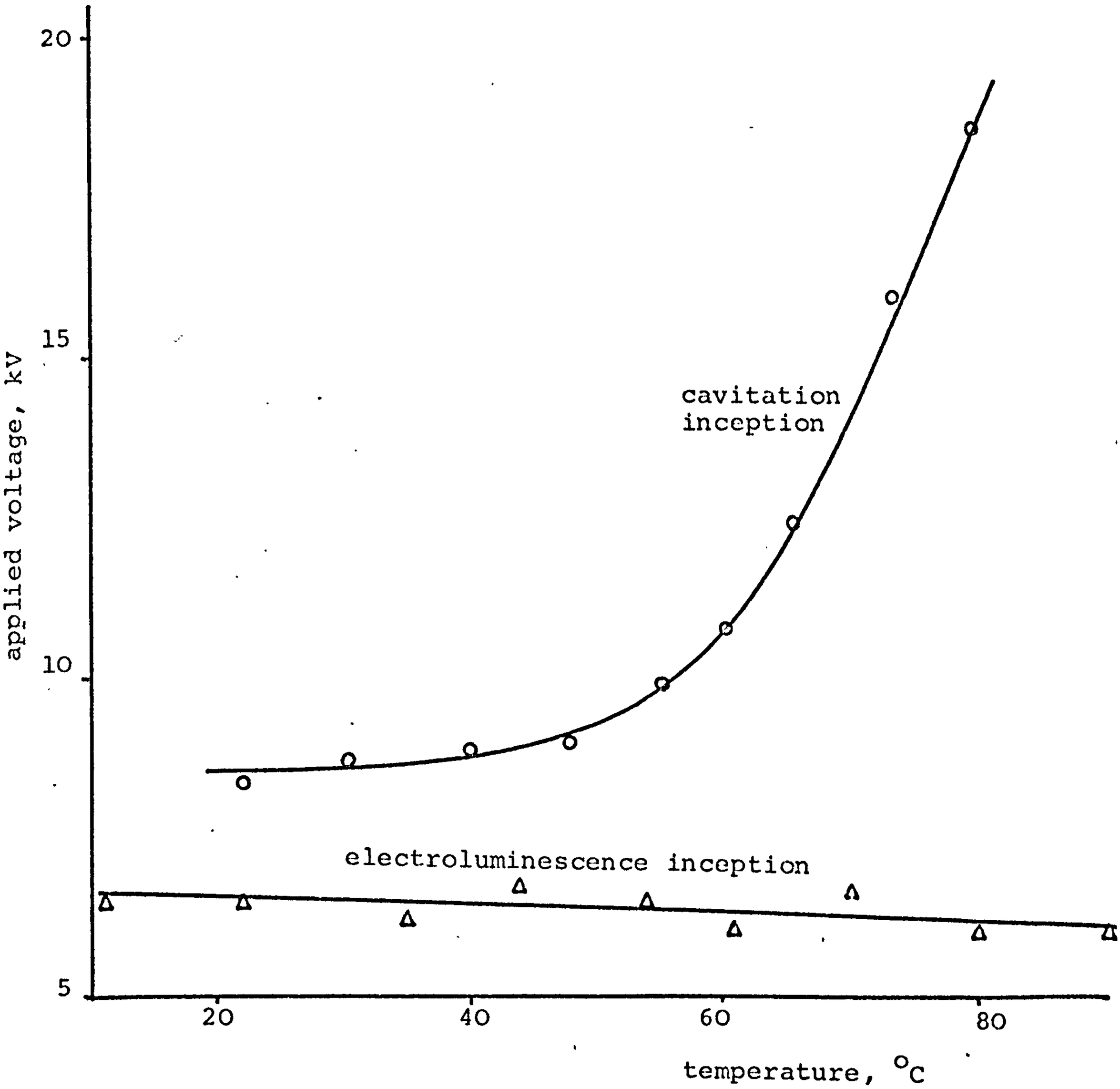

Fig. 4.8 Temperature dependence of electroluminescence and cavitation inception in transformer oil. Negative point/sphere electrodes, 3.0mm gap.

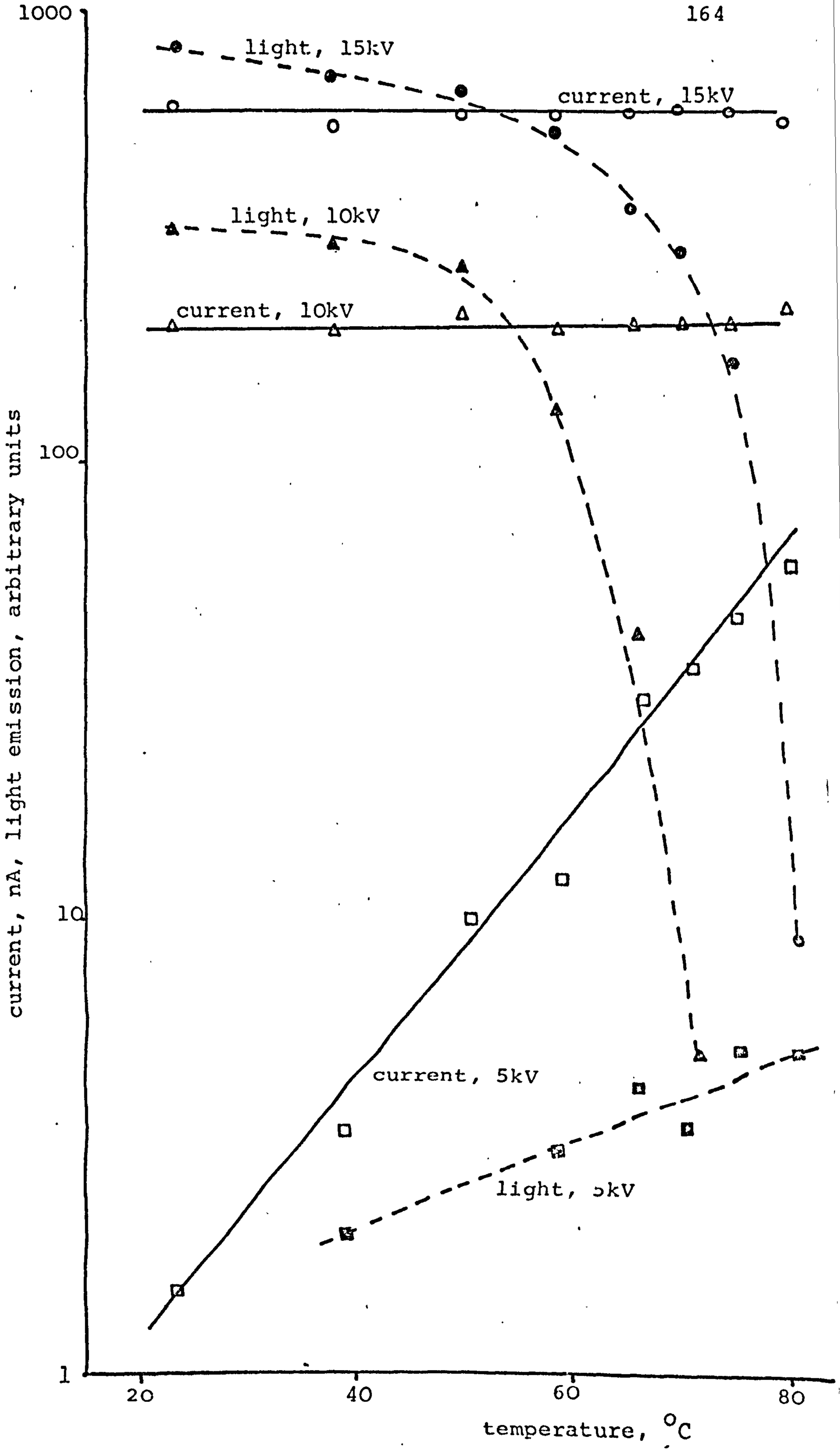

Fig. 4.9 Temperature dependence of conduction current and the associated light emission in transformer oil. Negative point/sphere electrodes, 3.0mm gap.

temperature,value.

4.3.6.4 Plots at 15kV

Increasing the voltage to 15kV produces essentially similar characteristics, with a small increase in the conduction current and the knee of the light emission curve forced to 60°C.

4.3.7 Spectral measurements

4.3.7.1 The dependence of light emission wavelength on electric stress

Using the photomultiplier in conjunction with calibrated narrow band optical filters the spectral nature of the emitted light was investigated. For a bi-spherical electrode geometry in transformer oil, figure 4.10 depicts the spectra that were measured for several chosen fixed voltages applied to the gap. A peak at about 420nm is evident for an applied voltage in excess of 11kV. Figure 4.11(a) shows that on changing the cathode to a sharp needle the peak is shifted to approximately 450nm. The peak becomes increasingly pronounced as the voltage is raised. After some deterioration of the electrode point, the larger radius of curvature allows the existence of an intermediate situation as illustrated by figure 4.11(b). For the lower applied voltages a peak appears at 420nm, but on increasing the voltage a transitional state exists before the 450nm peak is attained at 18kV.

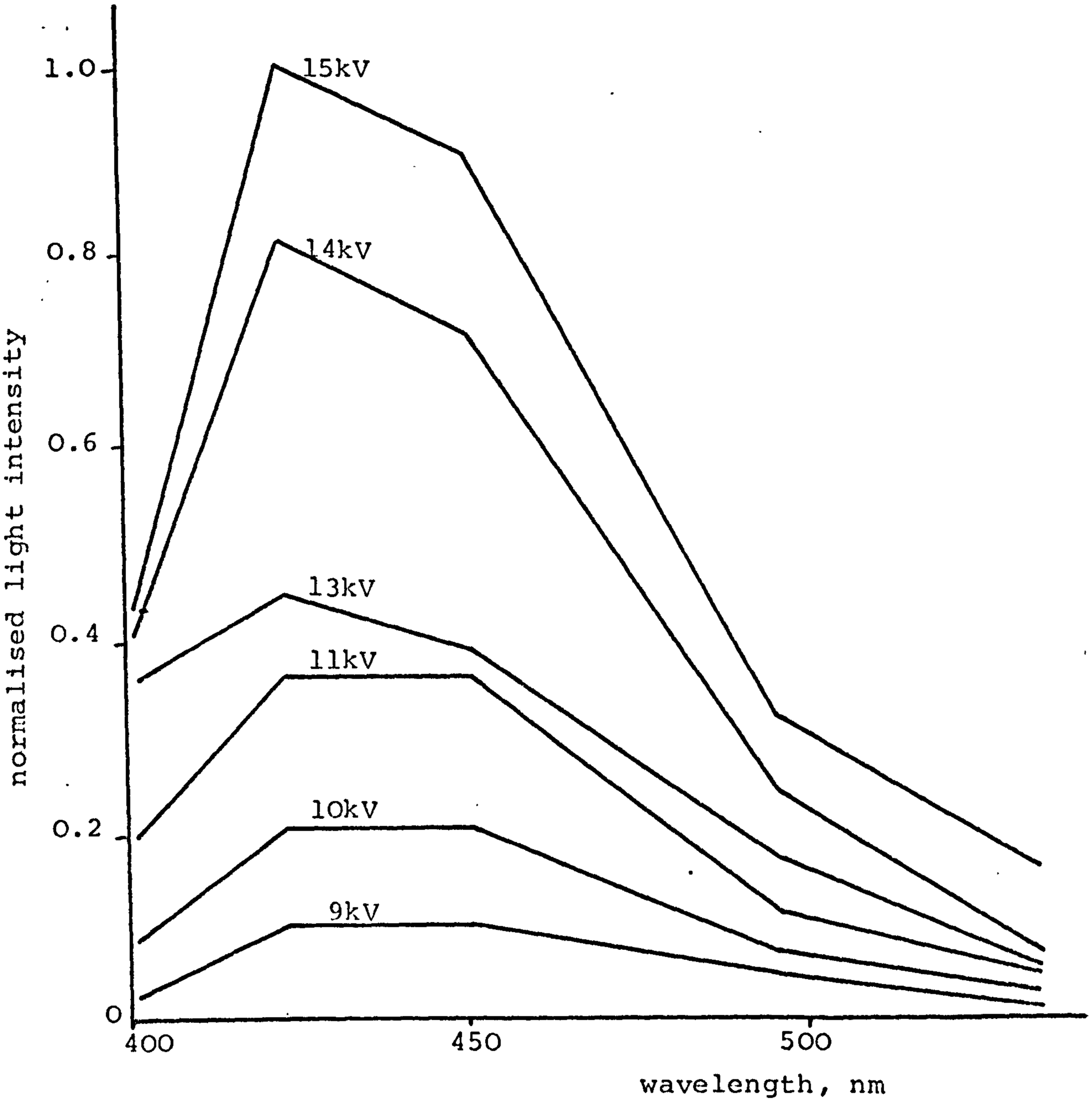

Fig. 4.10 Spectra of light emitted from stressed transformer oil.
Sphere/sphere electrodes, 0.75mm gap, 22°C.

Fig. 4.11(a)

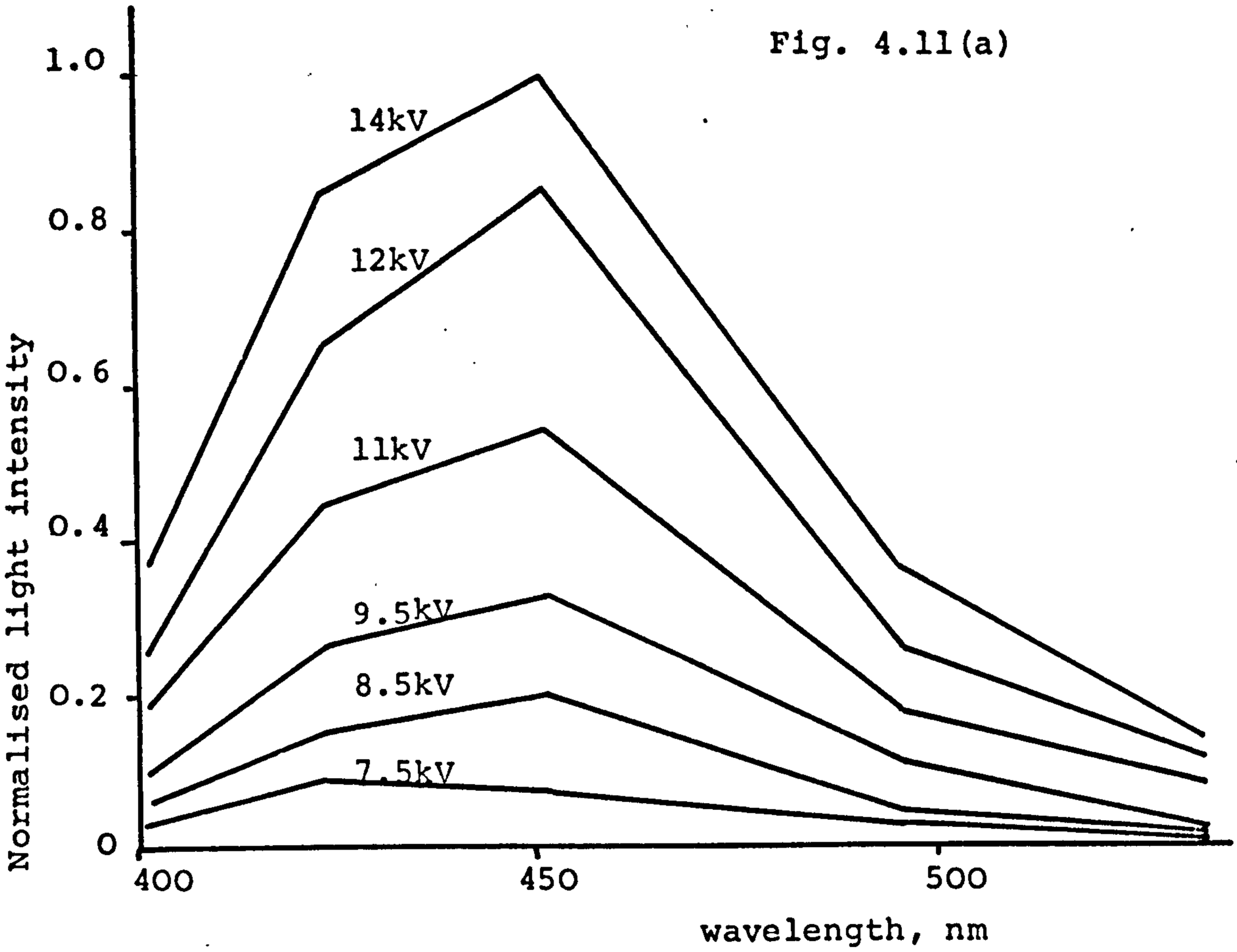

Fig. 4.11(b)

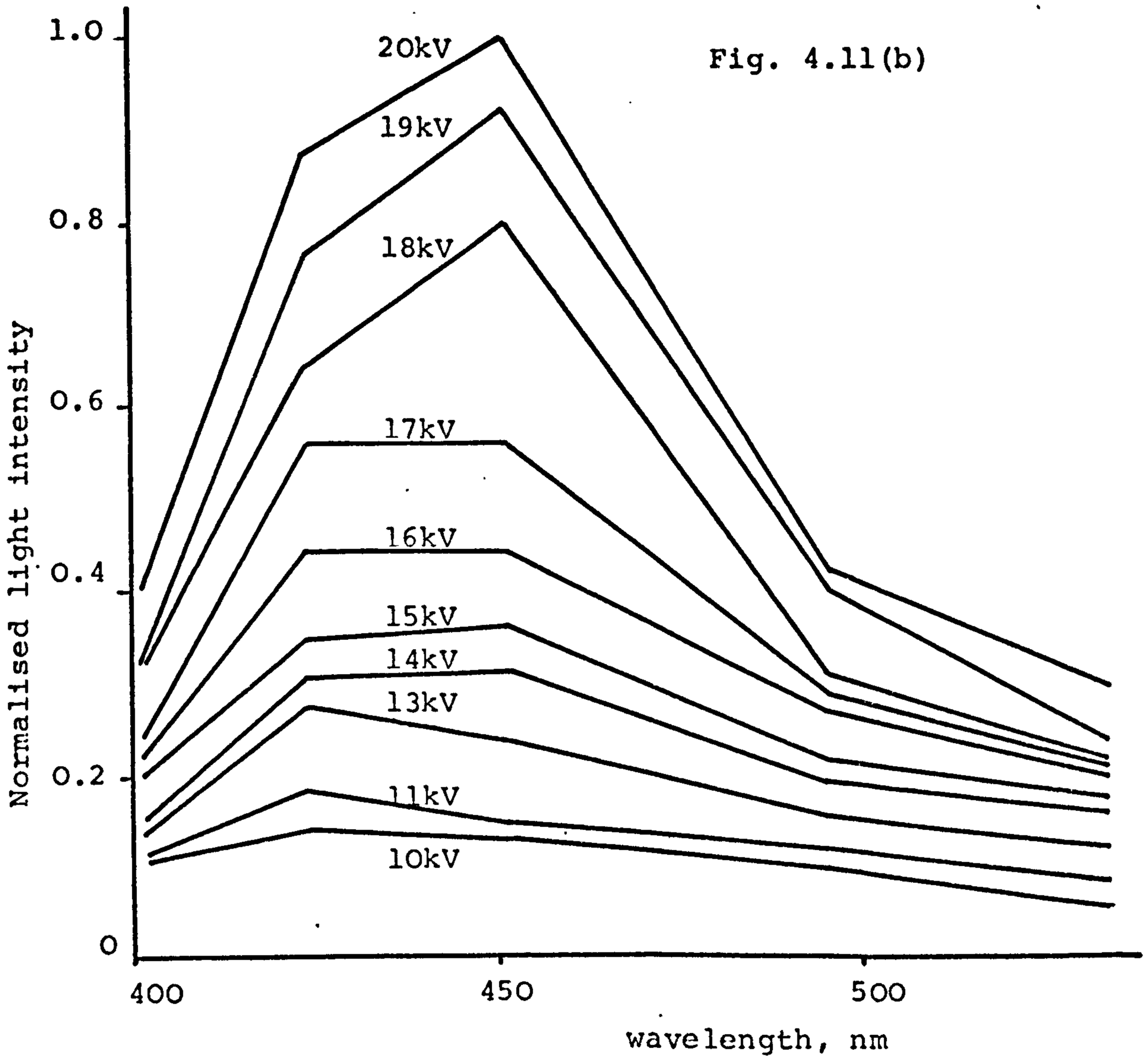

Fig. 4.11 Spectra of light emitted from stressed transformer oil. Negative point/sphere electrodes, 1.5mm gap, 22°C.

4.3.7.2 Thermally shifted characteristics

The electrodes used to produce figure 4.11(b) were retained and utilised to provide data for figure 4.12. This figure shows that for a fixed voltage of 15kV the transition in the spectral peak can be effected by a temperature change. At room temperature the peak occurs at 450nm. However, on increasing the sample temperature to 65^{o}C, the peak is forced to the lower wavelength of 420nm.

4.3.8 Light emission from n-hexane resulting from step voltage application

When the directly stressed test gap was viewed with the dark adapted eye it was possible to discern the cone of light at the tip of the point cathode shown by plate 4.30. The light emitted when a step voltage was impressed on the gap was found more difficult to visually detect and record directly. A photomultiplier was used to view the gap which produced a pulse response of pre-breakdown light emission immediately following voltage application. For a negative point polarity several pulses were commonly seen and a typical record is shown by the oscillograph of plate 4.35. From this record it can be seen that the first light pulse appears 1.5μs after voltage application, with several pulses following over a further 4.5μs period. Reversing the polarity set a more demanding task. Usually if sufficient voltage was applied to produce pre-breakdown emission, the single light pulse was followed by total gap

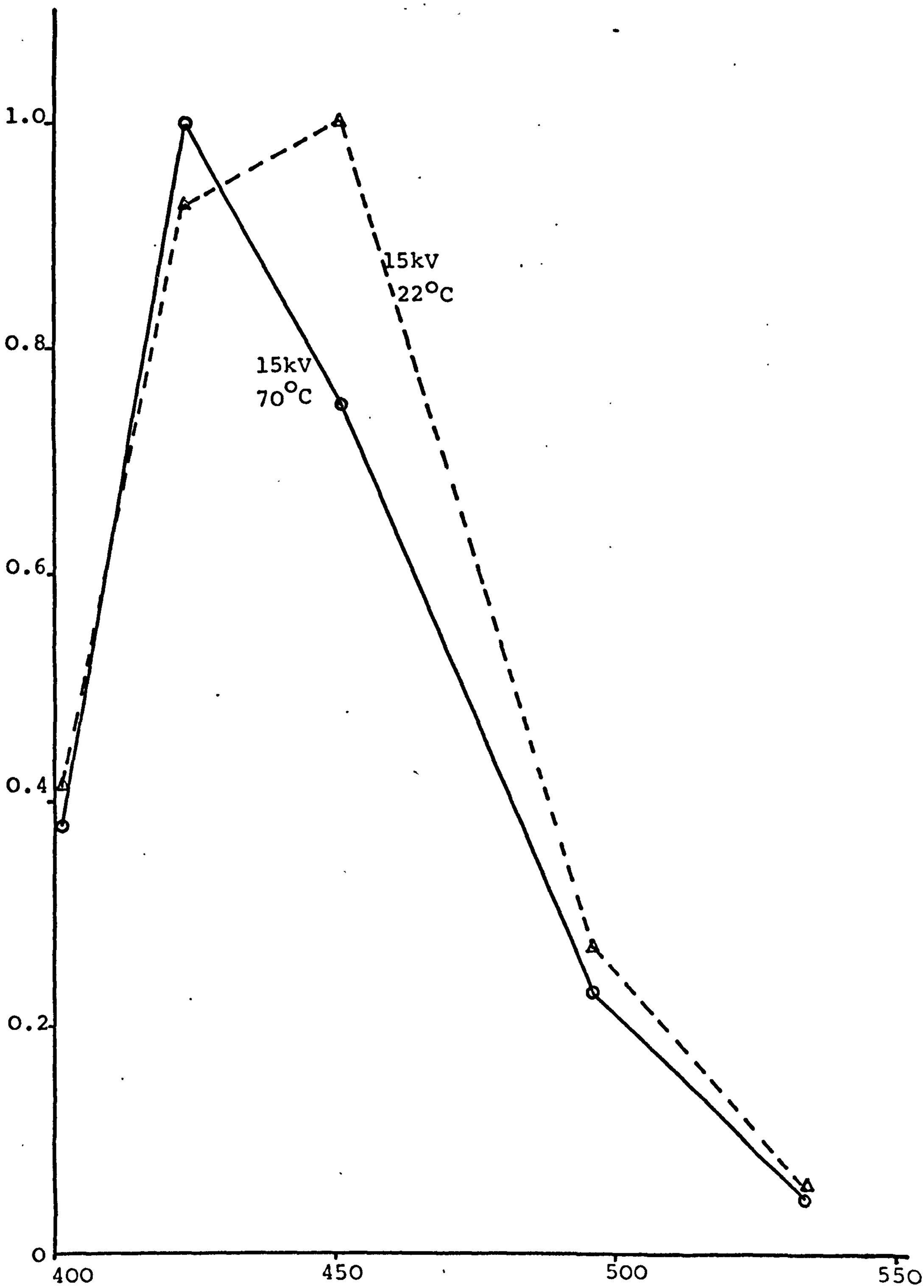

Fig. 4.12 Temperature dependence of light emission spectrum from stressed transformer oil. Negative point/sphere, 3.0mm gap.

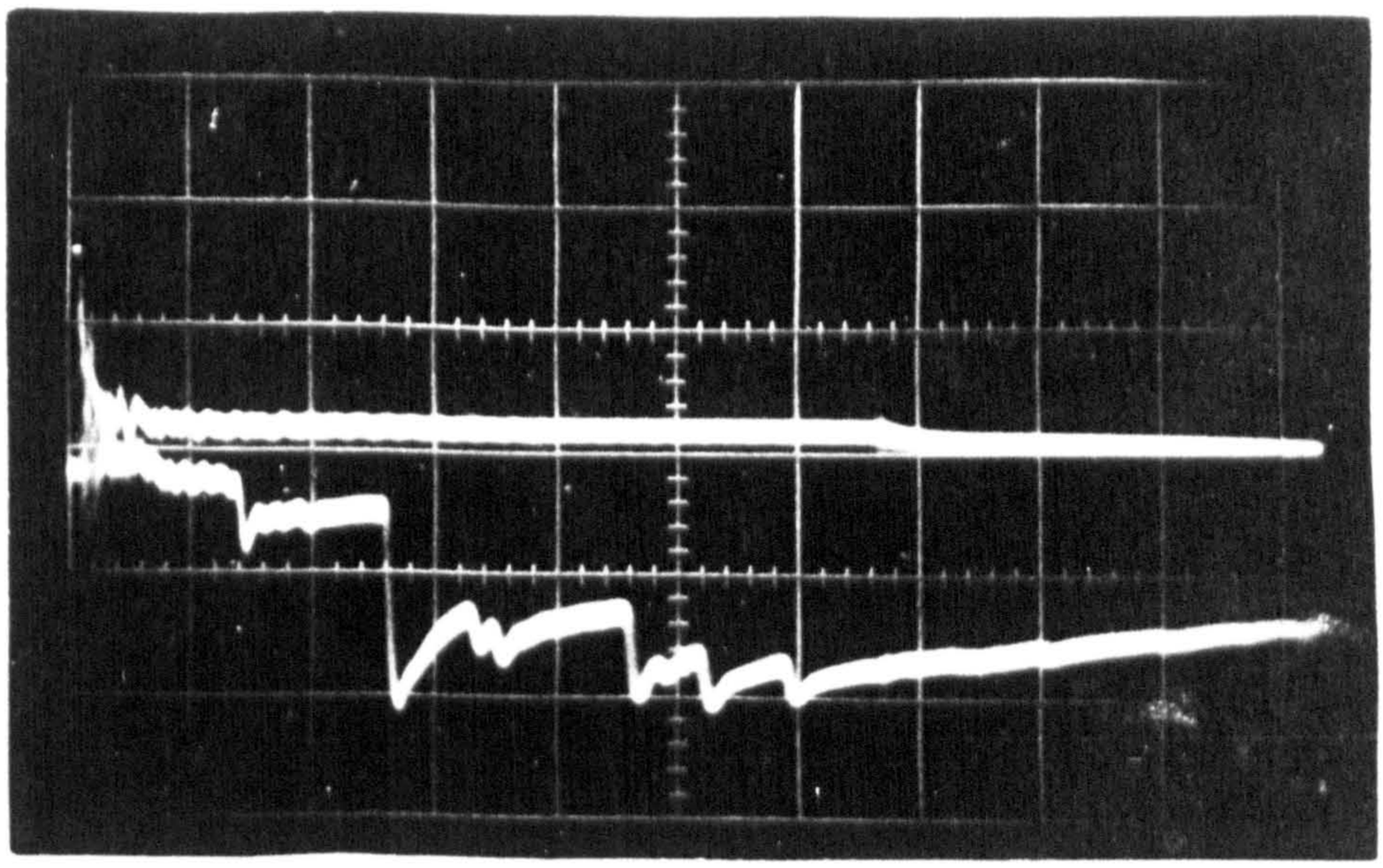

Plate 4.35 Oscillograph showing: upper, step voltage; lower, light emission. Time scale: 1μs cm^{-1}. Voltage: 18kV, negative point polarity. Liquid: n-hexane. Gap: 1.5mm.

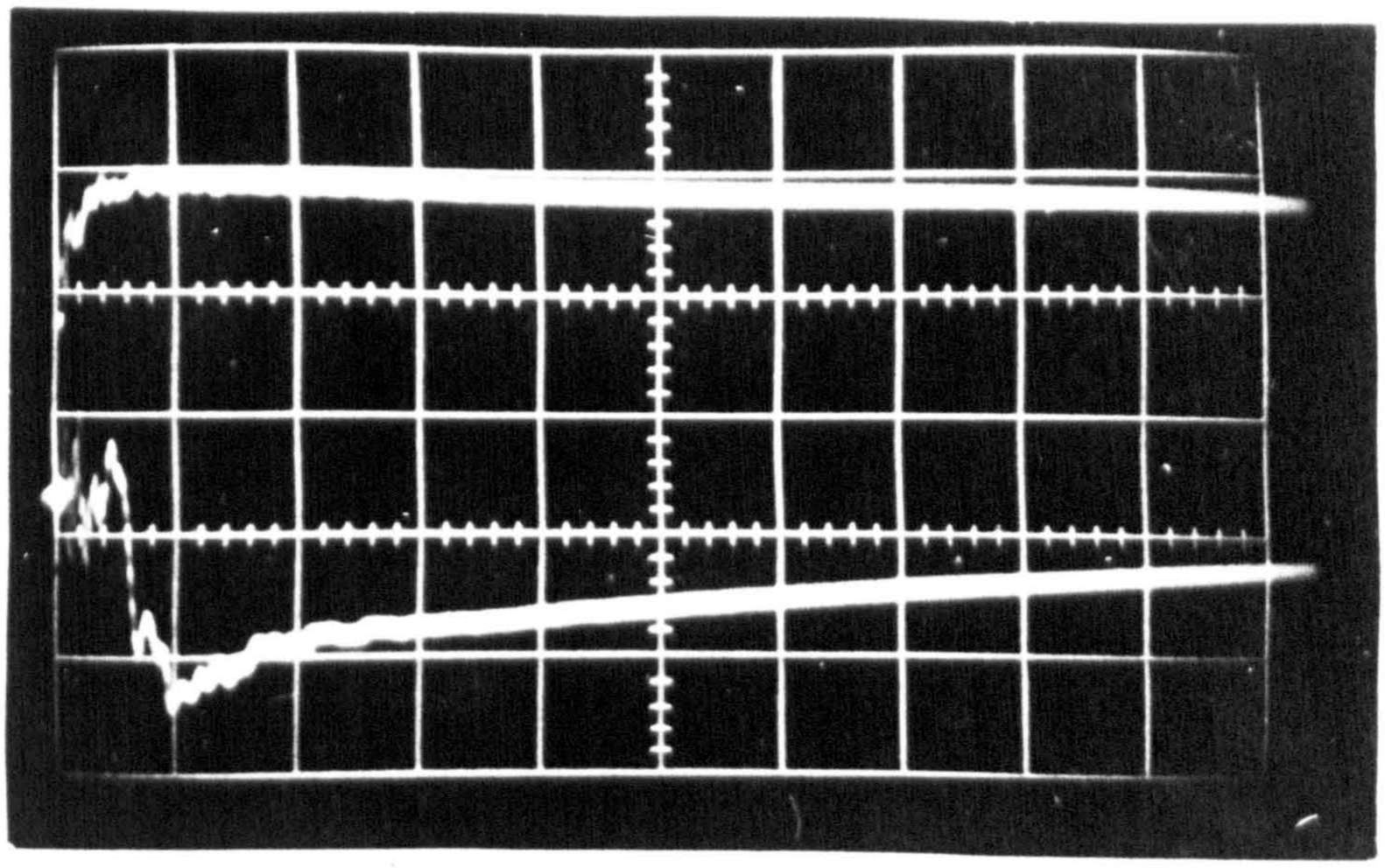

Plate 4.36 Oscillograph showing: upper step voltage; lower, light emission. Time scale: 1μs cm^{-1}. Voltage: 20kV, positive point polarity. Liquid: n-hexane. Gap: 1.5mm.

failure. However, by careful electrode preparation and voltage selection plate 4.36 was recorded. From this oscillogram a single light pulse can be seen 1μs after voltage application.

In order to locate the area of the gap from which the light was emitted a shield was introduced into the photomultiplier viewing plane. For a negative point polarity it was found that light was predominantly emitted from the region in which the point electrode was located. It was found that the tip located light emission was restricted to an area that extended less than 250μm into the gap.

When the point was made positive light pulses were rarely detected near the tip of the point anode. If the gap was viewed directly with the dark adapted eye, light scintillations were occasionally seen randomly distributed over the hemispherical cathode.

4.4 Measurements Derived from Schlieren and Photomultiplier Studies

4.4.1 The velocity of pre-breakdown events

The propagation velocity for disturbances appearing after voltage application were estimated from the time resolved Schlieren records. Direct measurements of the pre-breakdown profile were taken from each frame of a photographic sequence. The size of each event was measured from the tip of the point electrode along a line joining this electrode to the centre of the earthed

hemisphere. The propagation velocity was then calculated from the dimensions of each event and the time interval between frames. Each plot was constructed from an average of 5 trials.

From the characteristics presented, a division is apparent between the positive and negative point polarity results. Assuming the velocity of sound in n-hexane to be $1.11 kms^{-1}$ (11). the propagation velocity for the pre-breakdown event was found to be subsonic for a negative point and supersonic for a positive point polarity.

As illustrated by figure 4.13, the propagation velocity characteristic for a negative point polarity with and without pre-stress exhibits a decay after the application of a step voltage insufficient to precipitate breakdown. The initial velocity can be seen to be typically $100ms^{-1}$, but this decays to zero after 15μs. For a situation leading to gap failure, figure 4.14 shows the propagation velocity decaying to $50ms^{-1}$ but increasing to $100ms^{-1}$ just prior to the appearance of the breakdown spark.

The velocity plot for a positive point breakdown is illustrated by figure 4.15. As for the negative point breakdown characteristic, the curve exhibits a minimum before the advent of gap failure. However, in contrast with the point cathode results, the calculated velocity of propagation can be seen to lie between 3 and 4 kms^{-1} (for the total lifetime of the pre-breakdown event).

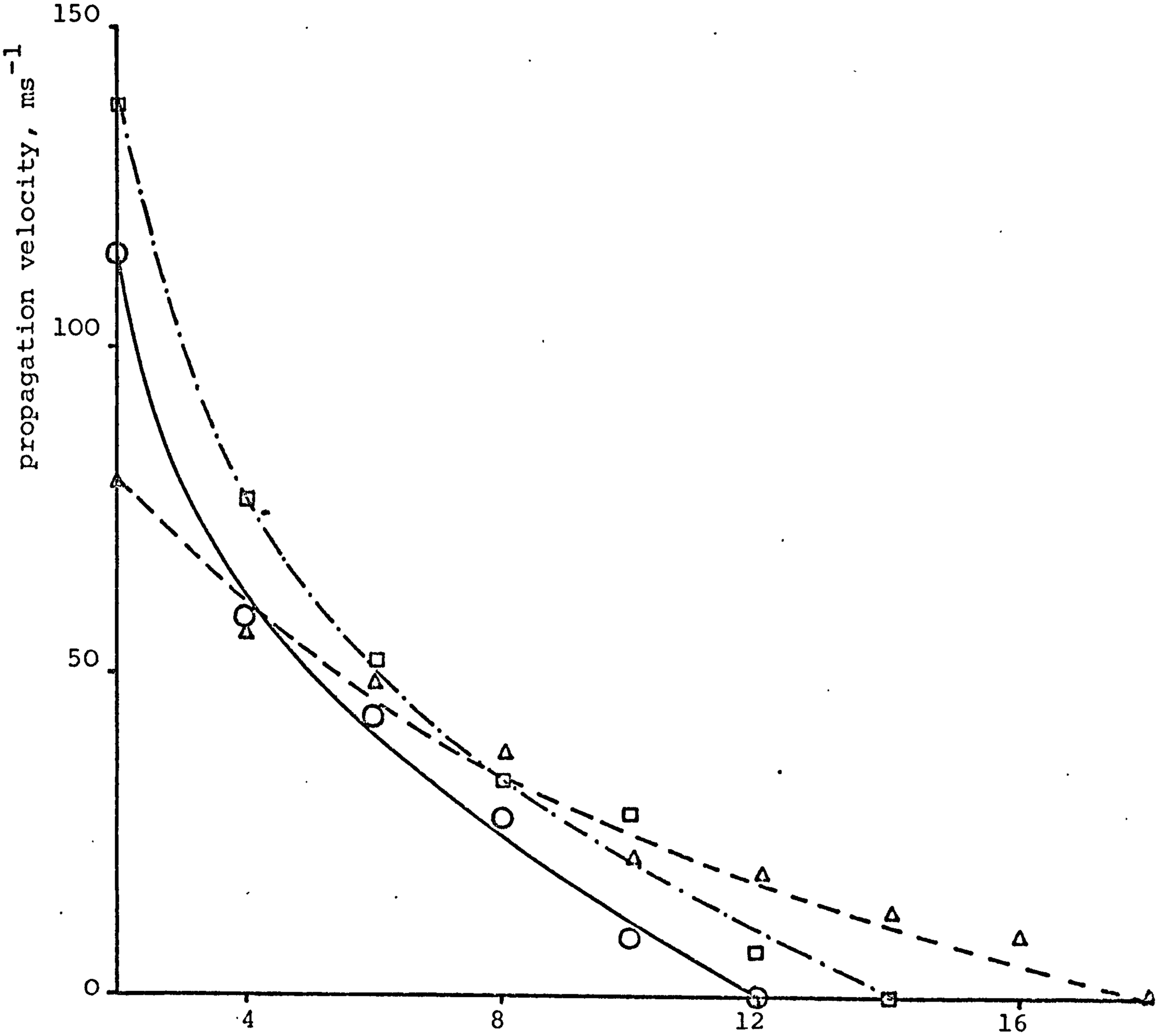

Fig. 4.13 Pre-breakdown event propagation derived from time resolved Schlieren records
(a) solid line, negative step voltage applied to point/sphere electrodes, 1.5mm gap, ambient temperature
(b) chain dotted line as (a) with negative point direct pre-stress
(c) broken line as (a) with positive point direct pre-stress

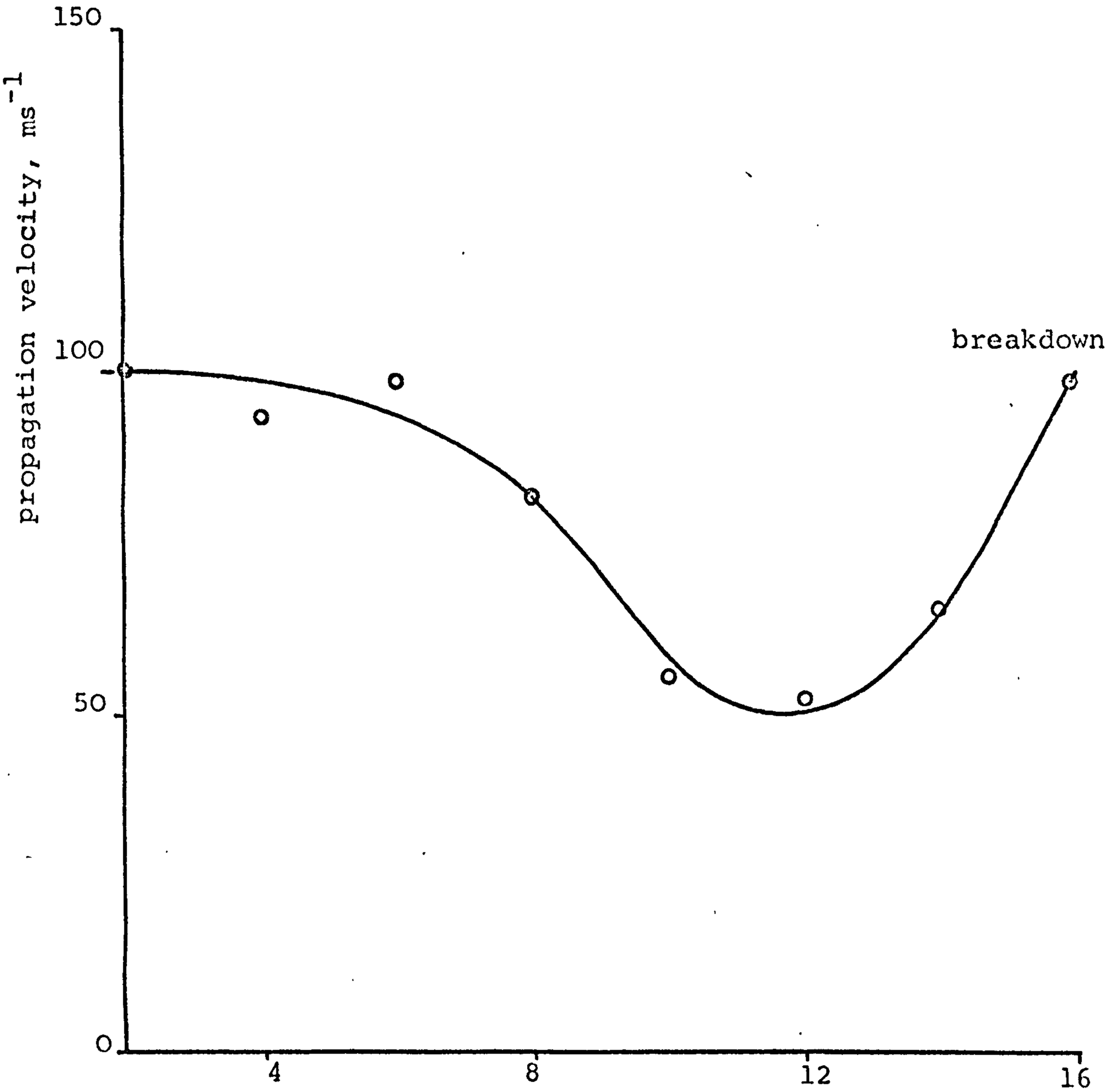

Fig. 4.14 Event propagation leading to breakdown with velocity derived from time resolved Schlieren records.

Negative point/sphere electrodes, 1.5mm gap, ambient temperature.

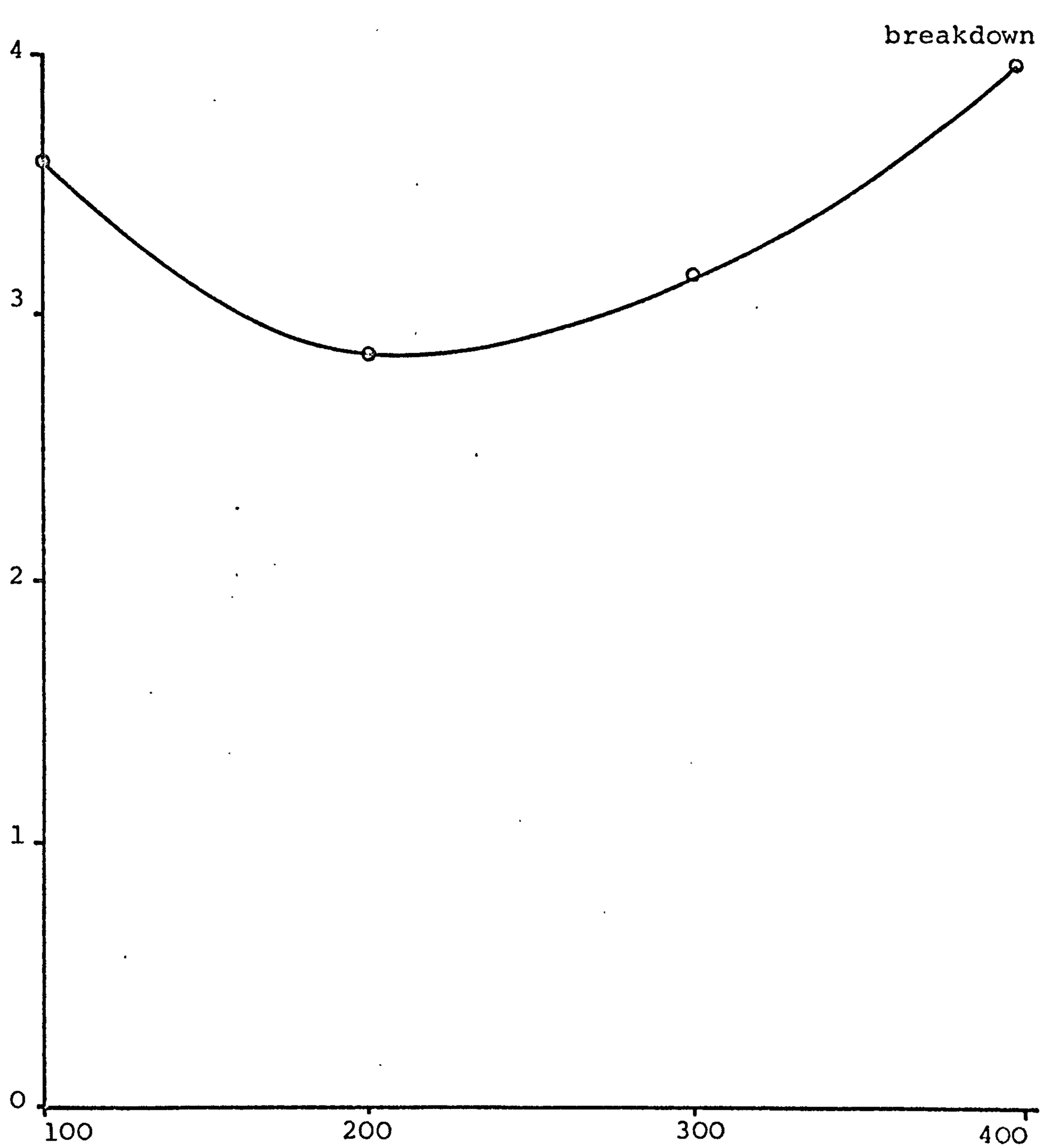

Fig. 4.15 Event propagation leading to breakdown with velocity derived from time resolved Schlieren records. Positive point/sphere electrodes, 1.5mm gap, ambient temperature.

4.4.2 Time to appearance of events for a point cathode

From the time resolved Schlieren records and associated oscillograms, it is evident that a delay exists between the time the step voltage is impressed on the gap and the first appearance of the disturbance. Similarly, a photomultiplier study reveals a time delay to the appearance of the first light pulse after voltage application.

The histogram shown by the solid line of figure 4.16 was obtained from the records showing the time delay to the first light pulse after voltage application to the gap. The broken line superimposed on this plot was derived from the Schlieren records and indicates the time to appearance of the disturbance. Although the accuracy available from the photographic records limits the time resolution to 1μs the plots show a marked similarity with a peak in the frequency of events occurring in the 2μs range.

Applying a pre-stress of either polarity to the gap prior to the step voltage produced a shortening in the time to appearance of the events detected by both methods. As can be seen from figure 4.17, the peak in the distribution is shifted towards a delay to appearance of 1μs.

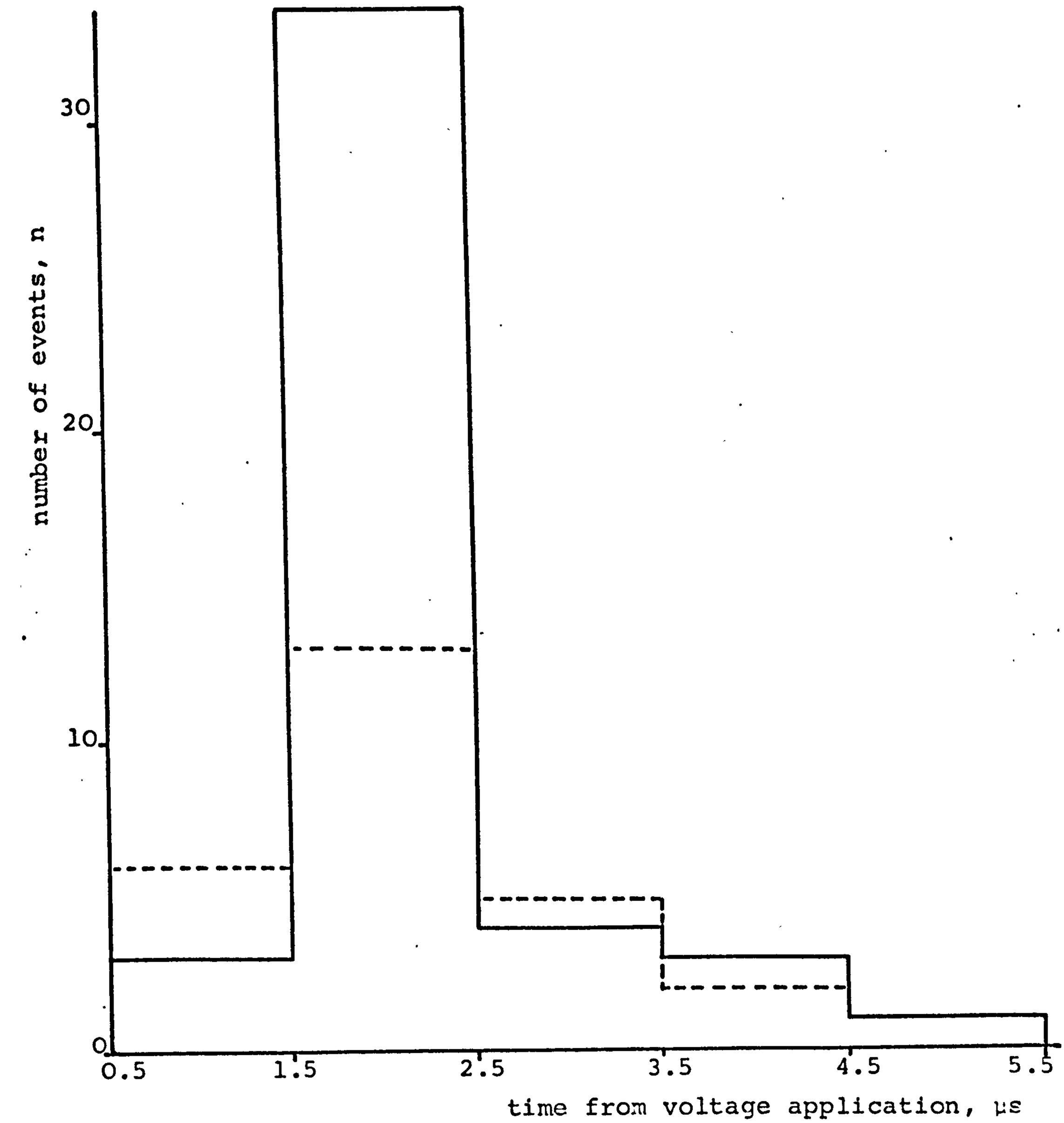

Fig. 4.16 Histograms showing:(a) the time delay to the first photographically recorded event, solid line, and (b) the first light pulse detected by photomultiplier studies, broken line. Negative step voltage applied to point/sphere electrodes, 1.5mm gap, ambient temperature.

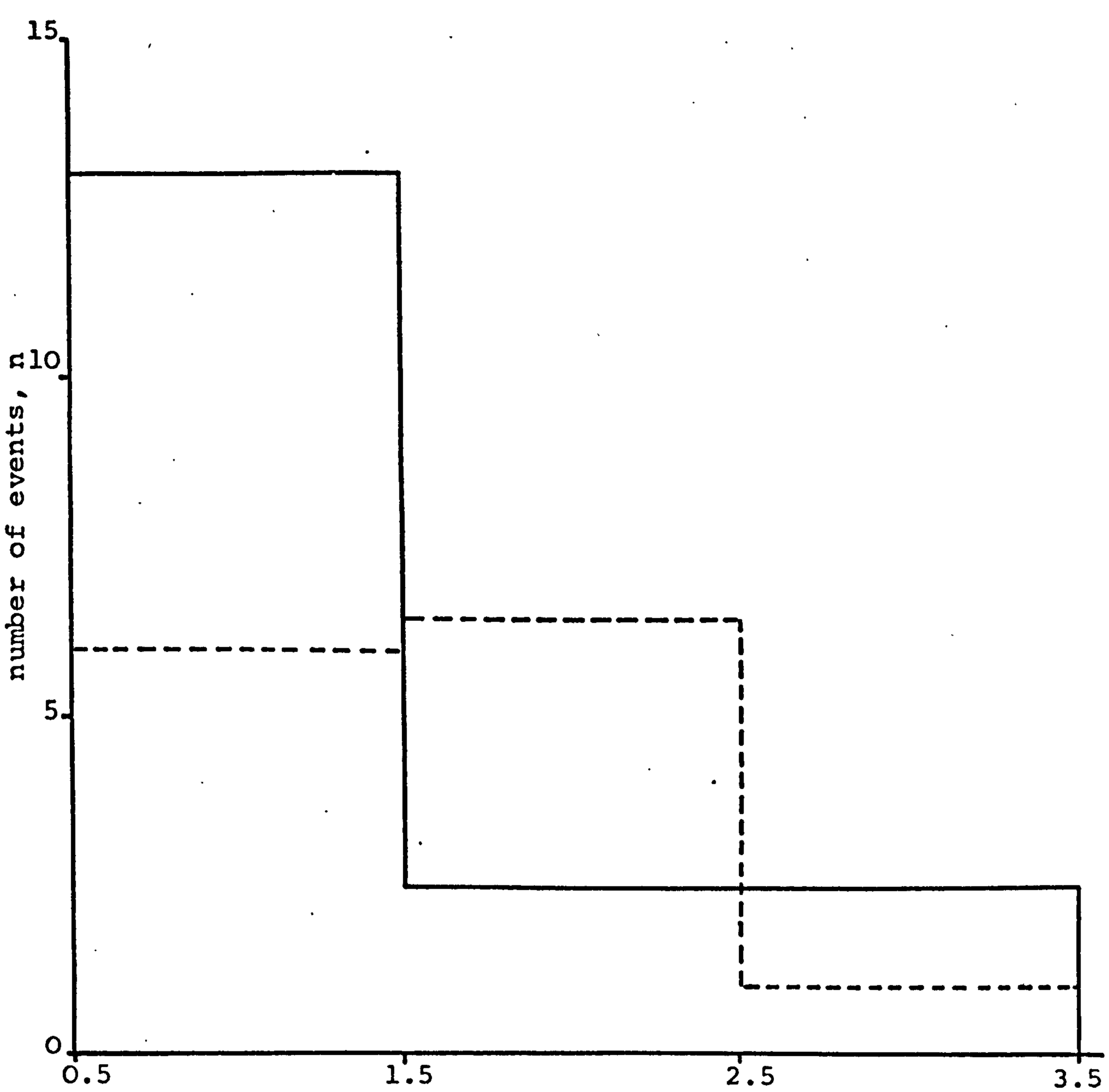

Fig. 4.17 Histogram showing: (a) the time delay to the first photographically recorded event, broken line, and (b) the first light pulse detected by photomultiplier studies, solid line. Negative step voltage applied to point/sphere electrodes, with negative point direct pre-stress, 1.5mm gap, ambient temperature.

4.5 Observations of Direct Voltage Spraying in n-hexane

Using a divergent electrode geometry it was found that a direct electric stress produced localised cavitation in the liquid near the tip of the point, with the subsequent spraying of bubbles into the gap. For the chosen electrode spacing of 1.5mm, this phenomenon occurred more readily for a point cathode than for a point anode. For a point cathode the cavitation inception voltage was found to be a repeatable slowly varying function of pressure at room temperature, being typically 14kV at vapour pressure and 16kV at atmospheric pressure. At inception, spraying was seen to be intermittent, pulsing at approximately 1 per second. The repetition frequency and disturbance size were found to increase with applied voltage. The most obvious pressure effect was on the dimensions of the disturbance and the gas produced. Near vapour pressure, gas was seen to collect in the upper region of the test cell. On allowing the pressure to rise less gas was collected, and at atmospheric pressure, gas collection ceased to accompany spraying. Spraying and gas collection were easily precipitated immediately following a pressure reduction. Conversely, if a degassed liquid at vapour pressure was brought to atmospheric pressure then spraying was not seen until breakdown followed at approximately 35kV.

CHAPTER FIVE

DISCUSSION

5.1 Step Voltage Induced Events

5.1.1 Introduction

It has been shown that on applying a step voltage to a divergent electrode geometry, immersed in a dielectric liquid, that an inhomogenity is generated. Propagation from the point electrode into the bulk of the liquid occurs in all cases. Progress to breakdown is dependent on voltage polarity and amplitude, and in this connection, particularly for a point cathode, the event expansion may cease if an undervoltage is applied. Providing breakdown does not intervene, the pre-breakdown disturbance fragments, and disperses throughout the liquid.

Evidence of pre-breakdown activity has been gathered by the use of sensitive Schlieren, shadowgraph and scattered light probe techniques. In all cases the records present a marked similarity in event profile. The low sensitivity Schlieren or shadowgraph setting of the system revealed a branched bulk disturbance possessing a steep refractive index gradient. When using a sensitive Schlieren setting spherical wavefronts were seen to emanate both from the point cathode and at mid gap located branching sites. For negative point conditions the event propagation remained subsonic. Scattered light photography provides strong evidence for the existence of

cavities throughout the lifetime of the pre-breakdown disturbance. Point anode events were generally shown to propagate at supersonic velocity, and once generated, the disturbance invariably precipitated breakdown. The expanding disturbance appeared to assume a field line path as highlighted by the bubble distribution photographically captured by the scattered light technique.

The nature of this study invites a certain degree of speculation regarding the interpretation of the recorded phenomena and the construction of a plausible breakdown mechanism. Based on the experimental findings accrued from the optical studies, cavitation is advanced as the dominant factor precipitating gap failure. The observations do not preclude the possibility of streamer mechanisms, and indeed a cavitation streamer model is advanced. Luminous streamers were, however, not detected in n-hexane using either the co-axial or orthogonal port test cell. Streamers have previously been observed during tests on transformer oil in this laboratory[36], but these were seen to span the electrode gap without precipitating breakdown.

Refractive index perturbations have been attributed to an elevated temperature liquid plasma[19]. In all cases the temperature rise was calculated to be 48^{o}C, by measuring the cut-off of the Schlieren image and the event persisted for 200μs before fading completely. The present Schlieren study revealed similar events irrespective of the Schlieren sensitivity setting and initial temperature

of the liquid. Dispersion of the disturbance was also observed if breakdown did not intervene with complete disappearance after 100μs[28, 120]. The pre-breakdown sequence depicted by plate 4.3 was recorded with a liquid temperature of 50°C. This elevated temperature behaviour can be seen to differ little from the room temperature trial shown by plate 4.1(a). From this comparison it appears unlikely that a liquid temperature increase of 48°C is responsible for the observed disturbance. On resorting to direct macrophotography, a light scattering region of similar profile was revealed which appeared within the first microsecond of voltage application and persisted for several milliseconds into a discrete dispersion phase. This technique is insensitive to small refractive index perturbations and an interface is necessary to account for the orthogonal scattering behaviour[26]. Persistent light scattering centres may however be readily furnished by a bubble field.

5.1.2 The initiating phase of the cavitation mechanism

It is suggested that the initiating phase results from liquid lift from the point electrode. An electrostatic interpretation is preferred to the alternative of local vapourisation[121]; on the simple premis that a well defined inception voltage exists for the event appearance. In experimental trials, below this critical stress, no refractive index perturbation was detected when using a sensitive Schlieren setting. The thermal mechanism would

be expected to produce an elevated temperature region over a continuous range of stress below boiling inception. Conversely, electrostatic traction exhibits its discontinuity only when liquid lift occurs.

5.1.3 Electrostatic traction

Initially, electrostatic traction acting on interfaces presented by the co-existence of solid, liquid and gaseous phases in a uniform field will be considered. The additional effects of field divergence will then be presented.

The force exerted on a dielectric element of unit volume due to an applied field, E, is given by[122]

$$\underline{t} = (\varepsilon + \frac{a_2 - a_1}{2})\underline{E}(\underline{E}.\underline{n}) - (\frac{\varepsilon + a_2}{2})E^2\underline{n} \qquad (5.1)$$

where $\underline{n}$ is the unit normal directed outwards from the element, a_1, a_2 are constants and ε the permittivity.

A discontinuity between two isotropic dielectric media is shown by fig. 5.1(a). From equation (5.1) using $\alpha = \varepsilon + \frac{a_2 - a_1}{2}$ and $\beta = \frac{\varepsilon + a_2}{2}$ the tractive force per unit area, t, acting from medium 1 to medium 2 is,

$$\underline{t} = [\alpha\underline{E}(\underline{E}.\underline{n})]_2 + [\alpha\underline{E}(\underline{E}.\underline{n})]_1 - [\beta E^2\underline{n}]_2 - [\beta E^2\underline{n}]_1 \qquad (5.2)$$

For an interface between two fluids[122]

$$a_1 = a_2 = -\tau \frac{\partial \varepsilon}{\partial t} = -\frac{\varepsilon_o}{3}(\varepsilon_r - 1)(\varepsilon_r + 2)$$

where τ is the liquid density

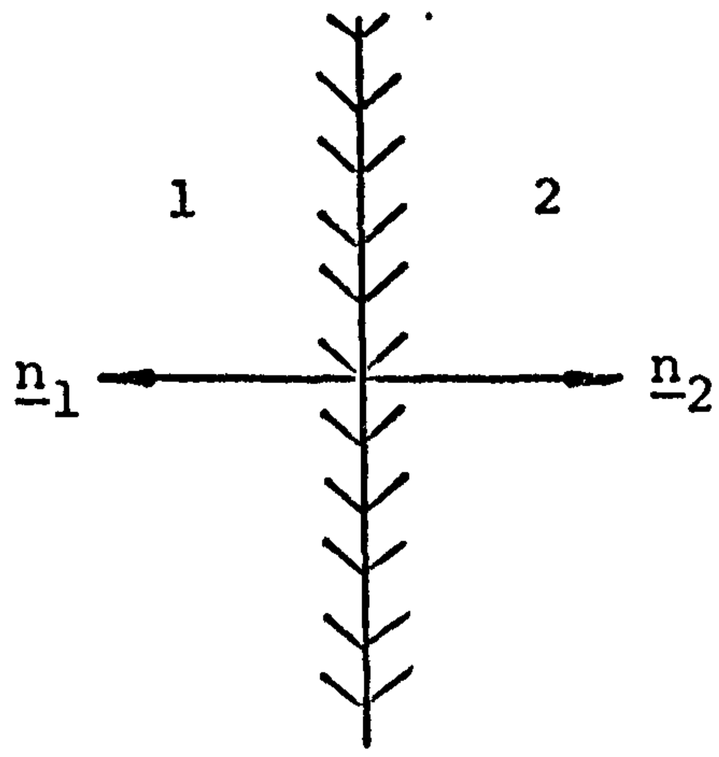

(a)

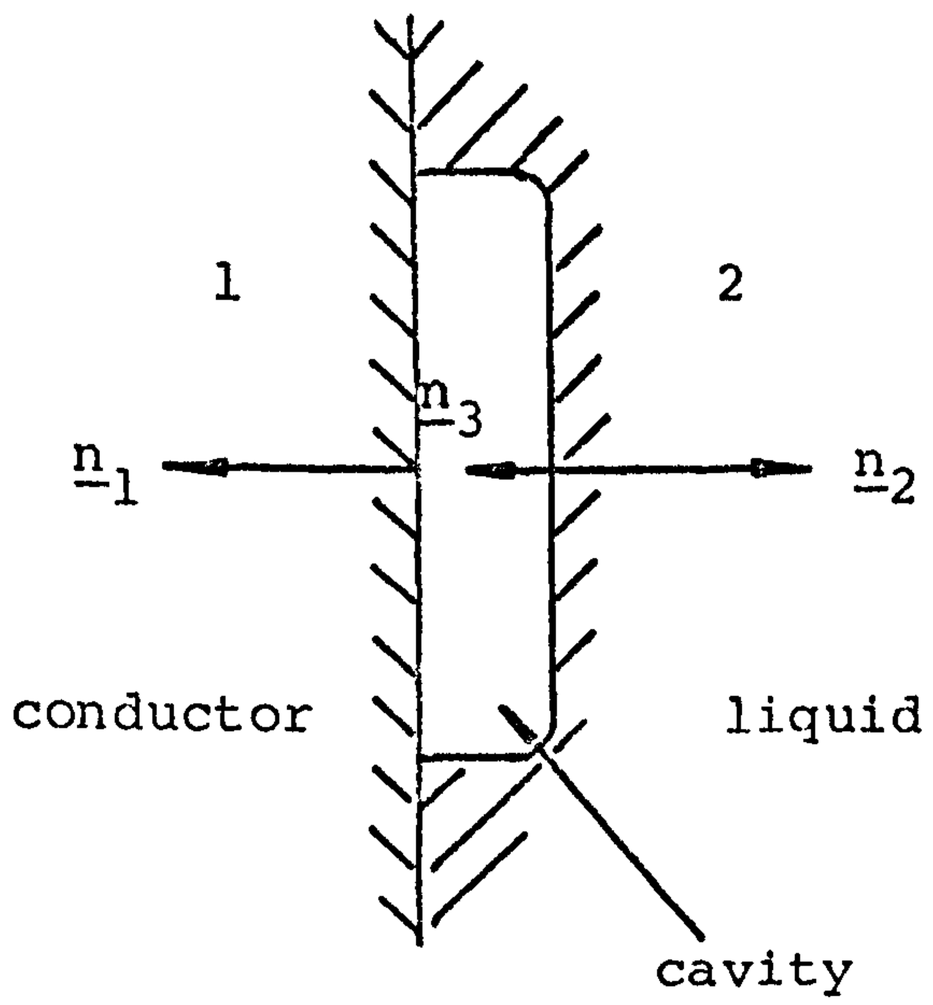

(b)

Fig. 5.1 Showing (a) a dielectric interface and (b) the intervention of a cavity at the boundary between a conductor and an insulating liquid.

$$\alpha = \varepsilon$$

$$\beta = -\frac{\varepsilon_o}{6}(\varepsilon_r{}^2-2\varepsilon_r-2)$$

$$\underline{t} = \frac{\varepsilon_o}{6}\left[\frac{1}{\varepsilon_{r_2}}(\varepsilon_{r_1}{}^2\varepsilon_{r_2}{}^2+4\varepsilon_{r_1}{}^2\varepsilon_{r_2}-6\varepsilon_{r_1}\varepsilon_{r_2}{}^2-3\varepsilon_{r_1}{}^2+2\varepsilon_{r_1}+2)E_{n_1}{}^2\right.$$

$$\left. + (\varepsilon_{r_2}(\varepsilon_{r_2}-2) - \varepsilon_{r_1}(\varepsilon_{r_1}-2))E_{t_1}{}^2\right]\underline{n}_2 \qquad (5.3)$$

This is a traction exerted by the field and is directed from medium 1 of relative permittivity ε_{r_1}, to medium 2, of relative permittivity ε_{r_2}.

$E_1 = 0$, $E_{t_2} = 0$ if medium 1 is a conductor and medium 2 is a liquid,

then (5.2) becomes

$$t = (\alpha-\beta)E_n{}^2\underline{n}$$

$$t = \frac{\varepsilon-a_1}{2}E_n{}^2 \qquad \text{but } a_1 = -\tau\frac{\partial\varepsilon}{\partial\tau} = -\frac{\varepsilon_o}{3}(\varepsilon_r-1)(\varepsilon_r+2)$$

$$t = \tfrac{1}{2}(\varepsilon+\tau\frac{\partial\varepsilon}{\partial\tau})E_n{}^2\underline{n} \qquad (5.4)$$

$$t = \tfrac{1}{2}(\varepsilon+\frac{\varepsilon_o}{3}(\varepsilon_r-1)(\varepsilon_r+2))E_n{}^2\underline{n}$$

where εr is the relative permittivity of the liquid.

This tractive force per unit area will be such that the liquid will be lifted from the electrode. However, there exists an excess pressure throughout the homogenous liquid due to electrostriction which will oppose the traction force.

For a liquid, $p - p_o = \tfrac{1}{2}E^2\tau\frac{\partial\varepsilon}{\partial\tau}$

$$p - p_o = \tfrac{1}{2}E^2\frac{\varepsilon_o}{3}(\varepsilon_r-1)(\varepsilon_r+2)$$

or, $$p - p_o = \frac{\varepsilon_o}{6}(\varepsilon_r-1)(\varepsilon_r+2)E^2 \qquad (5.5)$$

where p is the total pressure in the liquid and p_o the pressure in the liquid in the absence of electric stress.

This relationship has been experimentally verified[123] for n-hexane by the use of a Toepler-Schlieren system. The lift force per unit area, or pressure, will thus reduce to 5.4-5.5 giving,

$$t = \tfrac{1}{2}\,\varepsilon_o\varepsilon_r E^2 \qquad (5.6)$$

This electrically induced traction will be opposed by the work of adhesion $\sigma_{1,2}$ between the liquid dielectric and the electrode.

The adhesion $\sigma_{1,2}$ between the liquid and electrode surface is a specific property of the combination. An experiment was performed using n-hexane and a freshly etched tungsten rod. By measuring the load that could just be supported by a drop of n-hexane on the end of the rod, a value of $50 Nm^{-2}$ was obtained. This is comparable with the published finding[124] of $40 Nm^{-2}$ for n-heptane against stainless steel. This local adhesion pressure is easily overcome by a moderate voltage applied to a point electrode.

For a balance of forces at the electrode surface,

$$\tfrac{1}{2}\,\varepsilon_o\varepsilon_r E'^2 = \sigma_{1,2} \qquad (5.7)$$

using $\sigma_{1,2} = 50 Nm^{-2}$ gives $E' = 25 kV\ cm^{-1}$

For a stress > E' liquid lift may be considered to occur, at which point a new discontinuity is generated.

For the interface between 1 and 3 of fig. 5.1(b), equation 5.4 may be applied with $\varepsilon = \varepsilon_o$ and $\tau\frac{\partial\varepsilon}{\partial\tau} = 0$ for a gas or free space, then

$$t = \tfrac{1}{2}\,\varepsilon_o E_c^{\,2} \qquad (5.8)$$

This is the traction directed from medium 1 to medium 3, at the solid to gas interface, tending to expand the cavity.

The cavity electric stress E_c in equation 5.8 will exceed the previously prevailing homogenous stress in the liquid E due to a change in permittivity. If the section of the cavity represents a plane parallel to the electrode surface, $E_c = \varepsilon_r E$ which is the maximum value of stress enhancement.

Referring to fig. 5.1(b) there will be a traction force acting between the cavity, medium 3, and the liquid, medium 2. For the cavity ε_{r_3} may be taken as unity and equation 5.3 becomes,

$$t = \frac{1}{6}\,\varepsilon_o(\varepsilon_{r_2}-1)^2(2E_{n_3}^{\,2}-E_{t_3}^{\,2})\underline{n}_3$$

$$\text{or } t = \frac{1}{3}\,\varepsilon_o(\varepsilon_r-1)^2E^2 \qquad (5.9)$$

this traction acts from the liquid towards the cavity. The resultant electrostatic traction acting to expand the cavity is given by 5.8-5.9.

$$t = \tfrac{1}{2}\,\varepsilon_o E_c^{\,2} - \frac{1}{3}\,\varepsilon_o(\varepsilon_r-1)^2E^2 \qquad (5.10)$$

Let the initial cavity be a plane as shown by fig. 5.2(a) then, $E_c = \varepsilon_r E$, and

$$t = \tfrac{1}{2}\,\varepsilon_o\varepsilon_r^{\,2}E^2 - \frac{1}{3}\,\varepsilon_o(\varepsilon_r-1)^2E^2 \qquad (5.11)$$

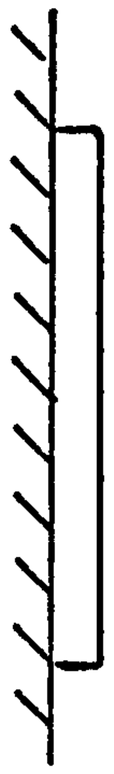

(a)

$E_c = \varepsilon_r E$

(b)

$E_c = \varepsilon_r E$

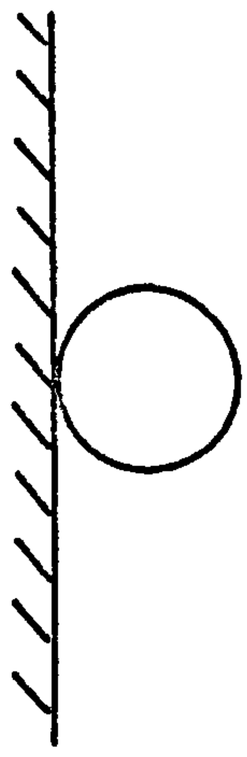

(c)

$E_c = (\frac{\varepsilon_r+2}{3})E$

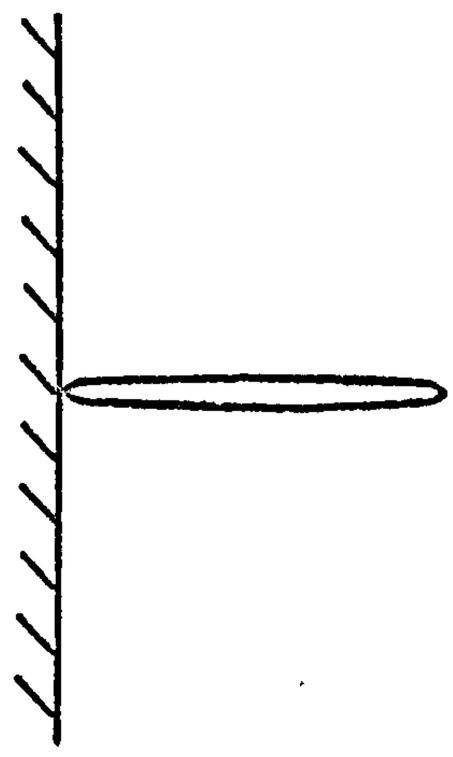

(d)

$E_c = E$

Fig. 5.2 The electric field within: (a) a plane; (b) disc; (c) sphere and (d) a needle shaped cavity.

In addition to the boundary traction the liquid will experience electrostriction due to the homogenous field. This has a value given by equation, 5.5, $\frac{\varepsilon_o}{6}(\varepsilon_r-1)(\varepsilon_r+2)E^2$ and acts as an overpressure throughout the liquid tending to compress the cavity. The resultant traction

$$t = \tfrac{1}{2}\varepsilon_o\varepsilon_r^2E^2 - \frac{1}{3}\varepsilon_o(\varepsilon_r-1)^2E^2 - \frac{\varepsilon_o}{6}(\varepsilon_r-1)(\varepsilon_r+2)E^2 \quad (5.12)$$

$$= \frac{1}{6}\left[3\varepsilon_r^2-2(\varepsilon_r-1)^2-(\varepsilon_r-1)(\varepsilon_r+2)\right]\varepsilon_oE^2$$

$$= \frac{1}{6}\left[3\varepsilon_r^2-2\varepsilon_r^2+4\varepsilon_r-2-\varepsilon_r^2-\varepsilon_r+2\right]\varepsilon_oE^2$$

$$\text{or } t = \tfrac{1}{2}\varepsilon_o\varepsilon_rE^2 \quad (5.13)$$

It can be seen that this result is the same as the initial lift traction. However, now there exist opposing forces stemming from a physical origin due to the co-existence of a gaseous and liquid phase. A pressure will act on the cavity given by $P_o = P_\infty - P_\nu$ where P_∞ is the external pressure applied to the liquid and P_ν is the vapour pressure of the cavity contents. A surface tension pressure also acts towards the centre of the cavity. If the conductor is a curved surface and the liquid lifts as an element following this electrode contour, let the radius of curvature be r, then

$P_s = \frac{2\sigma}{r}$ where σ is the surface tension

Equating pressure terms

$$\tfrac{1}{2}\varepsilon_o\varepsilon_rE^2 = P_\infty - P_\nu + \frac{2\sigma}{r} \quad (5.14)$$

If r = 1μm, $P_\infty = 10^5 Nm^{-2}$ and for n-hexane at ambient temperature, $P_\nu = 2 \times 10^4 Nm^{-2}$,

$\sigma = 18.4 mNm^{-1}$ and $\varepsilon_r = 1.89$

then $E = 1.18 MV\ cm^{-1}$

The simplified model for an homogenous field gives an indication of liquid traction and cavity formation at the electrode. Throughout the lifetime of the cavity additional factors arise that will influence its behaviour. These include: field divergence and distortion due to charge accumulation and the presence of the cavity; the electric stress within the cavity as a function of its shape; the formation of surface charge at the interface and the effect of electrostriction on the liquid structure and dynamic effects. Some of these factors are amenable to calculation and an account of their influence will be made.

5.1.4 The electric field within a cavity

The value of the field enhancement in the spherical cavity shown in fig. 5.2(c) may be calculated from Onsagers model[125].

In the absence of an orientation effect, for example n-hexane has no dipole moment[126], the moment, $\underline{\mu}$, can be identified with the elastic or induced moment $\alpha\underline{E}$, which is independent of temperature. Elastic polarisation is due to a change in the magnitude of the electric moment under the action of electric stress, and depends essentially on a deformation of the electron distribution about the nuclei of corresponding atoms.

The moment $\alpha\underline{E}$ is always parallel to $\underline{E}$ the homogenous stress in the liquid for elastic polarisation and,

$\underline{E}_i = \underline{E}_c + \underline{E}_r$ where $\underline{E}_c$ is the cavity field

$\underline{E}_r$ the reaction field

and $\underline{E}_i$ the resultant internal field.

$$\underline{E}_i = \frac{3\varepsilon_r}{2\varepsilon_r+1}\ \underline{E} + \frac{2(\varepsilon_r-1)}{2\varepsilon_r+1}\ \frac{\underline{\mu}}{4\pi\varepsilon_o R^3} \qquad (5.15)$$

Identifying the volume of the cavity containing a molecule with the volume per molecule,

$$\underline{\mu} = \frac{\underline{P}}{n'} \quad \text{and} \quad \frac{4}{3}\pi R^3 n' = 1$$

where $\underline{P}$ is the polarisation vector, n' the number of molecules and R the cavity radius.

$$\underline{E}_i = \frac{3\varepsilon_r}{2\varepsilon_r+1}\ \underline{E} + \frac{2(\varepsilon_r-1)}{2\varepsilon_r+1}\ \frac{\underline{P}}{3\varepsilon_o} \qquad (5.16)$$

This may be identified with the Lorentz equation,

$$\underline{E}_i = \underline{E} + \frac{1}{3\varepsilon_o}\ \underline{P}$$

putting $\underline{P} = \varepsilon_o(\varepsilon_r-1)\underline{E}$ in equation 5.16 gives,

$$\underline{E}_i = \frac{3\varepsilon_r}{2\varepsilon_r+1}\ \underline{E} + \frac{2(\varepsilon_r-1)(\varepsilon_r-1)}{3(2\varepsilon_r+1)}\ \underline{E}$$

$$\underline{E}_i = \frac{2\varepsilon_r^2+5\varepsilon_r+2}{3(2\varepsilon_r+1)}\ \underline{E}$$

$$\underline{E}_i = \frac{\varepsilon_r+2}{3}\ \underline{E} \qquad (5.17)$$

This is the same result as is obtained by substituting $\underline{P} = \varepsilon_o(\varepsilon_r-1)\underline{E}$ in the Lorentz equation[127,128]. This holds for non-polar materials which exhibit elastic polarisation

with relatively small values of ε_r. Thus for a cavity in n-hexane the electric stress in the cavity is 1.3 times greater than $\underline{E}$ prevailing in the essentially homogenous liquid prior to its existence.

5.1.5 Translation forces in a non-uniform field

If the cavity is formed at a point electrode it will be in a divergent field and experience a translation force acting to drive it into a region of lowest field strength.

$$\underline{F} = \underline{\mu}.\nabla\underline{E}$$

$\underline{\mu} = V_s\underline{P}$ where V_s is the volume of the spherical cavity

$$\underline{\mu} = \frac{4}{3}\pi R^3\underline{P}$$

$$\underline{P} = \varepsilon_o(\varepsilon_r-1)\underline{E}_c$$

but from equation 5.15, $E_c = \frac{3\varepsilon_r}{2\varepsilon_r+1}\ \underline{E}$

$$\underline{P} = \frac{3\varepsilon_o\varepsilon_r(\varepsilon_r-1)}{2\varepsilon_r+1}\ \underline{E}$$

and,

$$\underline{F} = 4\pi R^3\varepsilon_o\varepsilon_r\ \frac{(\varepsilon_r-1)}{2\varepsilon_r+1}\ \underline{E}\ \nabla\ \underline{E} \qquad (5.18)$$

For a charged point to sphere geometry[129] the electric stress falls off with the cube of the distance from the point. Thus it may be assumed that

$$E_\ell = \frac{E_T R_T^{\ 3}}{\ell^3}$$

where E_ℓ is the electric stress at a distance ℓ, measured along a line joining the point to the sphere, from the

centre of a point of tip radius R_T. E_T is the stress at the tip of the point.

$$VE_\ell = \frac{3E_T R_T^3}{\ell^4}$$

This is the field reduction as ℓ increases away from the point. Substituting $E_\ell = \underline{E}$ in equation 5.18

$$F = 4\pi r^3 \varepsilon_o \varepsilon_r \frac{(\varepsilon_r - 1)}{(2\varepsilon_r + 1)} \frac{E_T R_T^3}{\ell^3} \frac{3E_T R_T^3}{\ell^4}$$

This is the translation force acting on a spherical cavity directed away from the point electrode.

The translation pressure, $P_t = \frac{F}{A_n}$

where A_n is the normal projection of the area on which the force acts.

$$P_t = \frac{F}{\pi R^2}$$

$$P_t = 12R\, \varepsilon_o \varepsilon_r \frac{(\varepsilon_r - 1)}{(2\varepsilon_r + 1)} \frac{E_T^2 R_T^6}{\ell^7} \qquad (5.19)$$

Chossing a tip radius of 1μm and a tip stress of 1MV cm^{-1} a plot of the translation pressure, P_t, against cavity radius, R, is shown by fig. 5.3. This shows a peak in the translation pressure of approximately 1/5 Atm. at a cavity radius of 170nm.

At the initial liquid lift stage equation 5.13 gives a traction pressure on the liquid approaching 1 atmosphere at 1MV cm^{-1}. The additional translation pressure due to field divergence may be much less than this value for small cavity radii, as suggested by the plot of fig. 5.3.

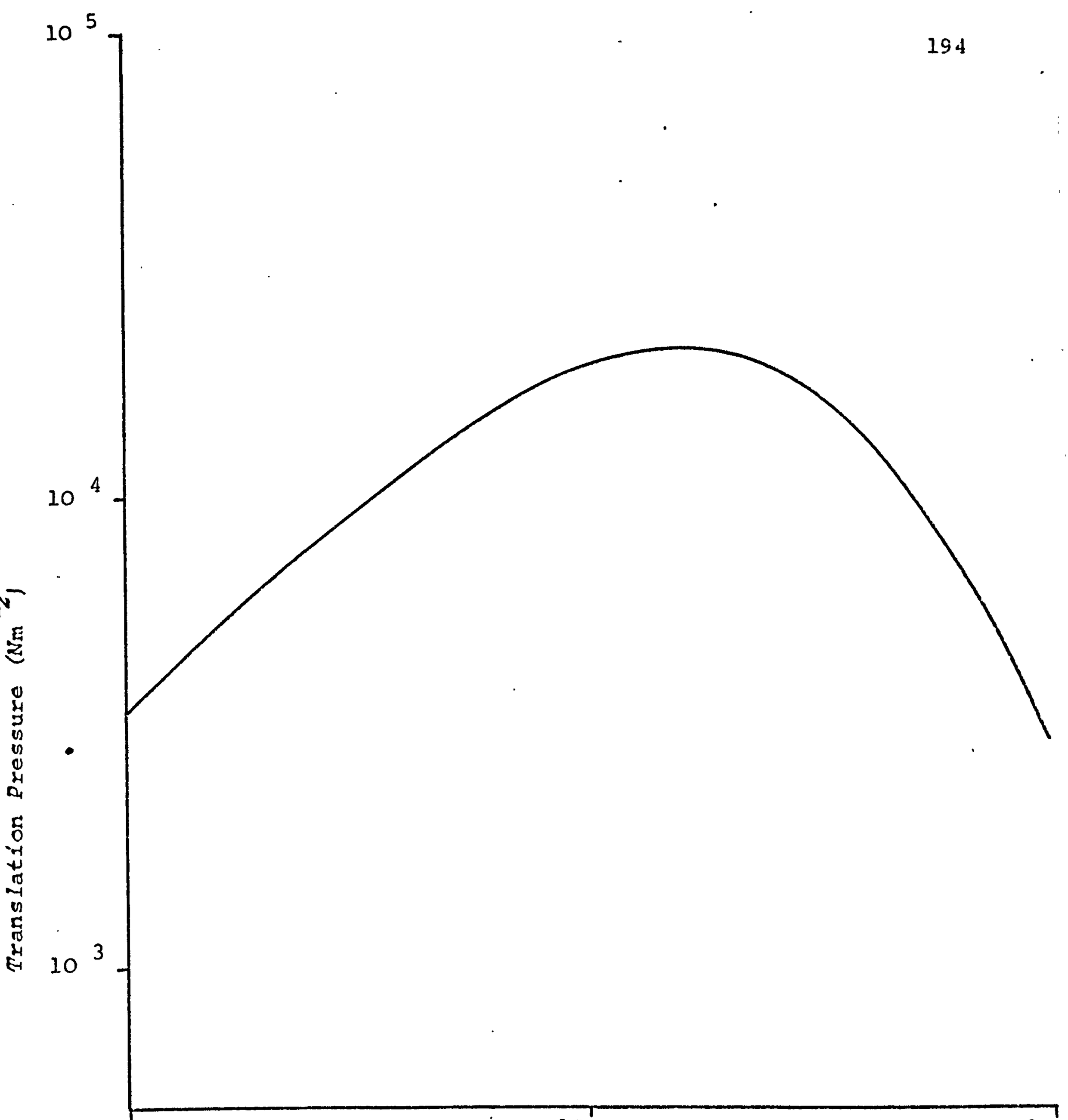

Fig. 5.3 Translation pressure on a cavity at the tip of a 1μm radius point electrode in n-hexane. Point stress: $1MVcm^{-1}$.

Under the influence of surface tension, the tangential component of stress and field divergence translation the plane cavity will extend in the normal field line direction into the gap.

If a spherical cavity is formed the supporting traction changes from the plane case, as described by equation 5.12 in section 5.1.3, and this becomes

$$t = \tfrac{1}{2}\,\varepsilon_o \left[\frac{\varepsilon_r+2}{3}\right]^2 E^2 - 1/3\varepsilon_o(\varepsilon_r-1)^2E^2 - \frac{\varepsilon_o}{6}(\varepsilon_r-1)(\varepsilon_r+2)E^2$$

$$t = \frac{1}{18}\left[\varepsilon_r^2+4\varepsilon_r+4-6\varepsilon_r^2+12\varepsilon_r-6-3\varepsilon_r^2-3\varepsilon_r+6\right]\varepsilon_o E^2$$

giving

$$t = \frac{1}{18}\left[-8\varepsilon_r^2+13\varepsilon_r+4\right]\varepsilon_o E^2$$

substituting $\varepsilon_r=1.89$ for n-hexane

$$t = -33\ \mathrm{Nm}^{-2}$$

The negative value of traction implies that the supporting forces are lost as the cavity forms a sphere, and collapse may follow under the action of surface tension and pressure differences.

If the spherical cavity should break away from the point due to the translation force stemming from field divergence as shown by fig. 5.3, then from equations 5.5 and 5.9

$$t = -\frac{1}{3}\,\varepsilon_o(\varepsilon_r-1)^2E^2 - \frac{\varepsilon_o}{6}(\varepsilon_r-1)(\varepsilon_r+2)E^2$$

which is also negative and again collapse will follow.

5.1.6 The collapse phase

The motion of a collapsing cavity may be approximated by considering the liquid to be incompressible[130,131,132,133] giving:

$$\frac{du}{dt} + \frac{3}{2R} u^2 = \frac{1}{\tau R} [p_L(t) - p_\infty(t)]$$

where, u is speed of interface,

R its radius,

p_L is the pressure in the liquid at the interface

p_∞ the pressure acting on the liquid

τ the liquid density

Direct integration gives

$$u^2 = \frac{2}{3} \frac{(P_{Lo} - P_c)}{\tau} \left[\frac{R_n^3}{R^3} - 1\right] \qquad (5.20)$$

and the time to collapse completely,

$$T_c = 0.915 R_n \frac{\tau}{P_{Lo} - P_c} \qquad (5.21)$$

where,

P_c is the cavity pressure

P_{Lo} is the initial static pressure

R_n the radius at which the bubble starts to collapse

T_c is the Rayleigh collapse time

If the cavity expands to a radius R_o, its speed u becomes zero, then collapse begins, and $R_n = R_o$ and $P_{Lo} >> P_c$.

In the absence of a homocharge at the cavity interface, and using $\tau = 660 Kg\ m^{-3}$ for n-hexane, and

$P_{LO} \simeq P_{\infty} = 10^5$ Nm^{-2} in equations 5.20 and 5.21 the plots of figs. 5.4 and 5.5 were obtained. Employing equation 5.5 to account for the addition of an electrostrictive overpressure in the liquid, supplementary plots on figs. 5.4 and 5.5 show the increase in collapse velocity and reduction of cavity lifetime. A comparison of the collapse speed for cavities in water was made by Flynn[132] and Mellen[134] showing close agreement between the behaviour of an incompressible Rayleigh cavity, the Herring approximation, which includes heat conduction and viscosity effects and the Kirkwood-Bethe form which includes the effect of compressibility. Although the motion of the cavity may be adequately predicted by the incompressible approximation, a true Rayleigh cavity emits only rarefaction waves. In reality the contents of the cavity will be compressed during the final collapse phase, and tend to arrest the motion. This deceleration of the cavity walls may then furnish conditions favourable for the emission of compression waves in the bulk of the liquid. In addition to the likelihood of a cavity containing gas and vapour, there is also the influence of the electric field at the point anode. Electrostriction will provide an additional pressure in the liquid acting to collapse the cavity as shown by figs. 5.4 and 5.5. A rapid single collapse is likely to occur with the attendant emission of a single light pulse[120,135,44] as shown by plate 4.36.

For a point cathode, the electrostatic traction

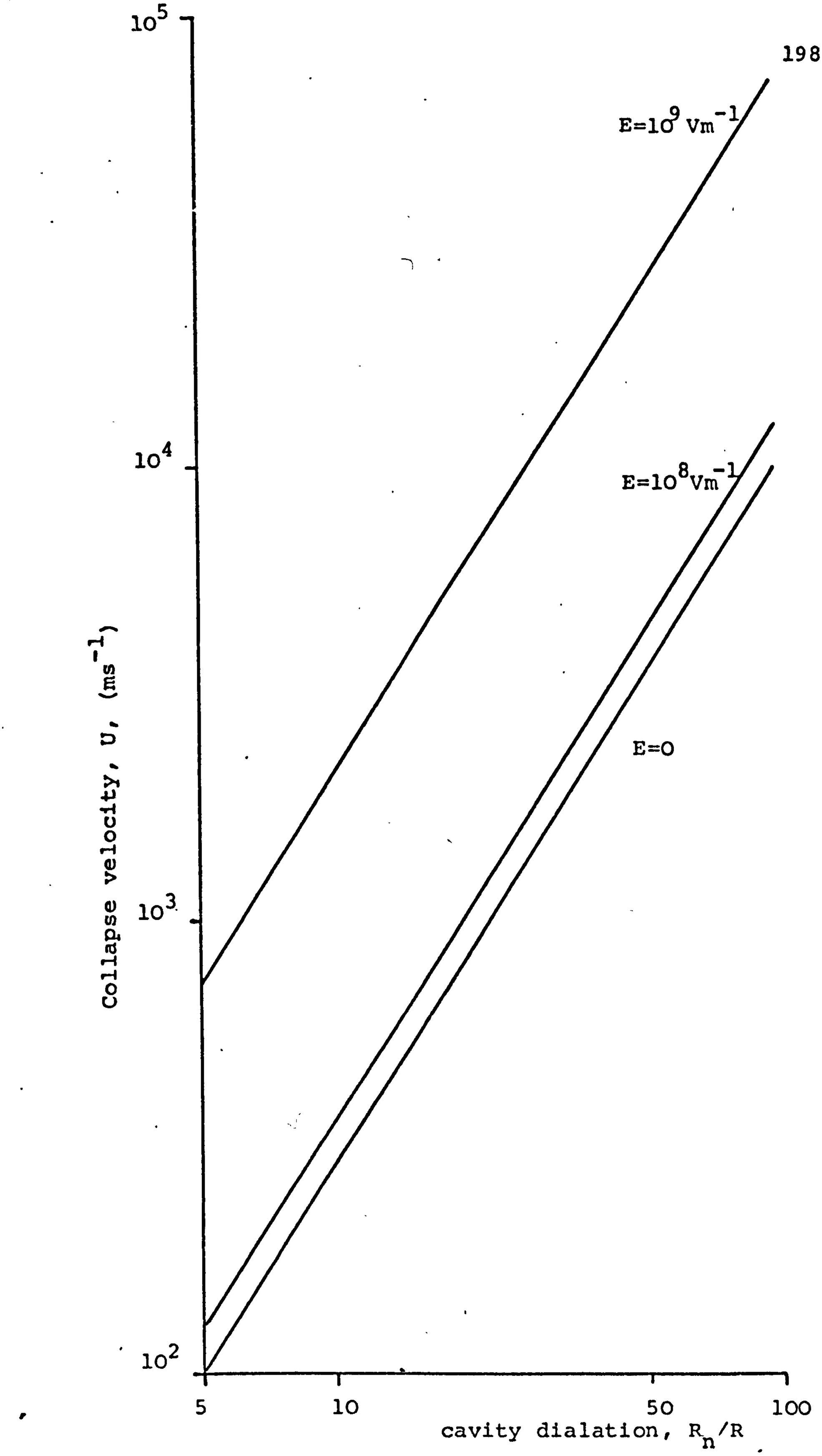

Fig. 5.4 A plot of collapse velocity U vs cavity dialation R_n/R for n-hexane with electrostrictive overpressure.

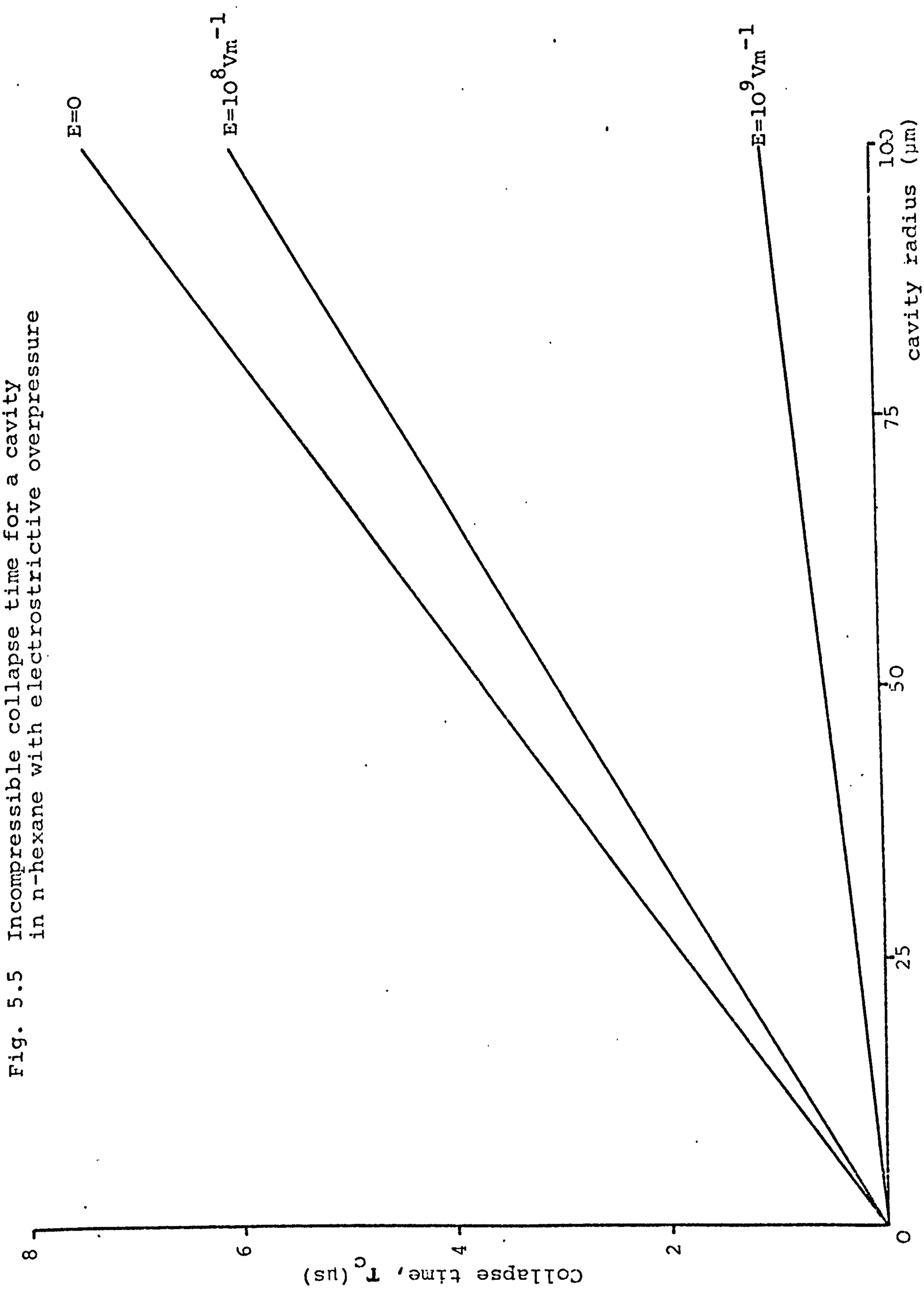

Fig. 5.5 Incompressible collapse time for a cavity in n-hexane with electrostrictive overpressure

equations will be identical to the point anode condition as the forces are quadratic functions of electric stress. The initial collapse behaviour will also be similar but during the final phase the influence of field emission in the vicinity of the point electrode is likely to dominate the motion of the cavity. The presence of a homocharge by accumulation at the gas/liquid interface will aid the final arrest stage by electrostatic repulsion. From the static field study it was observed that a small reduction in integrated conduction current accompanied the inception of point cathode cavitation and acoustic wave generation was associated with the superimposed conduction current pulses. Consequently it is suggested that most of the charge enters the liquid although a small proportion may remain at interfacial sites. Rebounding of the cavity is likely to occur which will generate a succession of weak shock waves in the surrounding liquid, as shown by the sensitive Schlieren record of plate 4.2. A rebounding cavity may give rise to the emission of several light pulses[120,44] as shown by the photomultiplier study and derived oscillograph, plate 4.35. The extended lifetime of the cavity may allow its contents to change by rectified diffusion at the interface. For a degassed liquid, evaporation into the cavity may take place. Gas dissolved in the liquid, even if it is undersaturated, may diffuse across the boundary into the cavity during the pulsating phase[132]. Increasing the gas content of the cavity will provide an additional repulsive force during the collapse

stage[131] and further limit the energy radiated into the liquid.

5.1.7 Cavitation

The advent of cavity collapse at the point electrode is consistent with the photographic evidence presented by plate 4.2. From this record it is apparent that the initiating stage of event propagation is accompanied by spherically radiating shock waves, rooted at the point. A collapsing cavity, with an interfacial velocity exceeding the local velocity of sound in the liquid,with a sudden arrest of the collapse phase may emit both rarefaction and then compressive waves. The compressive wave will overtake the rarefaction component, since velocity increases with density. This will form a steep compressive wavefront followed by rarefaction, propagating in excess of the small perturbation value of acoustic velocity in the liquid.

It is the rarefaction component of the shock wave that is likely to stimulate further cavitation in the bulk of the liquid. For cavitation to follow the passage of a shock wave, rupture of the liquid must occur under tension.

An estimate of the maximum tensile strength for a liquid may be made by the consideration of a free volume model for the liquid, the presence of free volume has been used to account for the change of specific volume with temperature[136], the pressure dependence of density and

viscoelastic behaviour[137], relaxation and viscosity[138, 139,140]. Above its crystallisation temperature, a substance in its liquid form may occupy typically 10% more volume than in the ordered crystalline phase. The free volume model suggests that a liquid is not truly homogenous. A real liquid may be permeated by a large number of rupture surfaces which, in the absence of external stimulation, do not coalesce to form macroscopic cavities. It is the system of microcavities that constitutes the free volume of the liquid.

To rupture or boil a liquid the internal and external pressures are required to be equal. Using the relationship for surface tension an estimate of this pressure may be obtained.

$$P = \frac{2\sigma}{r} \qquad \text{where } \sigma = 18.4 \text{ mNm}^{-1} \text{ for n-hexane,}$$

r is a microcavity of molecular dimensions $\sim 10^{-10}$m

$$p \simeq \frac{2\times 1.84\times 10^{-2}}{10^{-10}} \simeq 3.7 \times 10^{8}\text{Nm}^{-2} = 3\ 700 \text{ atmospheres}$$

This suggests that an upper limit exists for the tensile strength of a liquid. A limiting negative pressure of a few hundred atmospheres has been obtained by Flynn[132] for carefully prepared liquids. With less careful preparation, however, the tensile strength falls far below this value. It would therefore appear that it is contamination that is responsible for cavitation failure of real liquids under tension, and not the stimulation of true free volume.

The electrostrictive overpressure in the liquid is dependent on the square of the field, and consequently is a function of position throughout the electrode gap. Remote from the point, this effect may be small, but large positive pressures may be generated in the liquid close to the high field region. Based on the free volume model of a liquid, the viscosity will increase, and at sufficiently high stress the liquid may assume a behaviour normally attributed to that of a solid[141]. This may further modify the dynamic situation presented during cavity collapse and provide an additional arrest force acting against the motion of the cavity wall.

5.1.8 Cavitation nuclei

If nuclei were free macroscopic gas bubbles, these would soon float to the surface, or dissolve into the liquid, under the action of surface tension and diffusion[142]. Brownian motion may be used to describe the kinetic behaviour of particles in a colloidial suspension[141]. In the absence of electric stress, particles approaching 1μm in diameter may remain, on average, evenly distributed throughout the liquid, against buoyancy and gravitational forces. Persistent gas nuclei may exist in a liquid if additional forces are provided. A solid particle may provide the necessary interface to support the gas phase. A model was proposed by Strasberg[143] describing the behaviour of a gas bubble in a conical pit, forming part of the surface of a suspended particle in a liquid. If

the internal pressure, P_c, is greater than the equilibrium pressure of the gas in the liquid then to approach stability gas will diffuse out of the cavity and the bubble will creep into the apex of the cone, offering a concave surface to the liquid. The internal pressure $P_c = P_\infty - \frac{2\sigma}{R}$ where R is the radius of curvature of the gas to liquid interface and P_∞ the pressure in the liquid. When the internal pressure reaches the gas equilibrium pressure in the liquid, diffusion ceases. With increasing hydrostatic pressure the gas pushes the ring of contact into the apex of the cone, whilst maintaining a constant advancing angle of contact. However, decreasing the hydrostatic pressure does not cause the ring of contact to move away from the apex of the cone. The surface adjusts itself by increasing its radius of curvature and may become convex to accommodate the change of pressure. The position of the gas in the cone, will consequently depend on the maximum pressure to which the liquid has been subjected. If the hydrostatic pressure in the liquid is so low that the angle of contact becomes less than the receding angle of contact, the gas recedes from the apex and suffers unstable expansion.

Supporting the pressurising effect, Harvey et al[144] found that on applying hydrostatic pressure of 1000 Atmospheres to water before a test, that cavitation could not be precipitated in the liquid, although it exhibited a low cavitation threshold prior to pressurisation.

If a particle possesses an irregular surface such that the

ratio of surface area to volume is large, then it will have a high surface energy. Gas may adhere to the particle to form a sphere and provide a stable minimum energy surface. A gas bubble may also exist in a liquid in the presence of free charge. A homocharge distributed over the surface of the bubble will provide the necessary electrostatic repulsion to maintain a stable radius against the surface tension forces.

Substances dissolved in a liquid tend to migrate to interfacial sites. For a free surface or gas bubble, the surface tension will be lowered by the presence of a monomolecular layer. At a particle interface the work of adhesion between the liquid and the solid will be similarly reduced[127] by an adsorbed active surface layer of, for example, soap or resin[145].

5.1.9 The electrical origin of adhesion

In a metal the Fermi level lies in the conduction band but in an insulating media this lies between the conduction and inner valence bands. The dielectric may be considered to have a large energy gap between the conduction and inner valence band, prohibiting electron transition. For the metal, however, this transition readily occurs, and the conduction band may be partially filled at room temperature. A considerable amount of energy is required to remove an electron from the lowest state in the conduction band of an insulator to infinity. The magnitude of this energy may be regarded as the

electron affinity of the insulator.

When a metal is placed in contact with a dielectric, in the absence of an external field, an electron transfer may occur[146] to equalise the Fermi levels of the two materials at the interface. The transfer takes place from the high energy level or 'Fermi sea' of the metal, to the low level of the dielectric. This electron flow results in a positive charge on the metal and a corresponding negative charge in the dielectric. The electric double layer formed at the interface generates a force of attraction or adhesion between the two media[147], acting in addition to the short range London dispersion or Van der Waal attraction. Both terms combine to provide the adhesive force but their roles will depend on oxide or surface active layers[158].

The electric double layer can be considered to be a charged capacitor. The contained charge mechanically stresses the dielectric by a pressure of $\frac{1}{2}\varepsilon E^2$, where E is the gradient existing in the double layer. External electric stress may modify the double layer, adding to this if the metal is made positive, or conversely reducing the magnitude if the metal is negative. For a sufficiently large external voltage, the sign of the double layer may be reversed. When the external and internal stresses are equal the double layer must vanish[127]. The contribution made by the charge layer to adhesion is consequently removed at this point. These interfacial forces act in addition to those previously described on the basis of

electromagnetic theory for barriers of differing permittivity. The stress independent adhesion force may be smaller than the electric traction available at the point electrode due to local field intensification. However, the forces may be comparable at particle sites remote from the electrodes.

For a mixture of liquids, the higher permittivity media generally possesses a positive charge[145]. For example water or moist fibres suspended in an insulating oil will present a charged surface layer at the interface. The higher permittivity contaminant will assume a positive charge with respect to the surrounding liquid. When a positive potential is applied to the dielectric the electrically originating adhesion force will be reduced by this stress facilitating a lowering of the pressure required for separation.

From the foregoing, it is suggested that liquid lift at the electrode will be opposed by electrical adhesion to a limited extent for a positive polarity. Once event propagation is initiated, this is aided by electrostatic lowering of the adhesion forces at liquid/particle interfaces. For a point cathode, the lift process is somewhat eased by reduced adhesion but event propagation in the liquid is hindered by enhanced particle adhesion forces. When the liquid is separated from the contamination site, it is possible that light emission may result, depending on the nature of the materials in contact. Such light

emission, stemming from electrical discharge, is readily observed on the separation of adhesive tape in air.

5.1.10 The breakdown mechanism

The liquid, in this instance n-hexane, will be rapidly charged by the step voltage with a stress distribution dependent on the electrode geometry, in a time commensurate with electronic polarisation $\sim 10^{-15}$s[148]. After bubble expansion and collapse a shock wave is radiated into the liquid. The rarefaction component of the wave may form cavities at pre-existing nuclei in the liquid. The electric stress will aid the cavitation process particularly at contamination sites in the high field region. A combination of electric stress and acoustic stimulation may then initially form cavities in a field line direction. The expanding cavities will modify the field in the liquid.

Consider the expansion of a cavity from a small radius r_1, the dimension of a contamination particle, to a macroscopic bubble of radius r_2. The self capacitance of the sphere is initially $4\pi\varepsilon_o r_1$ and finally $4\pi\varepsilon_o r_2$, so the capacitance increases linearly with radius. The potential distribution and charge are appointed during the leading edge of the step voltage. A change in cavity dimension will not be accompanied by a change in its charge as the resistivity of the liquid provides an extended time constant in conjunction with the available capacitance. This interfacial polarisation action[128] is

similar to the behaviour of a void in a solid dielectric[148]. The time constant may be approximated by calculating the capacitance of a bubble and the resistance and capacitance of the associated column of liquid spanning the electrode gap, with a diameter equal to that of the bubble.

The resistance of the column $R_c = \frac{\rho \ell}{A}$

capacitance of the column $C_c = \frac{\varepsilon A}{\ell}$

capacitance of the sphere $C_s = 4\pi\varepsilon_o r$

with reference to fig. 5.6

Using

$\rho = 10^{13} \Omega m$

$\ell = 1.5$ mm

$r = 1$ μm .

$$C_c = \frac{\varepsilon \pi r^2}{\ell} = 3.5 \times 10^{-20} F$$

$$C_s = 4\pi\varepsilon_o r = 1.1 \times 10^{-16} F$$

$$R_c = \frac{\rho \ell}{\pi r^2} = 4.8 \times 10^{21} \Omega$$

As the capacitance of the sphere is considerably larger than that of the column, the charging of the sphere will occur with a time constant given by $C_s R_c \simeq 5 \times 10^5 s$. It is thus likely that no appreciable charging of a cavity will occur throughout the lifetime of a pre-breakdown event since this is $< 10^{-4} s$.

As no charging occurs in the lifetime of the event, the bubble may be considered to expand with constant charge.

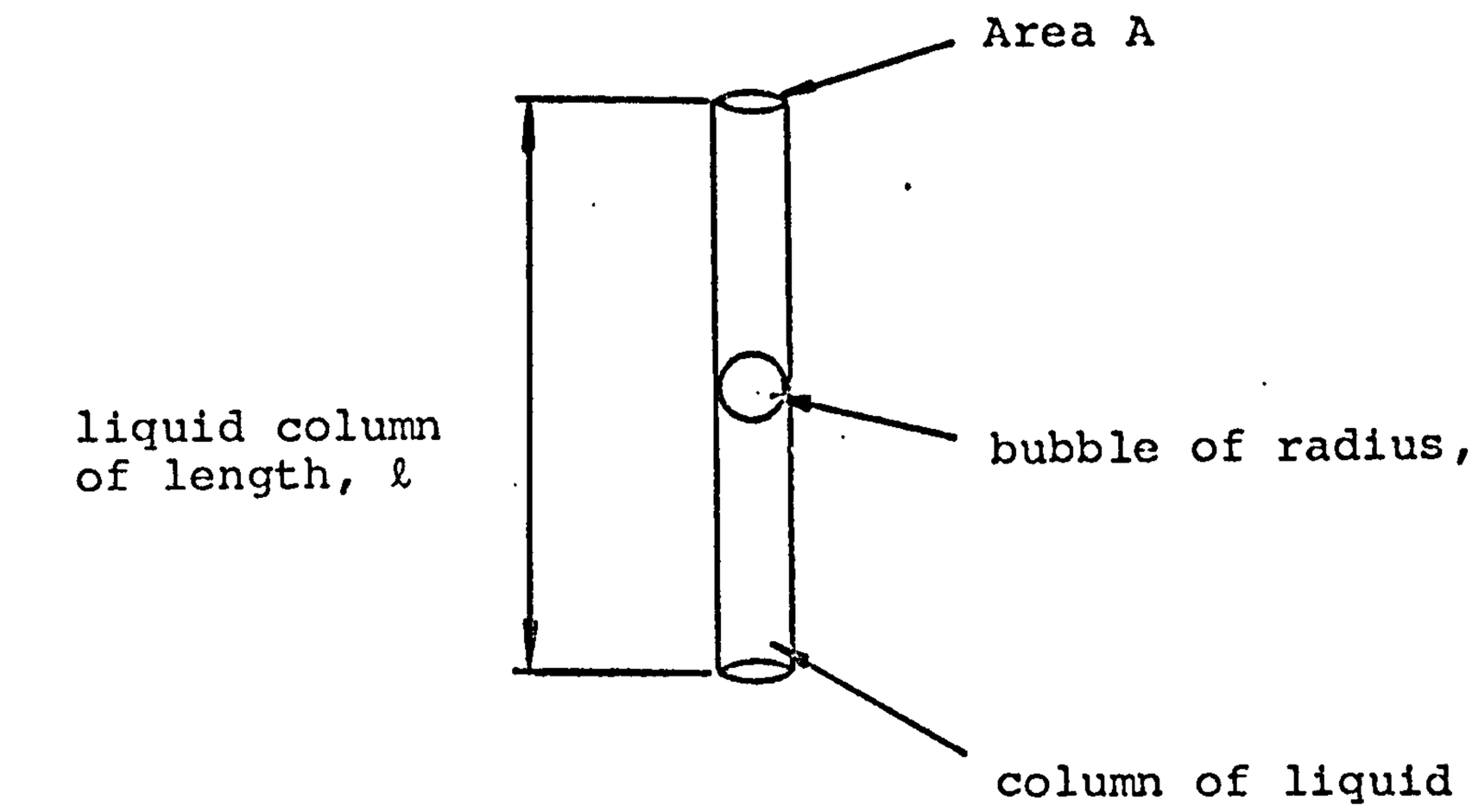

Fig. 5.6 Liquid column containing a bubble

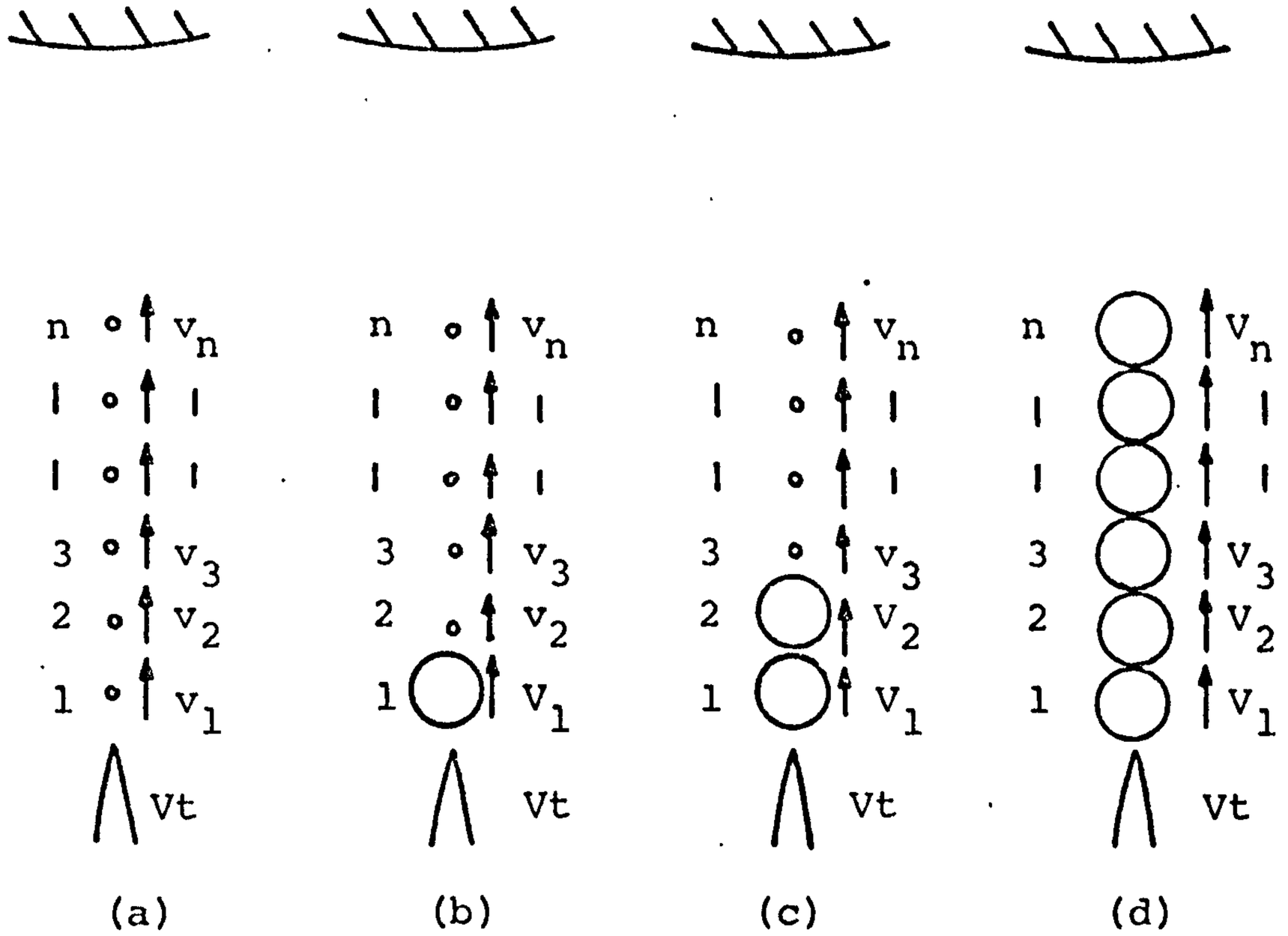

Fig. 5.7 Streamer formation from a series of expanding bubbles.

Using $Q = CV$

$$Q_1 = C_1 V_1 \qquad \text{or,}$$

$$V_1 = \frac{Q_1}{4\pi\varepsilon_o r_1}$$

on expansion from r_1 to r_2

$$V_2 = \frac{Q_1}{4\pi\varepsilon_o r_2}$$

so

$$\frac{V_2}{V_1} = \frac{r_1}{r_2}$$

Hence, the voltage across the cavity decreases linearly with increase in bubble radius.

The stored energy $W = \frac{1}{2}\frac{Q^2}{C}$

$$W_1 = \frac{Q_1^2}{8\pi\varepsilon_o r_1}$$

$$W_2 = \frac{Q_1^2}{8\pi\varepsilon_o r_2}$$

so

$$\frac{W_2}{W_1} = \frac{r_1}{r_2}$$

This shows that the stored energy is reduced in a similar manner with the voltage, as the radius increases. If the initial and final states are in equilibrium then the loss in stored energy suggests that work may be done by the cavity against dynamic electrostrictive and surface tension forces acting to collapse the cavity.

Referring to fig. 5.7 let (a) represent the gap immediately after switch on. Charge and voltage will be distributed throughout the gap at this stage and the voltage v_n across a nucleation site n may be determined from its location in the gap and the electrode geometry. At (b) after cavity collapse let the ensuing shock wave and electric stress form a bubble, 1, close to the point at a contamination site. If the bubble, 1, expands at constant charge, then the voltage across it, V_1, will be much less than the initial voltage v_1 at the embryonic site. The bubble now occupies a high field region but $V_1 \rightarrow 0$. A consequence of this expansion is that V_t appears at the site 2. Fig. (c) shows the event that follows the expansion of the first cavity. The increased voltage at the second site will aid the expansion process in the field line direction. Expansion of the second cavity results in a similar decrease in voltage across the bubble. The elevated voltage is consequently extended through neighbouring sites to any point n in the liquid along a field line, fig. (d). As the progress of the line of bubbles continues it may be considered to form a streamer with a relatively small potential drop across its length, extending the potential of the point electrode into the gap. As the event transverses the gap it is initially in a high field region and expansion may be rapid. Away from the point the potential gradient reduces and this may be accompanied by a reduction in propagation velocity. However, as the earthed electrode is approached, the

potential difference between the tip of the event and this electrode increases and again forms local field intensification. This results in an increase in propagation velocity in the latter stages of event expansion, as shown by figs. 4.14 and 4.15.

For a point anode the event often propagates in a field line direction and produces less cavities than a point cathode. On spanning the gap the line of bubbles may charge and the stress will be distributed throughout the length of the streamer. Breakdown may follow but this will depend on the size and number of bubbles. Plate 4.23(b) illustrates a bubble streamer with approximately 20μm cavities spanning the gap without precipitating breakdown.

At higher voltages breakdown may follow in the gaseous phase, although the liquid may not be disrupted. The spark may be self extinguishing when the interspaced liquid acquires a charge. A further increase in voltage may allow the discharge products to expand the cavities and form a complete breakdown channel between the electrodes.

In contrast with the point anode behaviour, the slower propagating negative point event may allow the stimulation of more nucleation sites in the bulk of the liquid by both electric stress and acoustic wave propagation. When sufficient voltage is applied, a densely packed region of microbubbles spans the gap.

Branching can be seen to occur which may be rooted at centres of transient cavity collapse. This can be seen throughout the extended expansion phase of the event. The presence of a gaseous channel between the electrodes may allow a bulk discharge to follow by a similar mechanism to that operating for a point anode with an overvoltage.

If an undervoltage is applied to a sufficiently divergent geometry, propagation is precipitated in the high field region but is arrested in the mid gap position where the field is much lower. This supports the experimental findings depicted by fig. 4.13. Temperature and pressure variations have been shown to influence the propagation of the pre-breakdown event both in this and other work[52,104].

Gaseous nuclation centres may behave in a similar manner to the free volume in a liquid. Either a temperature increase or pressure decrease increases the size of the embrionic cavity. This enlarged region will be more susceptible to stimulation by tractive forces to form unstable cavities. Large clouds of microcavities are evident from the scattered light photographs, plates 4.27(a) and 4.29(b).

Viscosity and liquid density decrease with temperature increase, and to a lesser extent pressure reduction. This allows an enhanced collapse speed and reduced lifetime for a transient cavity, and consequently aids the propagation of the event.

Although the thermal dependence is more complex, if the adhesion behaves as the surface tension this will be reduced by a temperature elevation. Consequently liquid lift from an interface will occur more readily at higher temperatures supporting the findings for step voltage trials. The temperature influence on direct voltage behaviour is discussed in section 5.3.

Studies using bubble chambers[149] suggest that cavities are generated in the wake of high energy particles passing through the liquid. However, the high degree of supersaturation and particle energy required suggests that this process is precluded from the situation of n-alkanes at ordinary temperatures and pressures.

5.2 Direct Stress and its Influence on Step Voltage Trials

5.2.1 Introduction

Direct pre-stress was found to dominate the behaviour of subsequent step voltage trials. In the absence of strong evidence, a tentative model is advanced to account for the interaction of an established space charge and a super-imposed transient event.

5.2.2 The creation of space charge

If sufficient negative direct voltage is applied to the point electrode, copious electron emission is possible due to field intensification. The electrons may attach to liquid, impurity or oxygen molecules[109] to form negative ions in the vicinity of the point cathode. The high field intensification may provide electrons and negative ions in such numbers that outside this region there is an insufficient

extracting field to remove them all. Some impurity molecules may dissociate as a result of the high field and form ions. The negative ions may then drift towards the anode. The positive dissociation ions may accumulate in the vicinity of the point cathode and its injected homocharge. Although neutralisation may occur in the region close to the point cathode the negative space charge will predominate.

For a positive point electrode at moderate voltages, field induced dissociation of impurity molecules may be the only mechanism[106]. Positive ions will drift to the cathode leaving negative ions close to the point anode. The formation of an electrode oxide layer may provide the necessary blocking action to prevent immediate space charge neutralisation[68,91,150].

An additional effect of pre-stress may be to deplete the mid gap region of suspended particles. Not only will charged particles be drawn to the electrodes but uncharged impurities will be impelled by dielectrophoretic forces which will depend on dimensions and gap location. Most particles are likely to possess a permittivity greater than that of n-hexane and so be drawn to the high field region presented by the point. Some contamination will, however, be present throughout the gap due to stress induced liquid motion.

A particle redistribution may also contribute to a lowering of the statistical time lag by increasing the particle count in the high field region and aid the

cavitation process. The additional impurity sites near the point may provide interfacial areas with a low work of adhesion , allowing ease of liquid separation. This is supported by the findings of the pre-stressed step voltage trials displayed by figure 4.17.

5.2.3 Negative step with negative pre-stress

Applying a negative step voltage to the point electrode whilst this was negatively pre-stressed produced a characteristic event profile. This behaviour may be attributed to the space charge created prior to the step voltage trial[151,152].

The initial stage of event formation may be inhibited by the presence of a negative space charge around the point electrode. A reduction of electrostatic traction will also be accompanied by a suppression of the travelling voltage wavefront in the presence of a homo-charge. Cavity collapse energy will be similarly reduced by the accumulation of a substantial interfacial charge.

On reaching the mid gap, forward propagation will be suppressed due to a reduction in the number of nucleation sites. As the anode is approached the event encounters the wall of negative ions forming the half diffuse space charge field, and consequently spreads in a plane normal to the inter-electrode axis; as shown by the Schlieren record, plate 4.8(a). A similar mechanism operates for a dual point electrode geometry when the event assumes a crescent profile on approaching the

anode as shown by plate 4.13(a).

5.2.4 Positive step with negative pre-stress

The influence of a negative pre-stress prior to a positive going step voltage trial is shown by plate 4.10. Then event propagation now appears similar to that encountered for a negative step voltage, and is readily precipitated at 13kV.

A reduced inception voltage would be expected in the presence of a negative space charge close to the point as this will enhance the local stress. Negative ions in the vicinity of an interface may accumulate at the boundary and limit the energy dissipated by electrostatic repulsion of the cavity walls during the initiating collapse phase. Once the event is formed, the progress of the bubble streamer mechanism will also be hampered by the presence of the negative space charge which modifies the field in which the bubble streamer propagates. The reduction of contamination in the gap by pre-stressing will also inhibit the propagation of the event. Consequently, a disturbance may be precipitated without leading to breakdown, which is contrary to the non pre-stressed behaviour.

5.2.5 Negative step with positive pre-stress

A negative step voltage applied in the presence of a positive pre-stress also produces an event with a modified profile. The lift process follows in a field of

negative space charge, with consequently reduced tractive forces. A reduction of the local field by the negative ions allows only a small disturbance to be formed at voltages approaching normal breakdown value as shown by plates 4.8(b), and 4.13(b). The mid gap may again possess a reduced particle count, contributing an additional factor in propagation suppression.

5.2.6 Positive step with positive pre-stress

Maintaining the same pre-stress but applying a positive going step voltage, will allow some reduction of the inception voltage for the event. The inhibiting mechanism may again be attributed to the negative ions formed near the point electrode, in this instance by field induced impurity dissociation.

5.3 Direct Voltage Study

5.3.1 Introduction

As can be seen from the scattered light photographs discrete bubbles appear to be swept from the point into the bulk of the liquid after several milliseconds from voltage application. This behaviour approaches that of direct voltage spraying which has been reported by Mirza et al[25].

For a point cathode a persistent light scattering cone is located at its tip. In the absence of background illumination the cone can be seen to emit light. Acoustic emissions were also detected, but only whilst the spraying phenomenon continued.

5.3.2 The influence of temperature variation

Oscillographically displaying the conduction current, light and acoustic emissions revealed a coincident pulse behaviour for the three parameters, when employing a point cathode. For transformer oil or n-hexane at room temperature, integrated plots of the three parameters exhibited a coincident transitional behaviour[153,154]. At elevated temperatures the conduction transition was suppressed whilst the light emission discontinuity was shifted to a higher stress. At high stresses the conduction current plots converge to a common value. As can be seen from fig. 4.6 it is the pre-transition conduction that increases with temperature whilst the post transition magnitudes show a lesser degree of dependence. The plots of fig. 4.9 show that the post-transition current is thermally invariant whilst the high level emission is suppressed at elevated temperatures.

The pre-transition light emission is relatively insensitive, whilst the conduction current increases by nearly two orders of magnitude over a 60^{o}C temperature rise. The pre-transition current may be identified with ionic conduction due to impurities in the liquid[69,88]: (see section 5.2).

The intimate relationship between emission and cavitation, and the evidence of differing thermal dependence of integrated conduction and light emission, reveals that conduction current is not a primary influence

on cavitation. Indeed, the 85^{o}C plot of fig. 4.6 suggests no interrelationship between integrated conduction and cavitation. However, returning to plate 4.34, it can be seen that the conduction current and light pulse behaviour is easily understood by a further oscillographic investigation. Fig. 4.7 shows a plot of the direct current offset, or pedestal, on which the conduction current pulses were superimposed. The high and low temperature conduction plots of fig. 4.6 are reproduced by this method. This stresses the important difference in magnitude between the pulse and pedestal conduction. The integrated contribution made by the superimposed pulses which were seen to have an amplitude of approximately 10^{-8}A, may be regarded as minimal compared with the pedestal current. This finding reinforces the view that direct voltage conduction is little influenced by the cavitation process.

If field emission occurs at sufficiently high stresses this will be influenced by space charge formation and charge transport by liquid motion in addition to impurity conduction. An increase in temperature may ease the formation of space charge layers and impurity conduction by decreasing viscosity and increasing mobility. The space charge created may, however, be modified by increased liquid motion associated with a reduced viscosity.

If cavitation resulted from a boiling process it is suggested that an increase in temperature would enhance the spraying process and force inception to a lower voltage.

If boiling resulted from a heating of the point electrode due to the current flowing through it, then as the current passes through a transition it would be expected that cavitation onset would be coincident with this large increase in current. This is contrary to the results depicted by fig. 4.6. Electrostatic lift due to permittivity differences is likely to be relatively insensitive to temperature. The physical properties of the liquid will, however, exhibit a thermal dependence.

For the dynamic situation of bubble collapse, there are several terms displaying differing thermal characteristics including: surface tension, vapour pressure, viscosity, density and thermal conductivity. The interrelationship between these parameters is further complicated during the final stages of collapse, making it difficult to predict a purely thermal dependence.

A distinction may be made between the transient and quasi-steady state conditions generated by step and direct voltage trials respectively. Step voltage tests performed on liquid paraffin and n-hexane showed a similar temperature dependence. Low temperature trials produced more filimentary events whilst at high temperatures bubble clouds appeared in the gap. Inception voltage decreased with increasing temperature. This behaviour is contrary to that observed for direct voltage. The extended stressing period may be responsible for the formation of space charge in the immediate vicinity of the cavities and allow interfacial polarisation. An increased mobility with temperature

could consequently assist this formation and hamper the cavitation process by modifying the tractive forces. The presence of the interfacial charge and cavities near the point has been shown to be only a second order influence on the total emission current.

5.3.3 The conduction process

Whilst integrated measurements were being taken, it was observed that when operating in the post transition conduction region, spraying was sometimes intermittent. A small decrease in conduction current accompanied the appearance of spraying and light emission, supporting the suggestion that this inhibited the integrated, or pedestal, charge injection process. After an extended spraying period the resultant electrode damage produced an enlarged tip radius. The intermediate region was then seen to depart from a true transition and extended over several kilovolts.

The nature of emission for a divergent electrode geometry has been the subject of studies by several other workers[88,89,91,106]. For a blade/plate geometry with a tip radius <60nm, a rectification effect was observed and as a near linear Fowler-Nordheim plot of $\ln \frac{I}{V^2}$ vs. $\frac{1}{V}$ was obtained, the forward mode, blade cathode, current enhancement was ascribed to a field injection process[88]. When blunt blades were used, with tip radii >100nm, no rectification was observed and current increased exponentially with voltage. Later[89] it was found that

increasing voltage led to a space charge limitation regime. A plot of I vs. V^2 suggested this behaviour for both blade/plate and point/plate configurations. When the water and benzene contaminants were removed from the hexane sample, the forward current was reduced which would tend to counter the original arguments for pure field emission.

5.3.4 Bubble relaxation

When point cathode spraying occurs this is associated with bubbles streaming away from the point, and possibly additional liquid motion. This effect will modify the conduction characteristic by providing discrete charge carriers whilst masking the tip by the cavitation region.

The pulsed behaviour of conduction current and emissions associated with cavitation may be explained by a bubble relaxation process at the tip of the point cathode. After the initial transient performance of the event, as shown by the step voltage trials, the cone at the tip of the point persists. This may be a site of continual cavitation, as bubbles stream out from its boundaries under the influence of electrostatic traction. Many small bubbles may be formed by a single collapse as was observed by Harrison[155] for a bubble collapse in water flowing through a venturi nozzle.

As the microbubbles emanate from the active high field region it is likely that they will continue to carry a surface charge. This will provide a repulsive force for

the cavity wall and extend its lifetime. This supports the earlier findings[49] of spraying from dual point electrodes, when light emission appeared as the bubbles met in a mid gap site.

5.3.5 Positive point polarity

Positive point experiments were undertaken and transitions were observed in the conduction characteristics. However, the light emission was found to be weak and erratic and did not consistently appear close to the point electrode. Light scintillations were occasionally seen over the surface of the spherical cathode, perhaps stemming from particle activity in the liquid. Observations of light emission were only facilitated by applying voltages close to breakdown. This was associated with the difficulty of producing cavitation at low average stresses. A freshly etched tungsten needle and an extended gap length provided the necessary stress enhancement to initially observe a spraying phenomenon. No light scattering cone was seen at the tip of the anode and the bubbles were spherically distributed in the mid gap site, unlike the streaming conical form for a point cathode. Elevated temperature observations have not been reproduced as breakdown frequently intervened and consequently damaged the electrodes.

5.3.6 Point electrode deterioration

A scanning electron microscope study of the etched tungsten electrodes was made. A freshly prepared

electrode is shown by plate 5.1. In the absence of breakdown , electrode deterioration was observed for either electrode polarity. Damage appeared to result from the spraying process. For a point cathode some rounding of the tip followed extended stressing, as shown by plate 5.2 taken after 2 hours of cavitation. Tests involving conduction current, light and acoustic emission were performed with the minimum time necessary to take readings in the post transition, cavitation, regime in an attempt to restrict the influence of electrode deterioration on the measured parameters.

A point anode suffered substantial damage even after short periods of cavitation. Plate 5.3 clearly shows the degredation of a point anode after a 30 minute spraying period. Injection studies[89] have also led to the report of electrode damage when reversed fields were applied and local ionization was thought to occur. The damage may have resulted from the high energy acoustic radiation associated with complete cavity collapse near the point, or perhaps by ion bombardment of the electrode facilitated by the presence of cavities in close proximity to the tip of the emitter[93].

5.3.7 Light emission spectra

The integrated characteristics of light emission, depicted by figures 4.10 to 4.12, clearly show a shift in the emission peak. This shift may be accomplished by either stress or temperature variation, when using a

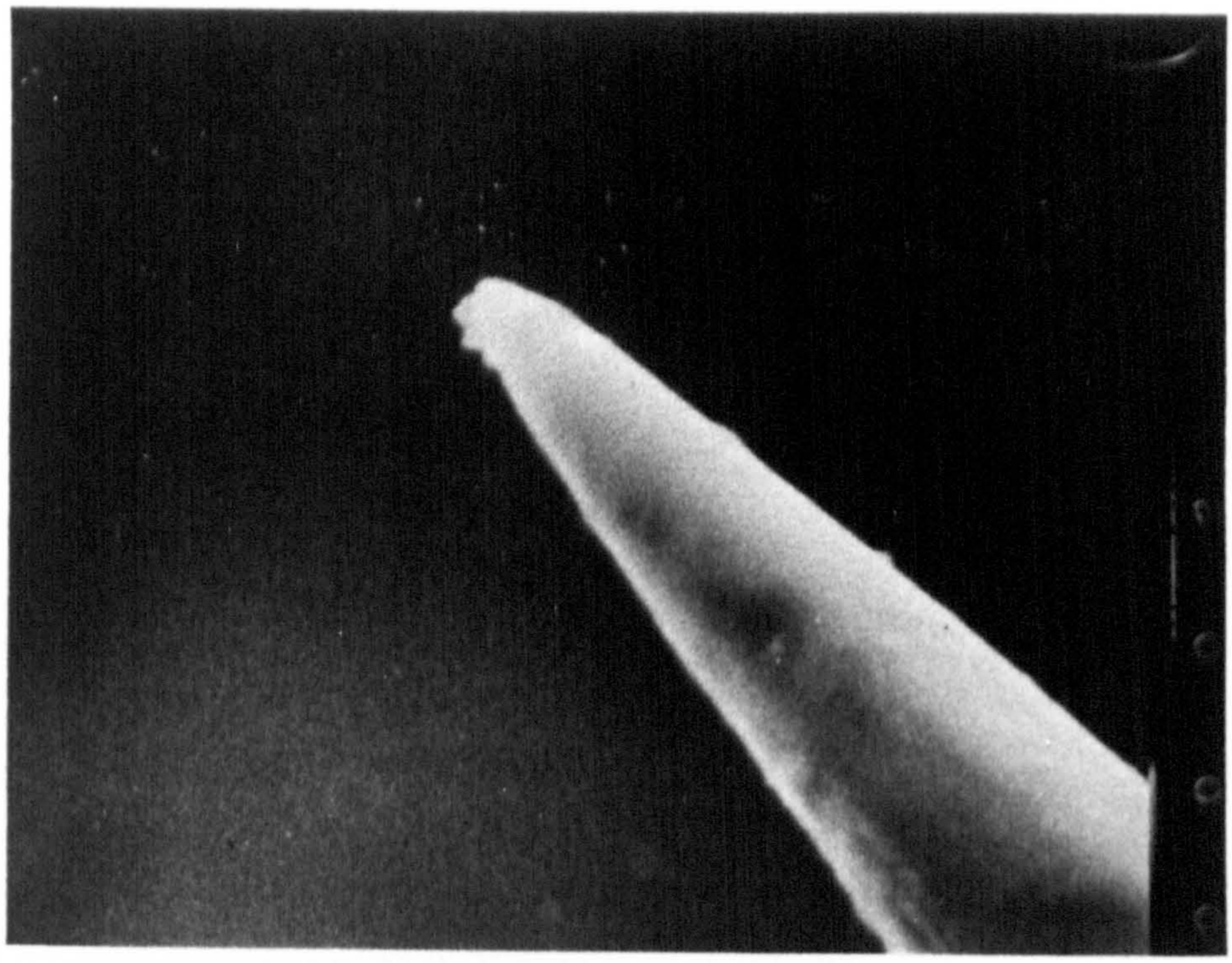

Plate 5.1 Photograph taken using a Scanning Electron Microscope. Freshly etched tungsten point electrode. Magnification: 10000.

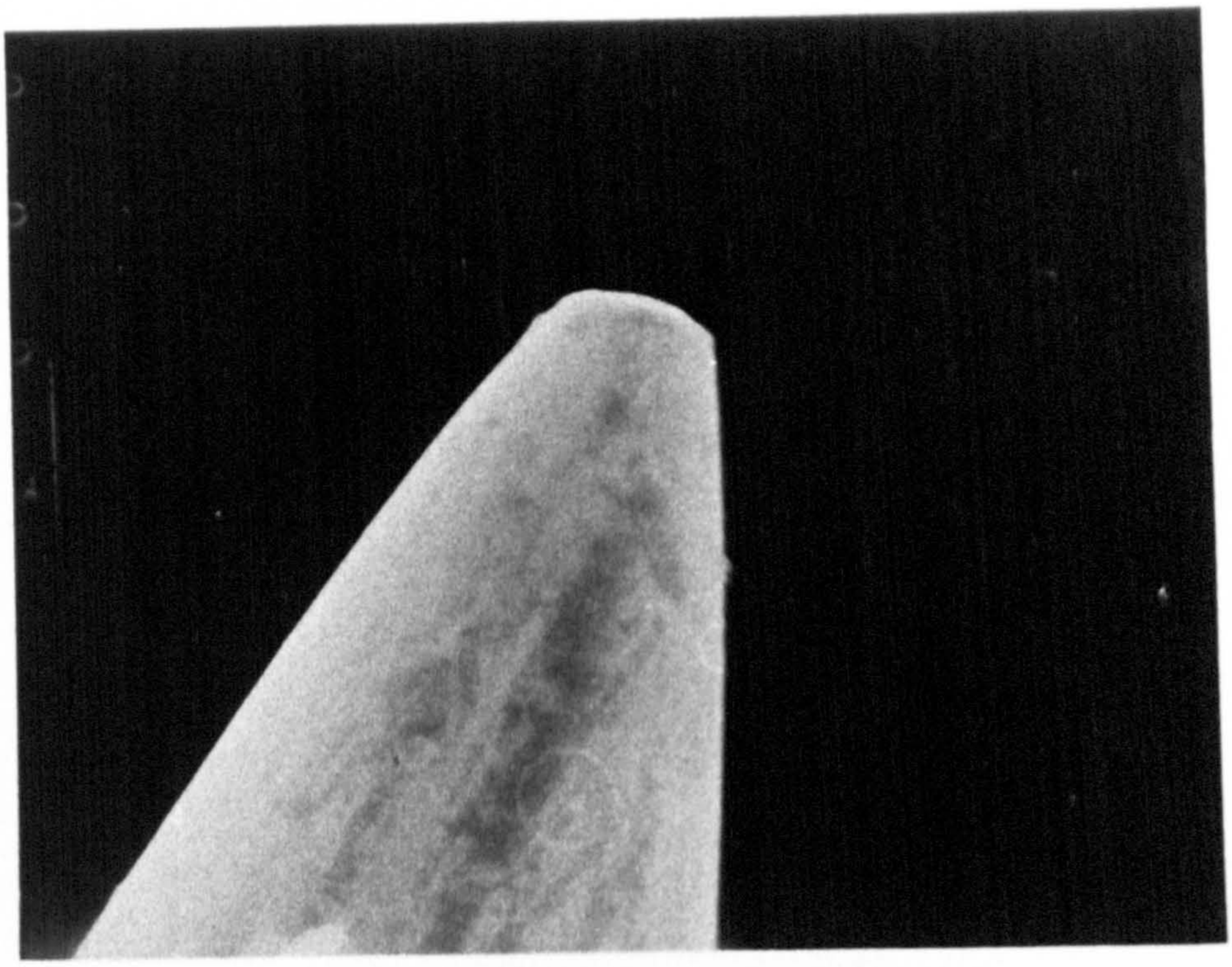

Plate 5.2 Photograph taken using a Scanning Electron Microscope. Point cathode after a 2 hour stressing period, showing cavitation damage. Magnification: 3000.

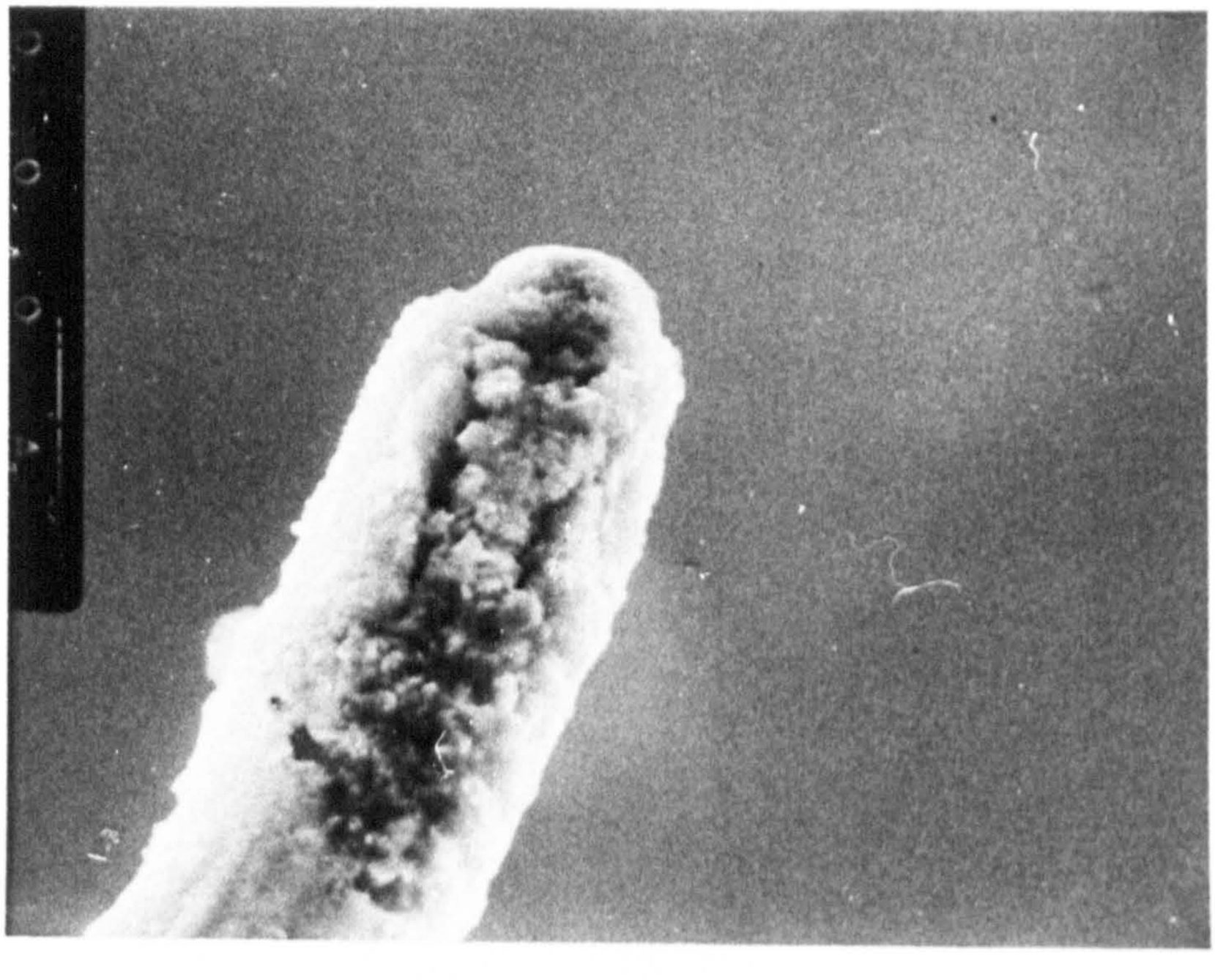

Plate 5.3 Photograph taken using a Scanning Electron Microscope. Point anode after a 30 minute stressing period, showing cavitation damage. Magnification: 3000.

divergent electrode geometry.

For bi-spherical electrodes an emission peak at approximately 420nm is evident for stresses extending between light inception and breakdown, as shown by fig. 4.10. Adopting a divergent electrode geometry, with a point cathode, the emission characteristics acquire a stress dependence. Fig. 4.11(a) shows that above 8.5kV, the emission peak occurs at 450nm. This behaviour depends on the cathode tip radius, and after an extended spraying period, the plot of fig. 4.11(b) was obtained. The low voltage peak is coincident with the bi-spherical value of 420nm. With increasing voltage a transition region is traversed and above 17kV the dominant emission wavelength becomes 450nm.

The lower wavelength peak is associated with the cavitation process, when large light scintillation pulses appear to be superimposed on a continuum of smaller emissions.

Choosing a high level of stress such that the room temperature emission peak occurs at 450nm, a temperature elevation can be used to shift the peak to 420nm, as shown by fig. 4.12. The establishment of an association between the lower wavelength emission peak with cavitation indicates that temperature elevation suppresses this form of emission, as was demonstrated by the transitional studies. A plot of the inception voltage for the two types of light emission is shown by fig. 4.8.

The low level inception for light emission is essentially independent of temperature, whilst the transitional state leading to high level emission is temperature sensitive, as suggested by fig. 4.6.

The peak in the emission spectra displayed by fig. 4.10 for uniform fields is stress invariant and coincident with that described by Malik[21]. The emission was attributed to the downward transitions of π-electrons of aromatic molecules. It was further suggested that anthracene or its derivatives furnish the dominant active luminescent centres in transformer oil.

For a divergent electrode geometry the low stress emission is the same as that exhibited by uniform fields and may be associated with an all electronic mechanism. The onset of cavitation marks a dominant emission shift to a lower wavelength which must be associated with a gas phase process. This may account for the differing emission behaviour of benzene and n-hexane when subjected to variation of temperature and pressure as observed by Rashwan and Kao[52]. The complex nature of transformer oil precludes the necessity for the species to be identical for both emission phases. The gas phase emission may, however, be rooted in a sonoluminescence or chemiluminescence mechanism. Increasing the pressure and temperature of the contents of a cavity in its final stages of collapse may give rise to the light emission, although microshocks within the cavity could generate black body radiation[135].

5.4 Conclusion and Suggestions for Further Work

The insulation failure of a liquid dielectric has been shown, in this divergent field study, to be preceded by the generation of a gaseous phase. It is suggested that the event is precipitated by electrostatic traction at the electrode surface. The findings suggest that a transient cavity is formed and during the collapse phase acoustic waves are radiated into the bulk of the liquid. In the rarefaction wake of the expanding acoustic disturbance there is the likelihood that further cavitation may ensue. Furthermore, the prevailing electric stress is locally enhanced in the presence of a cavity and interaction leads to the formation of a microbubble channel.

Point polarity differences were observed, and attributed to the nature of the space charge species generated. Corroborative evidence of space charge accumulation was furnished when pre-stressed tests were undertaken. A chosen polarity of static field applied prior to a step voltage trial was shown to dominate the subsequent event propagation. For a future study it is suggested that electron donating or trapping additives may be used to gain further insight into the control of pre-breakdown event behaviour in liquid dielectrics.

The techniques developed in this divergent field investigation may be used with uniform field electrodes. Unlike the present study, the location of an initiating event in a truely uniform field will be unpredictable and

may demand specialised optical techniques to capture a breakdown sequence. Whilst reliable optical instruments with framing rates in excess of 10^7 per second are available, the experimental methods are likely to be dictated by the limitations of event synchronisation and illumination levels.

The existence of bubble cloud formation in water is well documented. Observations made throughout the present study suggest common factors in event formation. Repeated trials of pressure cycling using liquid hydrocarbons in place of water may reveal further similarities in these studies, with particular emphasis on cavitation induced light and acoustic emissions. Valuable information may then be furnished to forge a link between pressure induced cavitation and the breakdown model presented in this thesis.

ACKNOWLEDGEMENTS

The author is indebted to Professor M.W. Humphrey Davies for the provision of laboratory facilities in the Department of Electrical and Electronic Engineering of Queen Mary College, and to the Science Research Council for the financial assistance that made this work possible.

Sincere thanks are extended to Dr. J.K. Nelson for continued encouragement and the many stimulating discussions that arose in connection with his supervision of this study.

The helpful co-operation and assistance of Mr. J. Honour of the Physical Electronics Laboratory is acknowledged with particular reference to his skills in optical and vacuum techniques. Thanks are also due to Mr. W. Solomons formerly of the Electrical Engineering Workshop for fabrication of the co-axial test cell.

Finally the author wishes to express his gratitude to Mrs. S.J. Reading for her patience and understanding in typing this thesis.

REFERENCES

1. Adamczewski, I., 1969, 'Ionization, Conductivity and Breakdown in Dielectric Liquids', (Taylor & Francis).

2. Progress in Dielectrics (Heywood & Co. Ltd.), a continuing series.

3. Macfadyen, K.A., 1955, Brit. J. Appl. Phys., 6, p.1-7, special article.

4. Swan, D.W., 1962, Brit. J. Appl. Phys., 13, p.208.

5. Digest of Literature on Dielectrics, National Academy of Science, Washington, D.C.

6. Gallagher, T.J., 1975, Simple Dielectric Liquids (Oxford University Press).

7. Hakim, S.S. and Higham, J.B., 1961, Nature, 189, p.996.

8. Holder, D.W. and North, R.J., 1963, Notes on Applied Science, 31: Schlieren Methods, (H.M.S.O.).

9. Farazmand, B., 1961, Brit. J. Appl. Phys., 12, p.251-4.

10. Chadband, W.G., 1962, M.Sc. Dissertation, Birmingham University.

11. Chadband, W.G. and Wright, G.T., 1965, Brit. J. Appl. Phys., 16, p.305-13.

12. Chadband, W.G., Coelho, R. and Debeu, J., 1971, J. Phys. D.: Appl. Phys., 4, p.539-40.

13. Morikawa, E., 1972, Elect. Eng. Japan, 92, 1, p.11-18.

14. Thomas, W.R.L., 1973, NRC-NAS Conference on Elect. Ins. and Diel. Phen., p.130-6.

15. Thomas, W.R.L., 1975, IEE Conference on Diel. Mats., Meas. and Appln., Cambridge, p.311-4.

16. Thomas, W.R.L. and Forster, E.O., 1975, Conference on Cond. and B/D in Diel. Liquids, Delft, p.49-54.

17. Thomas, W.R.L., 1974, NRC-NAS Conference on Diel. and Ins. Mats., CRL36, p.74.

18. Hizal, E.M., 1973, Ph.D. Thesis, Victoria University, Manchester.

19. Allen, R.N. and Hizal, E.M., 1974, Proc. IEE, 121, 3, p.227-31.

20. Nelson, J.K. and Hashad, I.F.M., 1975, Conference on Cond. and B/D in Diel. Liquids, Delft, p.41-4.

21. Malik, A.K., 1970, Ph.D. Thesis, London University.

22. Krasucki, Z., Church, H.F. and Garton, C.G., 1960, J. Electrochem. Soc., 107, 7, p.598-602.

23. Krasucki, Z., 1962, Proc. IEE, 109B, suppl. 21-22, p.435-9.

24. Krasucki, Z., 1966, Proc. Roy. Soc., A294, p.393-404.

25. Mirza, J.S., Smith, C.W. and Calderwood, J.H., 1970, J. Phys. D.: Appl. Phys., 3, 2, p.580-5.

26. Singh, B., Smith, C.W. and Calderwood, J.H., 1972, Conference on Cond. and B/D in Diel. Liquids, Dublin, p.202-5.

27. Singh, B., Chadband, W.G., Smith, C.W. and Calderwood, J.H., 1972, J. Phys. D.: Appl. Phys., 5, p.1457-64.

28. McGrath, P.B. and Nelson, J.K., 1975, Conference on Diel. Mats., Meas. and Appln., Cambridge, p.315-8.

29. Murooka, Y., Nagao, S. and Toriyama, Y., 1964, Brit. J. Appl. Phys., 15, p.1585-90.

30. Murooka, Y. and Toriyama, Y., 1973, NRC-NAS Conference on Elect. Ins. and Diel. Phen., p.161-8.

31. Murooka, Y. and Toriyama, Y., 1974, J. Appl. Phys., 45, 4, p.1707-12.

32. Yanshin, E.V., Ovchinnikov, I.T. and Vershinin, Yu, N., 1974, Sov. Phys. Tech. Phys., 18, 10, p.1303-6.

33. Toriyama, Y., 1964, Brit. J. Appl. Phys., 4, p.203-4.

34. Mitsui, H., Toriyama, Y. and Calderwood, J.H., 1975, Conference on Cond. and B/D in Diel. Liquids, Delft, p.209-12.

35. Race, H.H., 1940, AIEE Trans., 59, p.730-7.

36. Darveniza, M., 1959, Nature, 183, p.743.

37. Darveniza, M. and Tropper, H., 1961, Proc. Phys. Soc. 78, p.854-68.

38. Dakin, T.W. and Berg, D., 1959, Nature, 184, p.120.

39. Gosling, C.H., 1960, Ph.D. Thesis, London University.

40. Darveniza, M., 1959, Ph.D. Thesis, London University.

41. Kalinowski, J. and Dera, J., 1964, Acta Physica Polonica, 25, p.205-10.

42. Jones, E. and Angerer, L., 1966, Nature, 210, p.1219-20.

43. Gzowski, O.A., Wlodanski, R., Hesketh, T.R. and Lewis, T.J., 1966, Brit. J. Appl. Phys., 17, p.1483-9.

44. Kishida, H., Sato, T. and Toriyama, Y., 1975, Conference on Cond. and B/D in Diel. Liquids, Delft, p.171-4.

45. Palmer, A.W. and House, H., 1972, Opto-Electronics, 4, p.463-7.

46. Smith, C.W., Kao, K.C., Calderwood, C.W. and McGee, J.D., 1966, Nature, 210, p.192.

47. Smith, C.W., Kao, K.C. and Calderwood, C.W., 1966, NRC-NAS Conference on Elect. Ins., p.45-9.

48. Smith, C.W. and Calderwood, J.H., 1968, Phen. de Cond. dans les liq. isolants, Colloques Int. du Centre National de la Res. Sci., Grenoble, p.161-85.

49. Smith, C.W., Kao, K.C., Calderwood, J.H. and McGee, J.D., 1966, Adv. Electron., Electron. Phys., 22, p.1003-9.

50. Mirza, J.S., Smith, C.W. and Calderwood, J.H., 1972, Conference on Cond. and B/D in Diel. Liquids, Dublin, p.198-201.

51. Rashwan, M.M. and Kao, K.C., 1972, ibid., p.263-6.

52. Rashwan, M.M. and Kao, K.C., 1972, NRC-NAS Conference on Elect. Ins. and Diel. Phen., p.60-6.

53. Kao, K.C. and Rashwan, M.M., 1974, Proc. IEEE, 62, p.856-8.

54. Jayasakera, W.P., 1957, Ph.D. Thesis, London University.

55. Shammas, N., Smith, C.W. and Calderwood, J.H., 1974, J. Phys. D.: Appl. Phys., 7, p.2587-92.

56. Baker, E.B. and Boltz, H.A., 1937, Phys. Rev., 51, p.275-82.

57. Le Page, W.R. and Du Bridge, L.A., 1940, Phys. Rev., 58, p.61-6.

58. Dornite, R.W., 1940, Ind. Eng. Chem., 32, p.1529-34.

59. Plumley, H.J., 1941, Phys. Rev., 59, p.200-7.

60. Goodwin, D.W. and Macfadyen, K.A., 1953, Proc. Phys. Soc., 66B, p.85-96.

61. Fowler, R.H. and Nordheim, L., 1928, Proc. Roy. Soc., A,119, p.173.

62. Llewellyn Jones, F. and De La Perrelle, E.T., 1953, Proc. Roy. Soc., A, 213, p.267-79.

63. Green, W.B., 1955, J. Appl. Phys., 26, p.1257-64.

64. Green, W.B., 1956, J. Appl. Phys., 27, p.921-5.

65. House, H., 1955, Nature, 176, p.610-1.

66. House, H., 1957, Proc. Phys. Soc., 70, 10B, p.913-27.

67. Cullingford, M.C., Zaky, A.A., Zein Eldine, M.E. and Hawley, R., 1963, Nature, 199, p.1082.

68. Zaky, A.A. and House, H., 1963, J. Appl. Phys., 34, 11, p.3194-9.

69. Zaky, A.A., Tropper, H. and House, H., 1963, Brit. J. Appl. Phys., 14, p.651-6.

70. Macfadyen, K.A. and Helliwell, G.C., 1959, J. Electrochem. Soc., 106, p.1022-7.

71. Watson, P.K. and Sharbaugh, A.H., 1957, NRC-NAS Conference on Elect. Ins., pub. number 570, p.1-5.

72. Sharbaugh, A.H. and Watson, P.K., 1959, Nature, 184, p.2006.

73. Watson, P.K. and Sharbaugh, A.H., 1960, J. Electrochem. Soc., 107, 6, p.516-21.

74. Watson, P.K., 1965, NRC-NAS Conference on Elect. Ins., p.39-41.

75. Watson, P.K. and Sharbaugh, A.H., 1961, NRC-NAS Conference on Elect. Ins., p.95-6.

76. Chadband, W.G. and Calderwood, J.H., 1970, Conference on Diel. Mats. Meas. and Appln., Lancaster, p.105-9.

77. Chadband, W.G. and Calderwood, J.H., 1972, Proc. IEE, 119, 11, p.1661-6.

78. Huq, A.M.Z. and Tropper, H., 1964, Brit. J. Appl. Phys., 15, p.481-90.

79. Nosseir, A. and Megahed, I., 1970, J. Phys. D.: Appl. Phys., 3, p.1205-11.

80. Nosseir, A., 1973, IEEE Trans., E18, 4, p.118-22.

81. Huq, A.M.Z., 1962, Ph.D. Thesis, London University.

82. Nosseir, A., 1964, Ph.D. Thesis, London University.

83. Megahed, I., 1965, Ph.D. Thesis, London University.

84. Megahed, I., 1965, Nature, 205, p.686-7.

85. Megahead, I. and Nosseir, A., 1969, J. Phys. E.: Sci. Inst., 2, p.880-4.

86. Nelson, J.K. and McGrath, P.B., 1972, J. Phys. D.: Appl. Phys., 5, p.1111-6.

87. Ostroumov, G.A., 1962, Sov. Phys. JETP, 14, 2, p.317-9.

88. Secker, P.E. and Aplin, K.W., 1970, Conference on Diel. Mats. Meas. and Appln., Lancaster, p.129-33.

89. Aplin, K.W. and Secker, P.E., 1972, Conference on Cond. and B/D in Diel. Liquids, Dublin, p.158-61.

90. Coelho, R., 1961, NRC-NAS Conference on Elect. Ins., p.31-33.

91. Pugh, D.R., 1973, NRC-NAS Conference on Elect. Ins., and Diel. Phen., p.185-92.

92. Coelho, R., 1970, Conference on Diel. Mats. Meas. and Appln., Lancaster, p.105-9.

93. Halpern, B. and Gomer, R., 1969, J. Chem. Phys., 51, 3, p.1031-47.

94. Coelho, R. and Sibillot, P., 1969, Nature, 221, p.757.

95. Clark, F.M., 1933, J. Franklin Inst., 215, p.39-67.

96. Clark, F.M., 1935, AIEE Trans., 54, p.50-5.

97. Hoover, W.G. and Hixson, W.A., 1949, AIEE Trans., 68, 2, p.1047-50.

98. Salvage, B., 1951, IEE Monograph 2, p.15-22.

99. Lewis, T.J., 1953, Proc. IEE, 100, 2A, p.141-8.

100. Crowe, R.W., Bragg, J.K. and Sharbaugh, A.H., 1954, J. Appl. Phys., 25, 3, p.392-5.

101. Zein Eldine, M.E. and Tropper, H., 1955, IEE Monograph 135S, p.35-45.

102. Lewis, T.J., 1957, J. Appl. Phys., 28, 4, p.503-5.

103. Lewis, T.J., 1960, J. Electrochem. Soc., 107, 3, p.185-91.

104. Kao, K.C. and Higham, J.B., 1961, J. Electrochem. Soc., 108, 6, p.522-8.

105. Kao, K.C. and Calderwood, J.H., 1965, NRC-NAS Conference on Elect. Ins., p.44-52.

106. Kao, K.C., 1969, NRC-NAS Conference on Elect. Ins., p.122-7.

107. Watson, P.K. and Higham, J.B., 1953, Proc. IEE, 100, 2A, p.168-74.

108. Khambanonda, A., 1958, Ph.D. Thesis, London University.

109. Sletten, A.M., 1959, Nature, 183, p.311-2

110. Sletten, A.M., 1960, Ph.D. Thesis, London University.

111. Tropper, H., 1961, J. Electrochem. Soc., 108, 2, p.144-50.

112. Schopfle, C.S. and Connell, L.H., 1929, Ind. Eng. Chem., 21, p.529-36.

113. Schopfle, C.S. and Fellows, C.H., 1931, Ind. Eng. Chem., 23, p.1396-8.

114. Thomas, C.L., Egloff, G. and Morell, J.C., 1941, Chem. Rev., 28, p.1-70.

115. Basseches, H. and Barnes, M.W., 1958, Ind. Eng. Chem., 50, p.959-66.

116. Blodgett, R.B. and Bartlett, S.C., 1961, AIEE, Power App. and Syst., p.528-36.

117. Reynolds, E.H. and Black, R.M., 1972, Proc. IEE, 119, 4, p.497-504.

118. Spitzer, F.R.J., 1967, Ph.D. Thesis, London University.

119. Sletten, A.M. and Lewis, T.J., 1956, IEE Monograph,193M.

120. McGrath, P.B. and Nelson, J.K., 1977, Proc. IEE, 124, 2, p.183-7.

121. Watson, P.K., 1965, NRC-NAS Conference on Elect. Ins., p.39-41.

122. Stratton, J.A., Electromagnetic Theory (McGraw-Hill 1941).

123. Hakim, S.S. and Higham, J.B., 1962, Proc. Phys. Soc., 80, p.190-8.

124. Derjaguin, B., 1940, Trans. Faraday Soc., 56, p.204.

125. Onsager, L., 1936, J. Amer. Chem. Soc., 58, p.1486-93.

126. McClellan, A.L., Tables of Experimental Dipole Moments (W.H. Freeman and Co., 1963).

127. Frenkel, J., Kinetic Theory of Liquids (Clarendon Press, Oxford 1946).

128. Von Hippel, A.R., Dielectrics and Waves (John Wiley and Sons, Inc., 1954).

129. Nussbaum, A., Field Theory (C.E. Merrill Books, Ohio, 1966).

130. Rayleigh, 1917, Phil. Mag. 34, p.94-98.

131. Noltingk, B.E. and Neppiras, E.A., 1950, Proc. Phys. Soc., B63, p.674-85.

132. Mason, W.P., (Ed.) Physics of Acoustics, 1B (Academic Press 1964).

133. Knapp, R.T. and Hollander, A., 1948, Trans. Am. Soc. Eng., 70, p.419-35.

134. Mellen, R.H., 1956, J. Acoust. Soc. Am., 28, p.447-54.

135. Jarman, P., 1960,ibid., 32, p.1459-62.

136. Fox, T.G. and Flory, P.J., 1950, J. Appl. Phys., 21, p.581-91.

137. Singh, H. and Nolle, A.W., 1959, ibid., 30, p.337-41.

138. Williams, M.L., Landel, R.F. and Ferry J.D., 1955, J. Amer. Chem. Soc., 77, p.3701-7.

139. Doolittle, A.K., 1951, J. Appl. Phys., 22, p.1471-5.

140. Eyring, H., 1936, J. Chem. Phys., 4, p.283-91.

141. Tabor, D., Gases Liquids and Solids (Penguin, 1969).

142. Moelwyn-Hughes, E.A., Physical Chemistry (Pergamon Press, 1961).

143. Strasberg, M., 1959, J. Acoust. Soc. Am., 31, p.163-76.

144. Harvey, E.N., et al, 1947, J. Appl. Phys., 18, p.162-72.

145. Kok, J.A., Electrical Breakdown of Insulating Liquids, (Philips Technical Lib. 1961).

146. Skinner, S.M., Savage, R.L. and Rutzler, J.E., 1953, J. Appl. Phys., 24, 438-50.

147. Raff, R.A.V. and Sharan, A.M., 1969, 13, p.1129-57.

148. Anderson, J.C., Dielectrics (Chapman, Hall and Science Paperbacks, 1967).

149. Glaser, D.A., Phys. Rev., 1952, 87, p.665.

150. Gallagher, T.J. and Lewis, T.J., 1964, Brit. J. Appl. Phys., 15, p.491-8.

151. Croitoru, Z., Columbeau, M. and Coelho, R., 1961, NAS-NRC Conference on Elect. Ins., p.21-4.

152. Nelson, J.K. and McGrath, P.B., 1976, NAS-NRC Conference on Elect. Ins. and Diel. Phen., paper B-7.

153. McGrath, P.B. and Nelson, J.K., 1975, Conference on Cond. and B/D in Diel. Liquids, Delft, p.36-40.

154. Nelson, J.K. and McGrath, P.B., 1975, Proc. IEE, 122, p.1439-42.

155. Harrison, M., 1952, J. Acoust. Soc. Am., 24, p.776-82.

156. Krishnamurthy, N., 1966, Ph.D. Thesis, London University.

157. Priaroggia, P.G. and Palandri, G., 1960, J. Electrochem. Soc., 107, p.884-6.

158. McCarvill, W.T. and Bell, J.P., 1974, J. Appl. Poly. Sci., 18, p.343-9.